Numerical Simulations of Airflow and Weather during the Summer over the Island of Oahu

A THESIS SUBMITTED TO THE GRADUATE DIVISION OF THE UNIVERSITY OF HAWAI'I IN PARTIAL FULFILLMENT OF THE REQUIREMENTS FOR THE DEGREE OF

MASTER OF SCIENCE
IN
METEOROLOGY
DECEMBER 2006

By

Hiep Van Nguyen

Thesis Committee:

Yi-Leng Chen, Chairperson
Pao-Shin Chu
Yuqing Wang

We certify that we have read this thesis and that, in our opinion, it is satisfactory in scope and quality as a thesis for the degree of Master of Science in Meteorology.

THESIS COMMITTEE

Chairperson

ACKNOWLEDGMENTS

I would like to thank Prof. Yi-Leng Chen for his guidance, patience, and informative discussions. I also would like to thank Prof. Pao-Shin Chu, Prof. Yuqing Wang, Dr. Yang Yang, Dr. Yongxin Zhang, and DaNa Calis for their helpful suggestions and insightful discussions and Yang Yang and Yongxin Zhang for technical assistance. DaNa Calis provided the observation data at 13 hourly stations. I would like to thank my parents, my sisters, brothers, Hien Nguyen, friends, and colleagues at the Institute of Meteorology and Hydrology, Hanoi, Vietnam for their continuous love and support throughout my educational and life pursuits. I would like to acknowledge Vietnamese Government for financial support for my study in US. I would like to acknowledge US Forest Service (USFS) and UH/MHPCC (University of Hawaii/Maui High Performance Computing Center) for funding this research.

ABSTRACT

In this study, The MM5/LSM is used to simulate airflow and weather over Oahu for July and August, 2005. The forecasts from GFS provided by NCEP are used to initialize the model. The effects of trade-wind conditions, terrain height, and landuse on island-scale air flow and weather are investigated.

Simulated winds agree reasonably well with observations including weaker winds over the island interior, two regions with the strongest wind speeds over the ocean at the northwestern and southeastern corners of Oahu. During the diurnal cycle, both observed and simulated winds show mountain winds over the Waianae Mountains, weak winds over central Oahu and over the Ko'olau Mountains at night, stronger wind speeds and almost uniform wind directions during the day, weak onshore westerly winds offshore of the Waianae coast at 14 HST. Stronger surface wind speeds are simulated under strong trades than under weak trades. The wind direction errors are smaller at stations at windward side of the Ko'olau Mountains than at stations at other locations. Both wind speed and wind direction errors are smaller when winds are stronger during the day.

Simulated rainfalls of the two summer months agree reasonably well with observations including a maximum rainfall over the Ko'olau Mountains, a secondary maximum occurs at lee-side slope of the Waianae mountain ranges and a minimum at central Oahu. During the diurnal cycle, observed and simulated rainfall show a minimum in the afternoon, two maxima of rainfall, one at night caused by radiation cooling, stronger wind aloft as well as lower LCL, and the other in the morning. One of the important factors relates to the morning maximum rainfall is the increase in vertical motion at this time. However, the reason for larger vertical motion in the early morning is still under investigation. Both simulated and observed rainfalls are about four times larger in strong trades than in weak trades.

Overall, the simulated temperatures are better at windward stations than at other stations. The simulated temperatures at a specific station are generally better at night than during the day. The simulated dew point temperature shows the surface air is moister at night than during the day due to the mixing with dry air aloft. The abundant moisture area is simulated at windward side. The drier regions are simulated over the island interior and over the Waianae Mountains.

Sensitivity tests show that the island blocking effects result in decrease in wind speeds over central Oahu and at the windward coast of the Ko'olau Mountains. Wind speeds at these areas are stronger when one or both of the mountains are removed. Urbanization results in increase temperature 1-2°C at 14 HST due to urban heating and weaker wind speed over land at night due to the increase in stability and in roughness length.

No simulated rainfall over Oahu in the NM case reasonably proves that mountain terrains are crucial factors for the development of showers over Oahu. The NK case shows that the Ko'olau Mountains play an important role in producing rainfall over the Ko'olau Mountains and dry areas over central Oahu. A slight increase in rainfall was simulated at the leeward side of the Waianae Mountains in the UB case due to increase in daytime heating as a result of urbanization.

TABLE OF CONTENTS

LIST OF TABLES

LIST OF FIGURES

LIST OF APPENDICES

ABBREVIATIONS AND SYMBOLS

C	Celsius
BIAS	Mean Bias
d_i	Distances from the station to nearest grid points
Fr	Froude Number
F_s	Interpolation value at station
f_i	The grid values
GFS	Global Forecast System
hPa	Hecto-Pascal
h	Height
HaRP	Hawaiian Rainband Project
HST	Hawaii Standard Time
km	Kilometer (s)
K	Kelvin
LSM	Land Surface Model
mm	Millimeter (s)
m s^{-1}	Meters per second
MAE	Mean Absolute Error
MM5	Meso-scale Model 5
MSM	Meso-scale Spectrum Model
NCAR	National Center for Atmospheric Research
NCEP	National Centers for Environmental Prediction
NOAA	National Oceanic and Atmospheric Administration
N	Brunt-Vaisala frequency

NE	Northeast
NK	No Ko'olau Mountains
NM	No Mountains
NW	No Waianae Mountains
RMSE	Root Mean Square Error
SST	Sea Surface Temperature
UB	Urbanization
UTC	Universal Time
U	Wind speed of air upstream of island
Z_m	Model terrain Height at Station
Z_s	Real Station Altitude
%	Percent
>	Greater than
<	Less than
~	Approximately
°	Degree
α	The Lapse Rate
$\lvert\ \rvert$	Absolutes Value

Chapter I

Introduction

1.1 Motivation

The trade-wind belt has a minimum in the global distribution of rainfall. However, local trade-wind showers are frequent over the Hawaiian Islands (Chen and Nash, 1994) because of terrain and local winds. Besides orographic lifting on the windward slopes, the mountain also acts as a barrier to the approaching airflow and as a heat source (sink) during the day (night) (Leopold 1948, 1949; Chen and Nash 1994). With different sizes (< 140 km), shapes and mountain heights (500 m-4,100 m), and large variations in local microclimate ranging from humid tropical conditions on the windward side to dry conditions on the lee side including some areas with semi-arid terrain covered by lava rocks, the Hawaiian Islands are ideal to study the island flow response under different flow regimes and heterogeneous surface properties.

In terms of general statements of island effects on trade-wind flow, the tropical islands strongly affect the trade-wind flow on both direction and intensity. While the trade-wind flow is relatively uniform over the open ocean, it is distorted and disrupted by the mountains, hills, and valleys of the islands (Chen and Nash, 1994). The height of the mountains is one of the important factors affects the island flow response. High mountains split the trade winds and force it to flow around mountains. In contrast, low mountains allow the trade-wind flow to move over the top of the mountains (Leopold, 1949). Orographic lifting forces the air parcel to slow down and move upslope. On the other hand, island blocking causes flow deceleration upstream of the island. An orographic induced local high pressure is formed on the windward side because of orographic lifting aloft. As the air is forced upslope, it cools and becomes denser. As

the incoming trade winds encounter the high pressure and the pressure gradient forces it to slow down and the coming flow is deflected around the islands with strong winds at the southern and northern tips of the islands. In terms of intensity, the islands make the trade-wind weaken on windward side, and be calm on the lee side (Chen and Nash, 1994), stronger at southern and northern tips of the island.

In addition to dynamical blocking effect, the trade-wind flow is also affected by the diurnal heating cycle of the surface. In regions with weak winds, the diurnal land-sea breezes with upslope/onshore flow during the day, and downslope/offshore flow at night (Schroeder et al. 1977; Feng and Chen 1998; Chen and Nash, 1994) become important.

The interaction between island terrain and trade winds, resulting in orographic lifting, dynamic blocking, and the diurnal heating cycle affect the temporal and spatial distributions of rainfall. The rainfall maxima usually occur at the windward side because of orographic lifting, as the warm moist trade-wind flow is raised up the mountain slopes (Leopold 1949), convergence between the katabatic flow and coming trades, or the inland drifting of the offshore rainbands (Chen and Nash, 1994). On the other hands, the minimum rainfall usually occurs on the leeside where the trade-winds are blocked by mountains (Chen and Nash, 1994; Yang and Chen, 2003).

Rainfall at different regions of an island, which has varies properties of terrain, such as the Big Island, has different diurnal cycles. Over the windward lowlands, rainfall reach maximum at night (Schroeder et al., 1977) because of the convergence between the katabatic-land-breeze flow and the opposing trade-wind flow with abundant water vapor (Chen and Nash, 1994). During the day, windward lowlands have less rainfall due to the replacement of the nighttime convergence by a daytime divergence over the area (Chen and Nash, 1994). On the coastal regions, rainfall reaches maximum in the early morning because the offshore rainbands drift toward the island (Takahashi, 1977;

Fullerton, 1972; Chen and Nash, 1994). On the windward slopes, the maximum rainfall frequency occurs in the afternoon by orographic lifting as a result of anabatic-trade-wind flow moving up the slopes (Leopold, 1949; Chen and Nash, 1994). With cooling at night, the katabatic-land-breeze flow develops. As a consequence, the windward slope showers diminish (Chen and Nash, 1994). On the leeward side, rainfall accumulation is significantly less than on windward side (Giambelluca et al., 1986; Chen and Nash, 1994; Yang and Chen, 2003). On windward slopes a maximum rainfall occurs in the late afternoon due to orographic lifting (Leopold, 1949; Schroeder et al., 1977; Yang and Chen, 2003). Along the leeward side coast, maximum rainfall occurs in the early morning as a result of the lifting of moist air in the onshore flow by land-breeze front (Yang and Chen, 2003).

Oahu Island is much smaller with much lower heights than the Big Island. Oahu has two mountain ranges, the peaks of the two major mountains, 960 meters for Ko'olau, 1200 meters for Waianae, are lower than the normal trade wind inversion (TWI) height (~ 2 km, Yang et al, 2005; Chen and Nash, 1994). The two mountain ranges are oriented nearly perpendicular to the mean trade-wind direction (Leopold, 1948). Observations showed that rainfall over Oahu has a nocturnal maximum on the windward side and an afternoon maximum on the leeward side (Leopold, 1948).

Although there are many modeling studies on the terrain effects on airflow over and around flow barriers, the effects of the land surface heating/cooling during the diurnal cycle are only crudely estimated in these studies. Furthermore, there is only one modeling study (Lavioe, 1974) for Oahu.

Recently, using a mesoscale spectral model (Juang, 2000), Zhang et al. (2005) showed that adequate descriptions of vegetation and ground cover over Oahu with an advanced land surface model (LSM) are required in simulating weather conditions at

four major Oahu airport sites throughout the diurnal cycle. Using the surface properties compiled by Zhang et al (2005), Yang et al (2005) successfully simulated the island-induced airflow and weather over the Big Island during HaRP (Hawaiian Rain Band Project, 11 July- 24 August 1990) by applying the coupled MM5/LSM model (F. Chen and Dudhia 2001).

In the past, most high-resolution data sets over and around mountainous islands were collected during field experiments. For the Hawaiian Islands, special field studies were mainly conducted over the Big Island including HaRP. Although there are many studies on island effects on rainfall, few of them (Loveridge 1924; Leopold 1948) are done for the island of Oahu which accounts for 80% of the state population. These studies showed that rainfall occurrences at Honolulu and a few stations in the vicinity of the Ko'olau Mountain Range have a nocturnal maximum. Recently, with the deployment of rain gauges around the state by the National Weather Service and weather stations by various agencies, there are 69 hourly rain gauge stations and 13 weather stations with hourly weather data over Oahu allowing us to study the effects of terrain and the diurnal heating cycle on island weather over the island (Loos and Chen 2004). These data will be used to validate the results from high resolution weather models and to identify the model bias, if any. In addition, these models will be used as research tools to study island flow response to various weather conditions, including strong trades and weak trades.

1.2 Previous studies on weather and airflow over the Hawaiian Islands

1.2.1 Observation studies

One of the earliest studies on precipitation over Oahu was done by Loveridge (1924). He focused on diurnal variations of precipitation at the Honolulu Airport station. He stated that at the station, rainfall has a maximum in the winter and early spring, a minimum of rainfall in the summer. He stated that some winds are needed for rainfall formation but rainfall reaches maximum when wind speed is weak at night.

The diurnal weather patterns on Oahu were studied by Leopold (1948). In his study, he showed that the wind directions over most of Oahu were affected by local winds. He stated that the maximum wind speed during the day are caused by transferring of momentum from high wind speeds aloft to lower levels as a result of increase in instability during the day. Decrease in instability of the air makes wind speed much lower at night. On aspect of rainfall a maximum of rainfall at night, according to him, radiation cooling that makes the air more unstable, and higher wind speed aloft that makes more turbulence, result in the nocturnal rainfall maximum. On the leeward side, a secondary maximum of rainfall occurs from convective showers as a result of orographic lifting.

Interaction of trade-wind and see breeze was investigated by Leopold (1949). He divided interaction regimes between trade-wind and see breeze into different types based on three factors: (1) breadth of the area on which effects of heating and cooling occur, i.e. the area of the island; (2) the height and shape of the mountains; and (3) the locations i.e. leeward or windward side. For the low mountains (~1000 m), the trade wind flows over the mountain ridge and meets the leeward side sea-breeze in a front line perpendicular to trade direction. A long cloud line usually forms over the front. He further stated that if mountains are high (> 3000 m), they may split the trades into lateral flows.

In the high mountain case, at the leeward side, no trade winds but onshore/sea-breeze during the day and offshore/land breeze at night are prevalent. In general, the leeward onshore flow results in convective clouds producing leeward showers in the afternoon.

1.2.2 Model studies

The first modeling study over Oahu was done by Lavioe (1974). In his research, a simple, single-layer mesoscale model was used. At that time, the research contributed better understanding the effect of topography, the trade-wind inversion, and land-sea breeze regime on Oahu weather. Even though, one layer model can not well represent the real meteorological fields or do a good airflow simulation. To get better results, multi-level, non hydrostatic models such as MM5, MSM or WRF should be used. In addition, the horizontal resolution used on the work is 3 km, the Oahu Island is relatively small in side (East to West: 97km, North to South: 48 km), to simulate island-scale flow, higher resolution model should be used.

Recently, Zhang et al. (2005) used meso-scale spectral model (MSM) to simulate weather conditions at three stations on Oahu throughout the diurnal cycle for a month from 20 May to 20 Jun 2002. One heavy rainfall case during the period was also studied. He showed that adequate descriptions of vegetation and ground cover over Oahu with an advanced land surface model (LSM) are required to achieve good simulation of the diurnal variation of surface airflow and weather. He compared the results with that of regional spectral model (RSM) to show that high resolution MSM coupled with advanced LSM performed much better simulations than RSM. Zhang et al. (2005) also used MSM/LSM to perform rainfall simulations and showed that, compared with observations, the model simulated excessive rainfall on the windward side of Ko'olau, meanwhile less or no rainfall was simulated over the ridge axis of Ko'olau.

Yang et al. (2005) used the coupled MM5/LSM model and successfully simulated the island-induced airflow and weather over the Big Island during HaRP (Hawaiian Rain Band Project, 11 July- 24 August 1990). In the work, simulations of land-sea breezes, airflow patterns as well as thermodynamic fields are in good agreement with observations from 50 portable automatic mesonet stations. Overall, the simulations of wind speed and temperature in the research are better than that at leeside. In addition, the sensitivity tests showed that adequate depiction of the terrain and surface properties in the model and spinning up of soil temperature for a period of two month prior to the simulation period resulted in better simulation.

1.3 Questions and objectives

Above review section show that some interesting findings about Oahu flow and weather are stated in studies used observation data. The only prior modeling study over Oahu showed some limitations about grid resolution and model. Zhang et al. used the coupled MSM/LSM to focus only three locations and one heavy rainfall event; simulations of airflow and weather for Oahu have not been performed. In fact, Yang et al. (2005) gained some success in the coupled MSM/LSM model simulation for Hawaii Island. So, the questions stated here for this research are:

• Would it be possible to use MM5/LSM to simulate the island effects on airflow and weather for the island of Oahu which is considerable smaller than the island of Hawaii?

• Could MM5/LSM be used as a research tool to study island effects on weather for the island of Oahu?

To find the answers for these questions, following objectives are stated:

• With adequate depiction of the terrain and surface properties in the model, to what extent the effects of terrain and diurnal heating cycle on island-scale weather over Oahu could be simulated by the coupled MM5/LSM.

• What are the effects of trade-wind conditions, e.g., strong and week trades, on the island-scale airflow and weather over Oahu?

Chapter II

Data and Methods

2.1 Research Plan

The nonhydrostatic Mesoscale Model version 5 (MM5) coupled with an advanced land surface model (F. Chen and Duhia 2001) with a horizontal resolution of 1.5-km will be used as a research tool. The vegetation covers and soil properties compiled by Zhang et al. (2005) for Oahu will be used. The data collected during July-August 2005 will be used to validate the model results. During this two-month period, the daily model run will be initialized by the output of Global Forecast System (GFS) with a horizontal resolution of about 100 km provided by NCEP (National Centers for Environmental Prediction). Statistical analyses of model performance of the 1.5-km Oahu model during this two-month period will be evaluated at each station including the absolute errors, root mean square errors of simulated surface air temperatures, moisture and winds.

To study the effects of terrain and diurnal heating cycle on island-airflow and weather, model simulations are averaged for the two-month period and compared with corresponding averaged observations. The spatial distributions and diurnal variations of rainfall, wind speed, wind direction, and surface air temperature are investigated.

To investigate the effects of trade-wind conditions on island-scale airflow and weather, the model simulations and observations for two groups of strong and weak trade-wind categories are separately averaged and analyzed.

Sensitivity tests are conducted to investigate the effects of model terrain, differences in land-sea surface friction, daytime heating and nocturnal cooling on island-scale weather by changing the terrain height and model parameters. In the future, the model will also be used to study heavy rainfall events over Oahu.

2.2 Model descriptions

MM5, a limited-area, nonhydrostatic, terrain-following sigma-coordinate model (Dudhia, 1993), is used in this research. Four nested domains are employed in the model with a two-way nesting approach. The four nesting domains have horizontal resolutions of 40.5 km, 13.5 km, 4.5 km, and 1.5 km, and horizontal dimensions of 82 x 82, 70 x 70, 79 x 88, 52 x 64, respectively (Fig. 1). The finest nested domain with a 1.5-km resolution covers the entire island of Oahu. There are 28 vertical levels from the surface to the 100-hPa level. The details of these levels are shown in Table 1.

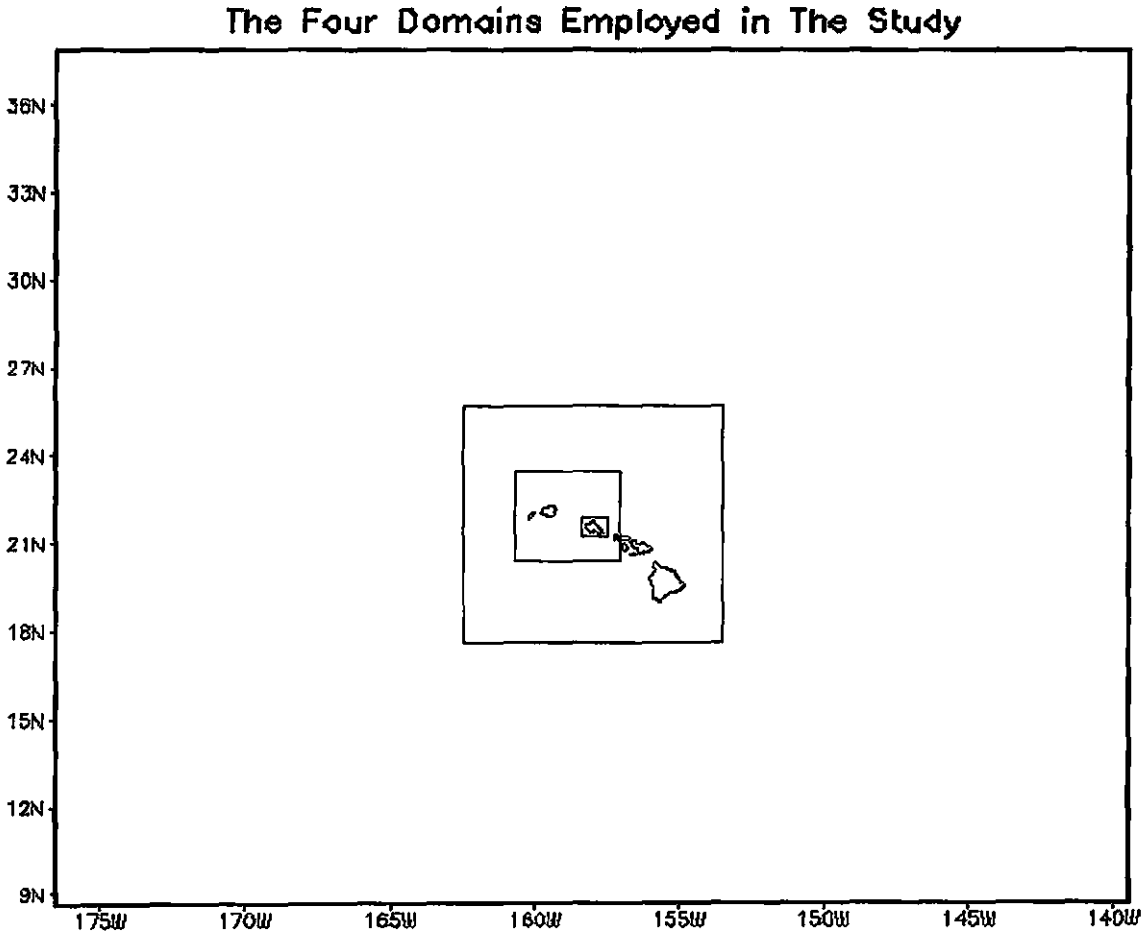

Figure 1 Four nested domains used in this study.

Table 1 Levels used in the mm5 model.

Level in the model	Sigma level
1	1
2	0.998
3	0.994
4	0.990
5	0.985
6	0.980
7	0.970
8	0.945
9	0.910
10	0.865
11	0.820
12	0.790
13	0.760
14	0.720
15	0.680
16	0.630
17	0.580
18	0.520
19	0.475
20	0.425
21	0.375
22	0.325
23	0.275
24	0.225
25	0.175
26	0.125
27	0.075
28	0.025

The physic options in the simulation are the same as those used in Yang et al. (2005) for the island of Hawaii including Grell cumulus parameterization scheme (Grell et al., 1994); MRF planetary boundary layer scheme (Hong and Pan, 1996); explicit warm rain microphysics (Hsie et al., 1984); Dudhia radiation scheme (1989). The cumulus parameterization scheme is not used for the 1.5-km Oahu domain.

An advanced land surface model (F. Chen and Dudhia, 2001) was employed using the vegetation cover and soil properties compiled by Zhang et al. (2005). Soil moisture and soil temperature input for LSM are spun up for two months prior to simulation period (Yang et al. 2005). To spin up soil moisture and soil temperatures, the model is run for 36 hours for every single day. Then, the soil moisture and soil temperature forecast at the 24th hour are used to update initial conditions for the model for the next day simulation.

The GFS outputs with the updated soil moisture and soil temperature are used for the daily 36-hour runs. In addition, sea surface temperature (SST) is updated at initial time by analysis SST data. 24-hour model forecast from the 12th to the 36th hour are used as simulated diurnal cycle for each day. The simulations are performed for two-month period, from July 1st to August 31st, during the summer 2005.

2.3 Data method

2.3.1 Observation data, interpolation method and error statistics

There are 13 hourly surface weather stations and 69 rain gage stations over Oahu. Data from these stations are used to validate the model simulations.

The simulated wind speed, wind direction, air temperature, and dew point temperature at 13 hourly stations are used to compile error statistics. A simple weigh-distance average interpolation formulation was used to interpolate the model data to station locations. Te formulated value of any meteorological fields at a station is computed from that of the four nearest model grid points:

$$F_s = \frac{1}{3D}\sum_{i=1}^{4}(D - d_i)f_i \qquad (1)$$

where

F_s is interpolation value at a station;

f_i, i =1,...,4 are the grid point values at the four nearest grid points;

d_i, i =1,...,4 are distances from the station to the grid points;

$$D = \sum_{i=1}^{4} d_i$$

For the surface air temperature, the interpolated value is adjusted to account for the difference between the model terrain height and real station terrain height using

$$F_s = F_1 + \alpha(Z_m - Z_s) \qquad (2)$$

where

F_1 is the temperature value computed from equation (1) ;

α is the lapse rate ~ 6.75 K km^{-1}; and

Z_m, Z_s are model terrain height and actual terrain height, respectively

In addition, for temperature interpolation, if one of the four nearest grid points is located over the ocean, then that grid point value is not used.

The error statistics including mean bias (BIAS), mean absolute error (MAE), root mean square of errors (RMSE) at stations are computed according to

$$\text{BIAS} = \frac{1}{N}\sum_{i=1}^{N}(F_i^m - F_i^s) \qquad (3)$$

$$\text{MAE} = \frac{1}{N}\sum_{i=1}^{N}\left|F_i^m - F_i^s\right| \qquad (4)$$

$$\text{RMSE} = \sqrt{\frac{1}{N}\sum_{i=1}^{N}(F_i^m - F_i^s)^2} \qquad (5)$$

Where, F_i^m, F_i^s are the i-th values in time series of simulated and observed values of a variable at a station, respectively; N is the number of data samples; and $|\ |$ denotes the absolute operation.

2.3.2 Strong and weak trade-wind categories

The wind data at the upstream point (21N, 152W) of Oahu from the National Center for Environment Prediction/National Center for Atmospheric Research (NCEP/NCAR) reanalysis data[1] are used to determine the strong and weak trade-wind categories in this study. The histograms for wind speed and wind direction during the period at the point at 12 UTC (Figs. 3a, and 3b) show that the prevailing wind speed is from 7 m s^{-1} to 10 m s^{-1} with wind direction from 70 to 90 degrees. The time series of wind speed and wind direction (Figs. 2a, 2b) for the two months show that the wind speed is relatively stronger from mid July to mid August and relatively weaker at the end of August. The wind direction is almost constant excepting at the beginning of July, mid July and the end of August. The criteria is used in this study to define strong and weak trade-wind categories based on wind speed and wind direction at the upstream point (21°N, 158°W) at 12 UTC. The reason only 12 UTC data are used is that there are no chaotic differences in wind speed and wind direction between 12 UTC and 00 UTC (Figs. 2a and 2b).

[1] NCEP/NCAR Reanalysis data is provided by the National Oceanic and Atmospheric Administration (NOAA) Cooperative Institute for Research in Environmental Sciences (CIRES) Climate Diagnostics Center (CDC)

To define strong and weak trade categories, the days with wind directions between 60 to 90 degrees are first selected from the two-month period to create a new data set. From the new data set, ten strong trades are defined as ten days of the strongest wind speed (>9.5 m s^{-1}). And ten weak trades are defined as ten days of the weakest wind speed (< 7 m s^{-1}) from the new data set.

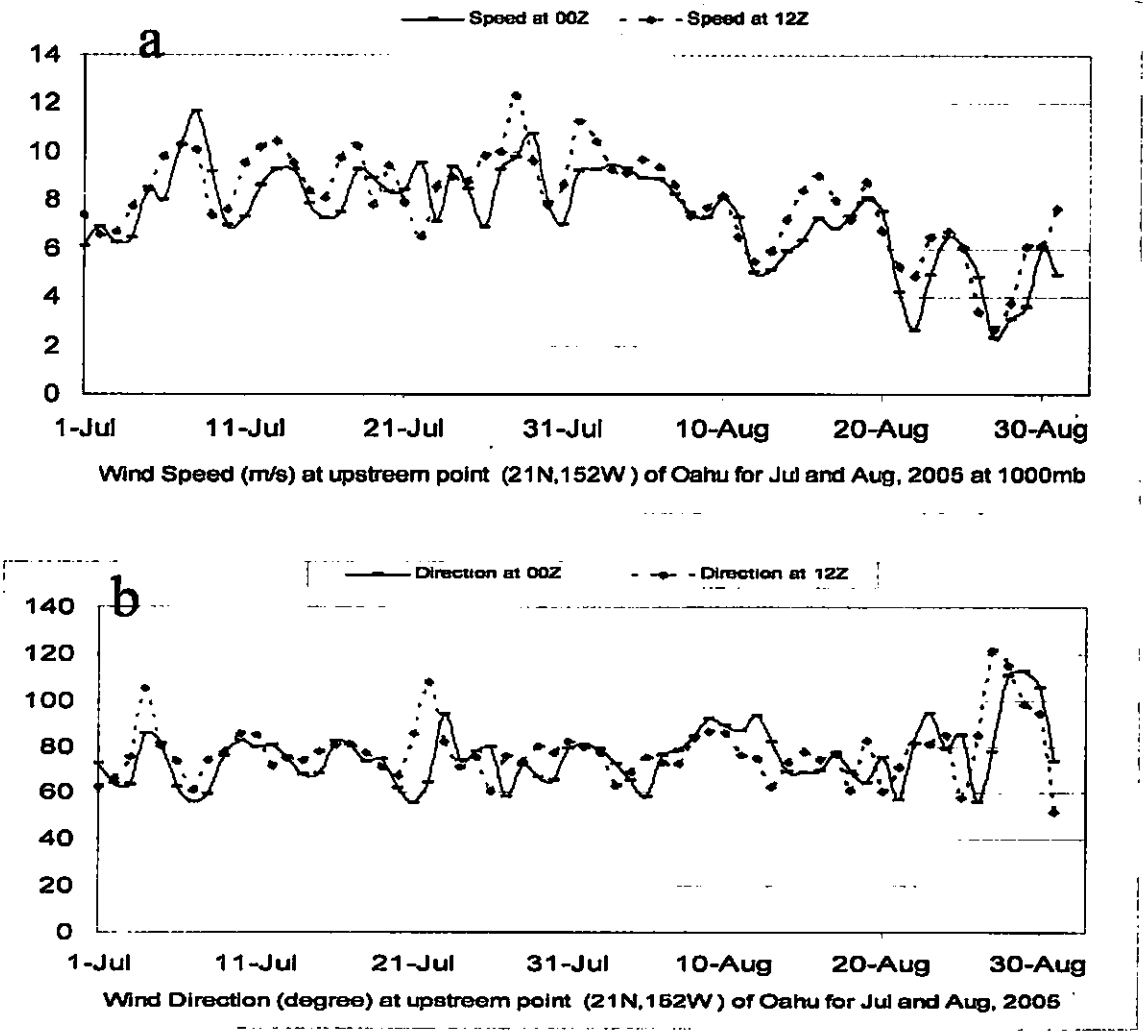

Figure 2 Time series of wind speed (a) and wind direction (b) at a upstream point (21N, 152W) for July-August 2005.

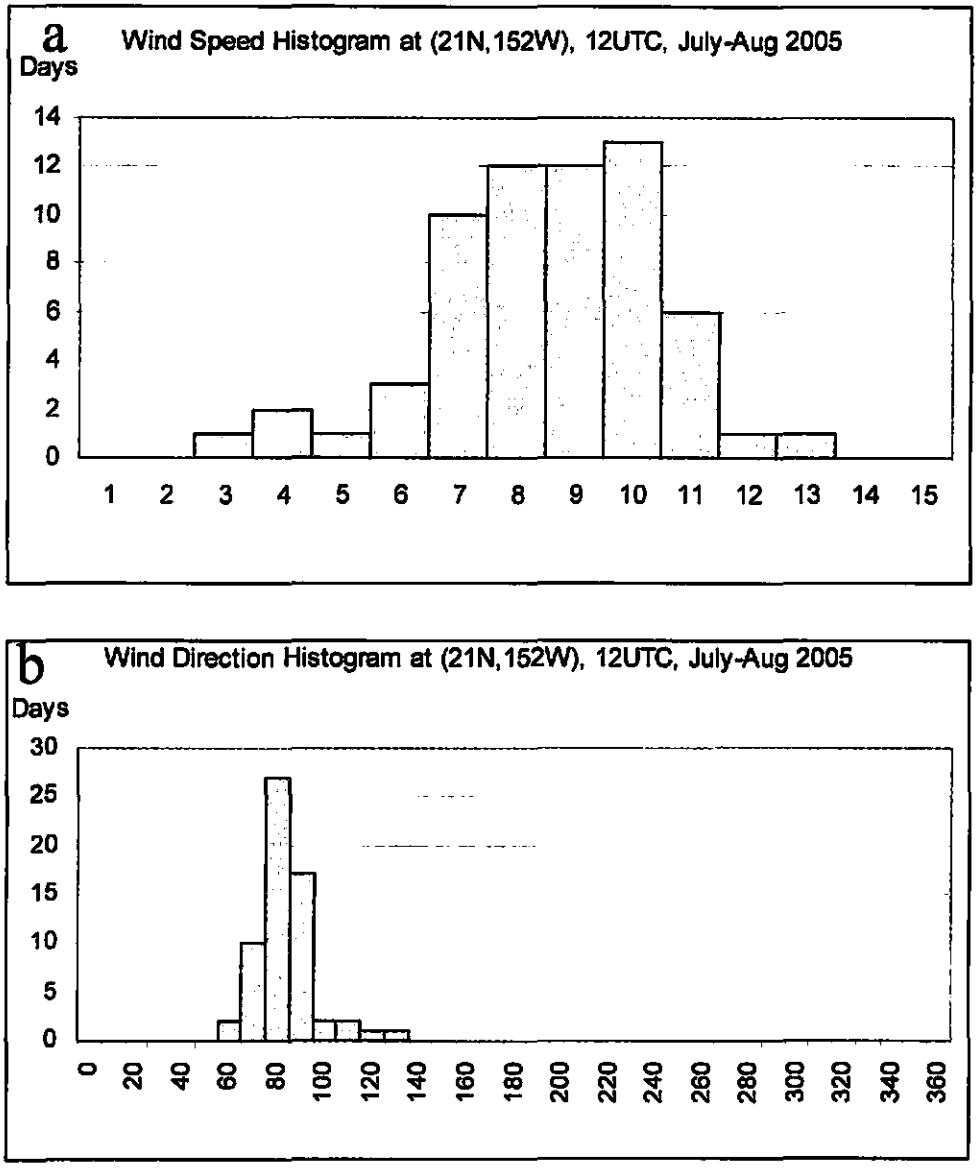

Figure 3 Histogram of wind speed (a) and wind direction (b) at a upstream point (21N, 152W) at 12UTC for July-August 2005.

Chapter III

Model simulations of air flow and weather during summer over the island of Oahu

3.1 Simulation of surface wind

3.1.1 *Surface mean wind simulations*

MM5/LSM model is run for a period of two summer months, July and August, 2005. The simulated results are used to diagnose the island-induced airflow and compare with observations.

Observations at 13 hourly weather stations over Oahu were used. The observations including wind speed, wind direction, air temperature, dew point temperature, were provided by Remote Automated Weather Station (RAWS), Marine Weather Transmitter (MWT), and Automated Surface Observing System (ASOS) (Table 2). Rainfall data used in this study were provided by National Weather Service (NWS) Hydronet.

Simulated mean winds and observed mean winds are shown in Figures 4, and 5. The simulated mean winds agree well with observations. Because of the effect of mountains, simulated winds show much stronger wind speed (6-8 m s^{-1}) over the opened ocean and on the windward side of the Ko'olau Mountains than that in the island interior and on the leeward side (1-5 m s^{-1}) of both the Ko'olau Mountains and the Waianae Mountains in agreement with observations and Leopold (1948).

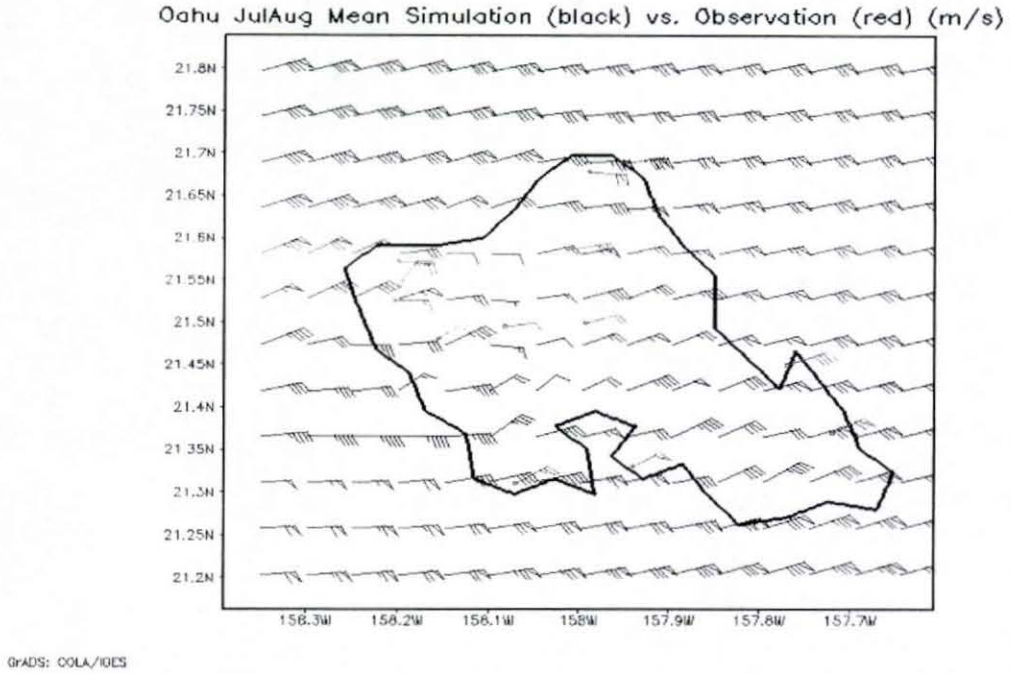

Figure 4 Mean simulated winds (back barb) and mean observed wind at 13 hourly weather stations (red barb) for July and August. One pennant: 5 m s^{-1}, full barb: 1 m s^{-1}.

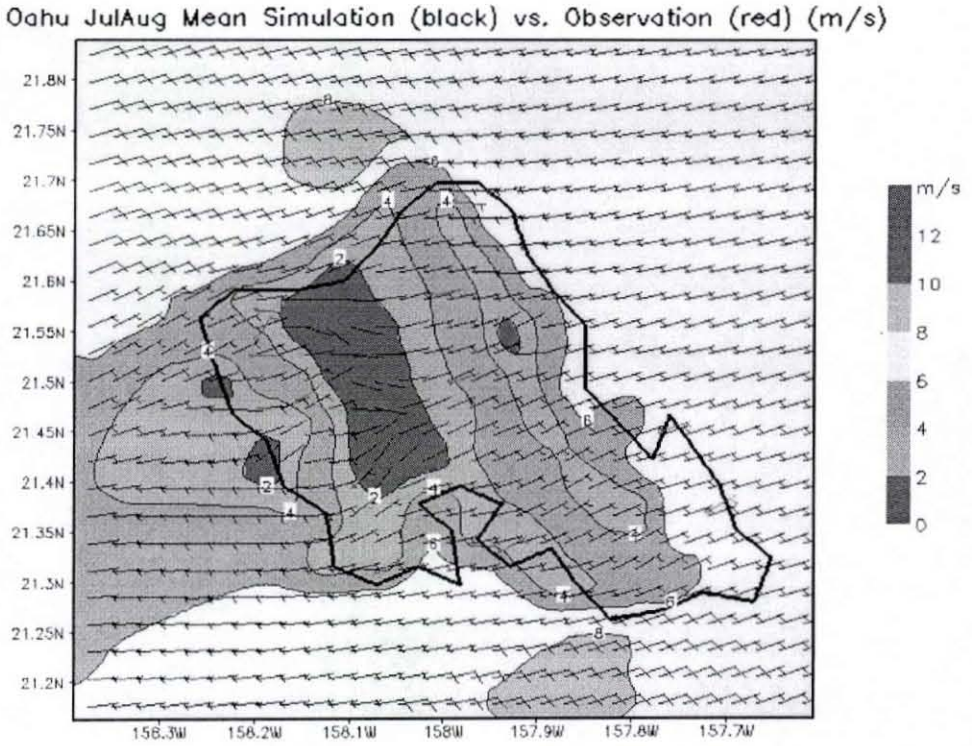

Figure 5 Mean observed winds at 13 hourly weather stations during July-August 2005. One full barb: 10 m/s; half barb: 5 m/s

The lowest mean wind speed is simulated over central Oahu extending from the leeward foothill of the Ko'olau to the ridge top of the Waianae, where wind speed is lower than 2 m s^{-1}. At the Schofield Barracks station, which is located at the central Oahu, simulated mean wind speeds are less than 1 m s^{-1} in agreement with observations. Another region of simulated low wind speed occurs along the leeside Waianae coast because of the effects of land surface forcing and island blocking and surface friction. The direction of the trade-wind flow does not change significantly as it approaches Oahu. There is no westerly onshore flow off the Waianae coast in the surface simulated mean wind (Figs. 4, and 5).

Figure 5 shows that there are two regions with the strongest wind speed at northwestern and southeastern corners of Oahu over the ocean. For these areas, the simulated mean wind speeds reach over 8 m s^{-1} and are stronger than the in-coming trade-wind over the open ocean (6-7 m s^{-1}). This result is consistent with previous observational studies (Leopold, 1948; Ramage and Oshiro 1977).

To evaluate the model performance in simulating surface air flow, the simulated winds are interpolated to 13 stations following Equation (1) every three hours during the period. Error statistics are computed. The locations of the hourly weather stations are shown in Figure 7 and Table 2.

Equations (3) to (5) are applied for wind speeds and wind directions at the 13 stations. These error statistics are shown in Table 3 and Table 4. Wind speed bias in table 4 shows that, of the five stations that have negative bias, only the Kawailoa station is located on the leeside of the Ko'olau Mountains. So, the model tends to simulate weaker wind speeds on the windward side. Of all other 9 stations which have positive bias, only the Kaneohe station is located on windward side. That means the model tends to over estimate wind speed over central Oahu and on the leeward sides of mountains.

Table 2 13-hourly stations at Oahu

Station #	Source	Station name	Station ID	Latitude	Longitude	Elevation (m)
1	ASOS	Kaneohe MCB	PHNG	21.4538	-157.7655	4.8
2	ASOS	Kalaeloa AP	PHJR	21.3083	-158.0686	10.0
3	ASOS	Honolulu AP	PHNL	21.3273	-157.943	4.0
4	RAWS	Dillingham	DLGH1	21.5719	-158.1986	31.1
5	MWT	Bellows	BELH1	21.3700	-157.7200	31.0
6	RAWS	Kii	KFWH1	21.6883	-157.9526	1.5
7	RAWS	Kahuku Training	KTAH1	21.6792	-157.9894	181.6
8	RAWS	Kawailoa TA	KWLH1	21.5872	-158.0131	388.3
9	RAWS	Makua Valley	MAPH1	21.5261	-158.2042	158.0
10	RAWS	Makua Ridge	MKGH1	21.5428	-158.1989	533.0
11	RAWS	Schofield Barracks	SCBH1	21.4950	-158.0819	298.7
12	RAWS	Schofield East	SCEH1	21.4994	-157.9933	318.0
13	RAWS	Waianae Valley	WNVH1	21.4806	-158.1553	291.7

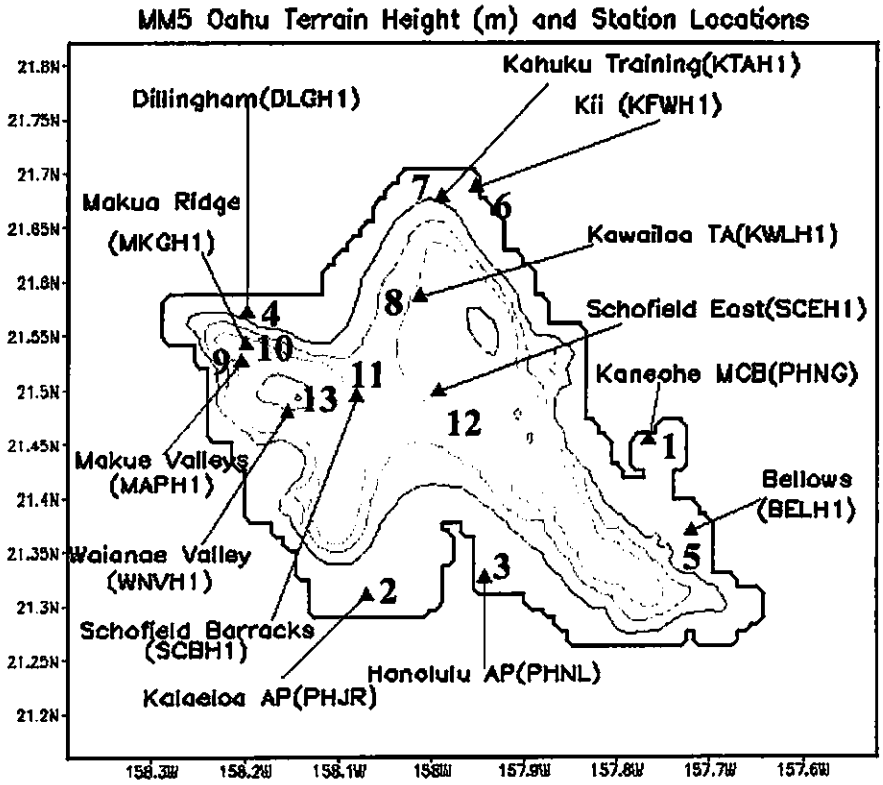

Figure 6 Locations of 13 hourly weather stations.

Table 3 Error statistics for wind speed at 13 hourly weather stations.

Station #	Station name	Station ID	BIAS (m/s)	RMSE (m/s)	MAE (m/s)
1	Kaneohe MCB	PHNG	1.2	2.5	1.6
2	Kalaeloa AP	PHJR	0.4	1.8	1.4
3	Honolulu AP	PHNL	-0.4	2.2	1.7
4	Dillingham	DLGH1	1.9	2.3	2.0
5	Bellows	BELH1	-0.9	1.6	1.3
6	Kii	KFWH1	-0.5	1.5	1.2
7	Kahuku Training	KTAH1	-0.9	1.7	1.4
8	Kawailoa TA	KWLH1	-0.8	2.2	1.8
9	Makua Valley	MAPH1	2.8	3.5	3.0
10	Makua Ridge	MKGH1	1.2	2.5	2.0
11	Schofield Barracks	SCBH1	0.3	1.5	1.3
12	Schofield East	SCEH1	0.9	2.1	1.7
13	Waianae Valley	WNVH1	2.3	3.4	1.8

Table 4 Error statistics for wind direction at 13 hourly weather stations.

Station #	Station name	Station ID	BIAS (degree)	RMSE (degree)	MAE (degree)
1	Kaneohe MCB	PHNG	0	24	13
2	Kalaeloa AP	PHJR	2	43	23
3	Honolulu AP	PHNL	11	62	34
4	Dillingham	DLGH1	-36	69	46
5	Bellows	BELH1	9	32	19
6	Kii	KFWH1	5	22	14
7	Kahuku Training	KTAH1	-15	25	18
8	Kawailoa TA	KWLH1	10	75	41
9	Makua Valley	MAPH1	-58	107	73
10	Makua Ridge	MKGH1	-18	105	70
11	Schofield Barracks	SCBH1	12	110	73
12	Schofield East	SCEH1	15	112	75
13	Waianae Valley	WNVH1	-71	138	105

The wind speed and wind direction errors (MAE) vary from 1.2 m s^{-1} to 3.0 m s^{-1} and from 13 to 105 degrees, respectively. Wind direction errors at windward stations are relatively small. All four windward stations including Bellows, Kaneohe MCB, Kahuku Training and Kii, have direction errors less than 20 degrees. Three stations near the southern coast of Oahu have rather small wind direction errors (Honolulu AP, Kalaeloa AP, and Dillingham). Wind direction errors of these stations vary from 23 to 46 degree. The largest errors in wind directions are at stations within the island interior where wind speeds are sensitive to the diurnal heating cycle. Although the distance between Makua Ridge and Makua Valleys is only about 3 km, there are large differences in wind directions between these stations (Fig. 4) because of the presence of complex terrain. The other factor that may contributes to large model errors in wind speed and wind direction at Makua Valleys is that the model terrain does not depict the step terrain in sufficient details with a 1.5 km grid. Note that the distance from the foothill to the top of Makua Valley Ridge is less than 1 km. On terrain used in the model (Figs. 6 and 11), no valley terrain characteristics but smooth slopes of Waianae Mountains are displayed. As a result, the two stations, Makua Valleys and Makua Ridge, located on the Makua Valley region, are presented in the model with terrain height between 300 m and 400 m (Fig. 4). In contrast, the real altitudes of Makua Valleys and Makua Ridge are 158 m and 533 m, respectively.

3.1.2 *Diurnal cycle of surface winds*

To investigate the simulated diurnal variations of airflow, model simulations during the two months are used to conduct mean diurnal variations of surface airflow with a 3-hour interval. The observed mean diurnal variations of surface winds at 13 hourly weather stations are also computed. The simulated and observed mean diurnal variations of surface winds are shown in Figures 7a to 7e.

Because of daytime heating and nighttime cooling of the island, both the wind speeds and wind directions change considerably during the diurnal cycle. The simulated island airflow throughout the day agrees well with observations at thirteen stations. Both mean simulated and observed wind speeds over Oahu are much stronger at daytime (Figs. 7b, 7c, and 7d) and weaker at night time (Figs. 7a, and 7e) in agreement with Leopold (1948). At night, the surface release OLR and become cool. Because of the cool surface, the air near the surface becomes cooler and heavier than the air aloft. As a result, low level air over the island is stable at night. Because the air is stable, there is no vertical mixing of trade-wind momentum at night (Leopold, 1948). Furthermore, surface friction reduces surface wind speeds. Therefore, surface wind speeds over the island are weak at night. The wind speeds are even weaker for central Oahu. The wind speeds at central Oahu at 05 HST and 23 HST are almost zero because of the meeting between two downslope winds in opposite directions as a result of surface cooling at night. One flows on the east side of the Waianae and the other flow on the west side of Ko'olau. Weak wind speeds at leeside of the Waianae from late morning (Fig. 7 c) to the early afternoon (Fig. 7d) are caused by wake circulations (Yang et al., 2005) developed during this time.

In terms of surface wind directions, wind directions are almost uniform from ENE to NE during the day except off the leeside coast of the Waianae Mountain Range. Where wind directions change from NE at 08 HST (Fig. 7b) to NW or completely W at 11 HST and 14 HST (Figs. 7c, 7d). The change in wind directions during the day is caused by onshore flows as a result of a daytime heating overland. At night (Figs. 7a, 7e), simulated surface mean winds are almost uniform in NE to ENE directions over the open ocean. Over the island, downslope winds are observed and simulated on the western slopes of the Ko'olau and the eastern slope of the Waianae. There is a clear transition from nighttime flow regime to daytime flow regime from 05 HST (Fig. 7a) to 08 HST (Fig. 7b) due to land surface heating after sunrise.

To evaluate the performance of model simulations of diurnal variations of surface wind quantitatively, simulated and observed wind speeds and wind directions at 13 stations at different time during the days are used to compute error statistics (Tables 5a, 5b). There is almost no wind speed bias in model simulation when wind speeds are relatively strong at 11 HST and 14 HST. At other periods, the simulated winds are stronger than observed (Table 5a). Wind speed errors during the diurnal cycle are less than or equal to 2 m s^{-1}. Both speed and direction errors (RMSE or MAE) are smaller when winds are stronger at 11 HST and 14 HST (Tables 5a, and 5b). Error statistics for wind directions show large errors especially for stations from the island interior (station number 8 to 12 in Table 4).

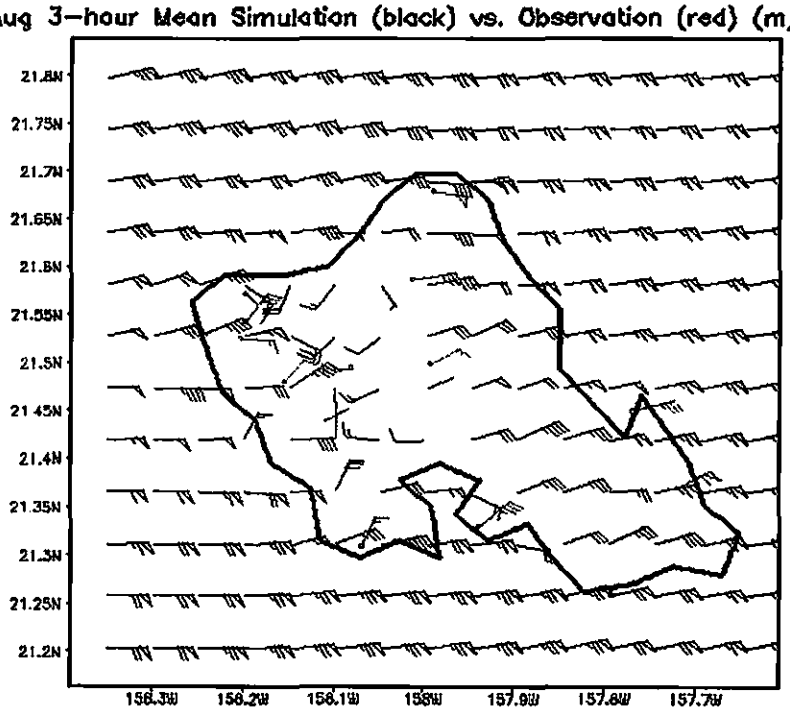

Figure7 a. Mean simulated winds (back barb) and mean observed wind at 13 hourly weather stations (red barb) at 05 HST for July and August 2005. One pennant: 5 m s^{-1}, one full barb: 1 m s^{-1}.

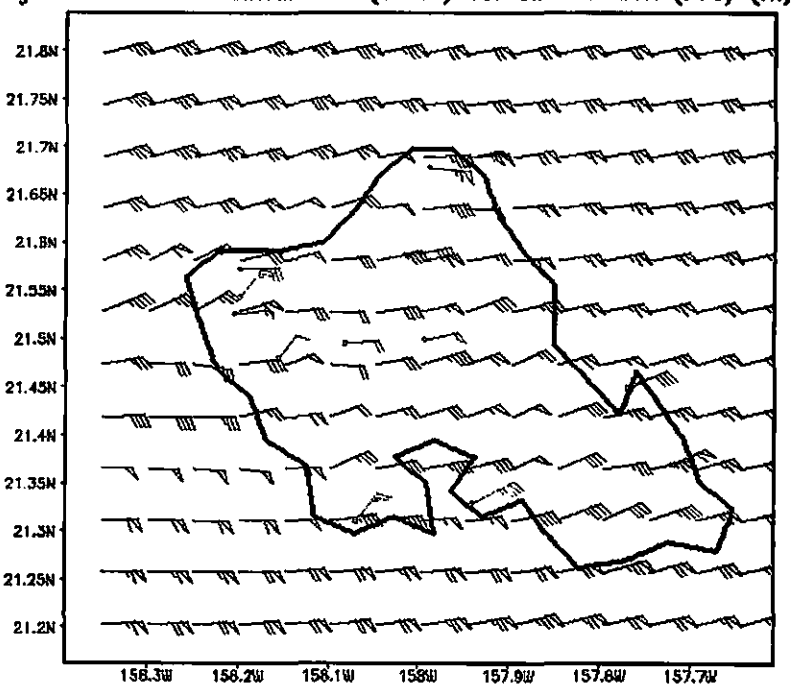

Figure 7b Same as Fig. 7a but for 08 HST.

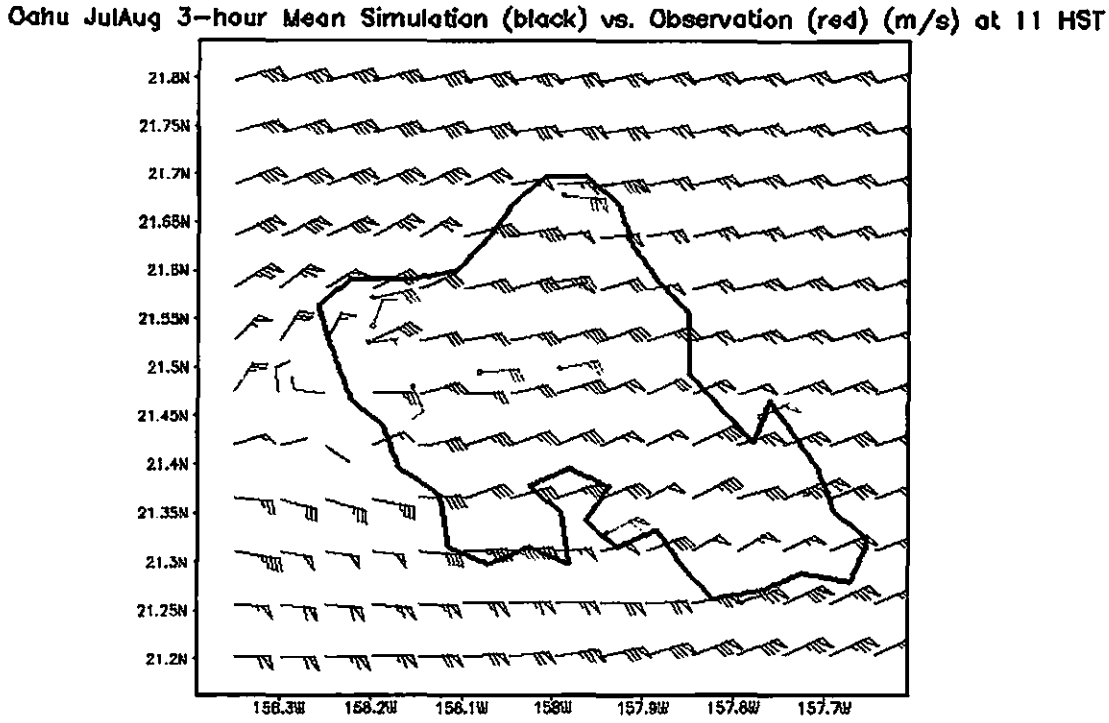

Figure 7c. Same as Fig. 7.a. but for 11 HST.

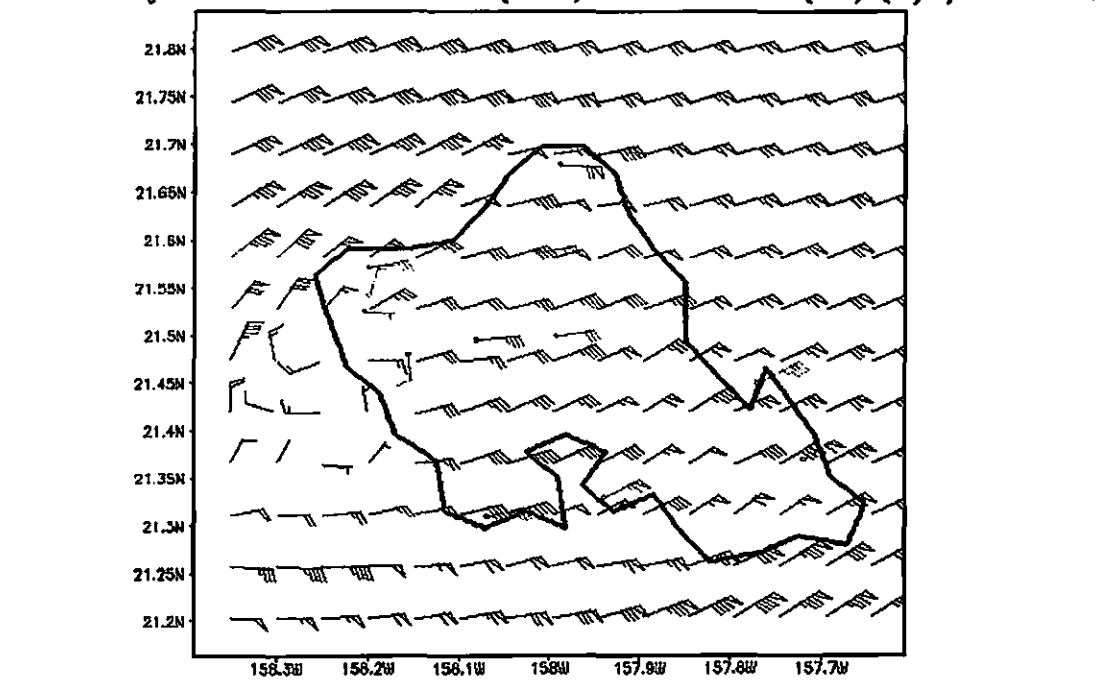

Figure 7d Same as Fig. 7a but for 14 HST.

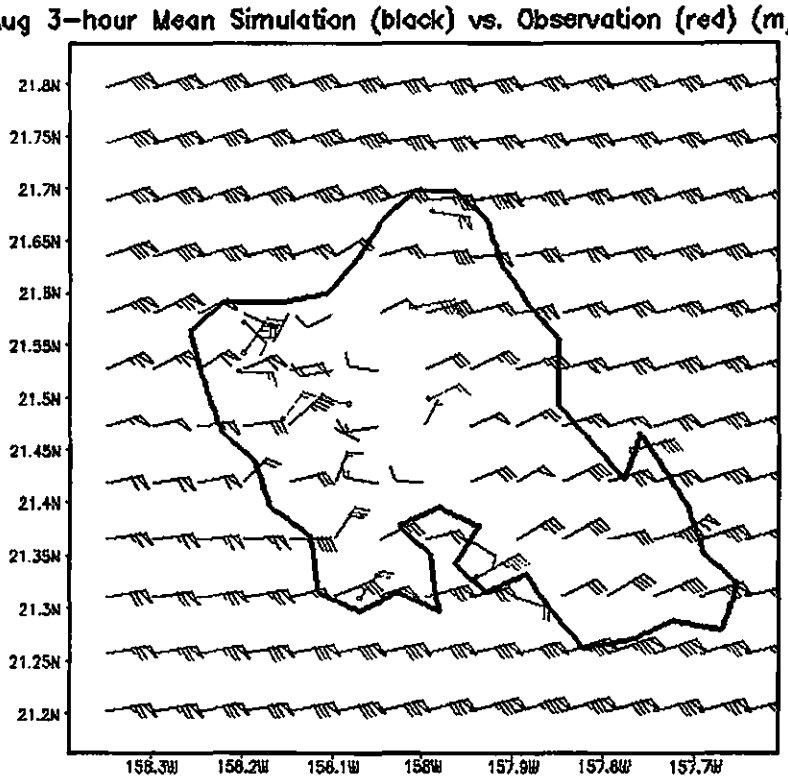

Figure 7e Same as Fig. 7a but for 23 HST.

Table 5a Diurnal cycle of error statistics for wind speed at 13 hourly Oahu stations.

	02HST	05HST	08HST	11HST	14HST	17HST	20HST	23HST
BIAS	0.8	0.7	1.1	0.0	-0.2	0.7	0.9	0.8
RMSE	2.1	2.0	2.6	2.1	2.1	2.2	2.1	2.1
MAE	1.8	1.7	2.0	1.7	1.8	1.8	1.8	1.8

Table 5.b Diurnal cycle of error statistics for wind direction at 13 hourly Oahu stations.

	02HST	05HST	08HST	11HST	14HST	17HST	20HST	23HST
BIAS	-2.7	1.6	-16.1	-15.0	-22.3	-24.2	-0.8	-1.8
MSE	75.3	81.6	70.8	56.4	64.2	63.4	68.5	66.8
MAE	54.5	56.8	45.7	38.4	42.2	40.0	47.1	48.4

3.1.3 Effects of trade-wind conditions on Island-scale surface air flow

To investigate the effects of trade-wind conditions on island-scale surface air flow, ten days of strong trades (Table 6a) and ten days of weak trades (Table 6b) during the two summer months of 2005 are selected.

Trade-wind conditions affect the mean wind speeds, wind directions over Oahu. For strong trades, the mean wind directions are almost uniform ENE. For weak trades, the mean wind directions vary over central Oahu. Overall, surface wind speeds over the island are stronger under strong trades than under weak trades. However, effects of trade-wind conditions are different at different locations.

On the western slope of the Ko'olau Mountains, under weak trades, the downslope flow is more pronounced than under strong trades (Figs. 8a and 8b). The mean wind speed at western slope of the Ko'olau Mountains can reach the same magnitudes of open ocean wind speed (~4.5 m s^{-1}) under weak trades (Fig. 8b). Under strong trades, mean wind speeds there (Fig. 8a) are much weaker (6 m s^{-1}) than that over open ocean (> 8 m s^{-1}).

At the leeside and adjacent to the coast of Waianae, under weak trades, wind speeds (Fig. 8b) there (1.5 m s^{-1}) are only about 35% of that of the open ocean (4.5 m s^{-1}). In contrast, in the case of strong trades (Fig. 8.a.) leeside Waianae wind speed value (~5 m s^{-1}) can reach about 60% of that of the open ocean (8.5 m s^{-1}).

The trade-wind conditions also have significant effects on diurnal cycle of island-scale airflow. The simulated and observed mean winds of 10 strong trade days and 10 weak trade days at 05 HST and 14 HST are given in Figures 9 and 10. At night, the cool air moving down from the Ko'olau Mountains (at 21.55° N, 157.95° W grid point for example) is more pronounced under weak trade-wind conditions. Under weak trades, the maximum wind speed on the western slope of the Ko'olau Mountains (Fig. 9b) can

reach 4.5 m s^{-1}. Meanwhile the maximum wind speed (5.5 m s^{-1}) on western slopes of the Ko'olau Mountains is much weaker than over the open ocean under strong trades (Fig. 9a). Especially, at night, wind direction can be completely opposite to coming trade-wind directions on eastern slope near the top the Ko'olau Mountain.

More profound effects can be seen during the day time. In the afternoon, the westerly onshore flow along the Waianae coast and adjacent waters due to land surface heating is more pronounced under weak trades (Fig. 10b). The simulated flows show a complete reversal on wind directions at leeside of the Waianae. The wind observation at Waianae Valley station also shows an upslope mean wind at this time. Complete reversal of wind direction occurs on the Waianae coast in the afternoon were mentioned by Leopold (1948) in his observations. The simulated winds under different trade-wind conditions show that the complete reversal of wind direction usually occurs under weak trade-wind and, maybe, in normal trade-wind conditions. Under strong trades, no mean westerly onshore flow or upslope winds on leeside of the Waianae are simulated or observed.

Table 6.a Ten strong trade wind days during the period of Jul to Aug, 2005

Ten strong trade wind days			
No	Date	Speed at 12Z	Direction at 12Z
1	6-Jul	9.81	73
2	8-Jul	10.10	74
3	12-Jul	10.21	72
4	13-Jul	10.45	75
5	17-Jul	9.72	81
6	18-Jul	10.24	74
7	27-Jul	9.99	76
8	01-Aug	11.28	80
9	02-Aug	10.46	77
10	28-Aug	12.31	74

Table 6.b Ten weak trade wind days during the period of Jul to Aug, 2005

Ten weak trade wind days			
No	Date	Speed at 12Z	Direction at 12Z
1	11-Aug	6.48	76
2	12-Aug	5.48	75
3	13-Aug	5.86	63
4	20-Aug	6.76	61
5	21-Aug	5.28	71
6	22-Aug	4.85	82
7	23-Aug	6.48	81
8	24-Aug	6.73	85
9	24-Aug	6.73	84
10	26-Aug	3.41	85

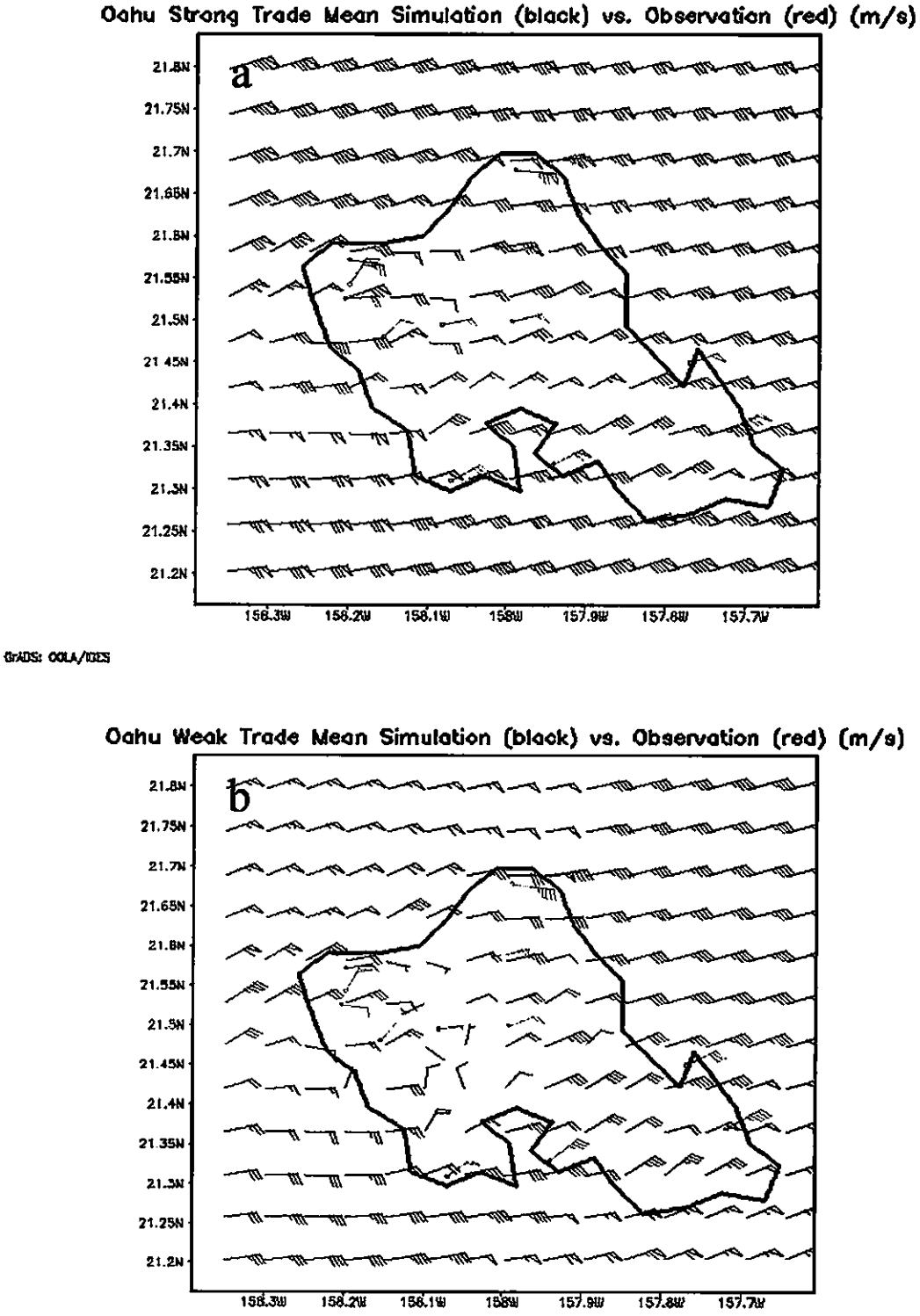

Figure 8 Averaged simulated winds (back barb) and averaged observed winds (red barb) at 13 hourly weather stations of (a) 10 strong trade days, (b) 10 weak trade days at 05 HST. One pennant: 5 m s^{-1}, full barb: 1 m s^{-1}.

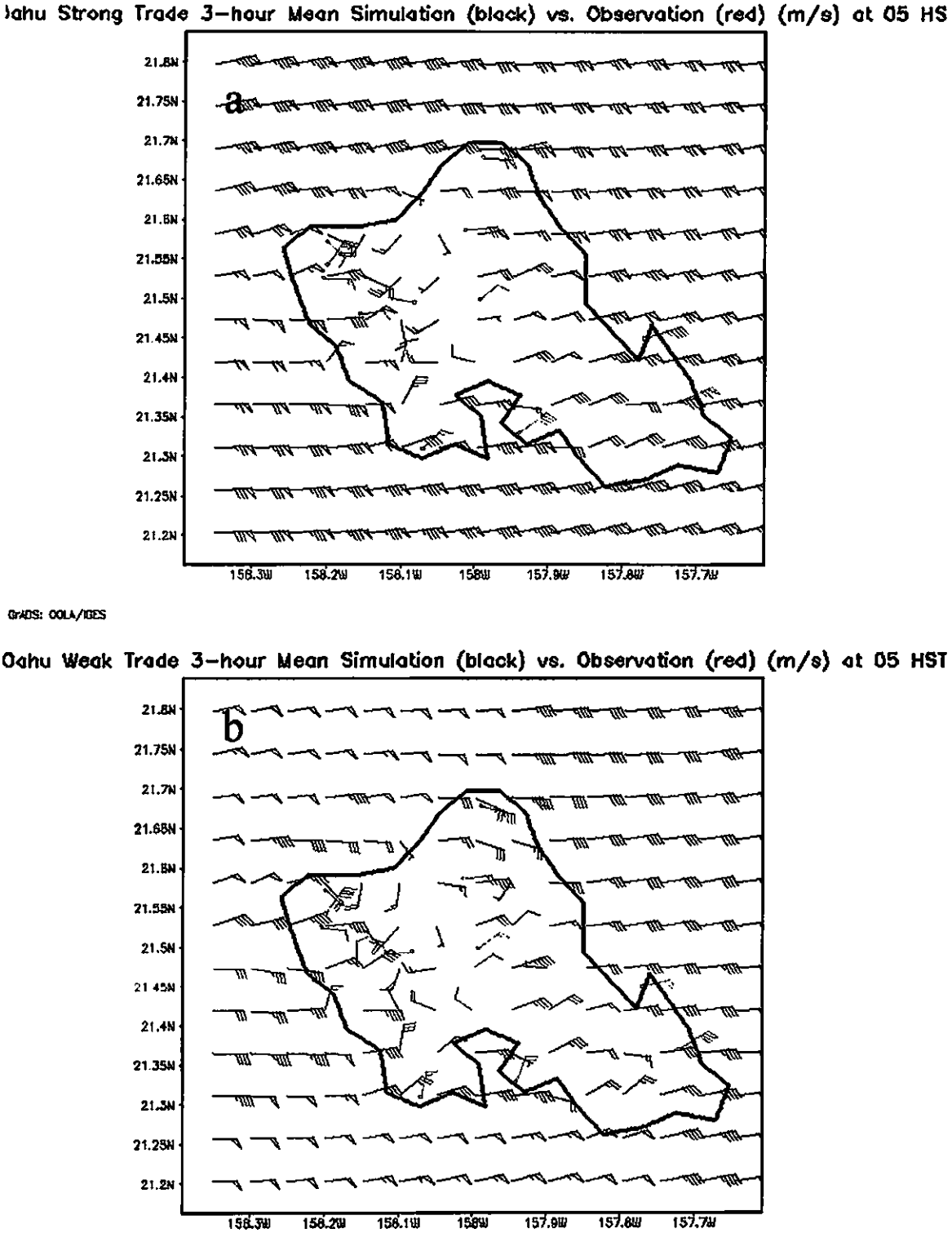

Figure 9 Same as Fig. 8 but (a) for strong trades at 05 HST, (b) for weak trades at 05 HST.

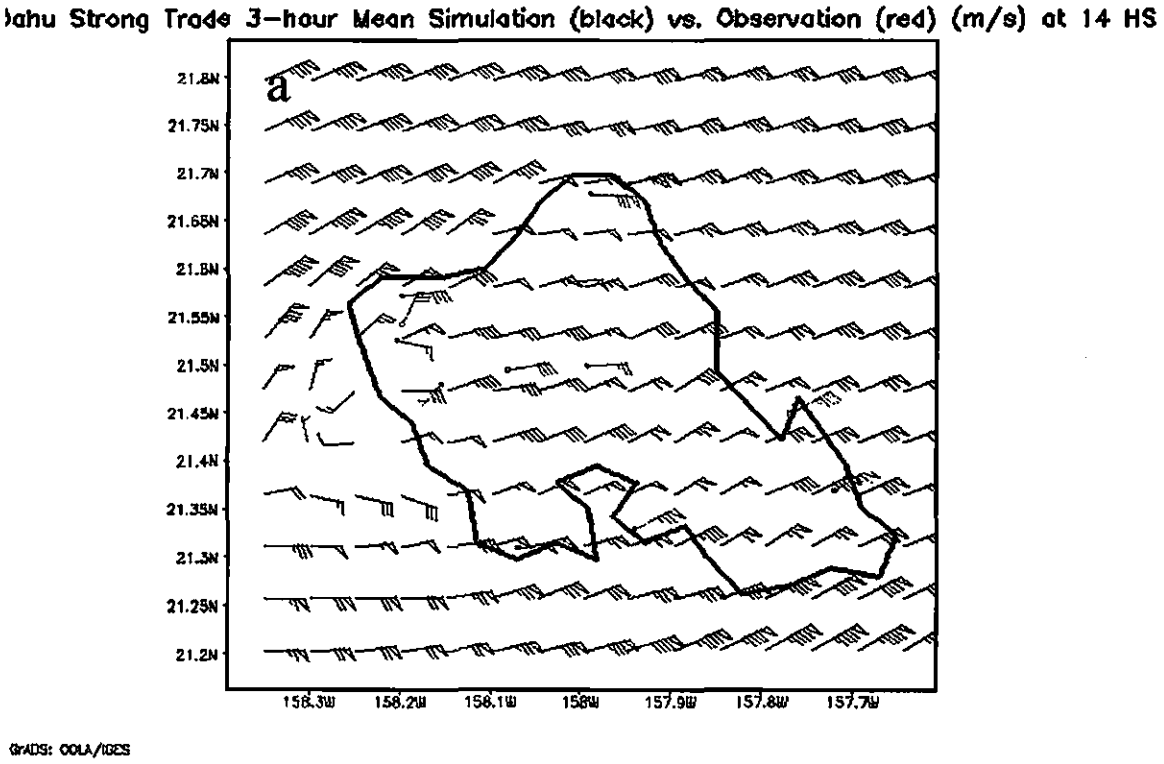

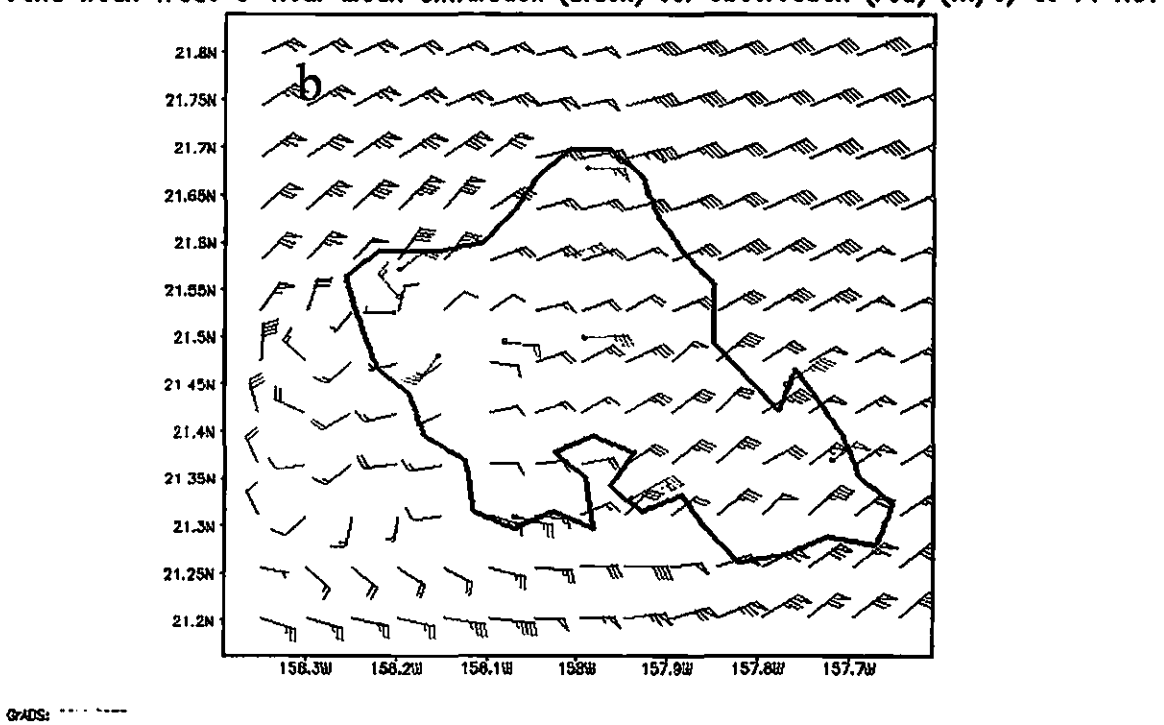

Figure 10 Same as Fig. 8 but (a) for strong trades at 14 HST, (b) for weak trades at 14 HST.

3.1.4 Diurnal cycle of winds aloft

Winds aloft are also significantly affected by the diurnal heating cycle. Vertical cross sections of mean zonal wind component along 21.45°N (Fig. 11) at 02 HST and 14 HST are plotted. Location 21.45° N is selected because the vertical cross sections at this latitude can capture the weak wind regions at leeside of the Waianae during the day, the weak wind areas at central Oahu as well as strong downslope winds on the lee-side slopes of both mountain ranges at night.

At night, these are strong easterly down-slope winds (>11 m s^{-1}) on the leeside slopes of both the Ko'olau and the Waianae mountains (Fig. 12a). The winds there are about 40% stronger than over the open ocean. These are the locations that would experience high winds under strong trade-wind conditions. The main reason for strong wind speed aloft over the leeside of the mountains probably is the stable stratification at night (Leopold, 1948). When the air parcels approach the mountains, they are forced to move upslope because of orographic lifting. As moving upslope to the higher level, the density of the air parcels is larger than that of the environment (stable stratification at night). As a result, the gravity force makes the air parcels move downward while continue to move horizontally with the mean flow. In addition, the aloft high wind speed regions are prevented from low wind speed regions near the surface because the low level air is stable at night due to cooling of the surface. The down slope wind at night also enhances the wind speed of the air parcel over the leeward side of the mountains.

In the afternoon, weak onshore flow develops off the Waianae coast near the ocean surface because of land surface heating. There is no strong downslope flow on the leeside slopes of the Waianae mountain ridge with weaker wind speed (~8 m s^{-1}) aloft (Fig. 12b) than at night (> 11 m s^{-1}) (Fig. 12a). The wind aloft on the leeside of the both mountains are decreased because the high momentum aloft are transferred to

lower levels because of the increase in instability during the day due to land surface heating (Leopold, 1948). The vertical mixing is the most significant in the afternoon as a result of development of thermal turbulences in the lowest levels when the surface heating is at its maximum. As a result, mean wind speeds aloft are weaker and mean surface and low level wind speeds are stronger during the day than at night.

3.1.5 Effects of trade-wind conditions on winds aloft

The winds aloft are also significantly affected by trade-wind conditions. At night, wind speeds aloft over leeside slopes of both the Waianae and Ko'olau mountains under strong trades (Fig. 12c) are much stronger than that under weak trades (Fig. 12e). The maximum wind speed regions over the both mountains under strong trades at 02 HST reach values of greater than 13 m s^{-1}.In contrast, the values under weak trades are only slightly lager than 8 m s^{-1}.

More significant effects of trade winds are simulated under strong trades than under weak trades during the day. Under strong trades, there are still two maximum regions of mean wind speeds on the leeside of both the Waianae and the Ko'olau Mountains. The maximum at Waianae is weaker than that at Ko'olau (Fig. 12d). No maximum wind speed regions over the leeward side slopes of the Waianae Mountains are simulated under weak trade case (Fig. 12e) and mean summer winds (Fig. 12b) during the day. At 14 HST, the westerly onshore flow along the Waianae coast and adjacent waters disappears under strong trades. For strong trades, the westerly onshore flow is not simulated along the leeside coast of the Waianae. Strong trade-wind flow blows through both the Ko'olau and Waianae Mountains in the afternoon hours. In contrast, the westerly onshore flow is rather pronounced under weak trades and extends vertically to a height of about 500 m offshore off the Waianae coast.

The effects of trade-wind conditions on leeside flow at Oahu seem to opposite to that at a bigger island such as the Big Island which has higher terrain height and horizontal scale. The return flow in the Big Island is stronger under strong trades (Yang and Chen, 2003). In contrast, the westerly onshore flow at leeward side coast of Oahu is weaker under strong trades. The lower terrain height and smaller in size probably explain for this difference. Because of lower terrain height and smaller in size, under strong trades, the trade flow can flow over the mountains preventing the development of the onshore flow along the lee-side coast in the afternoon hours. For the Big Island, with the mountain heights well above the trade-wind inversion, the trade-wind flow in lower level does not blow over the mountains but is forced to move around the island. For the Big Island, the island blocking and the wake circulations are more significant under strong trades (Yang and Chen, 2003).

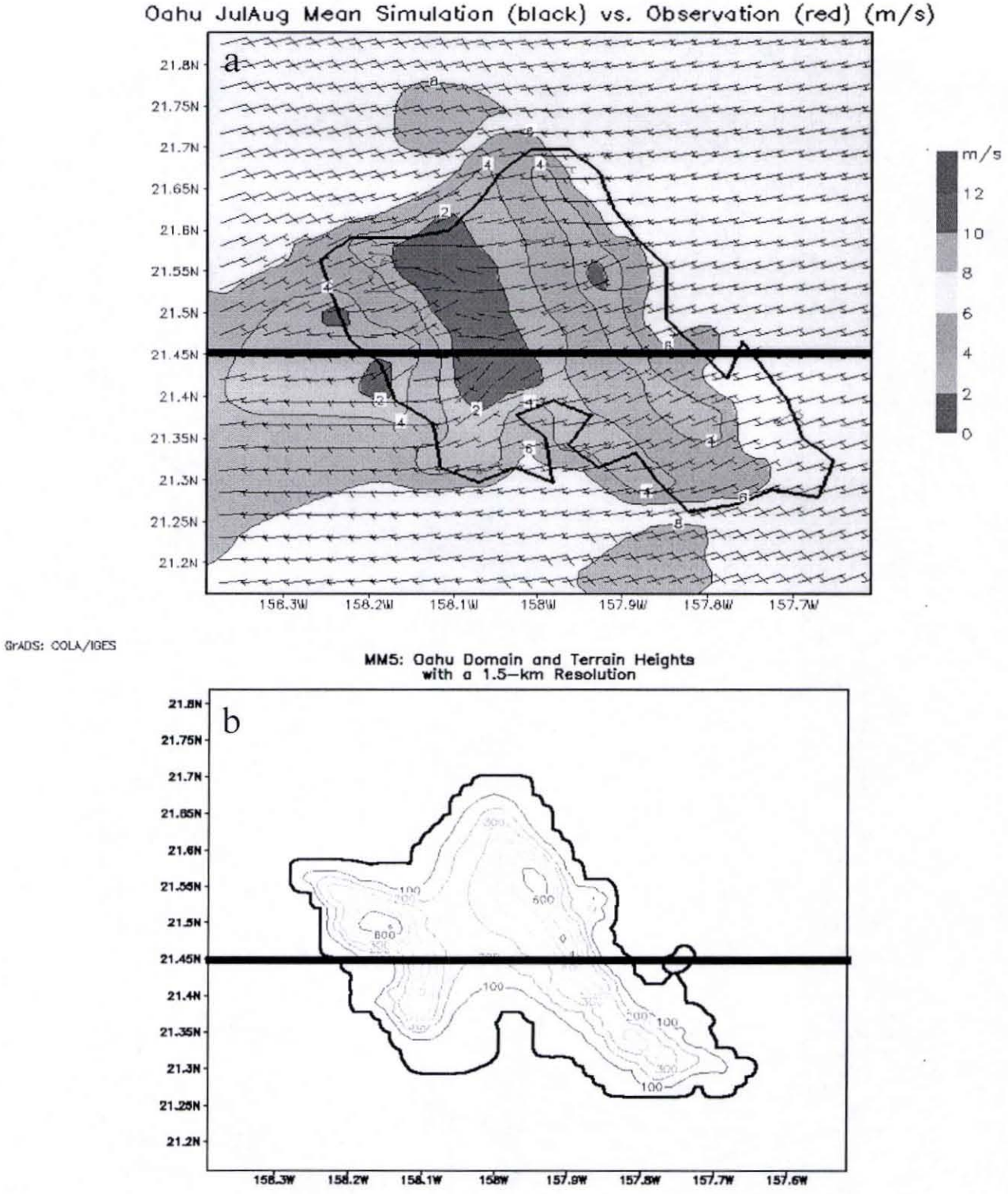

Figure 11 location of vertical cross section: 21.45° N (a) with the mean simulated wind map, and (b) with Oahu terrain of the mm5 model.

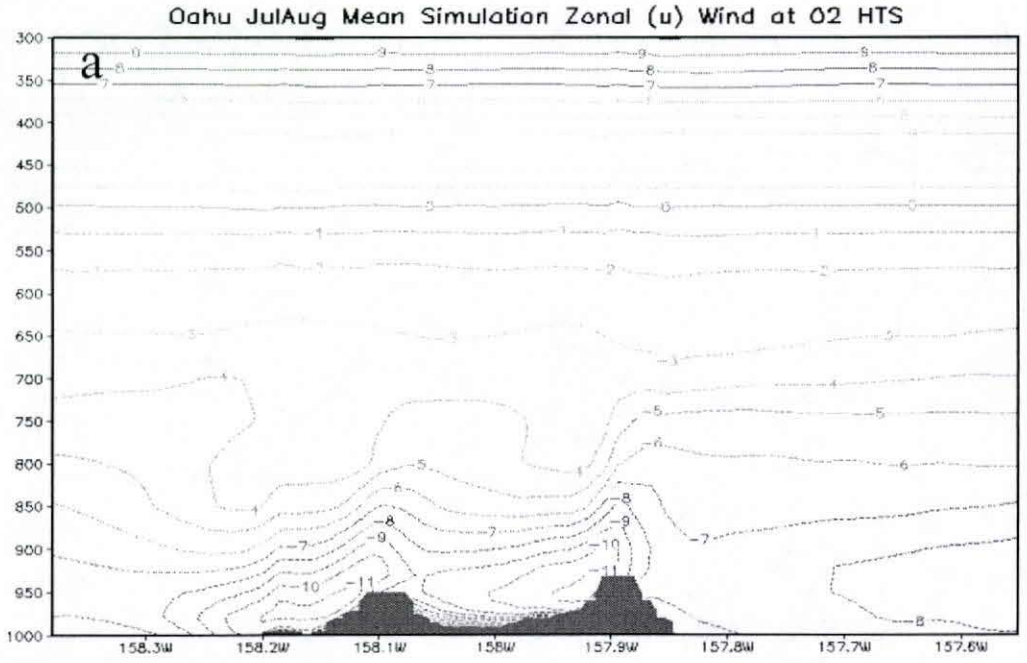

Figure 12a Vertical cross section at 21.45° N of zonal wind component at 02 HST for July-August 2005.

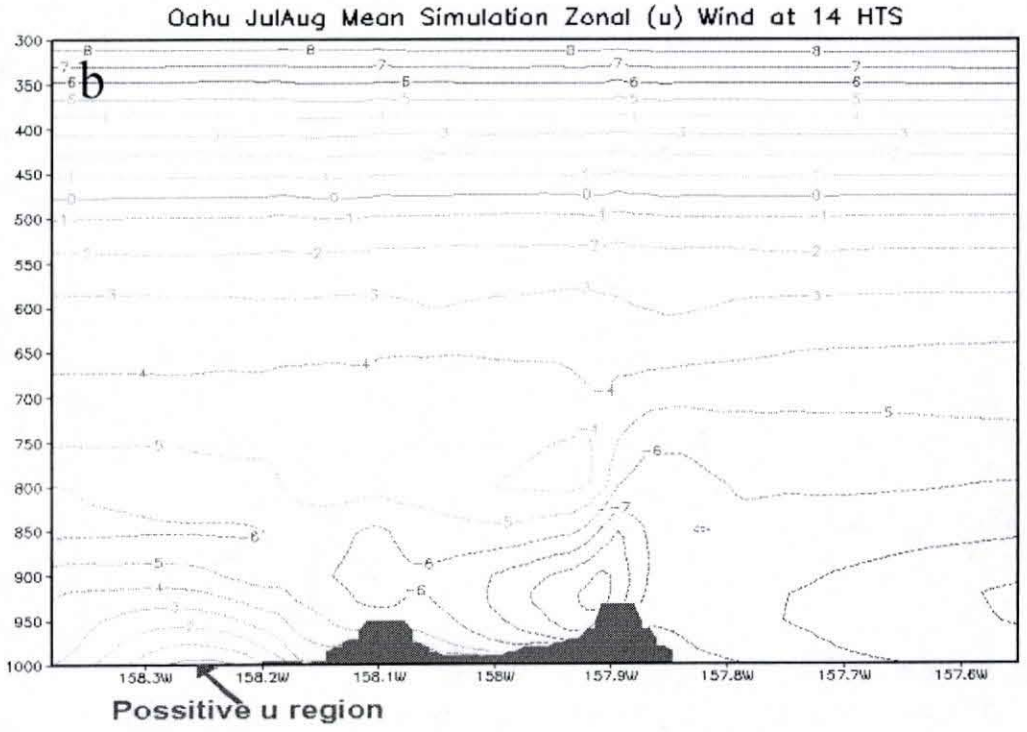

Figure 12b Same as Figure 12a but for 14 HST.

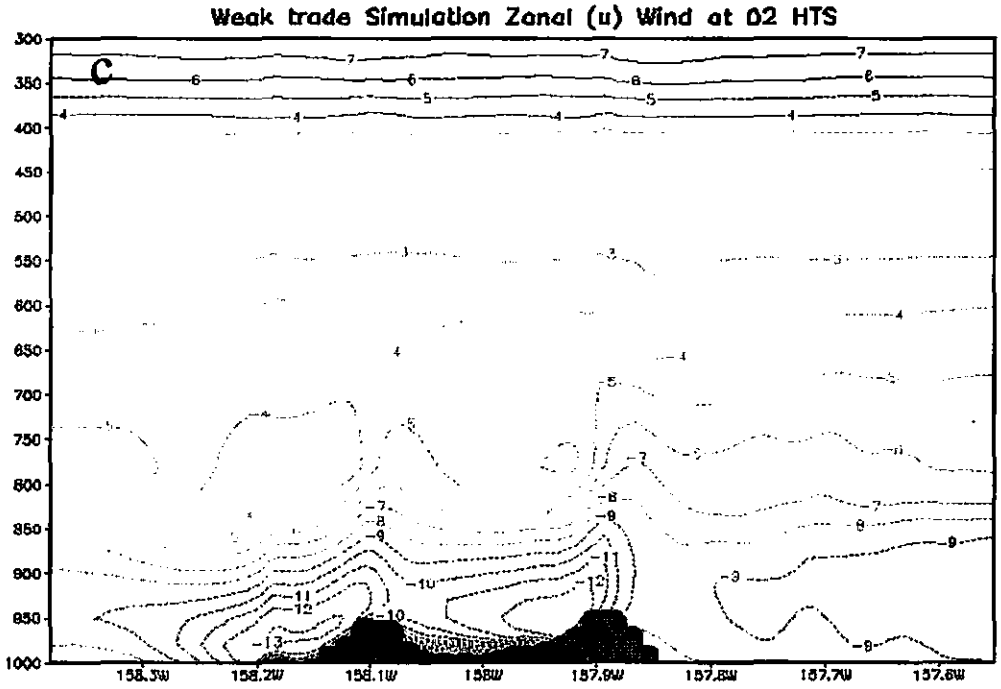

Figure 12c Vertical cross sections at 21.45° N of simulated mean zonal wind component under strong trades at 02 HST.

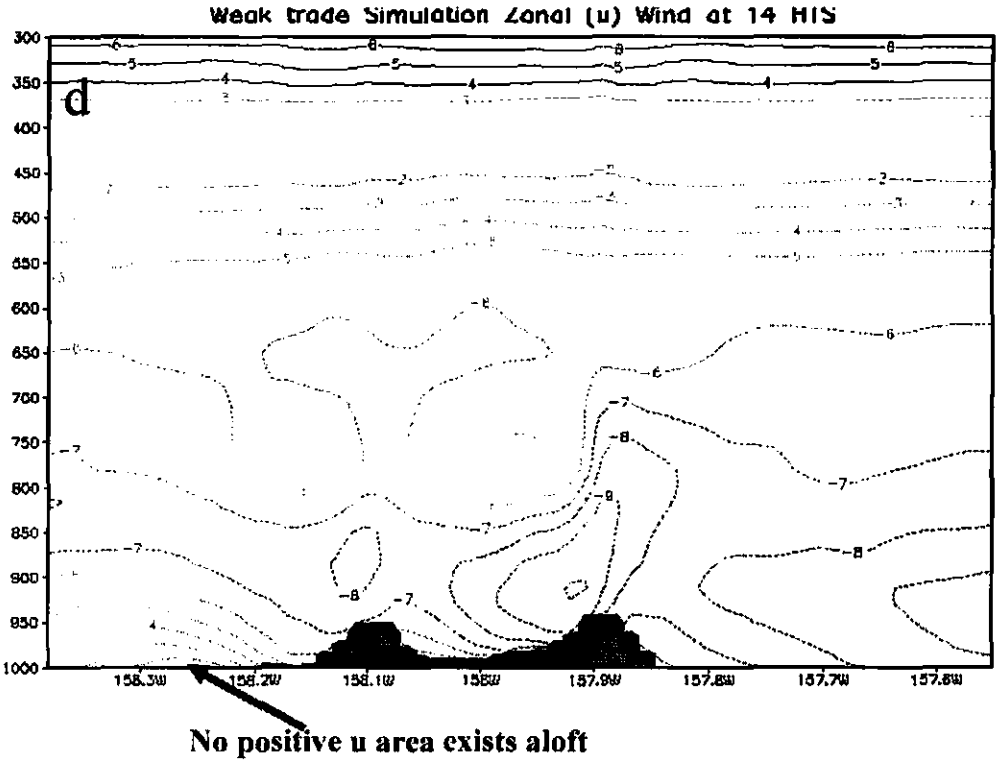

Figure 12d Same as Figure 12c but for 14 HST.

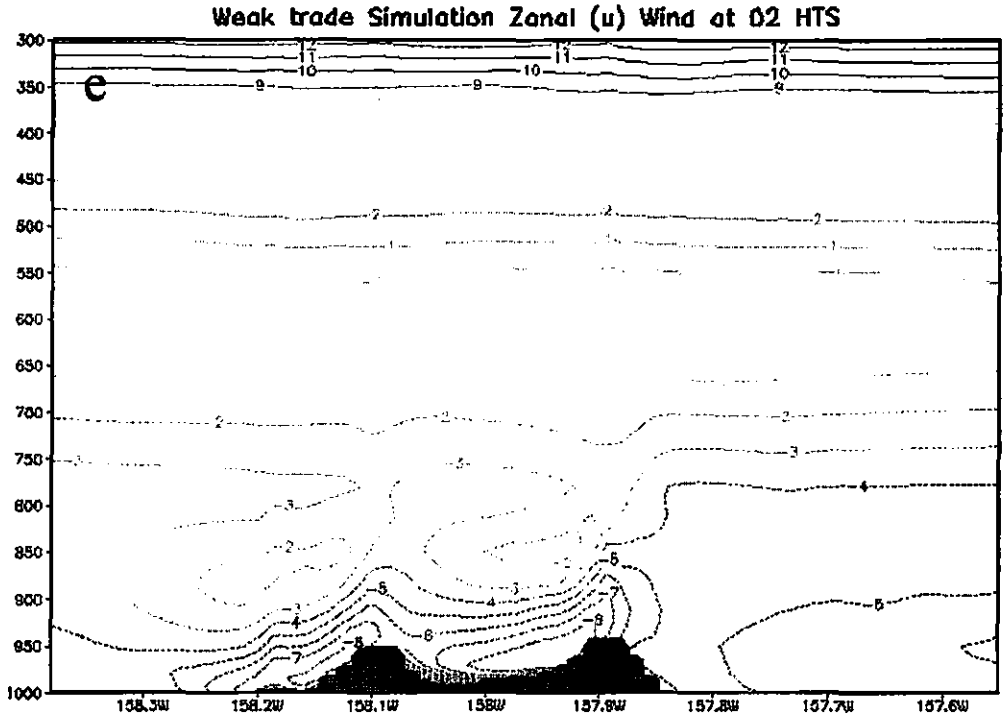

Figure 12e Vertical cross sections at 21.45° N of simulated mean zonal wind component under weak trades at 02 HST.

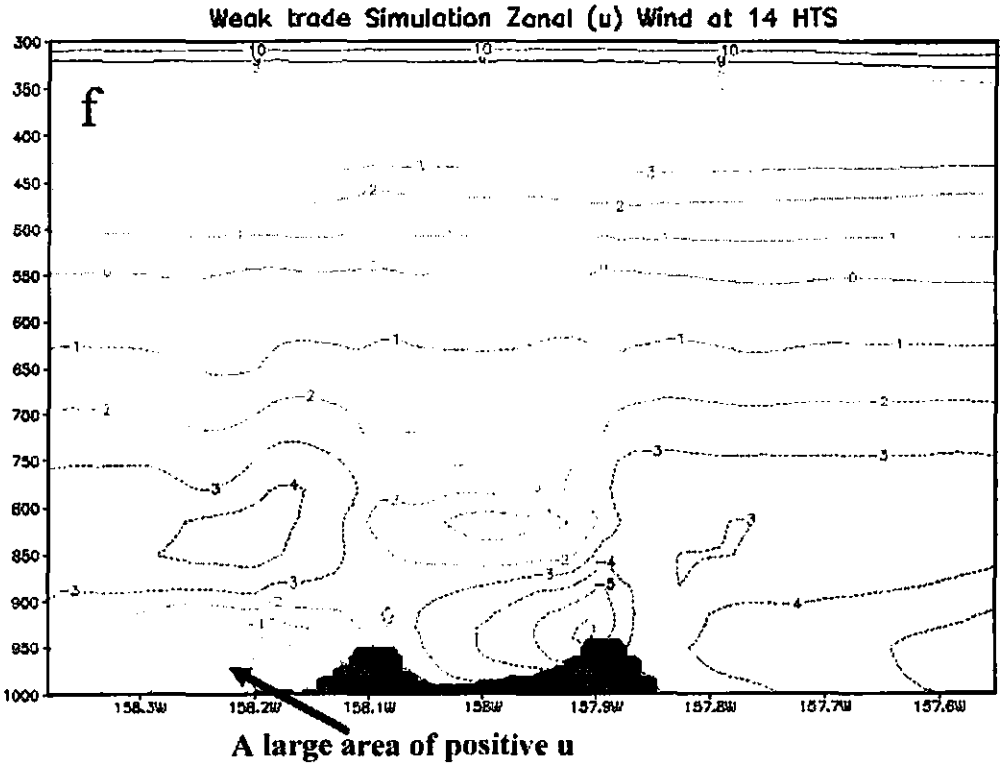

Figure 12f Same as Figure 12e but for 14 HST.

3.2 Simulation of rainfall

3.2.1 Simulation of total rainfall

Simulated rainfall accumulation for two summer months, July and August, 2005 is shown in Figure 13a. Observed rainfall accumulation of the two months from 29 Hydronet rain gages during the same period is shown in Figure 13b. Because no Hydronet rain gage at the rainfall maximum area over the Ko'olau Mountains, the observed total rainfall of the days without synoptic disturbances during summer months of 2002 (May to July, except: May 6, may 15) and 2003 (May to September: except: Sep 10, 11, Jun 4-8, Jul 24-27) from Loos (2004) (Fig. 14) is used to evaluate the spatial distribution of simulated rainfall accumulation. Even though the total rainfall in Loos's research is not from the same period as this research, Figure 14 is useful to evaluate spatial distribution of simulated rainfall accumulation.

Because of the mountains, there are large horizontal variations in simulated rainfall. Simulated rainfall accumulation (Fig. 13a) shows rainfall maximum over the Ko'olau Mountains. A secondary maximum occurs at lee-side slope of the Waianae Mountain Range and a minimum at central Oahu. These results are in agreement with observed rainfall during the same period (Fig. 13b) that shows a region of total rainfall less than 100 mm at central Oahu (Fig. 13a); and a rainfall maximum of 655 mm at one station at the southern Ko'olau rainfall maximum. The simulated rainfall in the area reaches 500 mm. Of the 29 rain gage used in this research, there is no station located over the areas of another rainfall maximum at the northern Ko'olau Mountains and the leeward Waianae maximum. However, the characteristics of spatial rainfall distribution are in agreement with Loos (2004) (Fig. 14).

For large islands with high mountains such as the Big Island, rainfall due to orographic lifting occurs mainly over windward slopes and windward lowland. For small islands such as Oahu, rainfall maximum region can spread to the western slopes of the Ko'olau Mountains (Figs, 13a, 13b, 14) because clouds and liquid water can be carried

by the prevailing winds over the mountains with rainfall extending to the lee side. Zhang et al. (2005) showed that MSM/LSM simulates less or no rainfall downstream of the ridge tops of the Ko'olau Mountains. MM5/LSM does a better job than MSM/LSM on simulating rainfall on the lee-side slopes.

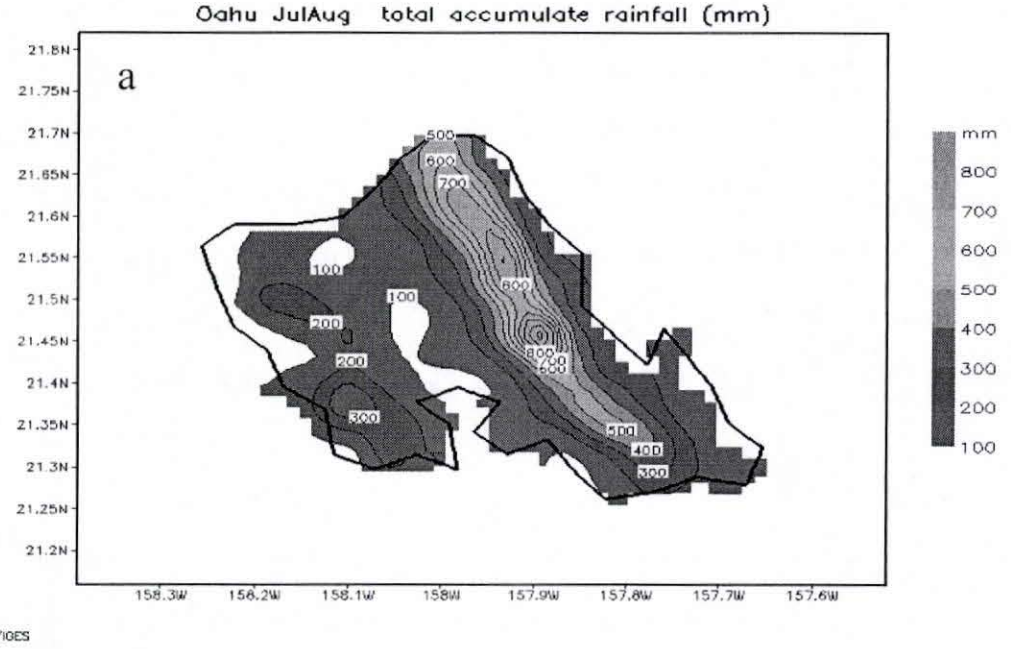

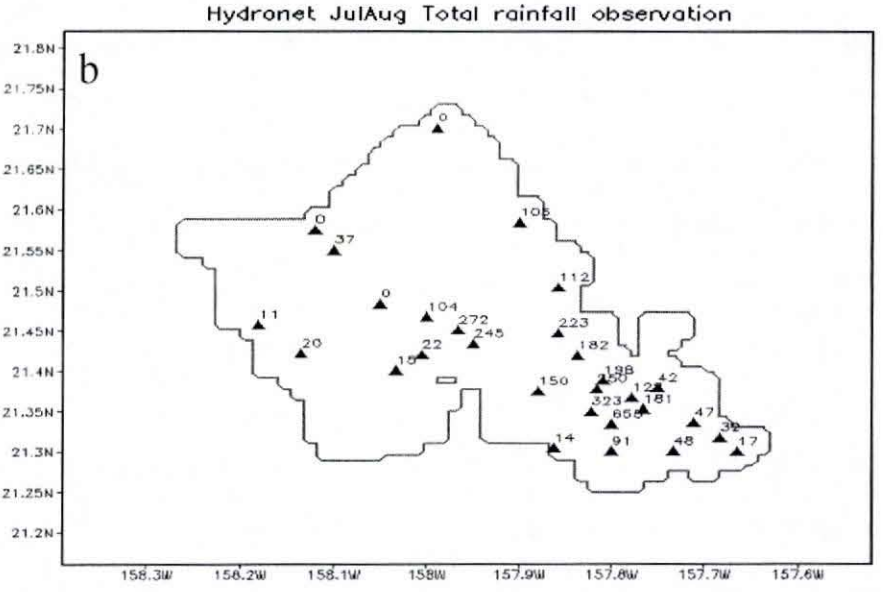

Figure 13a Total rainfall accumulation (mm) for July-August 2005 (a)simulation and (b) observation.

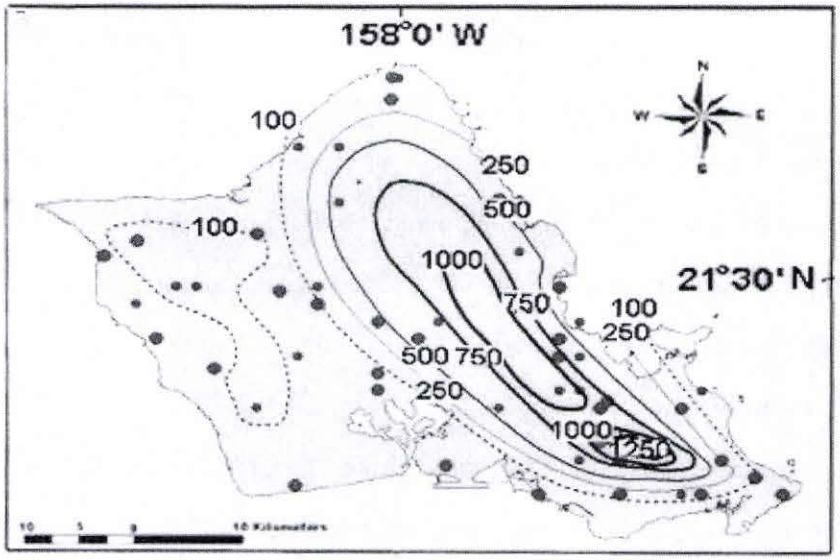

Figure 14 Total observed rainfall (mm) of days without synoptic disturbances during summer months 2002 (May to July except May 6, may 15) and 2003 (May to September except Sep 10, 11, Jun 4-8, Jul 24-27). (Fig. 2.3, page 18, Treena Marie Loos's thesis, 2004)

3.2.2 Diurnal variations of rainfall

To investigate the diurnal cycle of rainfall, simulations of 3-hour rainfall accumulation during the two summer months are averaged to obtain eight averaged maps of simulated 3-hour rainfall accumulation (Fig. 15).

Because of daytime heating and nighttime cooling, there are considerable diurnal variations in rainfall throughout the day. Diurnal variations of rainfall show a nocturnal rainfall maximum (Fig. 15a) and a secondary maximum in the morning from 8-11 HST (Fig 15e) over windward side and mountain interior in agreement with Loos (2004) and Leopold (1948). Under normal trade-wind conditions, Loos (2004) identified two rainfall maxima at 22 HST and 09 HST respectively. The double rainfall maxima during the diurnal cycle is also reported by Loveridge (1924, Fig. 1). On the lee side and southern part of the Waianae Mountains, there are secondary maxima occurs from the late afternoon through midnight hours (Figs. 15g, and 15h).

The nocturnal maximum is caused by cloud top radiation cooling, stronger wind speed aloft as well as lower lifting condensation level (LCL) (Leopold, 1948) and flow deceleration on the windward side of the Ko'olau Mountains at night. In the early evening, outgoing longwave radiation (OLR) is released at the cloud tops. Meanwhile the cloud base captures OLR emitted from below. As a result, radiation cooling at night enhances instability between cloud tops and cloud bases. Cooling also results in more significant flow deceleration than during the day as the air approaches the island. Moreover, cooling at all levels at night results in a lower LCL. All these factors are favorable for the development of the nocturnal rainfall maximum (Leopold, 1948).

Morning maximum is reported by Loos (2004) using rain gage observations over Oahu during normal trade-wind conditions. Loos compiled diurnal rainfall frequency and accumulation at every station. For windward Oahu foothill stations, two maxima in both rainfall frequency and accumulation are observed at 07 HST and 19 HST (Fig. 13, Loos, 2004). For stations over the Ko'olau Mountains, the simulated rainfall of two summer months of 2005 also shows two maxima in rainfall frequency as well as accumulation, one around 23 HST and the other around 09 HST. To explain the rainfall maximum in the morning, Loos suggested that it may be caused by morning airflow deceleration. But the deceleration should be most significant before sunrise, why does the rainfall maximum occur two to three hours latter after sunrise. Loos also stated two other possible factors to account for the early morning rainfall maximum: nocturnal cloud-top radiative cooling (Schroeder et al., 1977) and orographic lifting. The morning maximum was also reported by Leopold (1948). However, no previous studies clearly explain the morning rainfall maximum at Oahu. This problem will be investigated further.

Heating during the day and low LCL in the early morning are favorable conditions for morning maximum in rainfall accumulation from 08 HST to 11 HST. After a period of decrease in rainfall at night from 23 HST to 02 HST, mean rainfall slightly increases from 02 HST to 08 HST (Figs. 15c, and 15d). To find the factors account for this rainfall

maximum, mean vertical velocity and, equivalent potential temperature every three hour of the diurnal cycle is shown in Figure 16. The mean vertical velocities at the windward side of the Ko'olau Mountains also show two maxima at 23 HST (Fig. 16a) and at 08 HST (Fig. 16d). Because of maxima of vertical velocities at this two time sections, moist laden incoming trade-wind flow is forced to reach the relatively low LCL to condense and make rainfall. The diurnal variations on equivalent potential temperature in Figure 16 are also consistent with the morning rainfall maximum. Significant changes in the equivalent potential temperature on all figures occurs in the distance of about 5 km before the air parcels reach the island. With a mean speed of 8 m s^{-1}, air parcels take about 10 minutes to reach the island from 5 km offshore. With this short time, radiative heating/cooling is negligible when compare with condensation heating/evaporate cooling. Figures 16a to 16h show that equivalent potential temperatures at the time of rainfall maximum (Figs. 16a and 16d) increase more significantly before the airflow reaches the Ko'olau Mountains than at the other times. The rapid increase of equivalent potential temperature demonstrates that air parcels rise up to higher levels. The reason for larger vertical motions in the early morning is still under investigation.

In the early afternoon, even the surface heating effect is the strongest but the rainfall is at a minimum during the diurnal cycle (Fig. 15f). Less rainfall in the early afternoon occurs because surface is heated significantly. As a result, strong heat turbulence developed over land mix up air at low levels and aloft, no large vertical differences in temperature in the boundary layer. With land surface heating, LCL is higher than at night.

The afternoon maximum at leeward side agrees with Leopold (1948). Leopold explained that the rainfall maximum is caused by convective showers from orographic lifting. It occurs when sea breezes bring the warm, moist air from the ocean offshore of the Waianae Mountains to the island and moves upslope or converges with accelerated leeside flow to reach the LCL and produces clouds and possibly local showers.

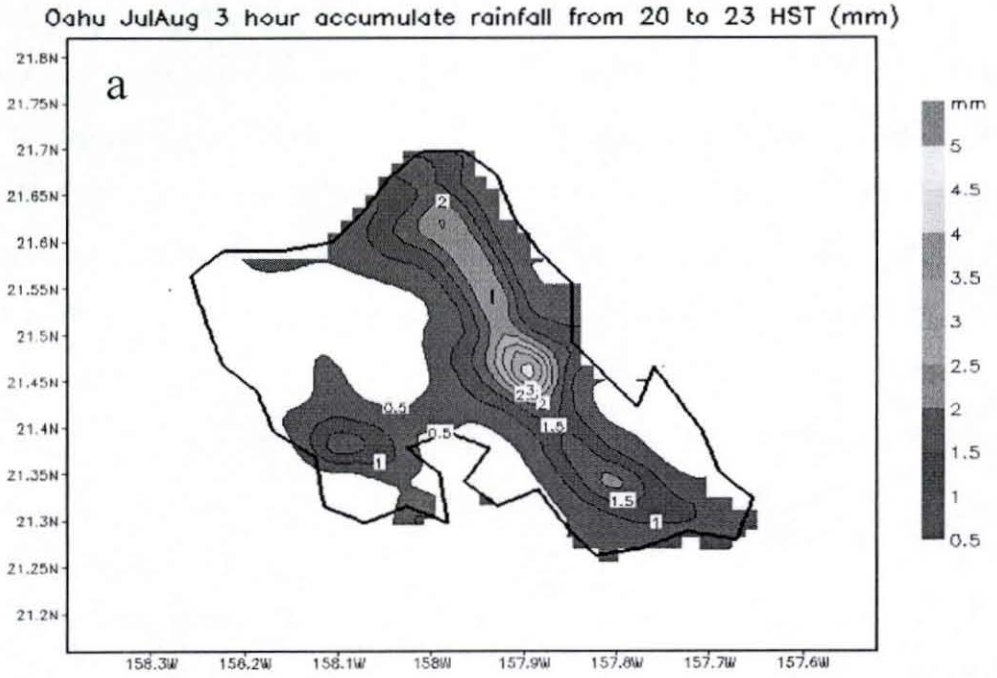

Figure 15a Mean simulated 3-hour rainfall accumulation (mm) from 20 HST to 23 HST

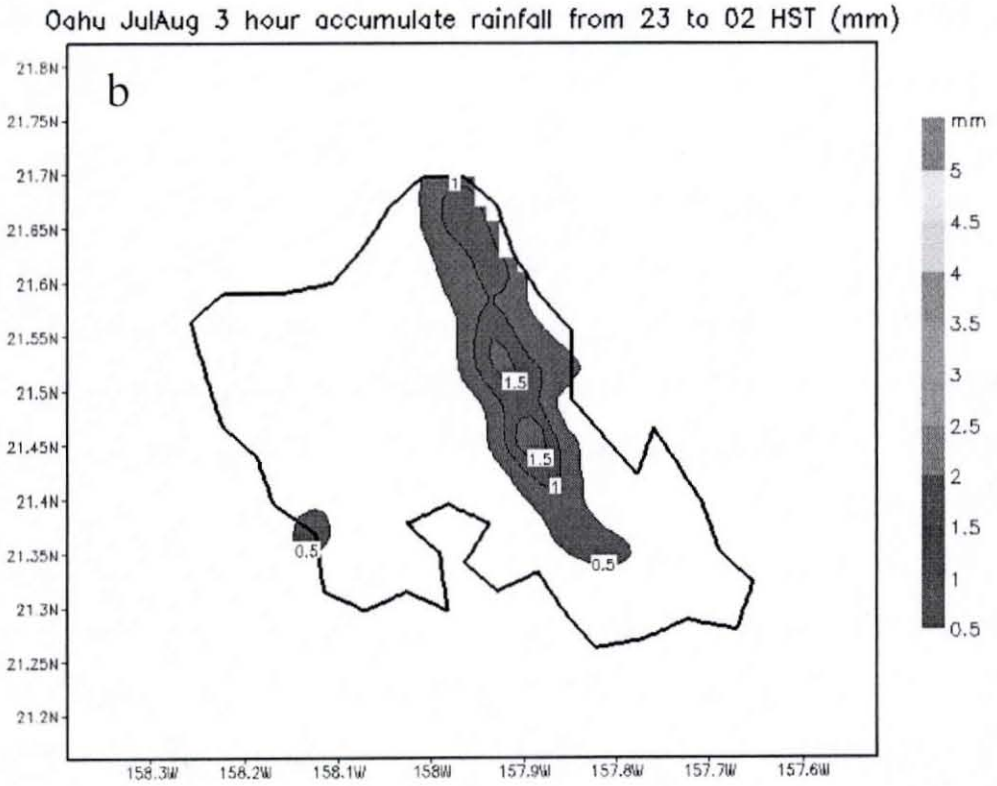

Figures 15b Mean simulated 3-hour rainfall accumulation (mm) from 23 HST to 02 HST.

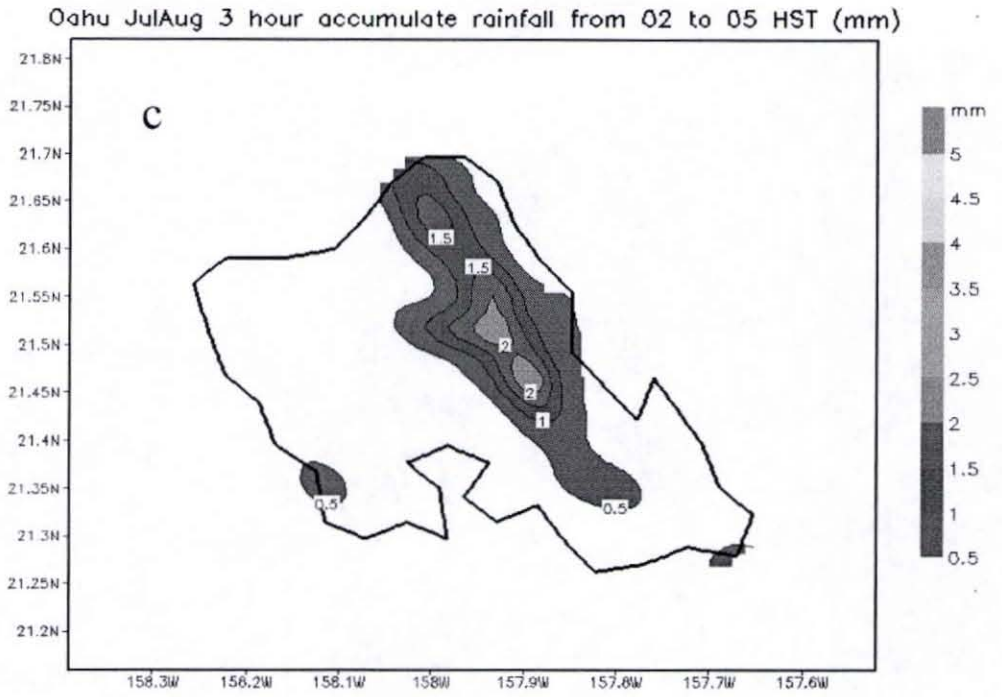

Figure 15c Mean simulated 3-hour rainfall accumulation (mm) from 02 HST to 05 HST.

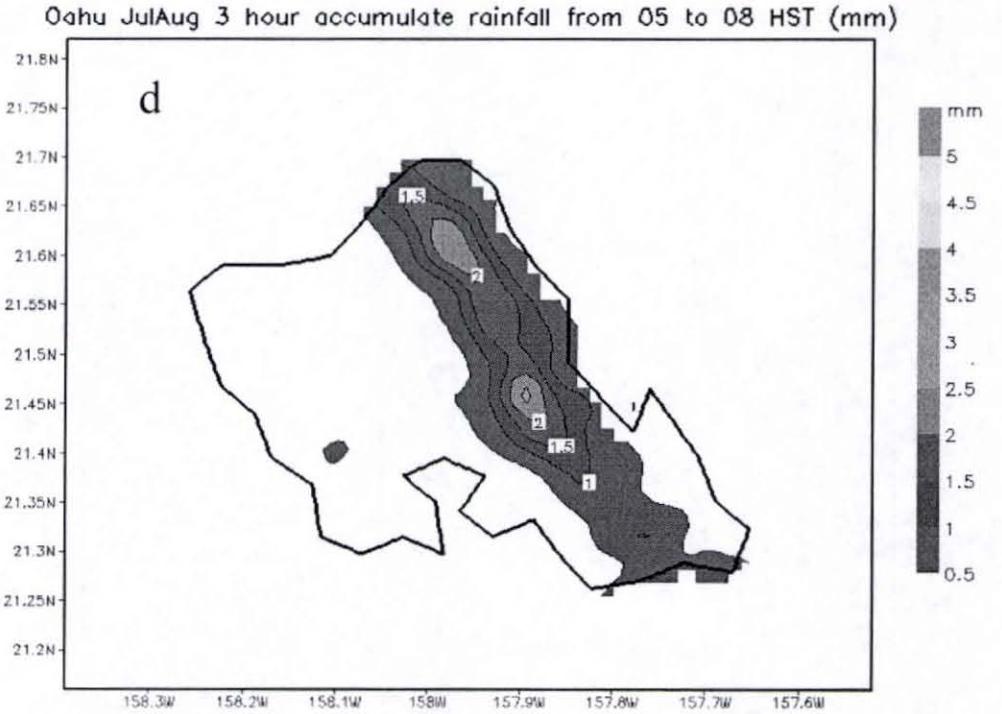

Figure 15d Mean simulated 3-hour rainfall accumulation (mm) from 05 HST to 08 HST.

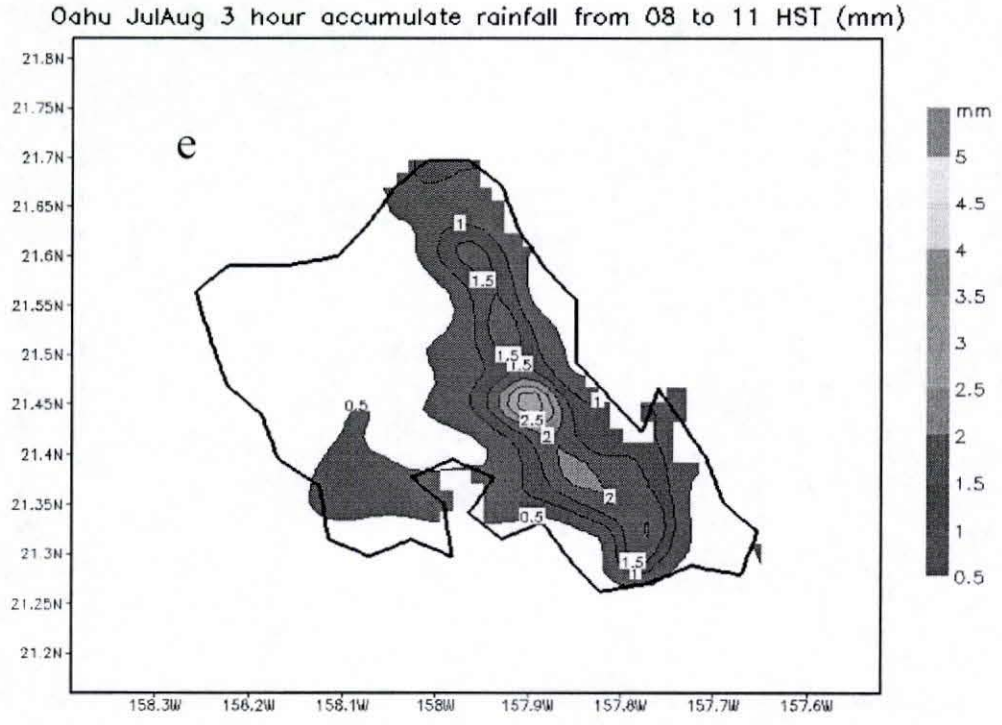

Figure 15e Mean simulated 3-hour rainfall accumulation (mm) from 08 HST to 11 HST.

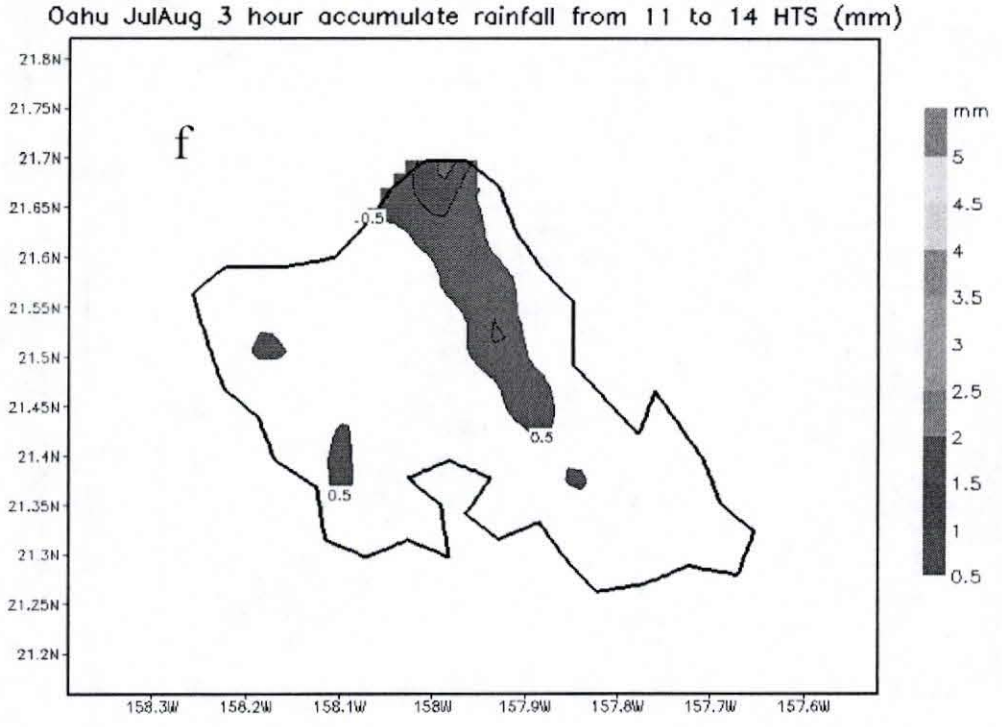

Figure 15f Mean simulated 3-hour rainfall accumulation (mm) from 11 HST to 14 HST.

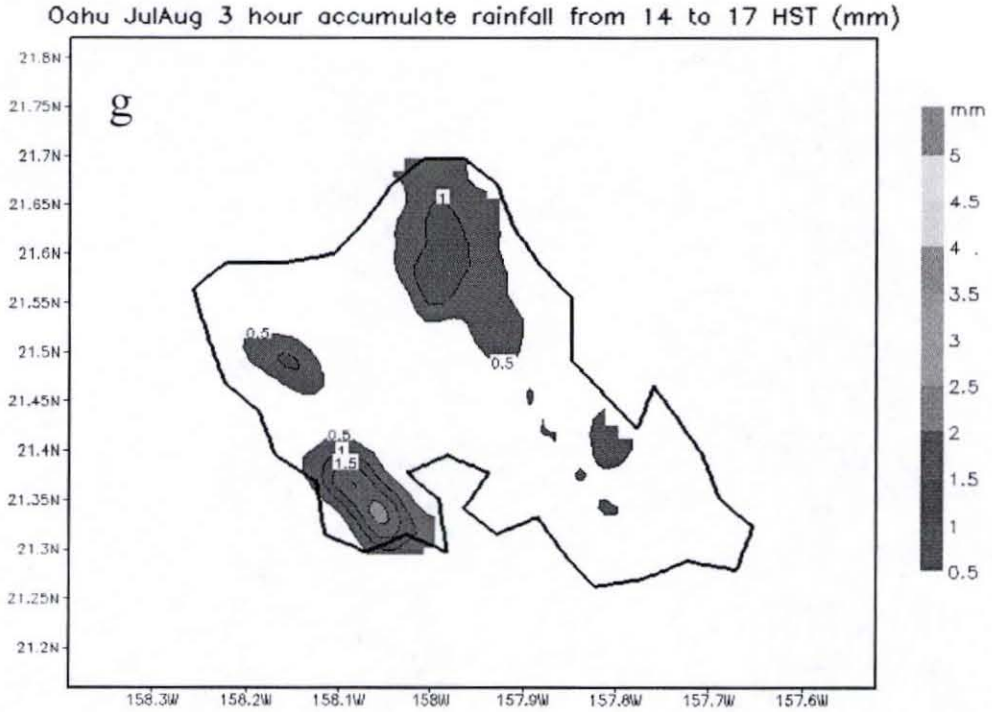

Figure 15g Mean simulated 3-hour rainfall accumulation (mm) from 14 HST to 17 HST.

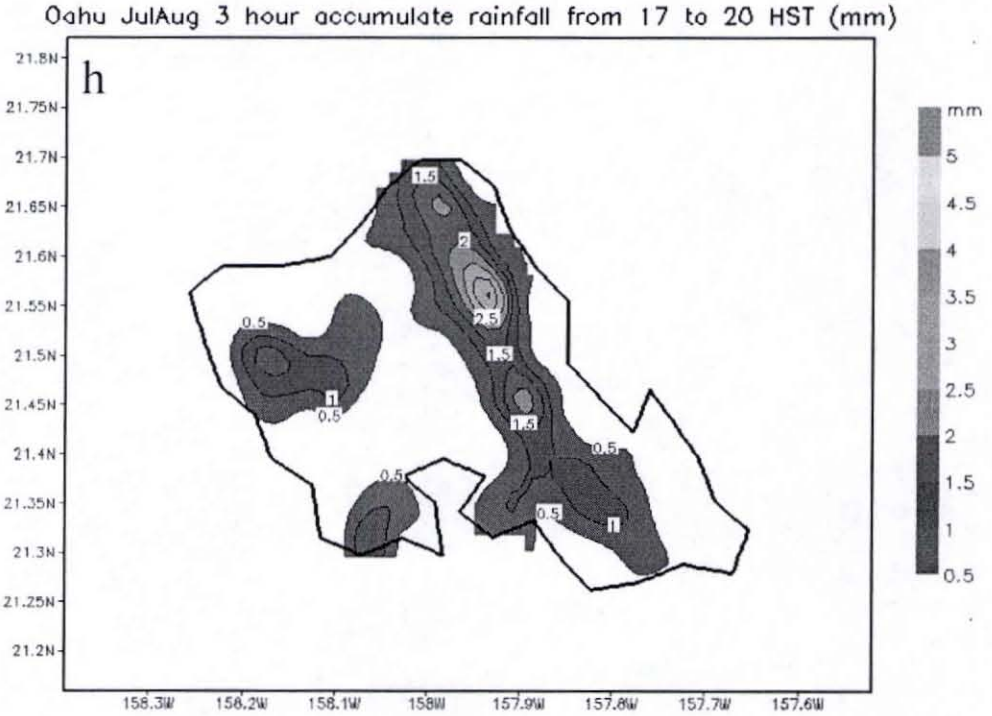

Figure 15h Mean simulated 3-hour rainfall accumulation (mm) from 17 HST to 20 HST.

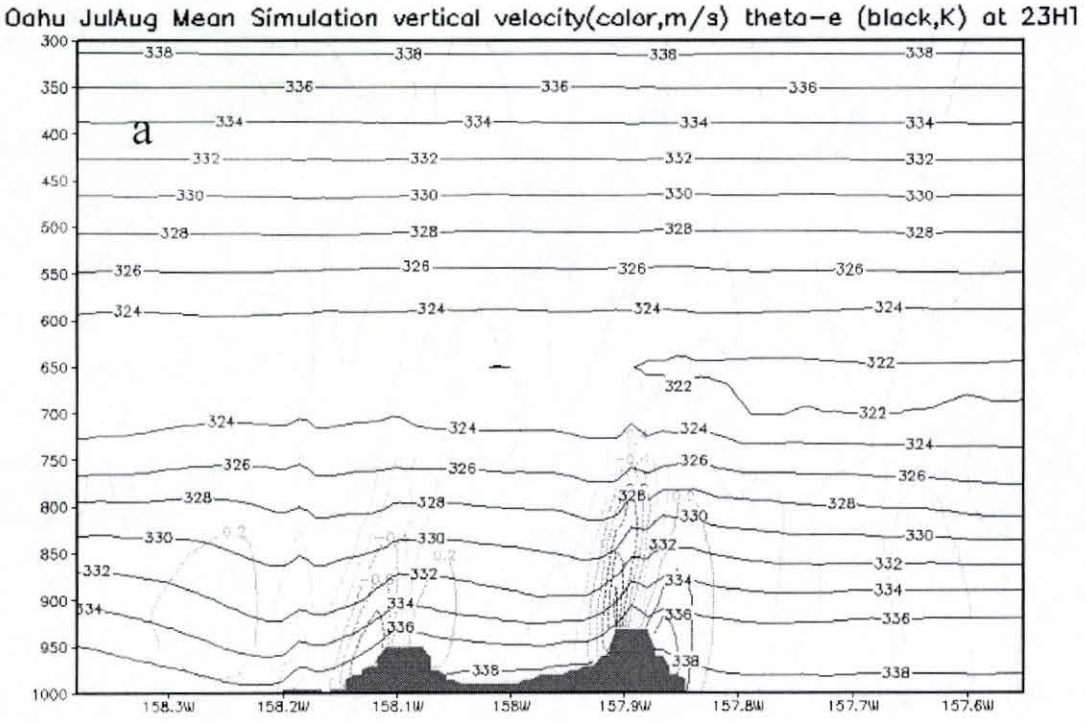

Figure 16a Simulated mean vertical velocity (color, m s^{-1}) and equivalent potential temperature during July –August 2005 at 23 HST.

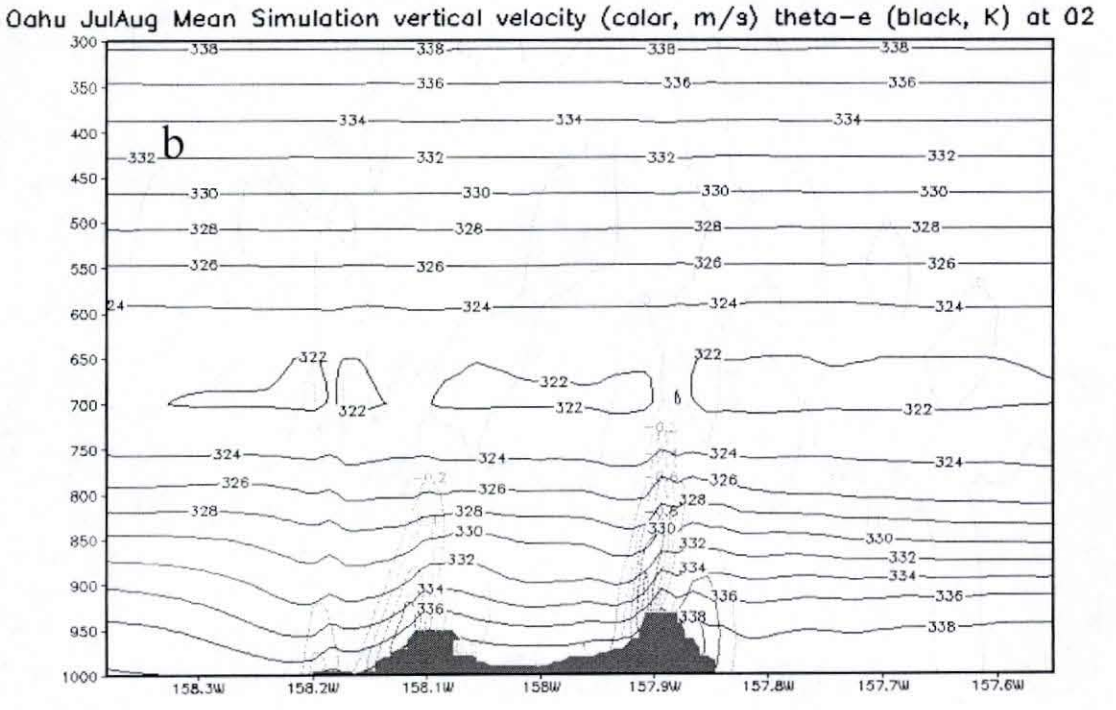

Figure 16b Simulated mean vertical velocity (color, m s^{-1}) and equivalent potential temperature during July –August 2005 at 02 HST.

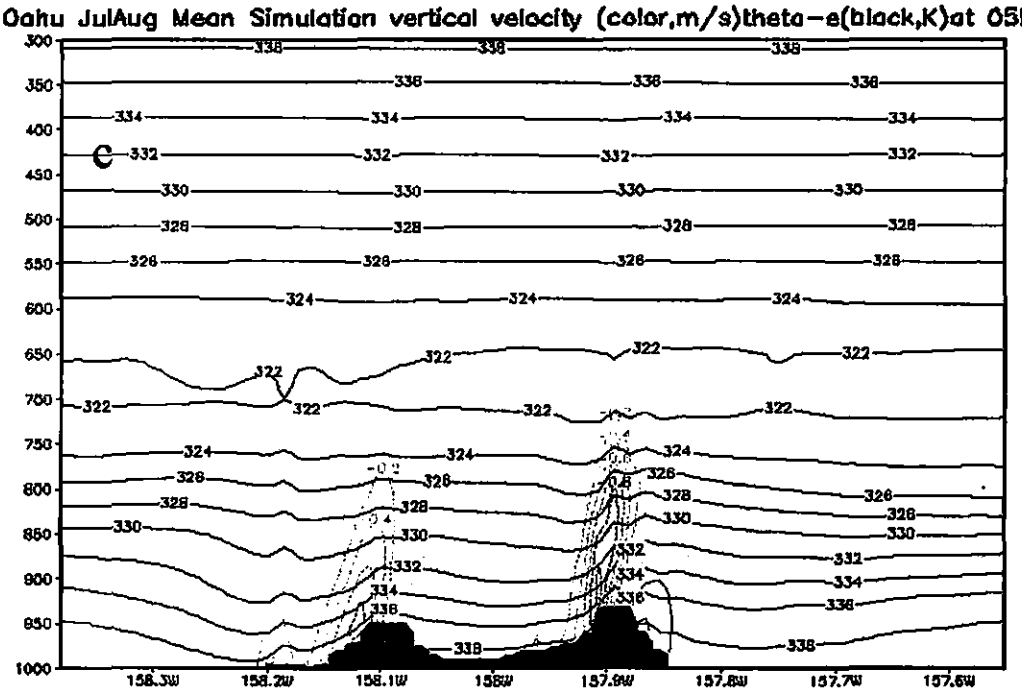

Figure 16c Simulated mean vertical velocity (color, m s^{-1}) and equivalent potential temperature during July –August 2005 at 05 HST.

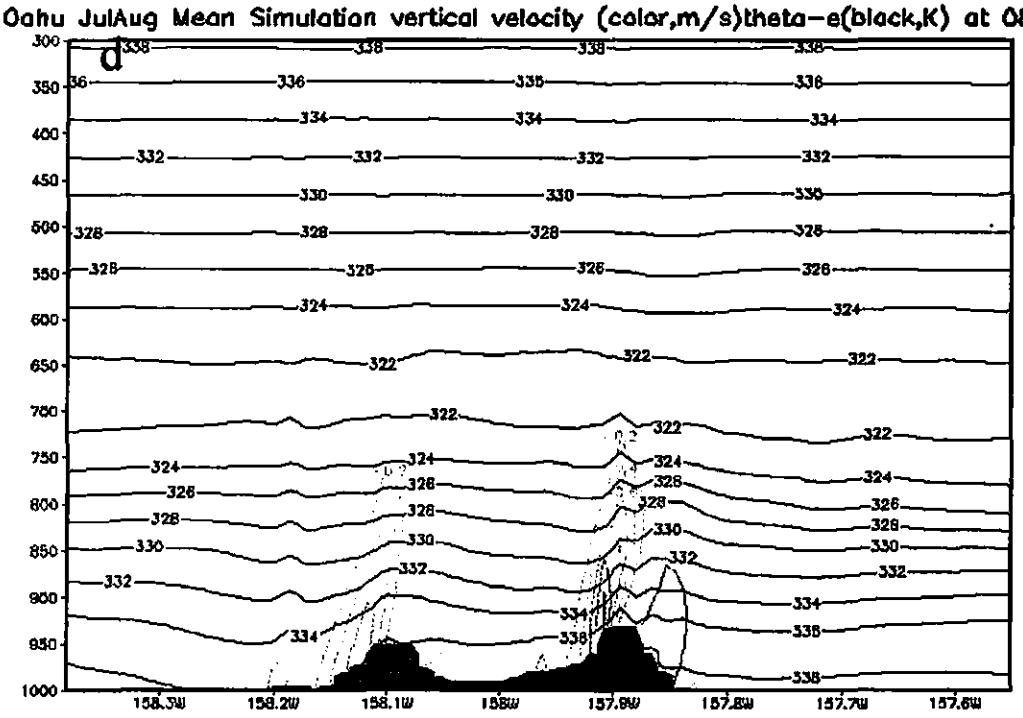

Figure 16d Simulated mean vertical velocity (color, m s^{-1}) and equivalent potential temperature during July –August 2005 at 08 HST.

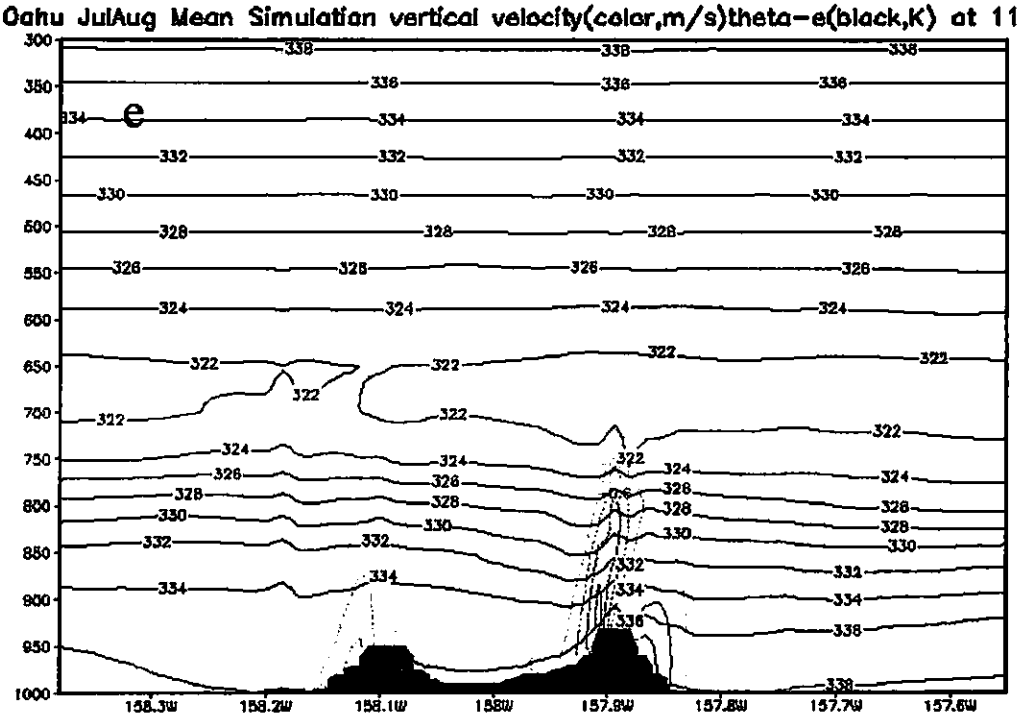

Figure 16e Simulated mean vertical velocity (color, m s^{-1}) and equivalent potential temperature during July –August 2005 at 11 HST.

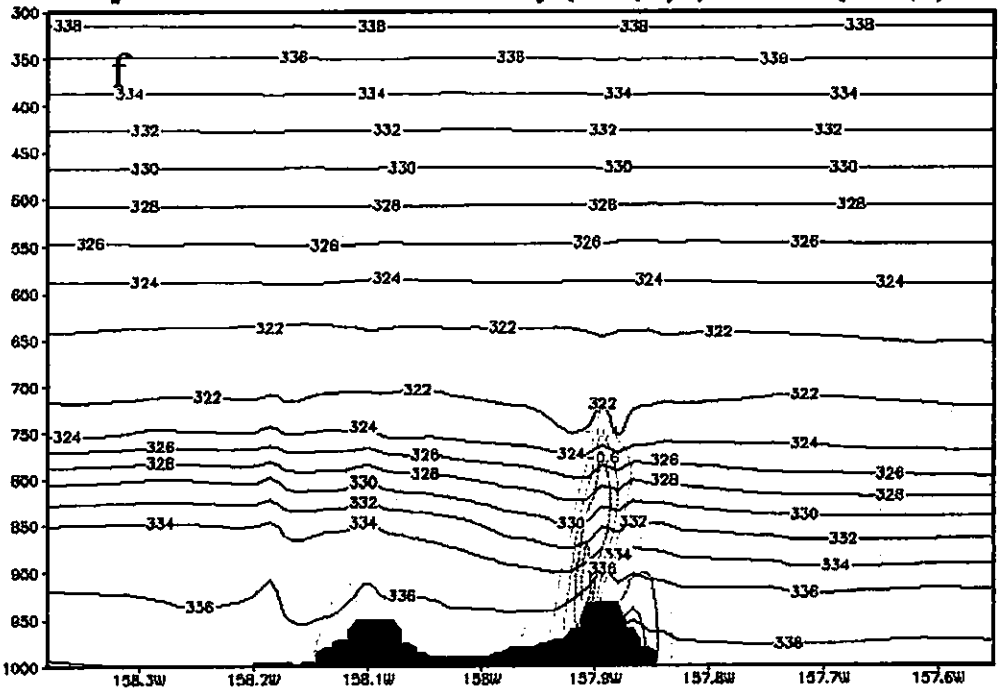

Figure 16f Simulated mean vertical velocity (color, m s^{-1}) and equivalent potential temperature during July –August 2005 at 14 HST.

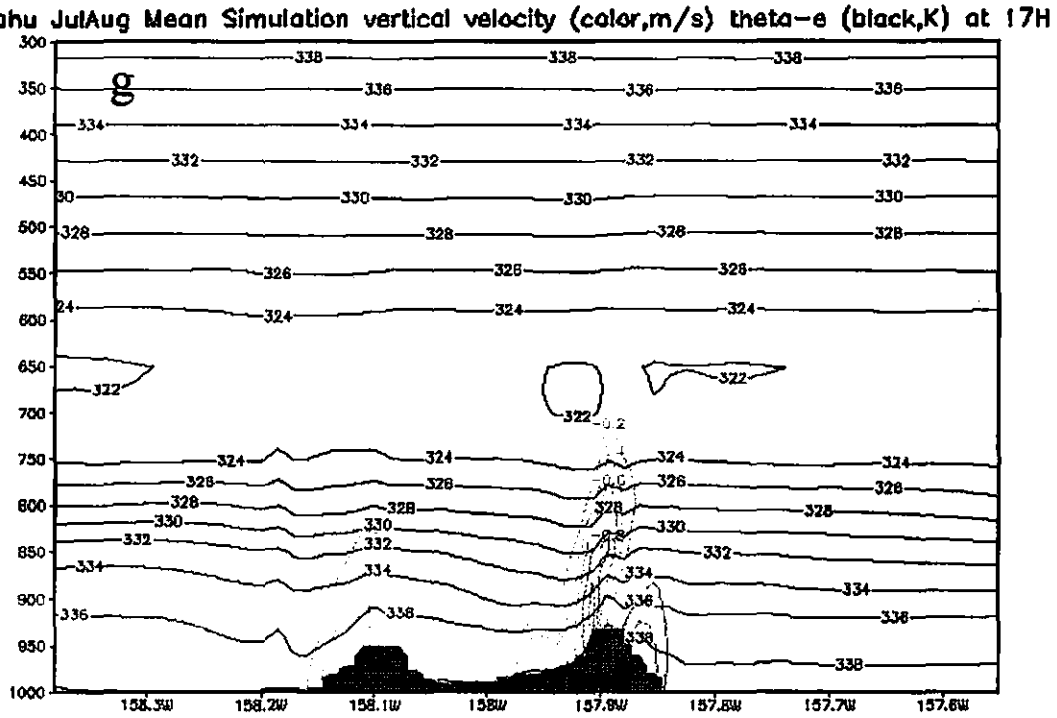

Figure 16g Simulated mean vertical velocity (color, m s^{-1}) and equivalent potential temperature during July –August 2005 at 17 HST.

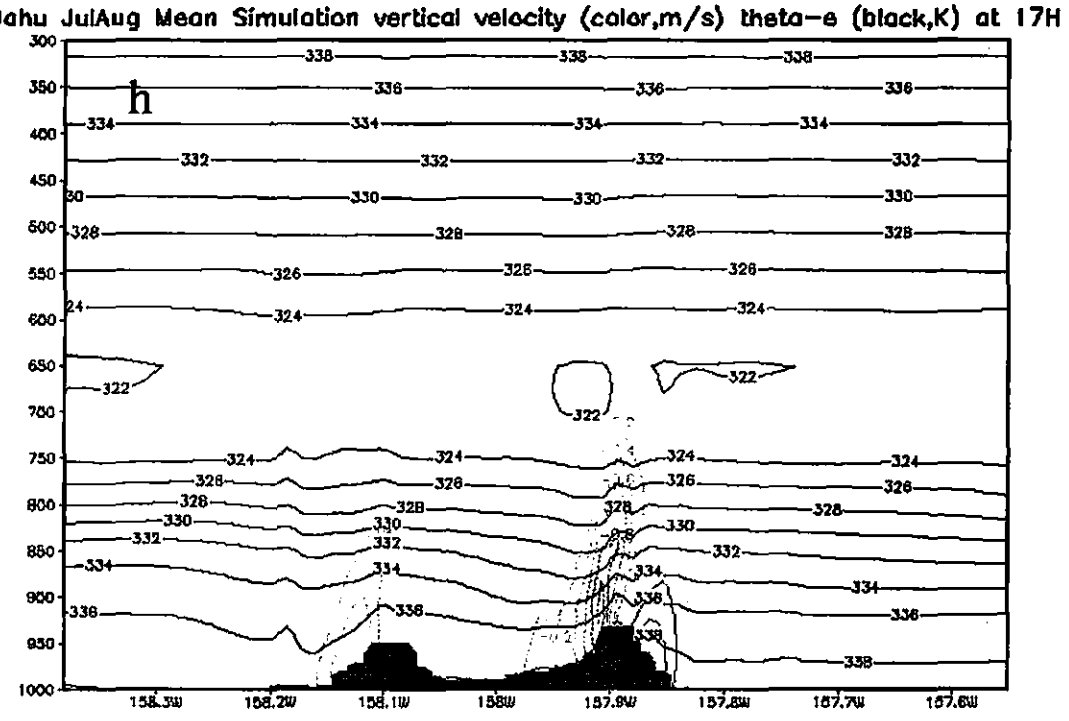

Figure 16h Simulated mean vertical velocity (color, m s^{-1}) and equivalent potential temperature during July –August 2005 at 20 HST.

3.2.3 Effects of trade-wind conditions on rainfall

To investigate the effects of trade-wind conditions on rainfall, total simulated rainfall accumulation for ten strong trade-wind (Table. 6a) and ten weak trade-wind days (Table. 6b) during the period of two summer months of 2005 are computed separately shown in Figures 17a, and 17b, respectively. The corresponding total observed rainfall at 29 Hydronet rain gage stations are shown in Figures 18a, and 18b.

Higher rainfall is simulated under strong trades (Fig. 17a) than under weak trades (Fig. 17b) in agreement with observations (Fig. 18a, and 18b) and Loos (2004). Overall, the simulated rainfall over Oahu is about four to five times greater under strong trades than under weak trades. The same situation is shown on Hydronet rain gage observations. Indeed, the value of maximum contour on simulated rainfall accumulation map (Fig. 17a) of ten weak trade days is 40 mm. Meanwhile, the value of the maximum contour on simulated rainfall accumulation map (Fig. 17b) of ten strong trade days at the same location is about 180 mm. From observed rainfall, the maximum of total rainfall accumulation under the weak trade case is 36 mm at a station located at southeast tip of Oahu near Honolulu. The maximum of total rainfall accumulation under the strong-trade cases occur at the same station at which total rainfall accumulation under the weak trade case reach maximum but with the value of about five times larger, 183 mm. Both simulation and observation show that trade-wind conditions do not significantly affect the locations of rainfall maxima but the values of the maxima.

In this study, total rainfall accumulation over Oahu is greater when the trades are stronger. However, trade-wind condition is not the only main factor affecting the total rainfall accumulation. Loos (2004) showed that the height of trade-wind inversions also strongly control the daily rainfall. In general, daily rainfall is greater when the trade-wind inversion is higher (Loos, 2004).

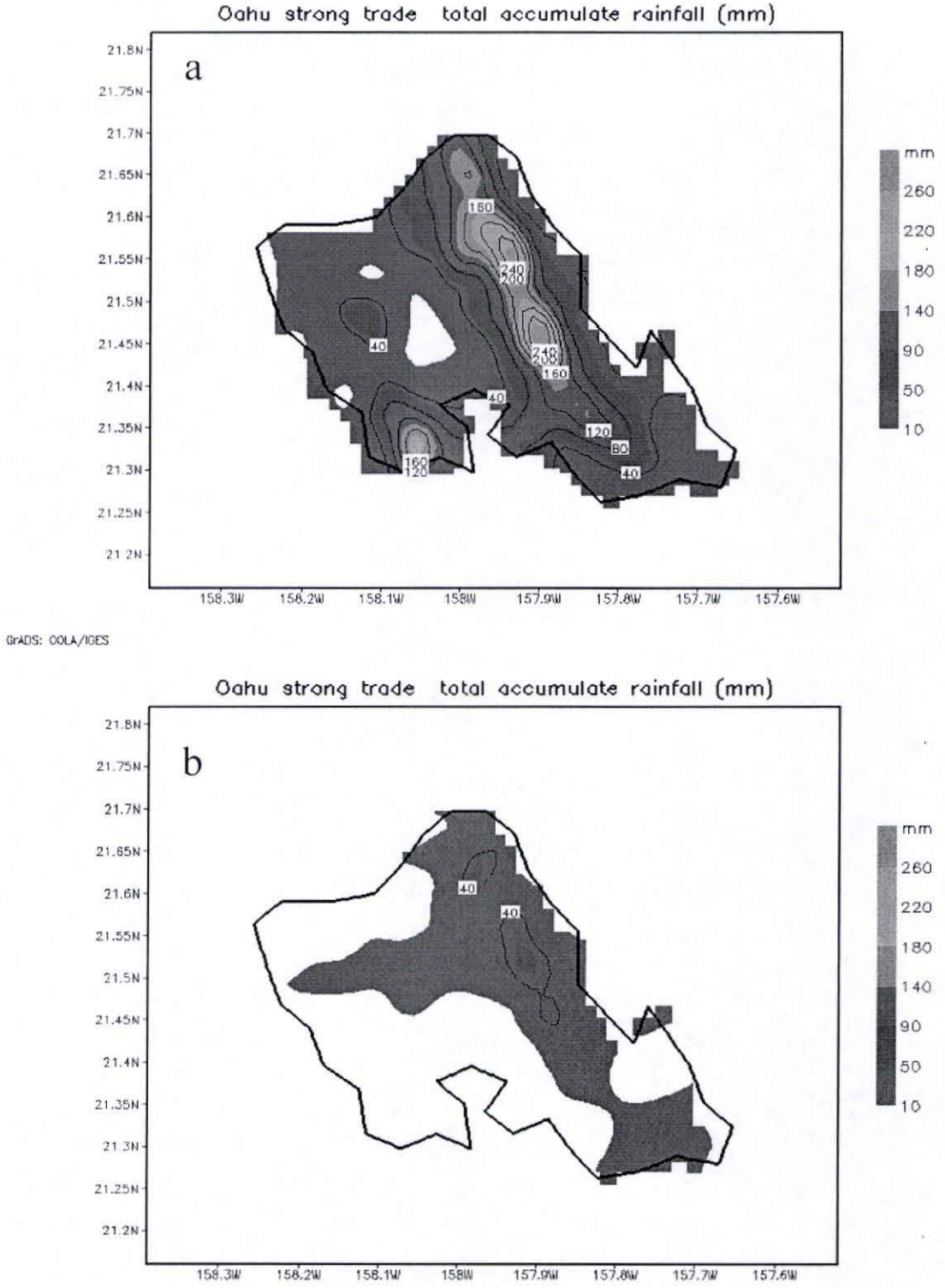

Figure 17 Simulated rainfall accumulations for (a) ten strong trade wind days and (b) ten weak trade wind days.

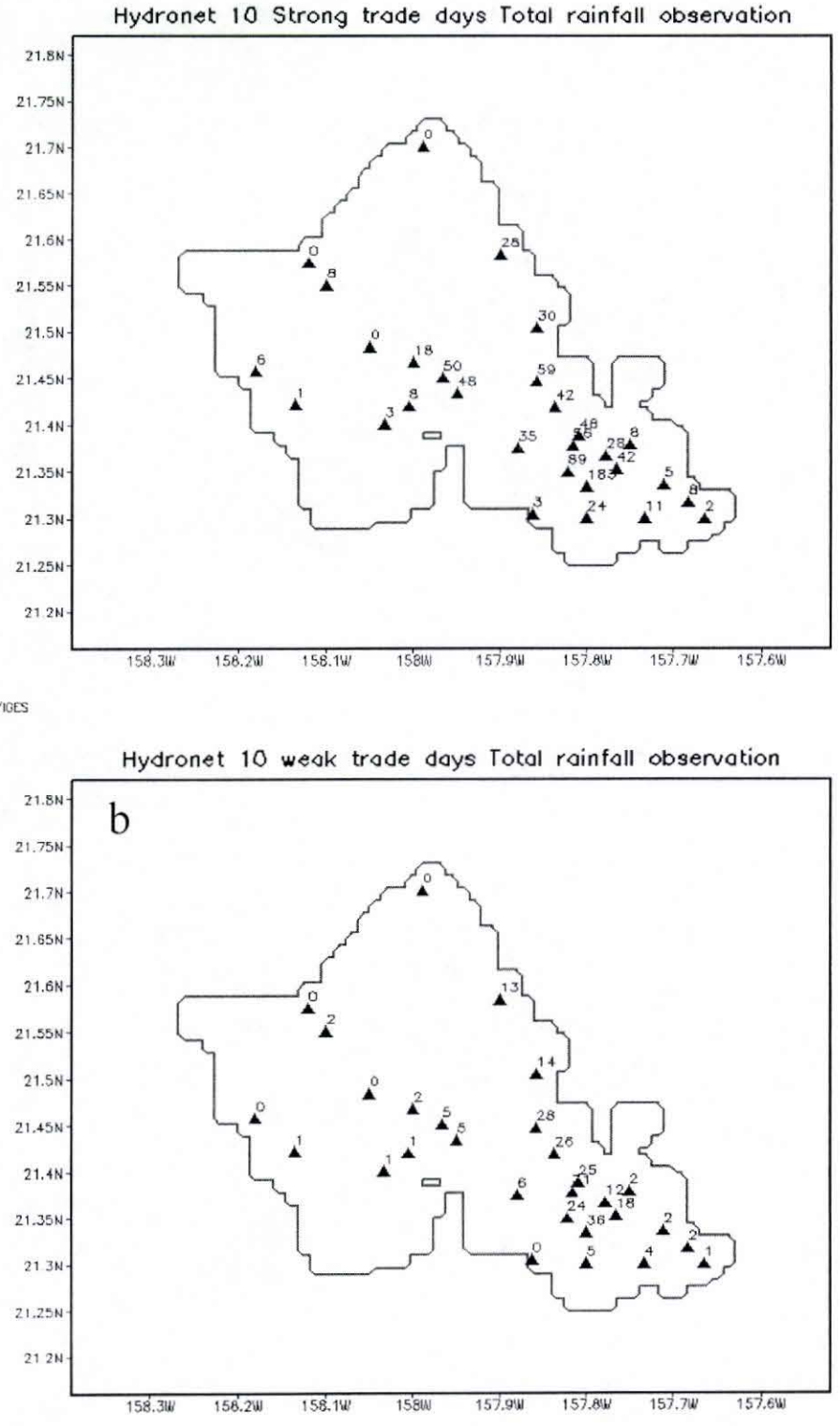

Figure 18 Observed rainfall accumulations for (a) ten strong trade wind days (a) and (b) ten weak trade wind days at 29 Hydronet rain gage stations.

3.2.4 Simulation of thermodynamic variables

3.2.4.1 Surface air temperature

Chen and Wang (1994) used observation from 50 PAM (Potable Automated Mesonet) to show that temperature at the Island of Hawaii has a significant diurnal cycle and the diurnal ranges are different from one place to another. Thermodynamic fields, according to Chen and Wang, depend not only on diurnal heating cycle but also orography, airflow, as well as the distribution of clouds and rains. In this section, simulations of thermodynamic fields over the island of Oahu are shown and the simulation of air surface temperature and dew point temperature are compared with corresponding observations at 13 weather stations. Error statistics are used to validate model simulations.

First of all, two-month mean of simulated temperature at 13 stations are compare with observations to evaluate possible model bias. The error statistics for temperature at every station are shown in Table 7, including mean bias (BIAS), root mean square error (RMSE), and mean absolute error (MAE) for the two-month period. The RSME and MAE values vary from 1.0°C to 2.2°C and from 0.7°C to 1.8°C, respectively. The average MAE values for 13 stations at 05 HST and 14 HST (Table 8a) are 1.2°C and 1.8°C, respectively. The average MAE values for 50 stations in Yang et al. (2005) simulation for the Big Island are 1.0°C and 1.4°C, respectively. Does it mean that MM5 simulations for bigger islands are better? The statement may not be true if spatial location distribution of stations is considered. Yang et al. (2005) showed that the errors at windward stations are much smaller than that at other locations. The same situation is shown in MM5 simulations for Oahu. Specifically, all MAE values at three windward stations of the Ko'olau are relatively small (<1.1°C). That means if more windward stations are used to compute MEA for all stations, the smaller the value would be. Of the 50 stations used in

Yang et al (2005), more than a half of these stations are located on the windward side. Meanwhile, only 3 of 12 stations (Bellows station is ignored because temperature observation is not available) on Oahu are windward stations. As a result, MEA indices for all Oahu stations are larger as compared to the work of Yang et al. (2005).

The mean temperature of Oahu during two summer months in 2005 is shown in Figure 19a. Although, the temperature has large diurnal cycle (Chen and Wang, 1994) because of heating during the day and cooling at night, the mean temperature simulation over the Waianae Mountains mainly depends on terrain height. The contours of isothermals (Fig. 19a) are almost coincided with the contour of constant altitude (Fig.11b). The temperatures at the top of the Waianae Mountains are 4-5 degrees lower than at the foothills and over the open ocean.

Because of the diurnal heating cycle, orography, distribution of clouds and rainfall (Chen and Wang, 1994), there are significant diurnal variations of air surface temperature over Oahu. Both simulation and observation at all stations show a minimum air temperature at 05 HST before sunrise and a maximum temperature around noon time between 13 HST and 14 HST (Figs. 21 to 33). Because coastal windward stations are strongly affected by the in-coming trade-wind flow, they have more oceanic climates (Chen and Wang, 1994; Riehl, 1979). Diurnal temperature ranges (maximum mean air temperature minus minimum mean air temperature) for stations on the windward side of the Ko'olau Mountains (Station 1, 5, 6, and 7) are smaller than that at the other stations. The diurnal ranges in temperatures at windward side stations are from 2° C to 4° C (Figs. 21d, 25d, 26d, and 27d). At other stations, these values vary from 6° C to 9° C.

With day time heating, the spatial distribution of surface air temperature is chaotic (Fig. 19b). The isotherms at 14 HST do not follow the contours of constant altitude like they are in the mean temperature (Fig. 19a). Low temperatures are simulated at windward coast (about 26°C) and high mountain areas (25°C over the Waianae and 23°C over the Ko'olau Mountains). Much higher temperatures are simulated over low land areas (31°C). The chaotic distribution should be a result of daytime heating of different landuse types at 14 HST. The temperatures over the Ko'olau Mountains are significantly lower than the temperatures over the Waianae Mountains. The temperature at the top of the Ko'olau Mountains can be as low as 22°C. Meanwhile, at the top of the Waianae Mountains, the lowest temperature only is about 25°C. The lower temperatures over the Ko'olau Mountains are results of adiabatic cooling due to orographic lifting of the incoming trade-wind flows (Chen and Wang, 1994) and different landuse categories between the two mountains.

The simulated air temperatures at 14 HST agree with observation reasonably well at windward stations (Table 9b). The RMSE and MAE at 14 HST (Table 9b) vary from 1.3-3°C and 1.0-2.4°C, respectively. The RMSE values for the Big Island (Yang et al., 2005) vary from 1-4°C. RMSE and MAE values at windward stations (Station 1, 6, and 7) are much smaller than at the other stations (Table 9b).

At night, temperature decreases because of radiative cooling. The isothermal contours are smoother than that during the day. The temperature at night strongly depends on terrain height. The smooth isothermal contours following the terrain indicate that air temperatures at night do not significantly depend on landuse categories like they do during the day. The lowest temperatures over the Ko'olau Mountains at night are comparable to the lowest temperatures over the Waianae Mountains (20° C). It implies that the stable conditions and weaken windward wind speeds at night reduce the effect

of adiabatic cooling due to orographic lifting on the surface air over the Ko'olau Mountains.

The simulated air temperatures are better at 05 HST than at 14 HST except at the two leeward coastal stations (Stations 2 and 4). All three windward stations have MAE less than 1° C at 05 HST. All other stations excepting station 2 and 4 have MAE less than 1.5° C. The large values on RMSE and MAE at Station 2 and 4 (Table 9a) probably result from an overestimation of wind speeds from the model at these locations. The overestimation of wind speeds results in strong mixing between cooler air over the island adjacent to the coast and warmer ocean air at night. As a result, the simulated air temperature is warmer than observed temperature (Figs. 22 and 24).

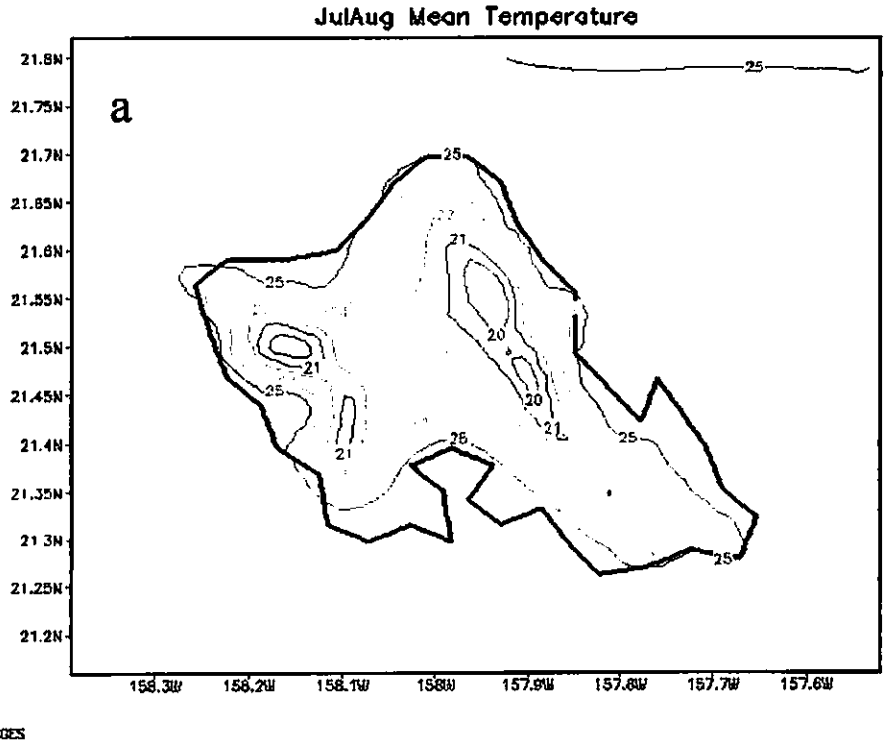

Figure 19a Simulated mean 10-m air temperature (°C) for July-August 2005.

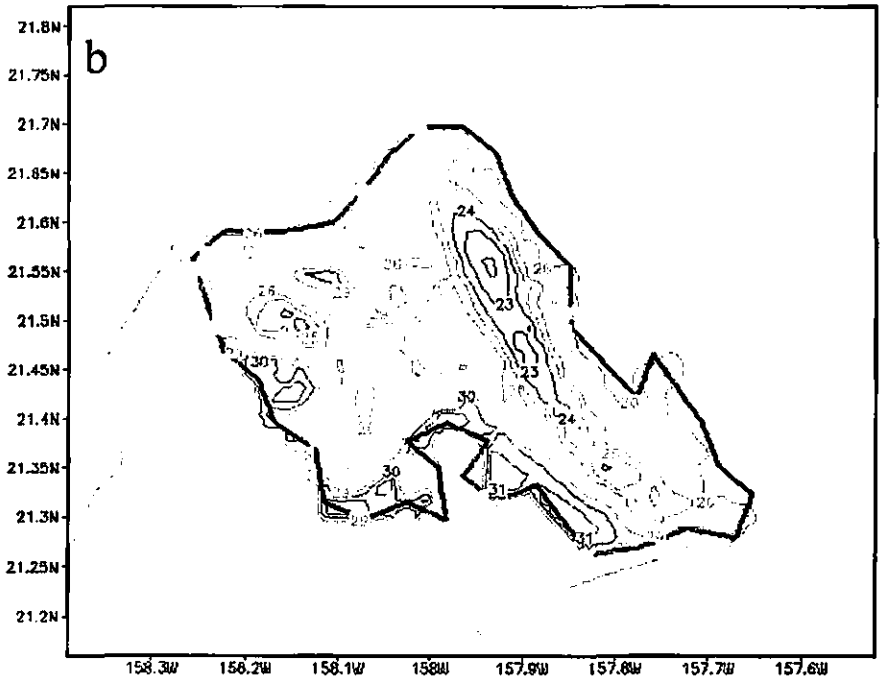

Figure 19b Simulated mean 10-m air temperature (°C) for July-August 2005 at 14HST.

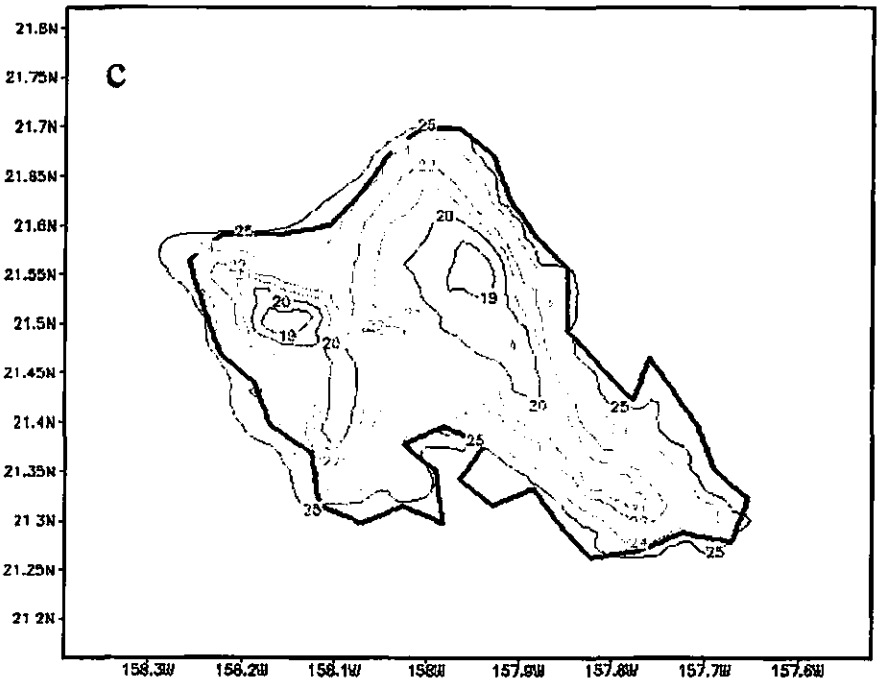

Figure 19c Same at Fig. 19a but for 05HST.

3.2.4.2 Surface dew point temperature and mixing ratio

The drying effect over the island of Oahu was discussed by Lavoie (1974). Lavoie stated that the reason for the drying effect stated in the work is caused by mixing between the low-level moist air over the island and dry air aloft (Lavoie, 1974), especially during the daytime. Another factor results in the air over the island of Oahu drier is descending trade winds aloft in the leeward side of the Ko'olau Mountains (Yang and Chen, 2003).

The simulated mean dew-point (Fig. 20a) and mixing ratio (Fig. 20d) for two summer month show low values of both dew point temperature and mixing ratio at the lee of the Ko'olau Mountains, over the Waianae Mountain area and over central Oahu, higher values occurs on the windward side of the Ko'olau Mountains. The dew point (19°C) on leeside of the Waianae Mountains and over the central Oahu are about 1.5 degrees lower than on the windward side of the Ko'olau Mountains and over the open ocean (20.5°C) (Fig. 20a). The lowest values of dew point temperatures are simulated at the top of the Waianae Mountains where the dew point temperatures (18°C) are 2.5°C lower than wind-ward values. The same trend is simulated in mixing ratio field. The moist area is on the windward side of the Ko'olau Mountains where the mixing ratio (15.6 g kg^{-1}) is not much different from that of the in-coming trade flow from the ocean (15.9 g kg^{-1}) (Fig. 20d).

Diurnal cycle of dew point temperature shows the air is moister at night than during the day. During the day, the dew point temperature values over central Oahu (18-18.5°C) are about 2-2.5°C lower than the values on the windward side of the Ko'olau Mountains. The lowest values occur over the top of the Waianae Mountains and are 3-3.5°C lower than the values on the windward side of the Ko'olau Mountains (Fig. 20b). In contrast, at night, the dew point temperatures over central Oahu and the Waianae Mountains are

higher than that during the day about 1°C (Fig. 20c). The lower dew point temperatures (dry air) during the day are probably due to the stronger vertical mixing as a result of day-time heating. The turbulence during the daytime brings drier air aloft to mix with low level air.

The error statistics of dew point temperatures at 11 stations (dew point temperature observations are not available at two stations, Bellows and Kii) are shown in Table 8b. The model tends to over (under) estimate dew point at night (during the day). The MAE varies from 1.4°C at night to 1.8°C at noon time. Both MAE and RMSE show lager values during the day than at night.

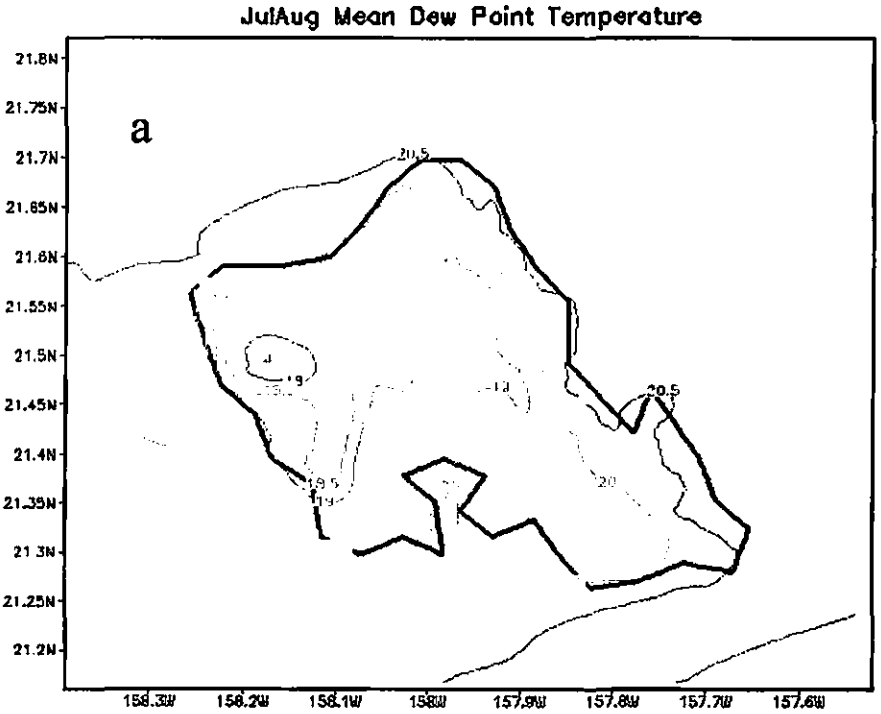

Figure 20a Simulated mean surface dew point (°C) for July-August 2005.

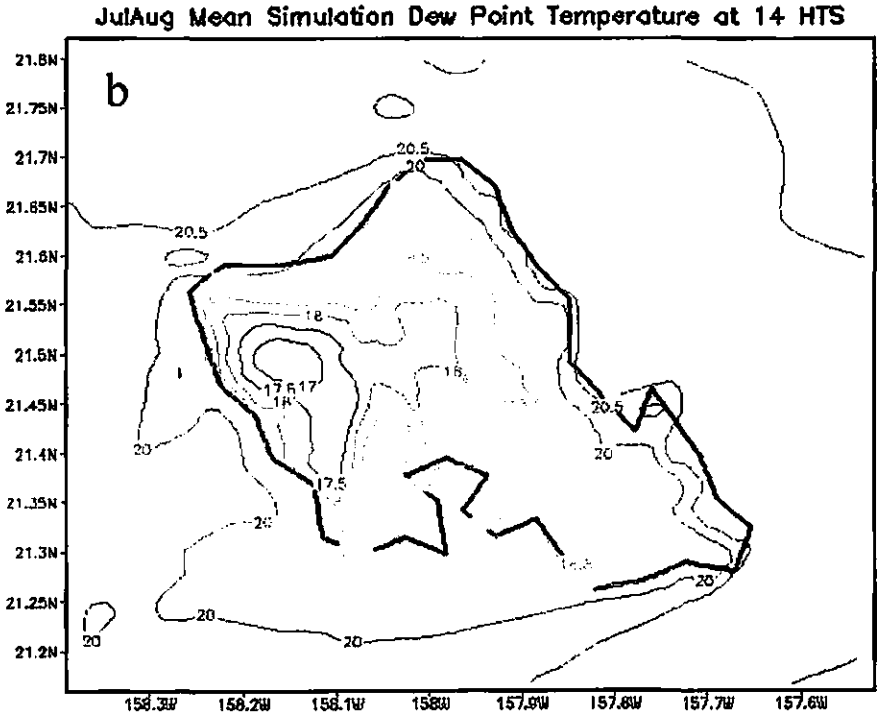

Figure 20b Same at Fig. 20a but for 14 HST.

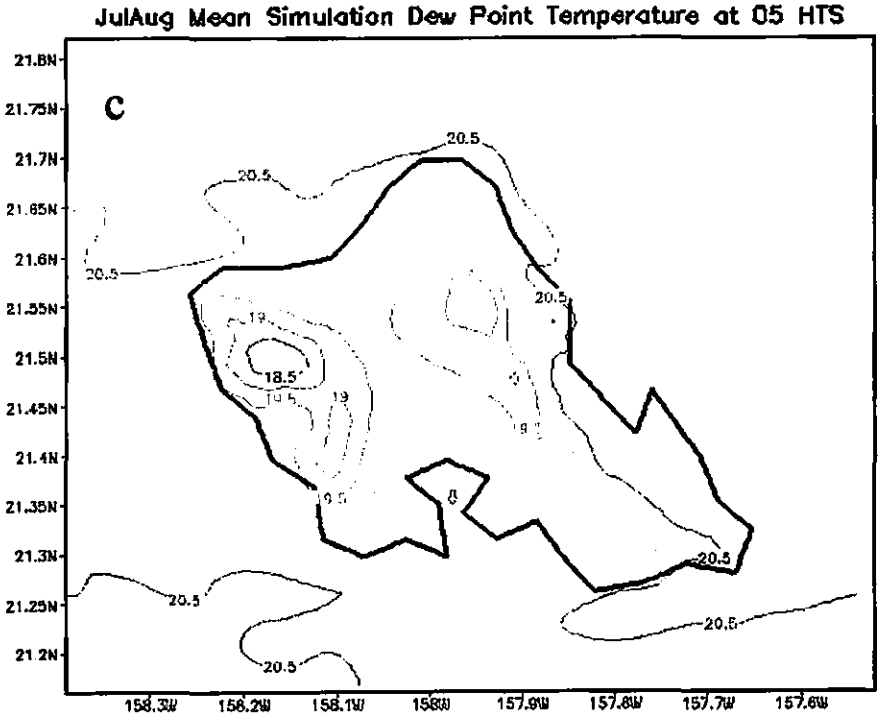

Figure 20c Same at Fig. 20a but for 05 HST.

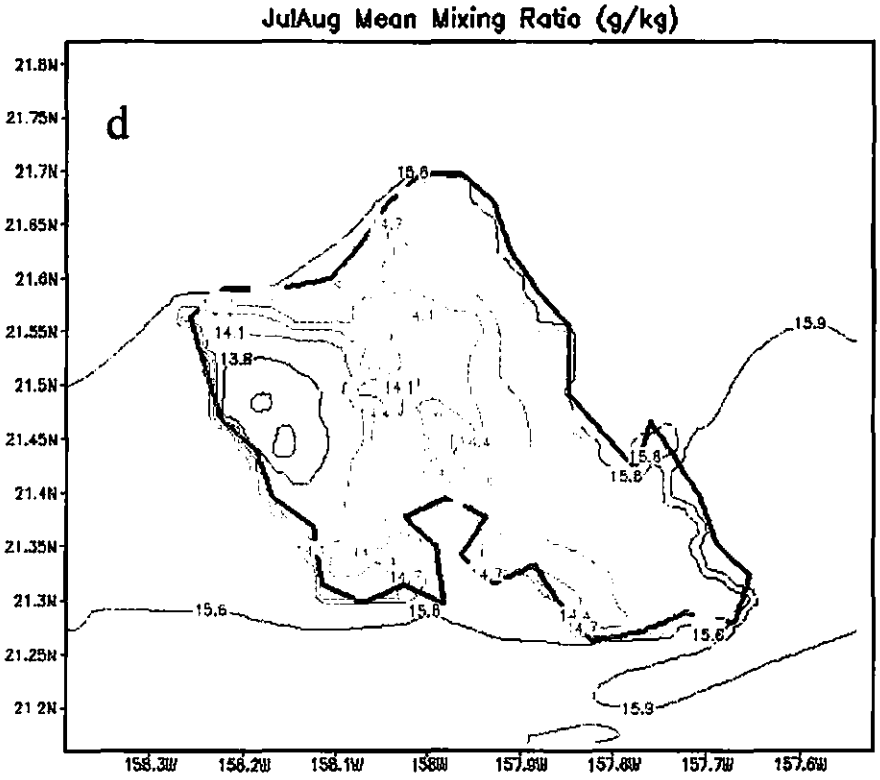

Figure 20d Same as Fig. 20a but for mixing ratio (g kg^{-1}).

Table 7 Error statistics of the 10-m air temperature at 13 hourly weather stations.

Station #	Station name	Station ID	BIAS (degree)	RMSE (degree)	MAE (degree)
1	Kaneohe MCB	PHNG	-0.1	1.0	0.7
2	Kalaeloa AP	PHJR	1.5	2.1	1.8
3	Honolulu AP	PHNL	-0.3	1.4	1.0
4	Dillingham	DLGH1	0	2.2	1.7
5	Bellows	BELH1	N/A	N/A	N/A
6	Kii	KFWH1	-1.0	1.4	1.1
7	Kahuku Training	KTAH1	-0.8	1.5	1.1
8	Kawailoa TA	KWLH1	-0.1	1.9	1.5
9	Makua Valley	MAPH1	-1.0	2.0	1.5
10	Makua Ridge	MKGH1	0	1.5	1.1
11	Schofield Barracks	SCBH1	0	1.7	1.3
12	Schofield East	SCEH1	0.7	1.9	1.4
13	Waianae Valley	WNVH1	-1.1	2.0	1.6

Table 8a Diurnal cycle of temperature errors (K) for 13 hourly Oahu stations.

	02HST	05HST	08HST	11HST	14HST	17HST	20HST	23HST
BIAS	0.4	0.4	0.0	-0.4	-0.3	-1.1	-0.3	-0.1
RMSE	1.4	1.5	1.5	2.1	2.2	1.9	1.2	1.2
MAE	1.1	1.2	1.2	1.8	1.8	1.6	0.9	1.0

Table 8b Diurnal cycle of dew point errors (K) at 13 hourly Oahu stations.

	02HST	05HST	08HST	11HST	14HST	17HST	20HST	23HST
BIAS	0.7	0.6	-0.7	-1.1	-1.0	-0.5	0.5	0.5
MSE	1.6	1.6	1.7	2.0	2.1	1.9	1.6	1.9
MAE	1.4	1.4	1.5	1.8	1.8	1.6	1.4	1.4

Table 9a Temperature errors (K) for 13 hourly Oahu stations at 05 HST.

Index	PHNG	PHJR	PHNL	DLGH1	BELH1	KFWH1	KTAH1	KWLH1	MAPH1	MKGH1	SCBH1	SCEH1	WNVH1
BIAS	0.2	2.6	-0.1	2.2	N/A	-0.4	-0.3	-1.3	-0.4	0.2	1.1	0.3	-0.8
RMSE	0.8	2.7	0.9	2.8	N/A	1.2	1.1	1.7	1.3	0.8	1.6	1.3	1.5
MAE	0.6	2.6	0.7	2.3	N/A	0.8	0.8	1.4	1.1	0.6	1.2	1.0	1.3

Table 9b Temperature errors (K) for 13 hourly Oahu stations at 14 HST.

Index	PHNG	PHJR	PHNL	DLGH1	BELH1	KFWH1	KTAH1	KWLH1	MAPH1	MKGH1	SCBH1	SCEH1	WNVH1
BIAS	0.0	0.1	0.3	-0.7	N/A	-1.3	-1.2	1.7	-1.4	0.1	-0.5	1.9	-2.0
RMSE	1.3	1.5	1.9	2.1	N/A	1.6	2.0	2.7	2.7	2.3	2.0	2.9	3.0
MAE	1.0	1.1	1.6	1.6	N/A	1.4	1.5	2.4	2.2	1.9	1.3	2.4	2.4

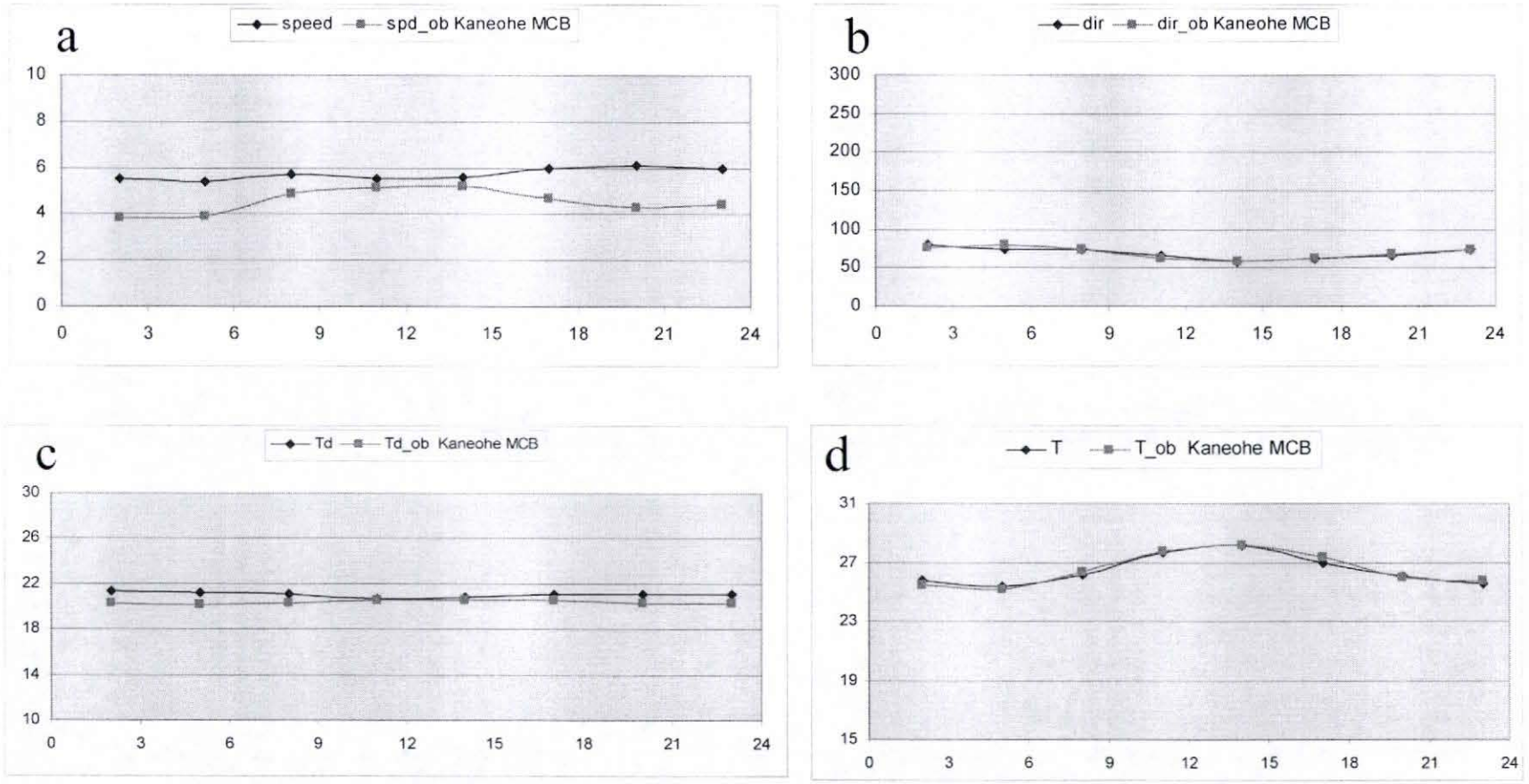

Figure 21 Simulated (lozenge) and observed (square) values at Kaneohe MCB (PHNG) of (a) wind speed (m s^{-1}); (b) wind direction (degrees); (c) dew point (^{o}C); and (d) air surface temperature (^{o}C).

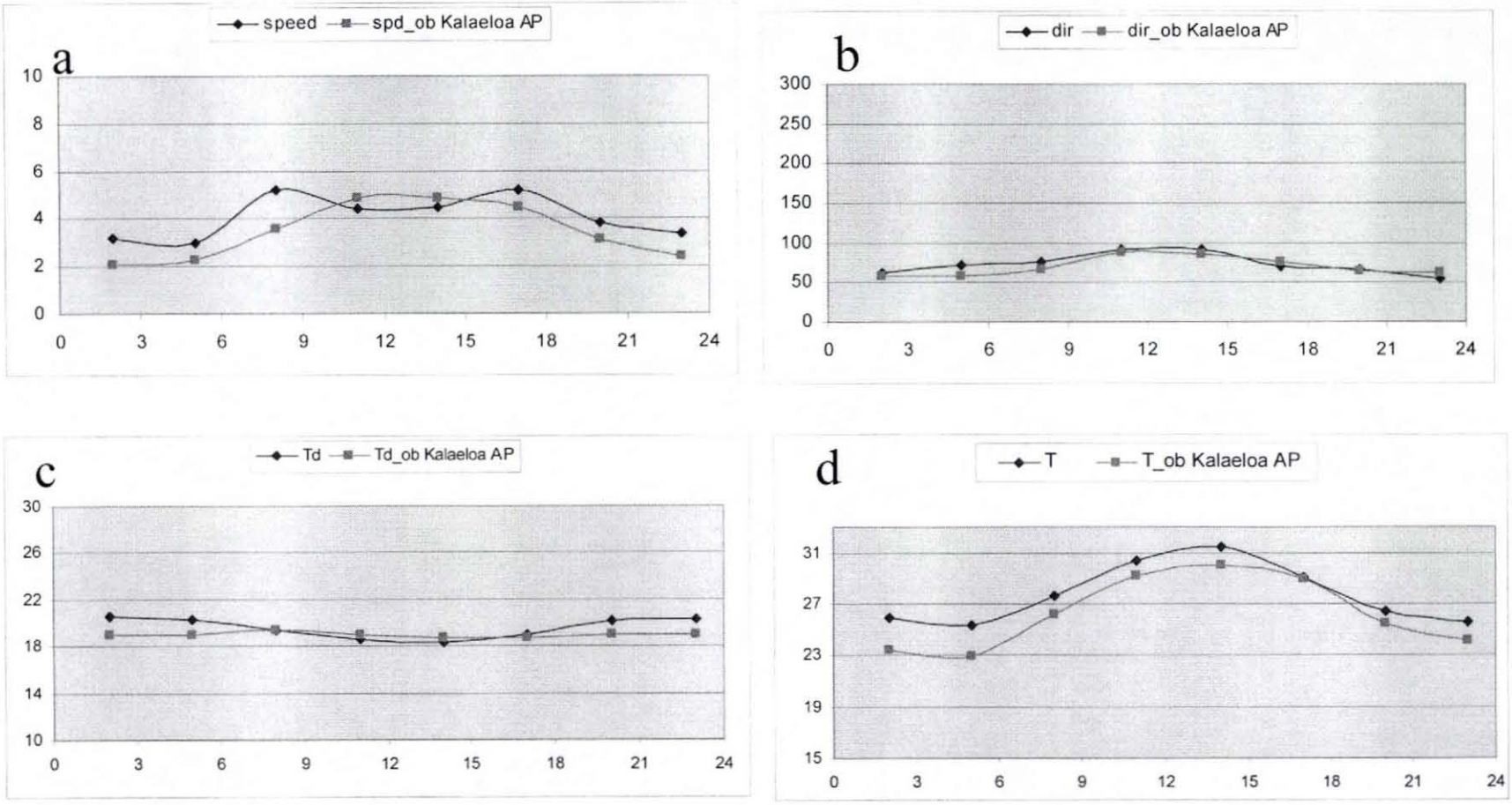

Figure 22 Same as Fig. 21 but for Kalaeloa AP (PHJR) station.

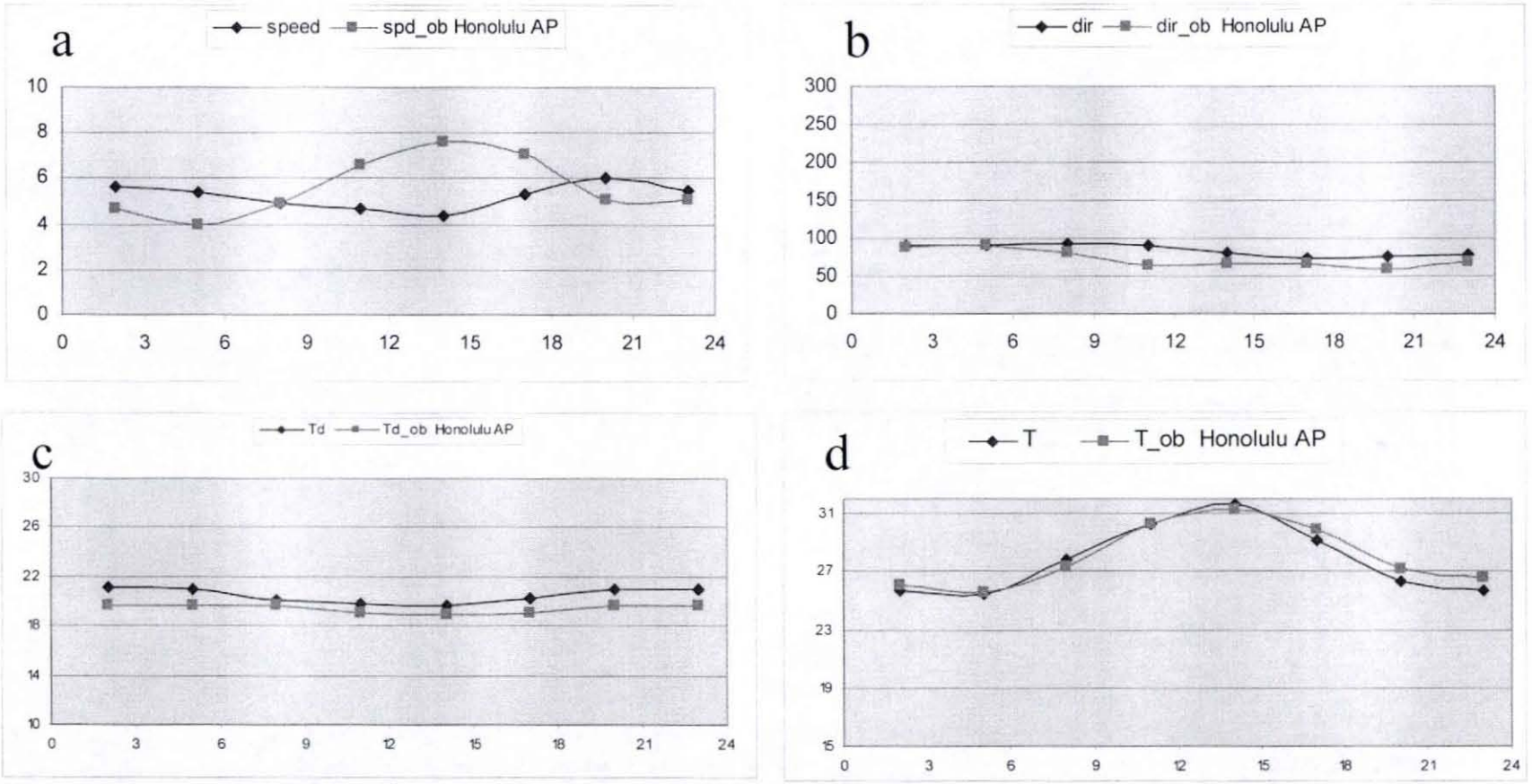

Figure 23 Same as Fig. 21 but for Honolulu AP (PHNL) station.

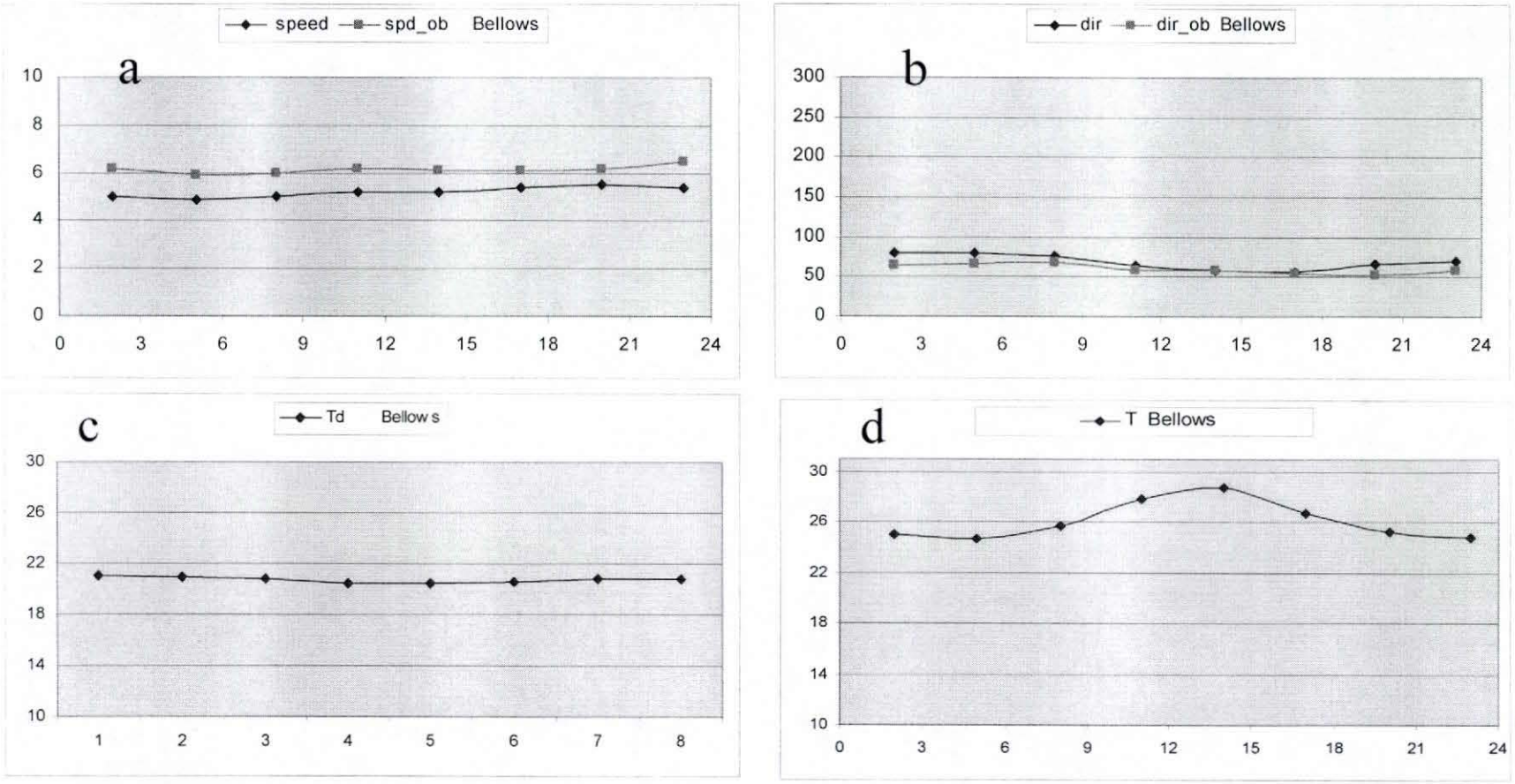

Figure 24 Same as Fig. 21 but for Dillingham (DLGH1) station.

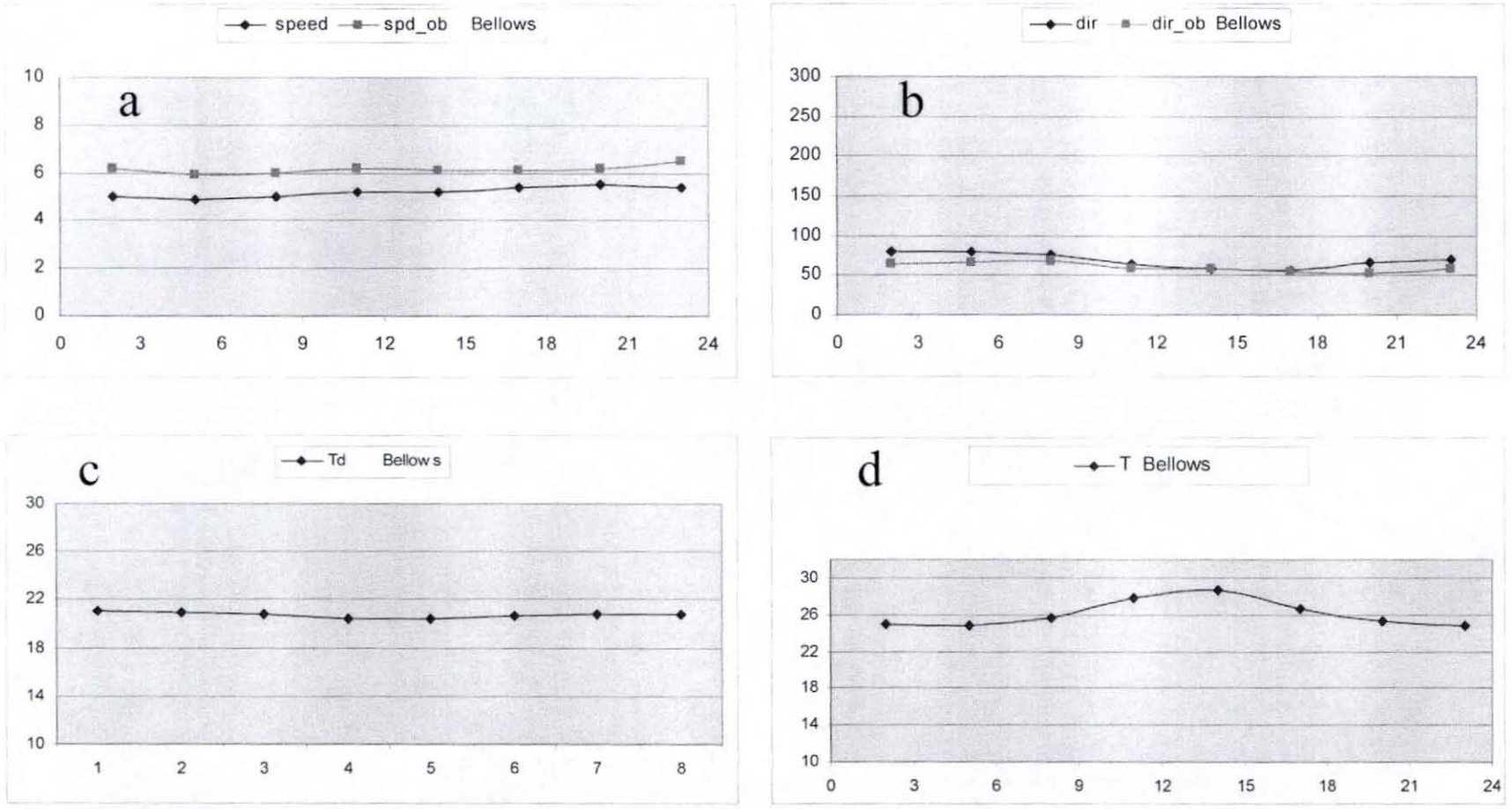

Figure 25 Same as Fig. 21 but for Bellows (BELH1) station (no dew point and temperature).

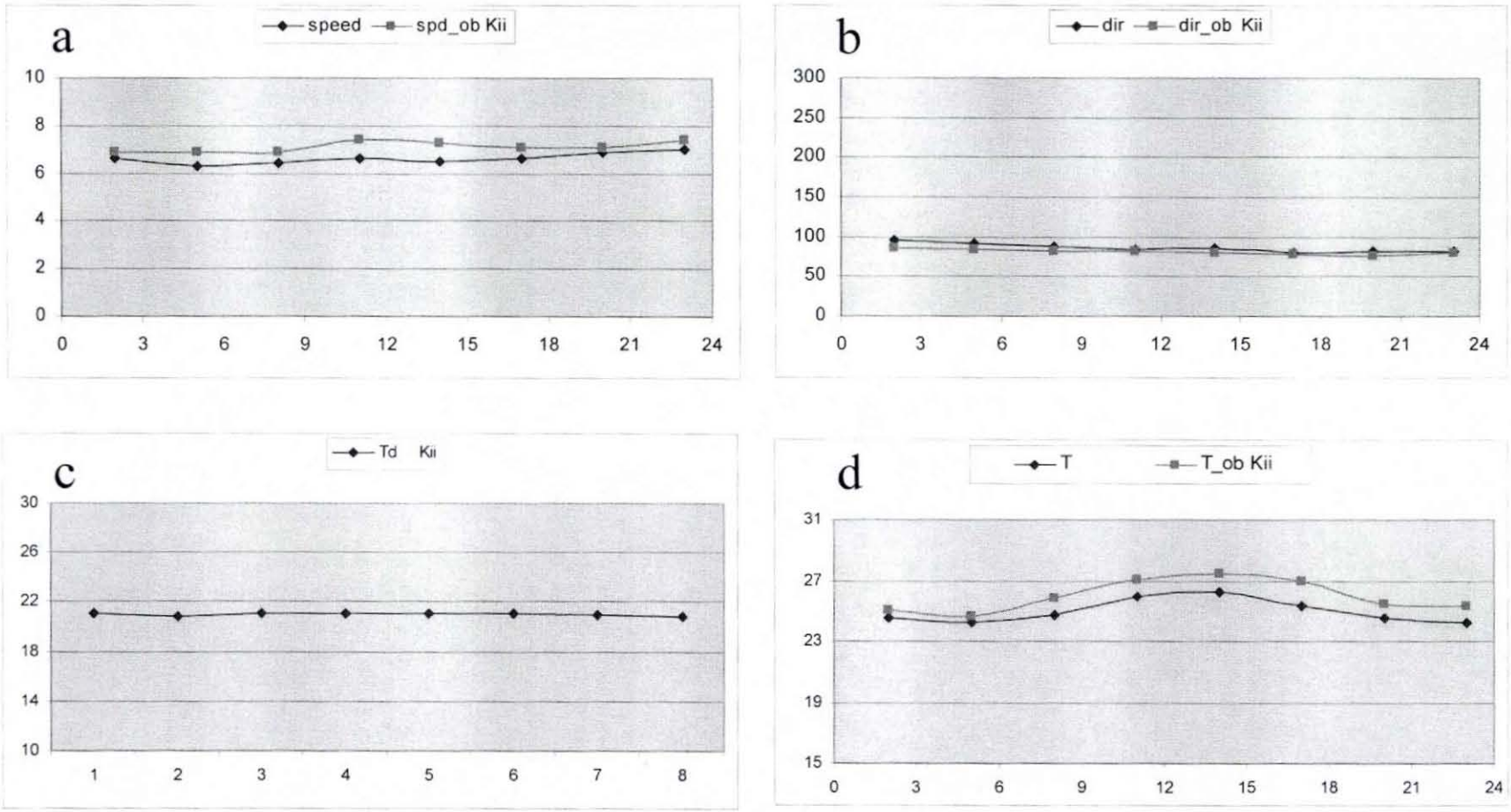

Figure 26 Same as Fig. 21 but for Kii (KFWH1) station (no dew point).

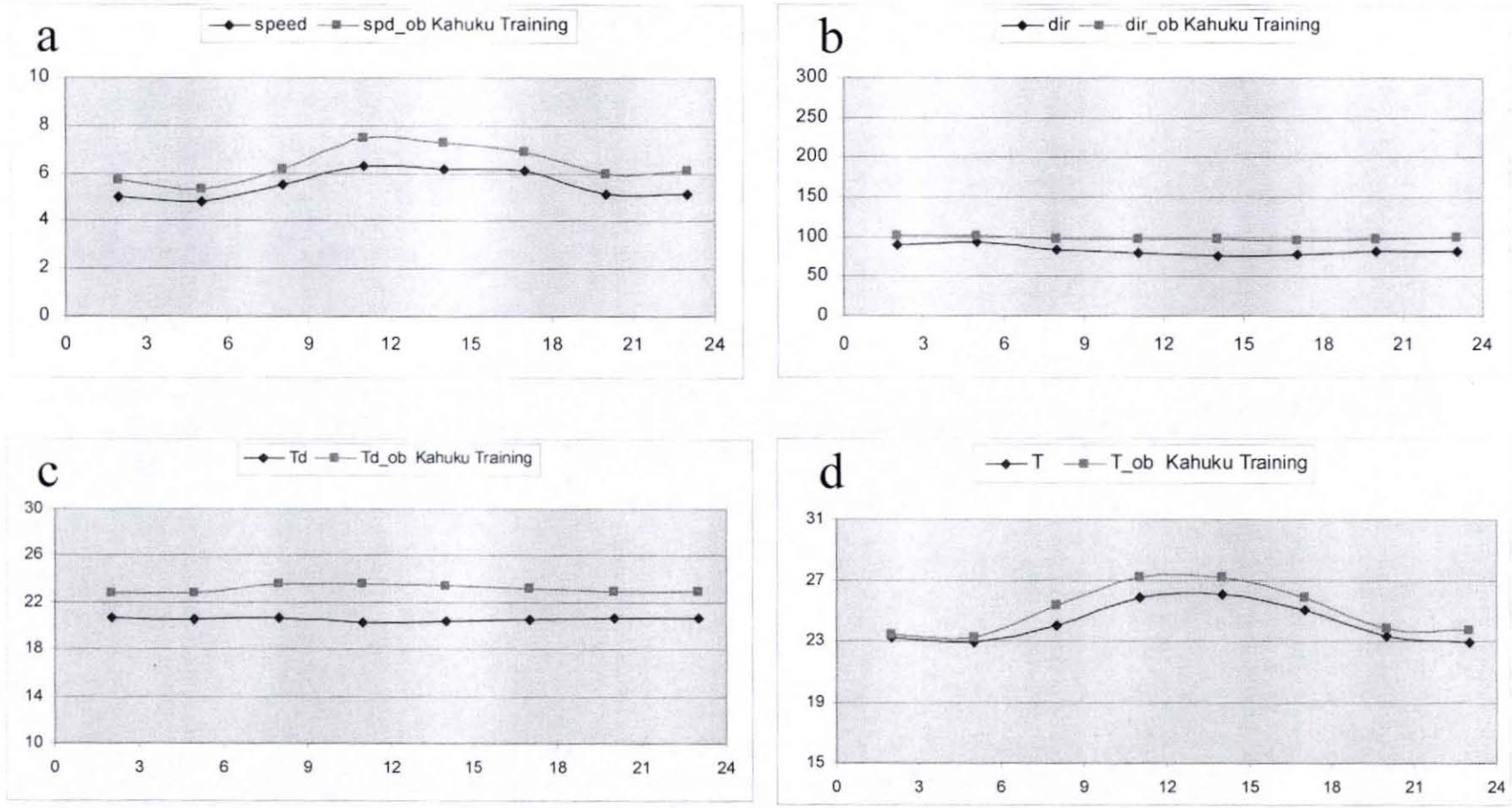

Figure 27 Same as Fig. 21 but for Kahuku Training (KTAH1) station.

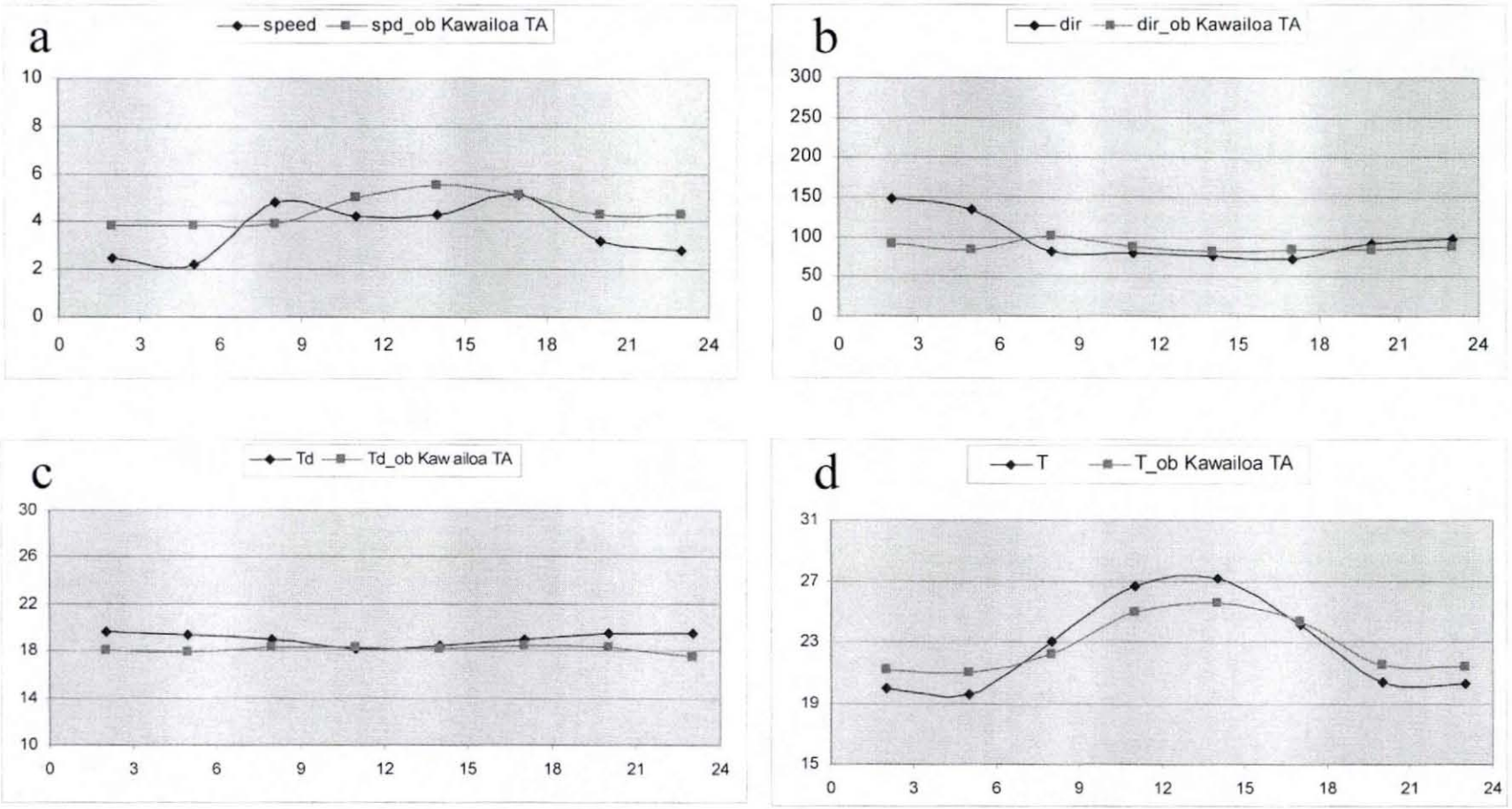

Figure 28 Same as Fig. 21 but for Kawailoa TA (MAPH1) station.

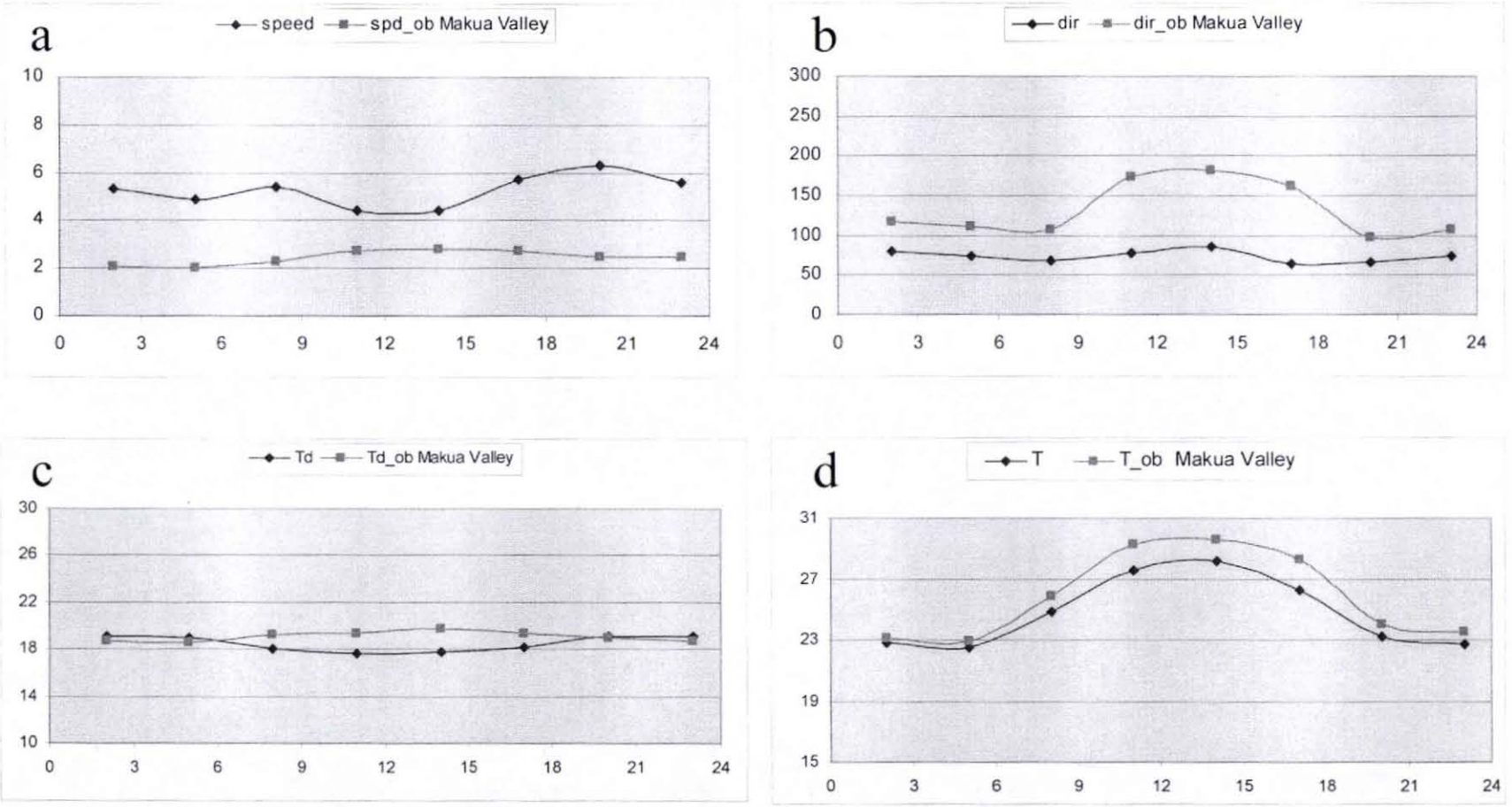

Figure 29 Same as Fig. 21 but for Makua Valley (MAPH1) station.

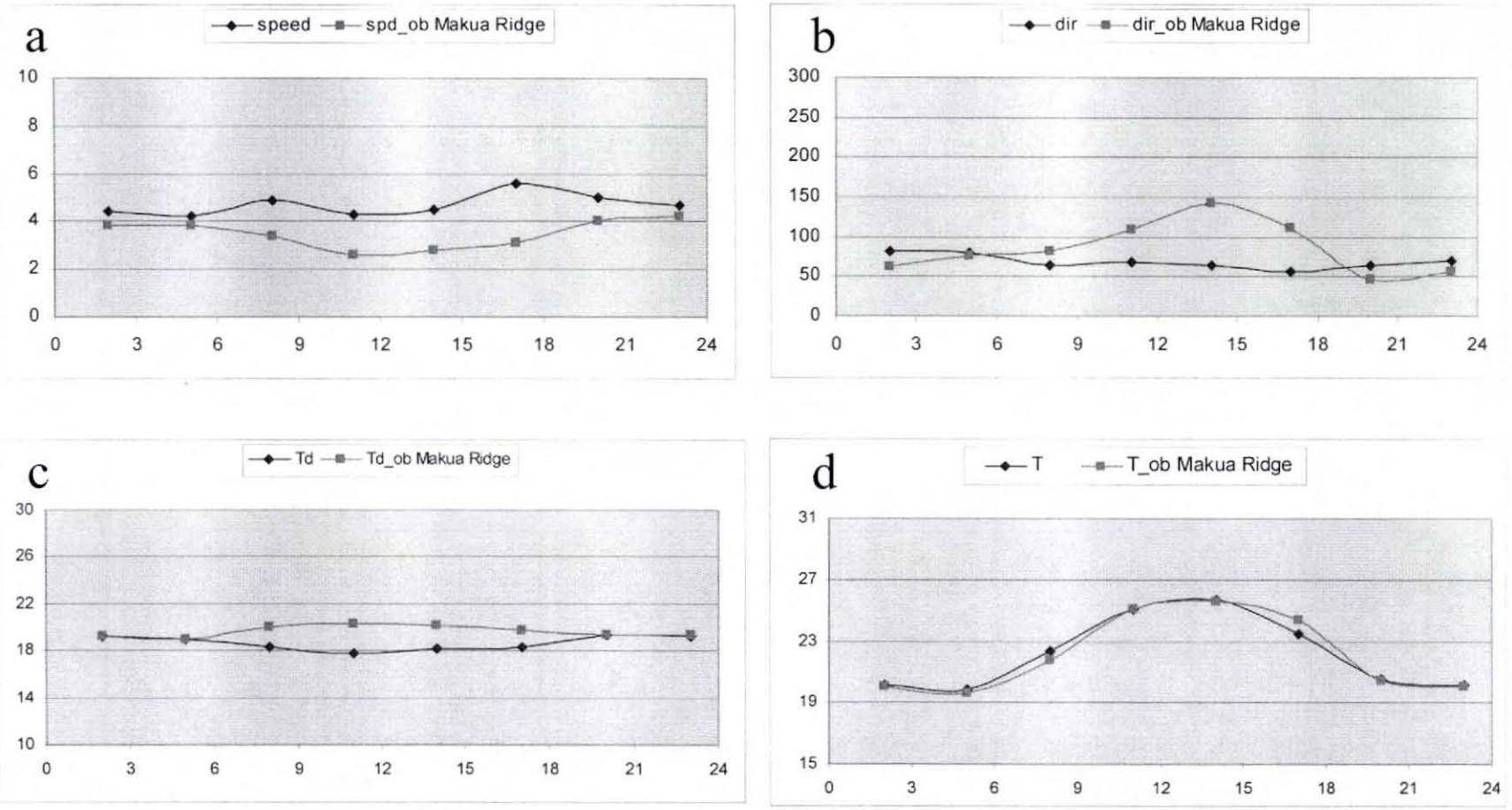

Figure 30 Same as Fig. 21 but for Makua Ridge (MKGH1) station.

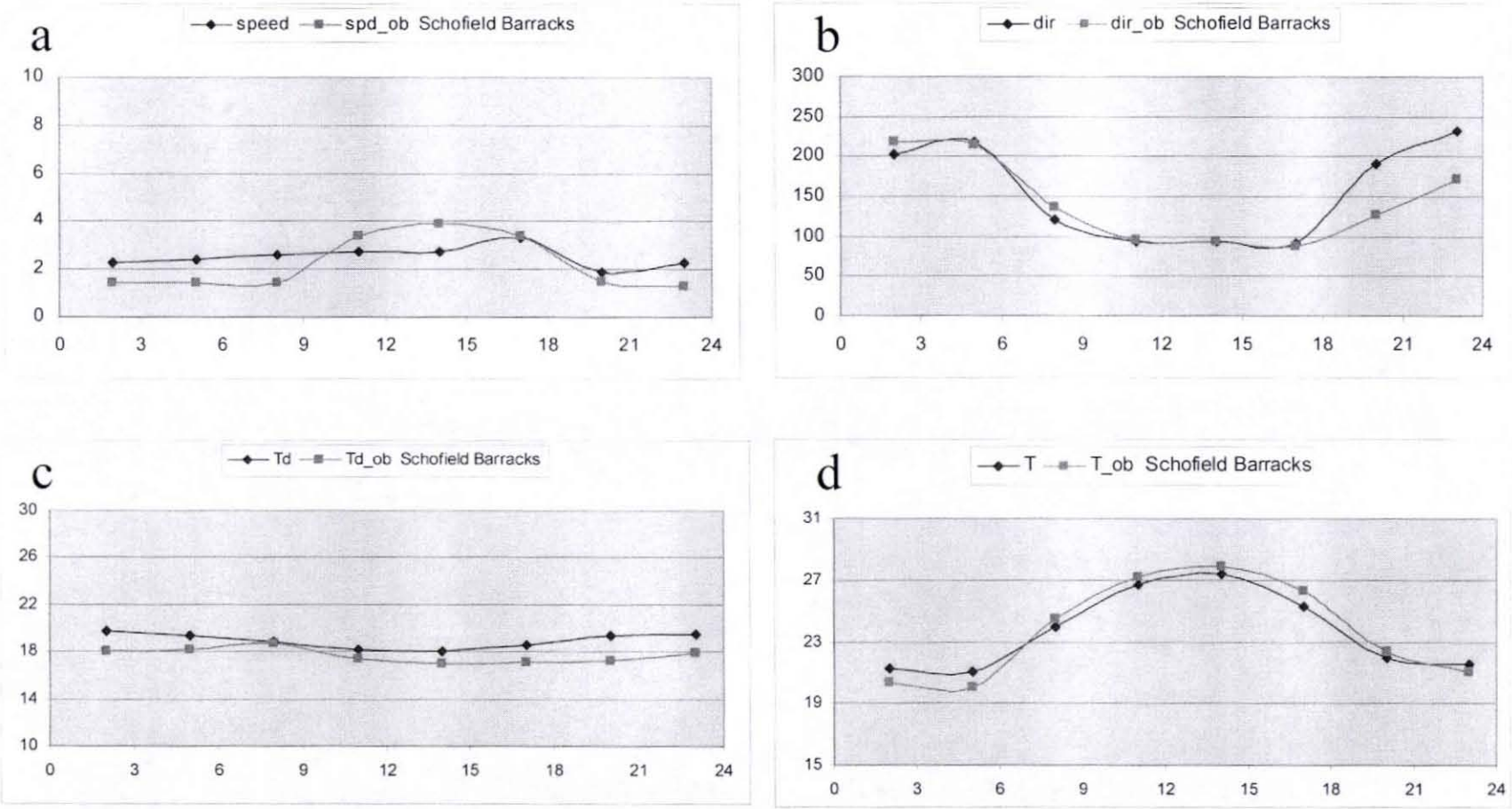

Figure 31 Same as Fig. 21 but for Schofield Barracks (SCBH1) station.

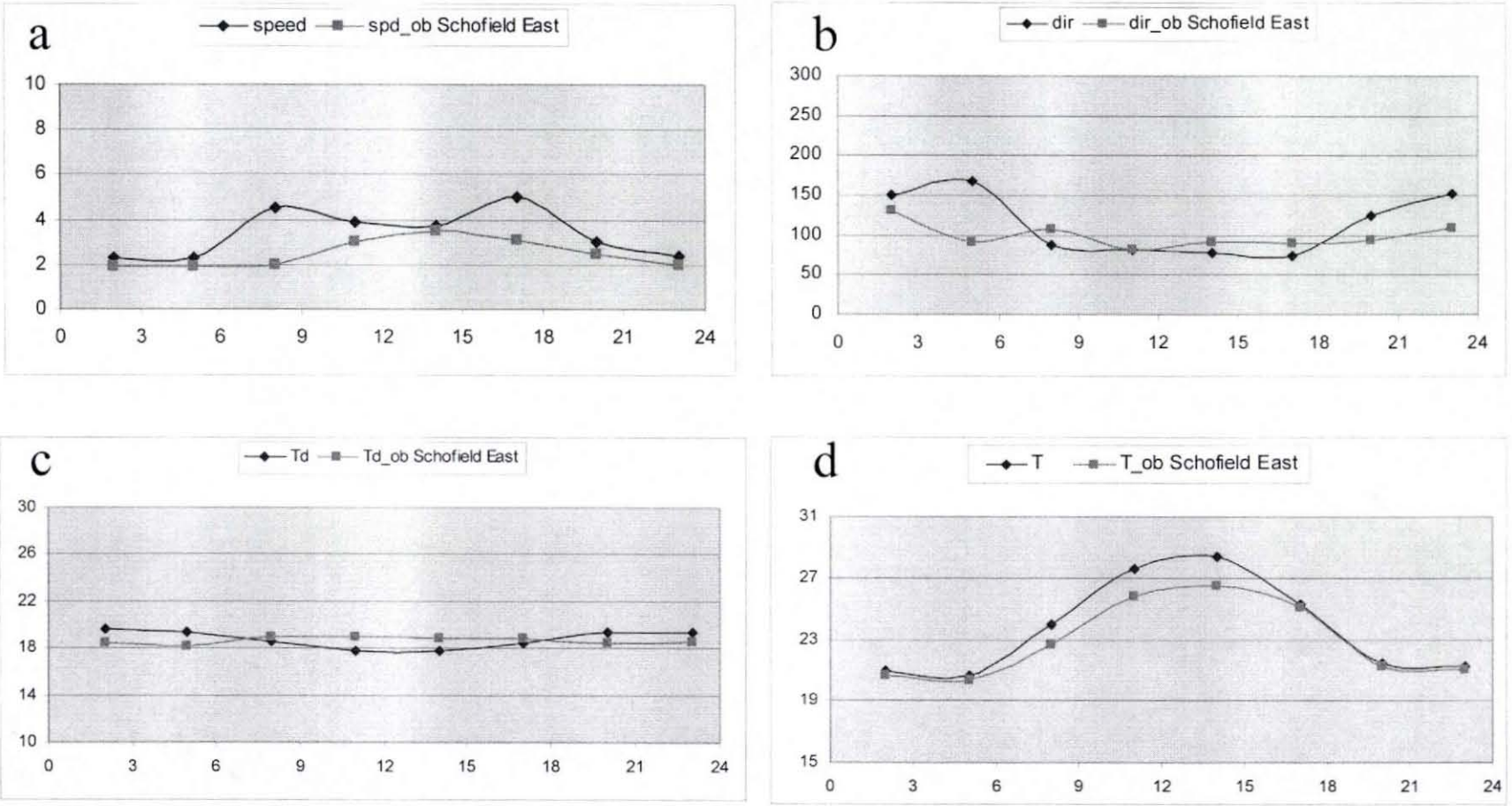

Figure 32 Same as Fig. 21 but for Schofield East (SCEH1) station.

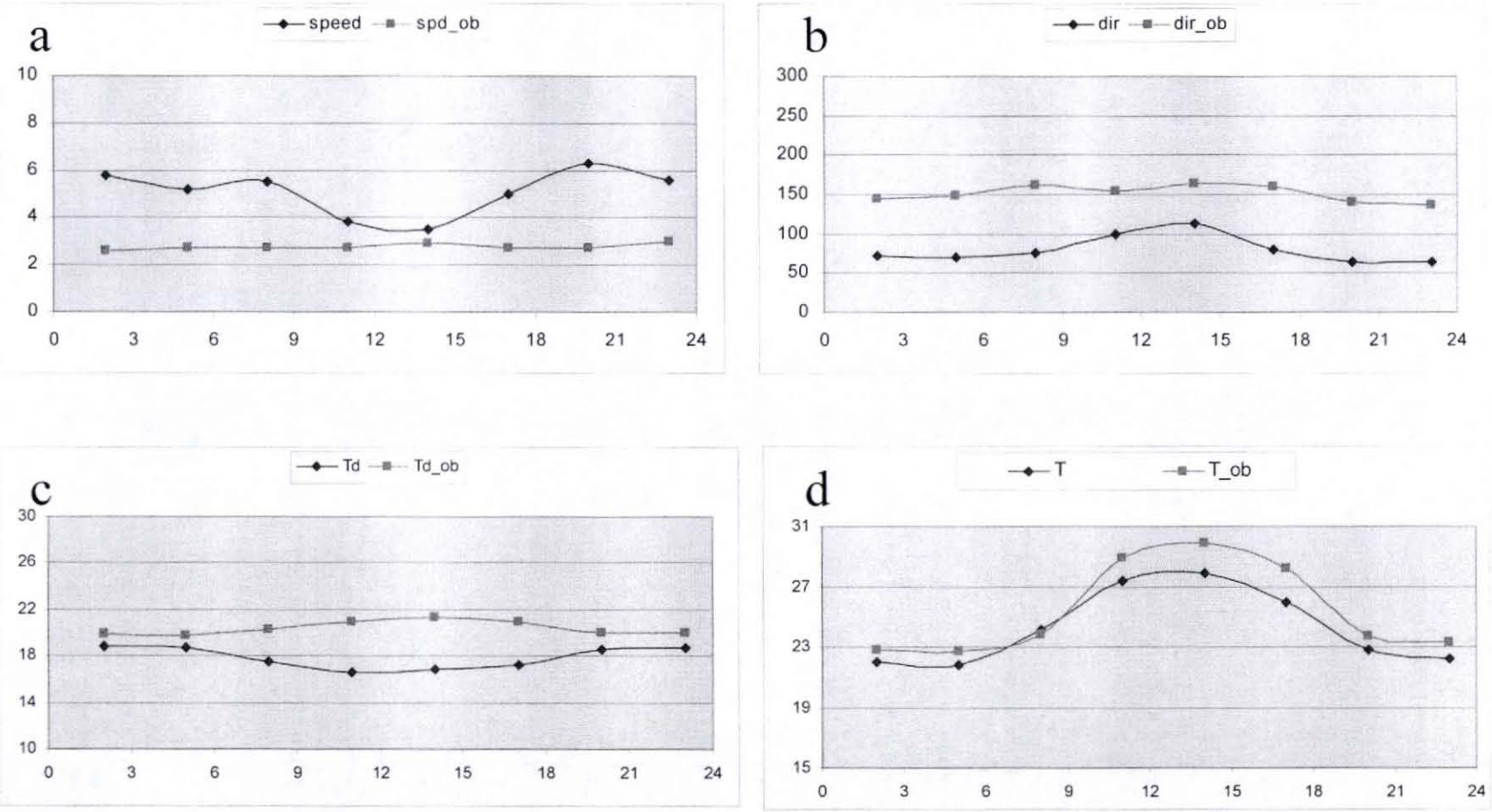

Figure 33 Same as Fig. 21 but for Waianae Valley (WVNH1) station.

3.3 Sensitivity tests

3.3.1 *Sensitivity test designs*

Previous studies (Leopold, 1948; 1949; Carbone et al., 1998; and others) and simulation results of this study showed that the island play a crucial role on island airflow and rainfall. Leopold (1949) found that for the mountains with tops above the trade-wind inversion, the trade-wind flow moves around the mountains. In contrast, low mountains allow the trade-wind aloft to move over the mountain tops. He also stated that rainfall regime over the islands is affected by the interaction between land-sea breezes and trade winds. In this research, terrain height and landuse of the two mountain ranges, the Ko'olau and the Waianae Mountains of the Oahu Island, are changed in the model to investigate the roles of terrain and landuse properties on weather and airflow of Oahu.

Four sensitivity tests with no mountains, no Ko'olau Mountains, no Waianae Mountains, and urbanization are conducted. The first case, no mountain case is employed to evaluate the effects of terrain on airflow and rainfall. The next two cases, no Ko'olau, no Waianae, are conducted to assess the roles of each mountain on weather and airflow of Oahu. The last case, urbanization, is used to investigate the effect of urbanization, e.g., the landuse over the entire island is specified as urban, on weather and airflow. The sensitivity tests are run for 36 hours, 24 hours of simulation from 12^{th} hour (00 HST) to 36^{th} hour (24 HST) for the 09 August, 2005 case. 09 August, 2005 is selected simply because that day is a normal trade-wind day. The wind speed at 12Z 09 August upstream point (21° N, 152° W) is 7.7 m s^{-1} (wind speed at 00Z is 7.3 m s^{-1}) and the wind direction is 86 degrees (Fig. 2).

For the no mountain case, both the Ko'olau Mountains and the Waianae Mountains are removed. To remove the mountains, terrain height at any grid points greater than 5 m is replaced by the value of 5 m. The landuse properties are unchanged.

The effects of the Ko'olau Mountains and the Waianae Mountains on island airflow and weather are tested in no Ko'olau and no Waianae cases. In these cases, either the terrain of the Ko'olau Mountains or the Waianae Mountains is removed without changes in landuse properties. The boundary used to separate between Ko'olau and Waianae is a line through central Oahu. Specifically, the line is drawn through two selected points: (21.2°N, 157.9°W) and (21.8°N, 158.21°W) (Fig. 34).

The altitude at the cut line at central Oahu is grater than 200 m (Fig. 34). The straight cut at the line will create a wall of 200 m at the boundary when one of the two mountains is removed. To eliminate the wall boundary at the cut position that may create unexpected spurious turbulences at the boundary in the model, the terrain height of mountain adjacent to the boundary is smoothly removed by a combination between real terrain height and a parabola function:

$$Z_{new} = \begin{cases} 5 & if\ x > d \\ \dfrac{Z_{org}}{2}\left(\dfrac{d-x}{d}\right)^2 & if\ x \le d \end{cases}$$

Here d is the threshold of the distance from the cut line to the point in the region where terrain height is smoothed. In this case, the selected value of d is 5 km; x is the distance from the smoothed point to the cut line (Fig. 34); Z_{org} and Z_{new} are the original real terrain height and new terrain height (m) in which either the Ko'olau or the Waianae Mountains are smoothly removed. The terrain height for no Ko'olau and no Waianae cases are shown in Figures 35a, and 35b, respectively.

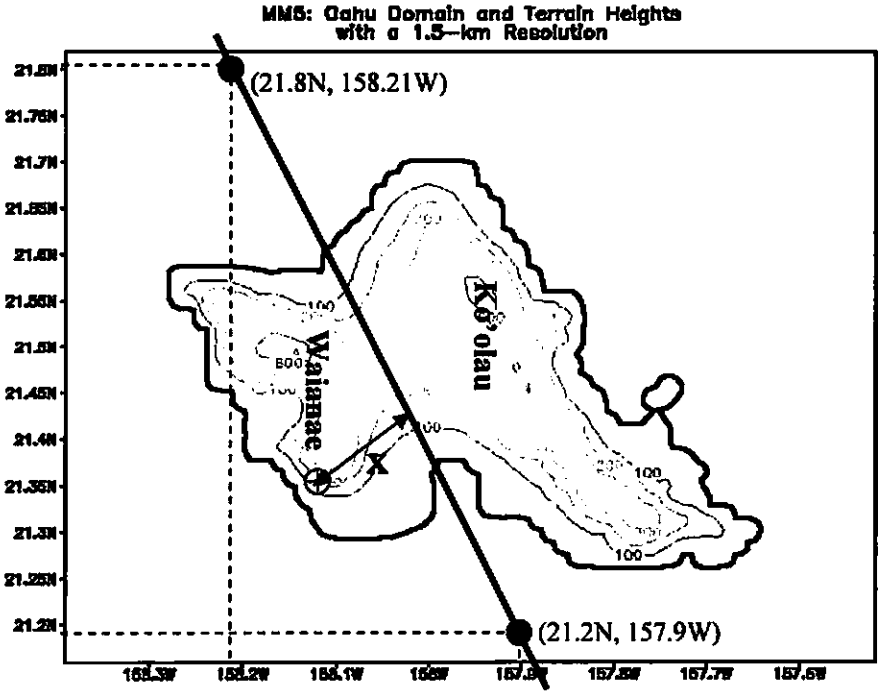

Figure 34 Position of boundary between the Ko'olau and the Waianae mountains.

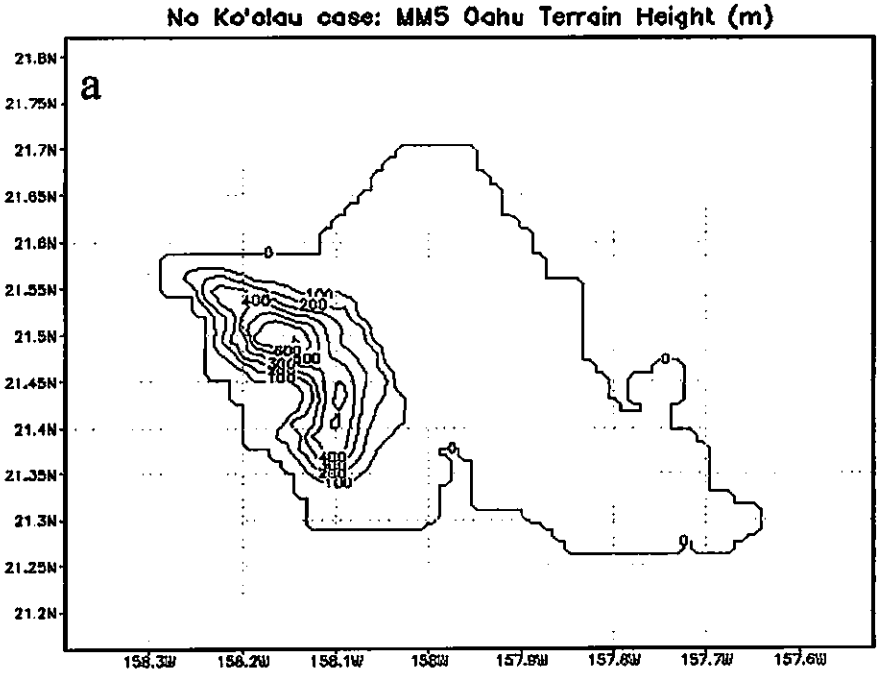

Figure 35a Terrain for the no Ko'olau case.

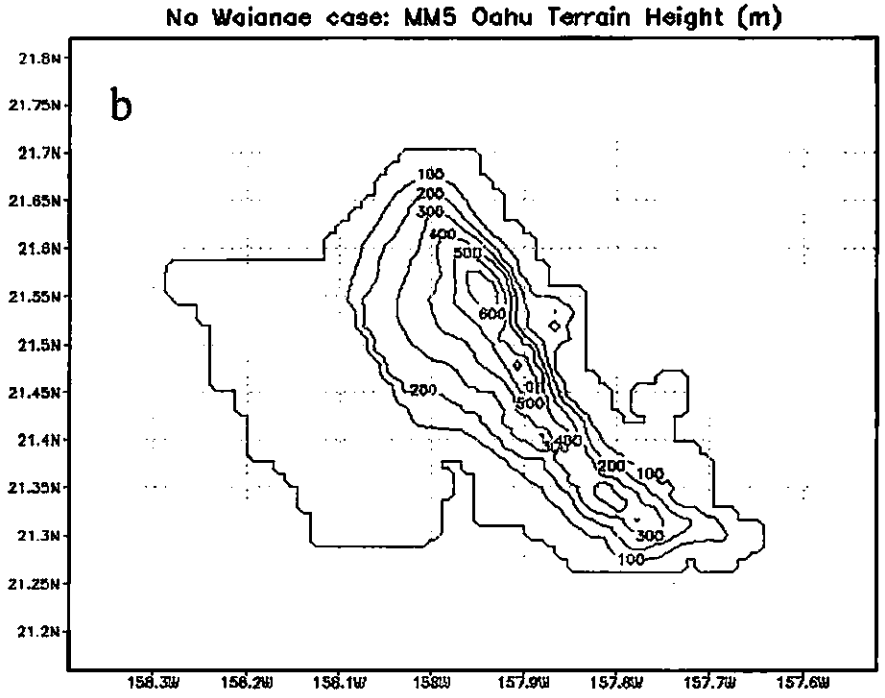

Figure 35b Terrain for the no Waianae case.

3.3.2 Sensitivity test results

3.3.2.1 *Island scale airflow*

The island-scale airflow for each sensitivity test is compared with the control run case (CRTL) at 05 HST and 14 HST (Fig. 36) to investigate the effects of terrain and landuse on the island-scale airflow.

a. No mountain case (NM)

For the no mountain case (NM), the wind directions over the island are rather uniform at 05 HST with weaker wind speed over the island interior than over the open ocean upstream (Figs. 37a, and 37c). When the mountains are removed, there are neither mountain winds at night nor the complete reversal of wind direction along the leeward coast of the Waianae Mountains in the afternoon hours. At the windward coast

offshore of the Ko'olau Mountains, wind speeds (>7.5 m s^{-1}) (Figs. 37a and 37c) are stronger than in CRTL (5-6.5 m s^{-1}) (Figs. 36a and 36c) because the island blocking effects are weakened when the terrain is removed. Over the island interior, wind speeds in the NM case (2-3 m s^{-1}) are significantly weaker than over open ocean upstream (>7 m s^{-1}) (Figs. 37a and 37c). Although there is no terrain, friction and a stable condition due to nighttime cooling over the island result in the wind speeds over the entire island 50% smaller than over the open ocean.

In the afternoon, the wind speeds at central Oahu and along the windward coast are stronger. While wind speeds at central Oahu in the CTRL vary from 3.5-5 m s^{-1} (Figs. 36b and 36d), the wind speeds at these areas increase to 4.5-6 m s^{-1} in the NM case (Figs. 37b and 37d). Over the windward coast, wind speeds in the CTRL and in the NM case vary from about 5-6m s^{-1} (Figs. 36b and 36d) and 6-7 m s^{-1} (Figs. 37b and 37d), respectively. Decrease in island blocking effects in the NM case is the reason for increase in wind speeds over central Oahu and along the windward coast.

In the NM case, the onshore flow (Fig. 37b) and a weak wind speed region off the Waianae coast (Fig. 37d) still exist at 14 HST as a result of island heating. The existence of the onshore flow off the Waianae coast in the NM case attests that the onshore flow in the afternoon is a result of both the wake circulation off the lee-side coast and island heating. However, with decrease in island blocking effect in the NM case, the weak wind speed (wind speed less than 4 m s^{-1}) region off the lee-side coast of the Waianae Mountains is smaller than in the CTRL. In the CTRL, the weak wind speed region extends from 21.23° N to 21.55° N (Fig. 36d). The region in the NM case extends from 21.27°N to 21.55°N (Fig. 37d).

Along the vertical cross sections, the simulated zonal winds aloft at night in the NM case are almost similar to over the open ocean (Fig. 42a) with no strong winds aloft as found in the CTRL. In the afternoon, effects of island on wind speed in the NM case are weaker than in the CTRL. The region of onshore flow aloft at 14 HST only extends about 50 hPa from the surface offshore of the Waianae Coast (Fig. 42b). Meanwhile it extends about 80 hPa in the CTRL (Fig. 41b).

b. No Waianae case (NW)

At night, winds are stronger on the leeward side of the Ko'olau Mountains. The mountain winds over the Waianae area are replaced by wake circulation (Fig. 38a) leeward side of the Ko'olau Mountains. When the Waianae Mountains are removed, downslope winds on the leeside of the Ko'olau Mountains are enhanced. In the region between 21.4°N to 21.55°N over the leeward slopes of the Ko'olau Mountains, wind speeds (5-6 m s^{-1}) (Figs. 38a and 38c) in the NW case are about 1 m s^{-1} stronger than in the CTRL (4-5 m s^{-1}) (Figs. 36a and 36c). Without the Waianae Mountains, the region of maximum wind (> 11 m s^{-1}) aloft over the leeside slopes of the Ko'olau Mountains is greater than in the CTRL (Fig. 41a) extends westward to the central Oahu (Fig. 43a).

The surface mountain wind regime in the CTRL over the Waianae Mountains area at night is replaced by a wake circulation on the leeside of the Ko'olau Mountains in the NW case with a area of westerly winds extending from the Waianae Coast to the central Oahu at 21.5°N (Figs. 38a and 38c). The speeds of the surface westerly flow at the wake reach 2 m s^{-1} (Fig. 38a). The vertical cross section of the simulated zonal wind (Fig. 43a) shows that the westerly flow shown in Figure 38a in the NM case at night only exists at the surface with easterly winds aloft over the entire island.

In the afternoon, the NW case shows stronger wind speeds over the windward coast of the Ko'olau Mountains (Fig. 38b). Without the Waianae Mountains, the simulated winds aloft over the leeside slopes of the Ko'olau Mountains are stronger in the NW case (Fig. 43b) than in CRTL (Fig. 41b). The surface wind speeds along the windward coast of the Ko'olau Mountains (5-6 m s^{-1}) in the NW case (Fig. 36d) are stronger than in the CTRL (4-5 m s^{-1}) (Fig. 38d). In addition, at 14 HST, vertical extent of the westerly onshore flow decreases in the NW case (Fig. 43b). The westerly wind region extends to 900 hPa in the CTRL (Fig. 41b). It only extends to 975 hPa in the NW case (Fig. 43b).

c. No Ko'olau case (NK)

For the NK case, without blocking effects of the Ko'olau Mountains, no mountain winds on the eastern slops of the Waianae Mountains (Fig. 39a) at night. In addition, the surface wind speeds (8-10 m s^{-1}) (Figs. 39a and 39c) on the western slopes of the Waianae Range are stronger than in the CTRL (<3 m s^{-1}) (Figs. 36a and 36c). The easterly wind speeds (8-10 m s^{-1}) on the western slops of the Waianae Mountains in the NK case also exceed the value (7 m s^{-1}) over the open ocean upstream (Figs. 39a and 39c). The winds aloft at night over the leeside of the Waianae Mountains also significantly increase when in the NK case. At 05 HST, the maximum wind speeds aloft over the leeside of the Waianae Mountains increase from 10 m s^{-1} in the CTRL (Fig. 41a) to 11 m s^{-1} in the NK case (Fig. 44a). Moreover, the region of high wind speed aloft (> 10 m s^{-1}) more extends in the NK case (Fig. 44a). These features are caused by a combination of trade-wind flow and offshore flow along the Waianae coast at night when the of the Ko'olau Mountains are removed.

During the day, stronger trades along the windward coast and over central Oahu are simulated for the NK case. Because of no blocking effects of the Ko'olau Mountains, the wind speeds along the windward coast (5-6 m s^{-1}) in the NK case (Figs. 39b and 39d) are about 1 m s^{-1} stronger than in the CTRL (4-5 m s^{-1}) (Figs. 36b and 36d). In addition, wind speeds on windward slope of Waianae also increase from 3-4.5 m s^{-1} in the CTRL (Figs. 36b and 36d) to 4-5.5 m s^{-1} in the NK case (Figs. 39b and 39d). The increase is probably caused by stronger wind speed aloft at the same level with grid points on the slope in the NK case (Fig. 44b). Wind speeds aloft over the windward side of the Waianae Mountains increase from 4-5 m s^{-1} in the CTRL (Fig. 41b) to 5-6 m s^{-1} in the NK case (Fig. 44b). Without blocking effect of the Ko'olau Mountains, wind speeds at the leeside slopes of the Waianae Mountains increase from 4-5 m s^{-1} in the CTRL (Fig. 41b) to over 6 m s^{-1} in the NK case (Fig. 44b). With strong easterly winds aloft, the vertical extent of the westerly winds at wake circulations leeward side of the Waianae Mountains decrease from 900 hPa in the CTRL (Fig. 41b) to 940 hPa in the NK case (Fig. 44b).

d. Urbanization case (UB)

At night, urbanization results in weaker wind speeds over central Oahu and the leeside of the Ko'olau Mountains. The wind speeds in these areas vary from 2-6 m s^{-1} in the CTRL (Figs. 36a and 36c). In comparison, the corresponding values in the UB case only vary from 2-5 m s^{-1} (Figs. 40a and 40c). The increase in stability at night as a result of more significant nocturnal cooling and the increase in roughness length in urban areas are two main factors that account for weaker wind speed over land. At night, wind speed at the top windward side of the Waianae Mountains reach 8 m s^{-1} in the CTRL (Fig. 41a). In the UB case, the value decreases to 7 m s^{-1} (Fig. 45a).

During the day, more significant onshore flows along the Waianae lee-side coast are simulated in the UB case due to the increase in island heating. The maximum onshore flow off the Waianae coast in the CTRL case (Figs. 36b and 36d) is about 4.5 m s^{-1}. This value increases to 5 m s^{-1} in the UB case (Figs. 40b and 40d). Furthermore, the area of the onshore flow is larger in the UB case than in the CTRL. The onshore flows are more significant in the UB case than in the CTRL because of the increase in island heating during the day due to urbanization.

3.3.2.2 Rainfalls *and 2-m surface air temperature*

In this section, the effects of urbanization on 2-m surface air temperature are investigated. The simulated total rainfall accumulation for 09 August 2005 in each sensitivity test is compared with that of the CTRL case to investigate the effects of terrain and landuse on total rainfall.

At 14 HST, urbanization results in higher temperature about 1 degree over Oahu. At central Oahu, the temperature is around 299 K in the CTRL (Fig. 41a) and increases to around 300 K in the UB case (Fig. 41b). There are two areas, one at Waialua area and the other at Waipahu area, where the temperatures reach 302 K at 14 HST in both CTRL and UB cases. However, the areas are larger in the UB case than in the CTRL.

The simulated total rainfall accumulation for the CTRL run (Fig. 42a) has a similar spatial distribution to the total rainfall distribution of the two summer months (Figs. 13). There is a maximum at the windward and over the Ko'olau Mountains, a secondary maximum at leeward side of the Waianae Mountains, a minimum over the central Oahu.

There is no rainfall simulated over the island in the NM case (Fig. 47b). It is apparent that mountain terrain is a crucial factor for the development of showers over Oahu. The effects of island heating and cooling alone are not adequate for the rainfall development over Oahu. The island terrain is needed to result in orographic lifting or an increase in upward motions due to the interactions between the trade-wind flow and the island-induce flow. In the NM case, the vertical motions, which are needed to force the air parcels to LCL, are negligibly small over the island at night (Fig. 49a). In the afternoon, the weaker vertical motions along leeward coast in the NM case (Fig. 49b) than in the CTRL case (Fig. 48b) with a shallower onshore flow offshore of the Waianae coast (Figs. 42b, and 41b) are not favorable for the development of afternoon showers.

In the NW case, there are slight increases in simulated total rainfall accumulation over the Ko'olau Mountains and the leeward side of the Waianae Mountains (Fig. 47c) than in the CTRL case (Fig. 47a). The contours of 4 mm and 8 mm rainfall amount cover larger areas over the Ko'olau Mountains in the NW case (Fig. 47c) than in the CTRL (Fig. 47a). At night, the vertical motions on the windward side of the Ko'olau Mountains in the NW case (Fig. 50a) are stronger than in the CTRL (Fig. 48a) resulting in greater nocturnal rainfall in the NW case. On the leeward side of the Waianae Mountains, the areas with rainfall amount greater than 4 mm and 0.5 mm are larger in the NW case (Fig. 47c) than in the CTRL (Fig. 47a). Note that at 14 HST, the vertical and horizontal extents of the positive vertical velocity regions are broader in the NW case (Fig. 50b) than in the CTRL (Fig. 48b). Moreover, at the leeward side of the Waianae Mountains, the maximum vertical velocity at 14 HST is 0.6 m s^{-1} at about 900 hPa in the CTRL (Fig. 48b). Whereas in the NW case, it is to 0.8 m s^{-1} at about 900 hPa and 1.6 m s^{-1} at about 830 hPa (Fig. 50b).

In the NK case, more rainfall is simulated at windward side of the Waianae Mountains with no rainfall over the Ko'olau area. More rainfall at windward side of the Waianae Mountains in the NK case (Fig. 47d) than in the CTRL is due to the orographic lifting of the moist laden in-coming trade flow. Without the Ko'olau Mountains the moisture content of the trade-wind flow is not removed by orographic precipitation before reaching the windward slopes of the Waianae Mountains. In the NK case, the simulated mixing ratio (g kg^{-1}) over the central Oahu and on the windward slopes of the Waianae Mountains are from 0.6 g kg^{-1} to 1 g kg^{-1} (Figs. 54a and 54b) greater than in the CTRL case (Figs. 53a and 53b) throughout the diurnal cycle. In the CTRL case, the simulated rainfall has maximum over the Ko'olau Mountains (Fig. 47a). No rainfall is simulated over the Ko'olau Mountain region in the NK case (Fig. 47d). Figure 50 also shows that, with the removal of the Ko'olau Mountains, the vertical motion over the Ko'olau Mountains region is very small in the NK case.

There is also less rainfall at the lee of the Waianae Mountains in the NK case (Fig. 47d) than in the CTRL (Fig. 47a). The increase in the strength of the descending air flow on the leeside slopes (see section 3.3.2.1.c) of the Waianae Mountains in the NK (Fig. 44b) is one of the reasons for the decrease in the rainfall along the lee-side coast. Furthermore, the onshore westerly flow during the day (Fig 44b) which brings moisture from the ocean to the island is also weakened in the NK case than in the CTRL case. In addition. the region of upward motion in the afternoon hours is also pushed toward the open ocean in the NK case (Fig. 51b) with the downward motion on the leeside slopes of the Waianae Mountains. As a result, less rainfall was simulated in the NK case.

A slightly increase in rainfall was simulated along the leeward side of the Waianae Mountains in the UB case than in the CTRL case. The increase may due to the increase in onshore flow in the afternoon (Fig 44b) resulting in enhancement of vertical motions (Fig. 52b) as well as an increase in orographic lifting on leeside slope of the Waianae Mountains in the UB case due to the development of stronger upslope flow. At 14 HST, a region of positive vertical velocity covers entire leeward slopes of the Waianae Mountains in the UB case. Moreover, the maximum of vertical velocity (0.8 m s^{-1}) over leeward slopes of the Waianae Mountains in the UB case (Fig. 52b) is larger than in CTRL (0.6 m s^{-1}) (Fig. 48b).

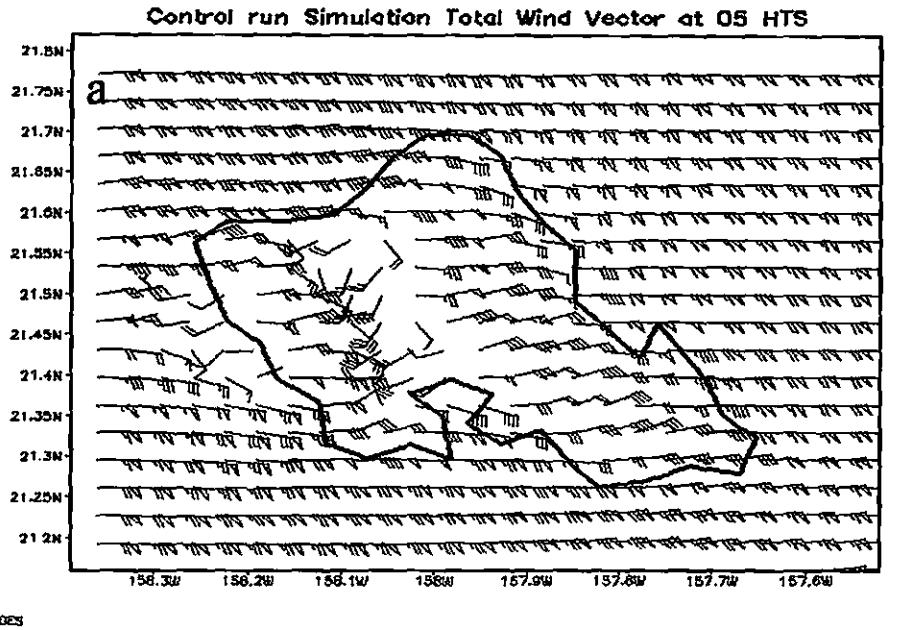

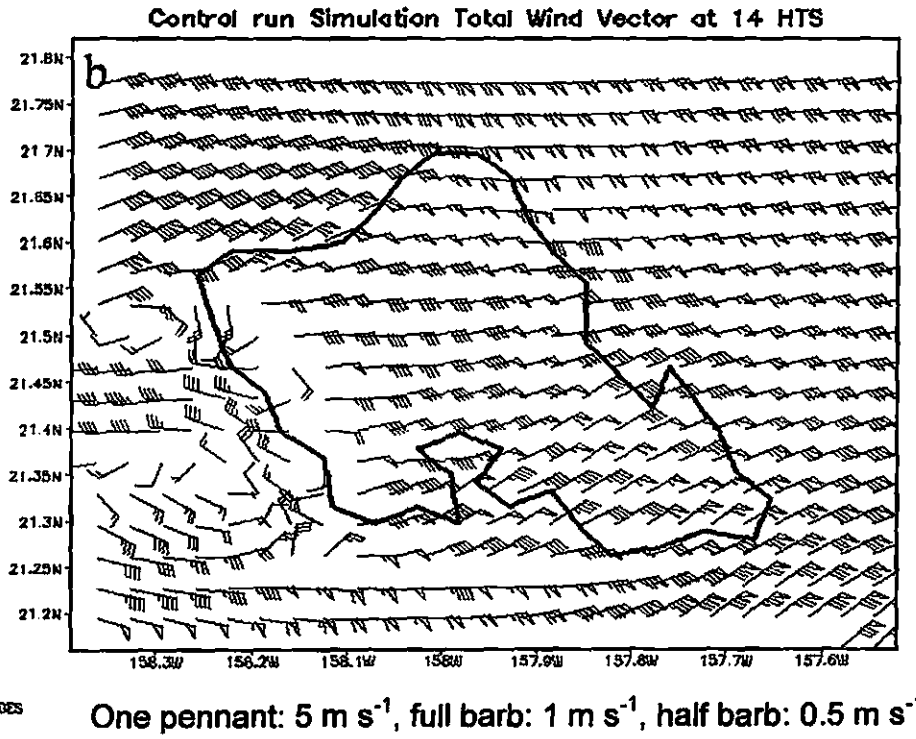

One pennant: 5 m s^{-1}, full barb: 1 m s^{-1}, half barb: 0.5 m s^{-1}

Figure 36 Simulated winds for 09 August 2005 at (a) 05 HST and (b) 14 HST in CTRL.

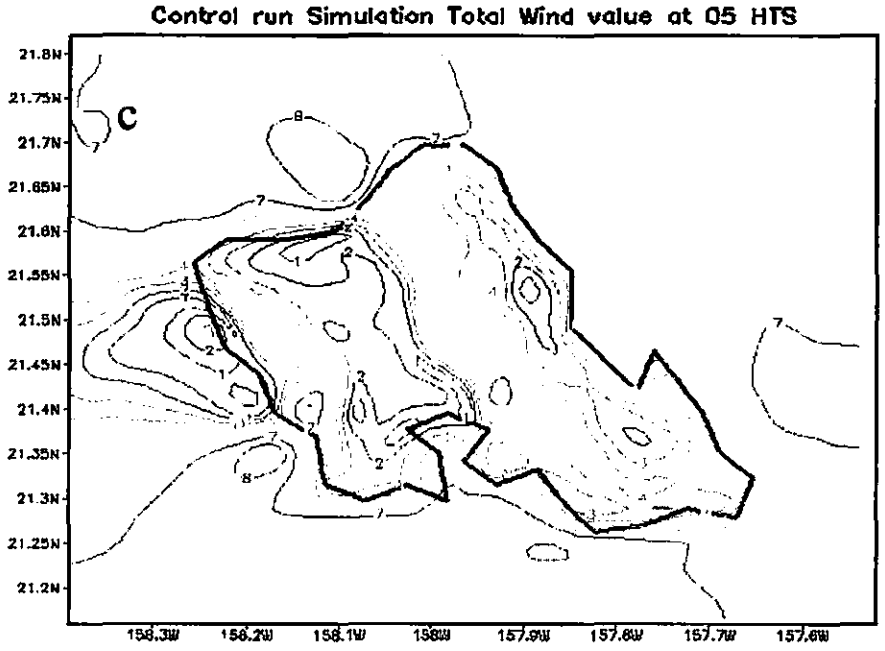

GrADS: COLA/IGES

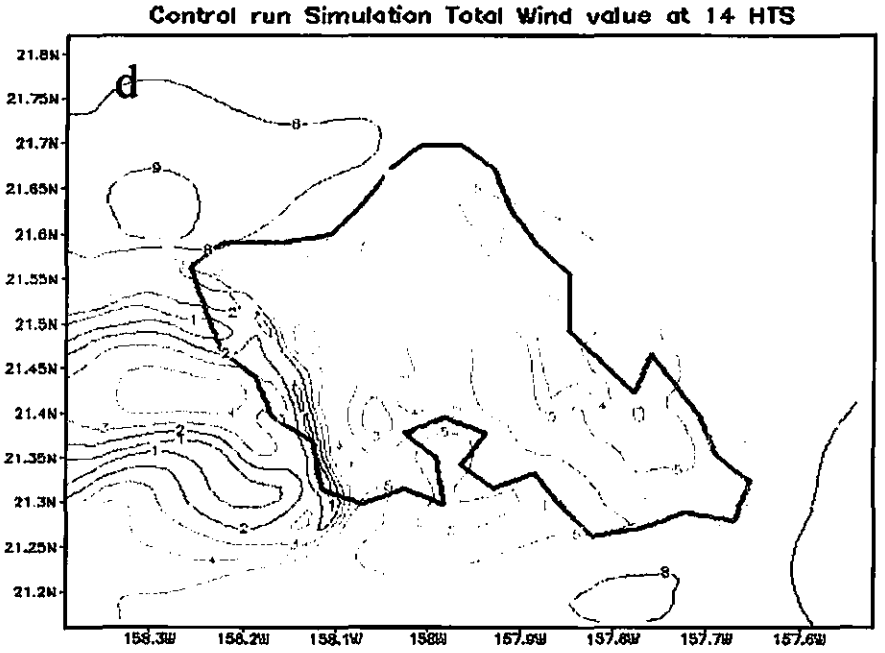

Figure 36 Simulated wind speeds for 09 August 2005 at (c) 05 HST and (d) 14 HST in CTRL.

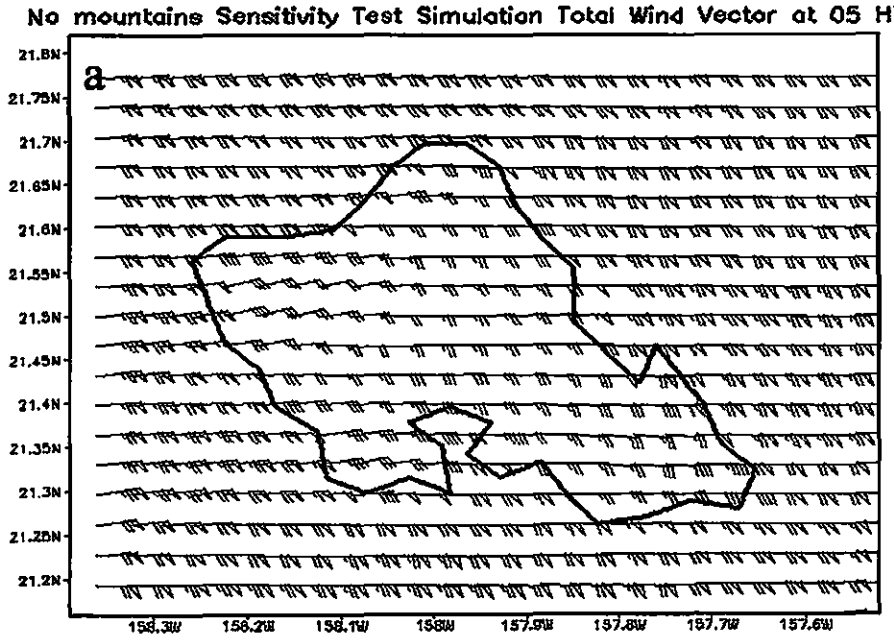

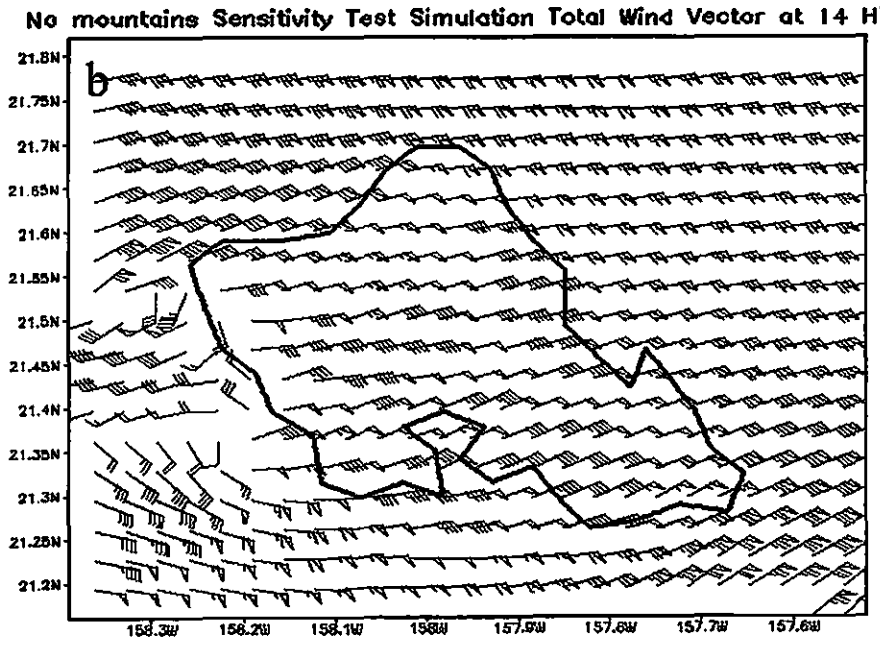

Figure 37 Same as Figs. 36a and 36b but for the no mountain case at (a) 05 HST and (b) 14 HST.

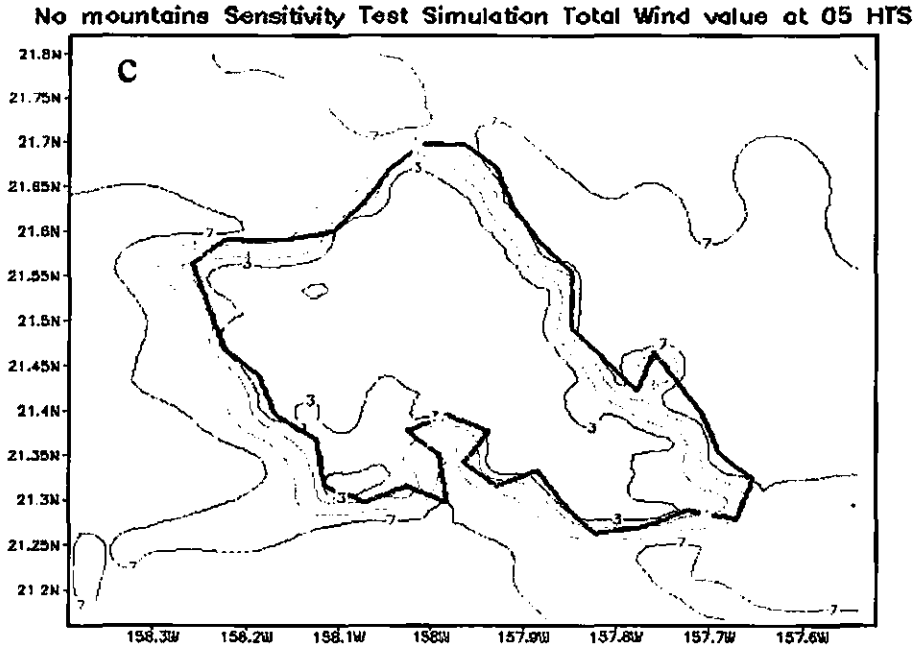

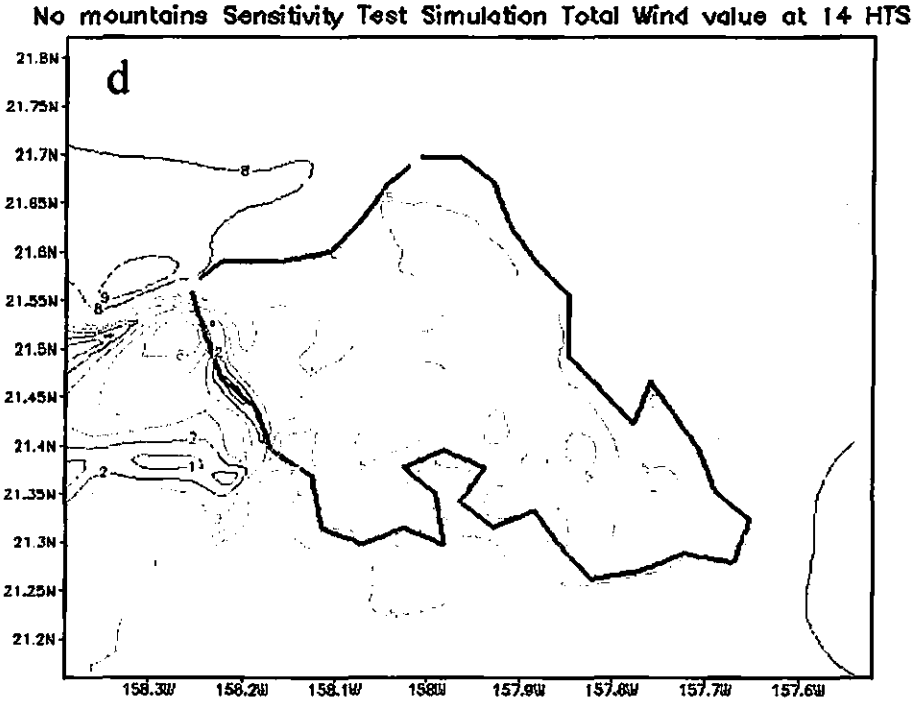

Figure 37 Same as Figs. 36c and 36d but for the no mountain case at (a) 05 HST and (b) 14 HST.

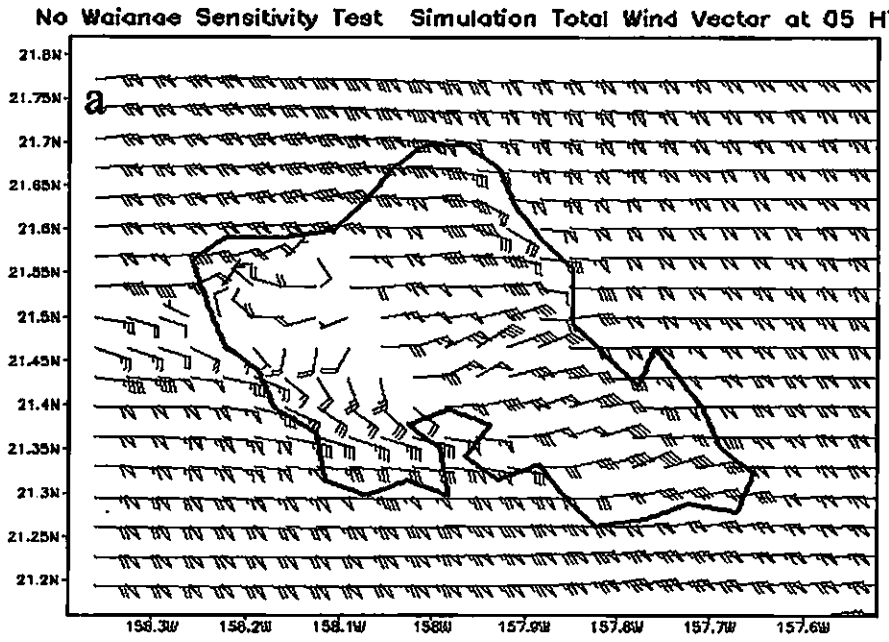

GrADS: COLA/IGES

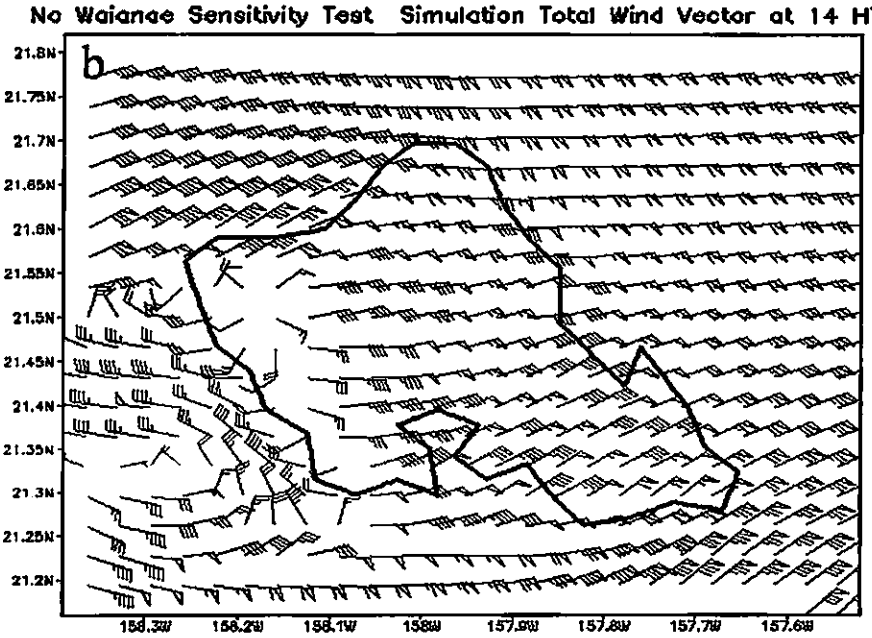

Figure 38 Same as Figs. 36a and 36b but for the no Waianae case at (a) 05 HST and (b) 14 HST.

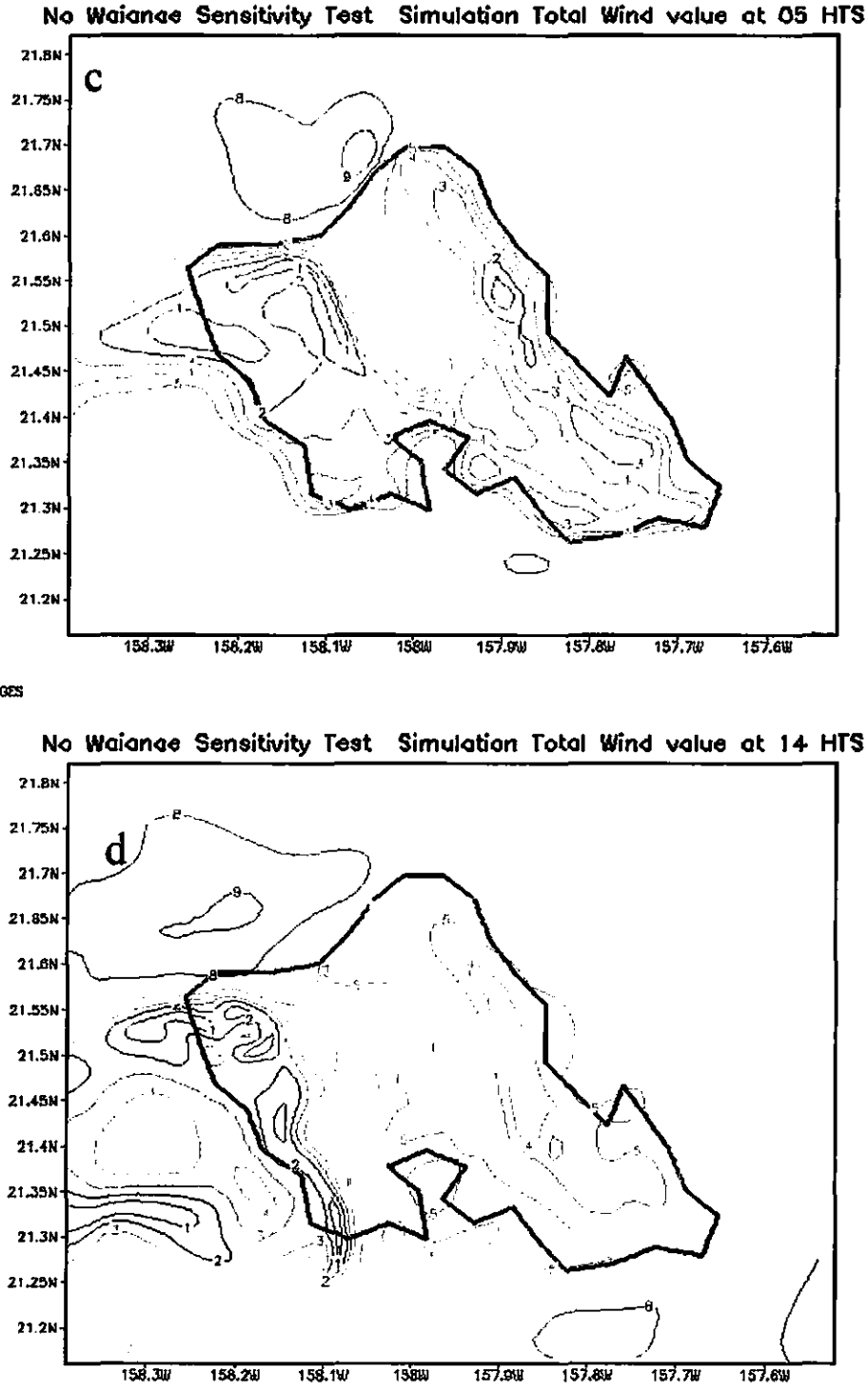

Figure 38 Same as Figs. 36c and 36d but for the no Waianae case at (a) 05 HST and (b) 14 HST.

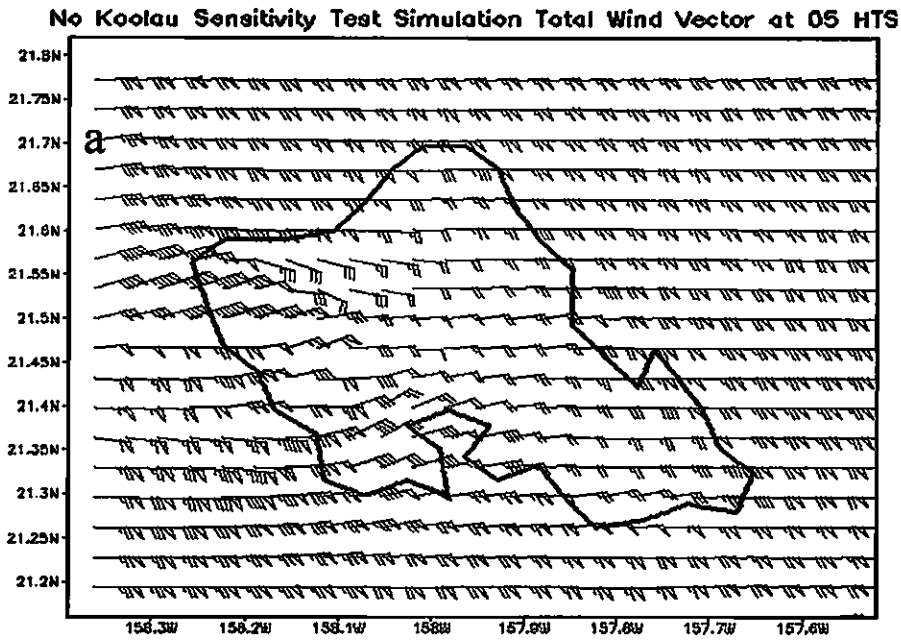

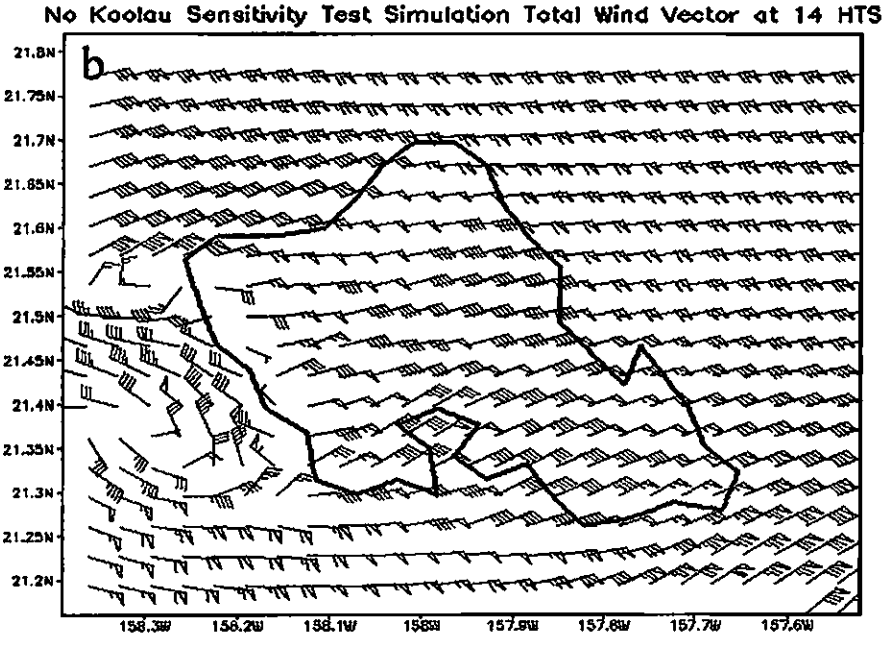

Figure 39 Same as Figs. 36a and 36b but for the no Ko'olau case at (a) 05 HST and (b) 14 HST.

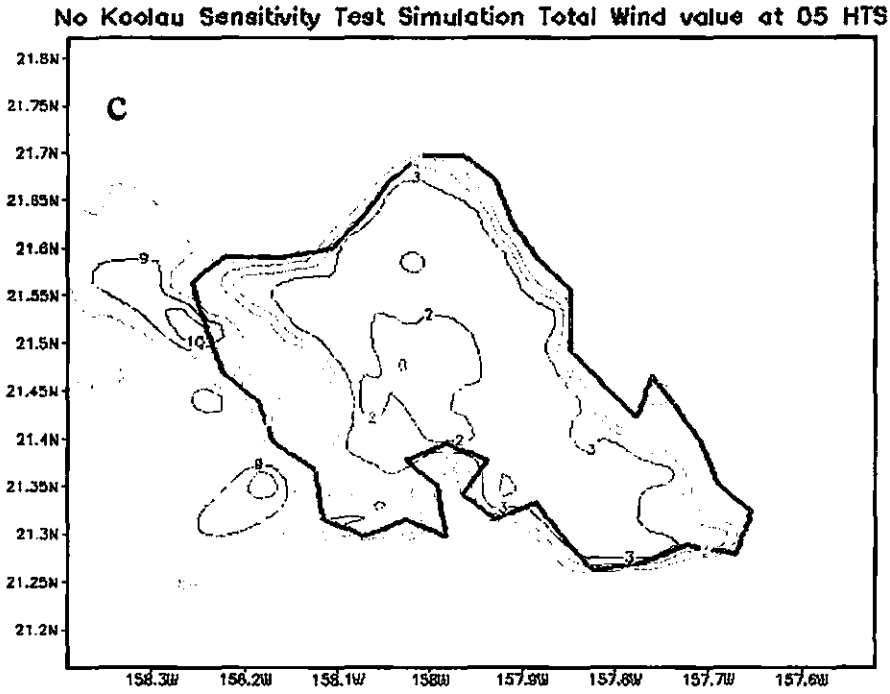

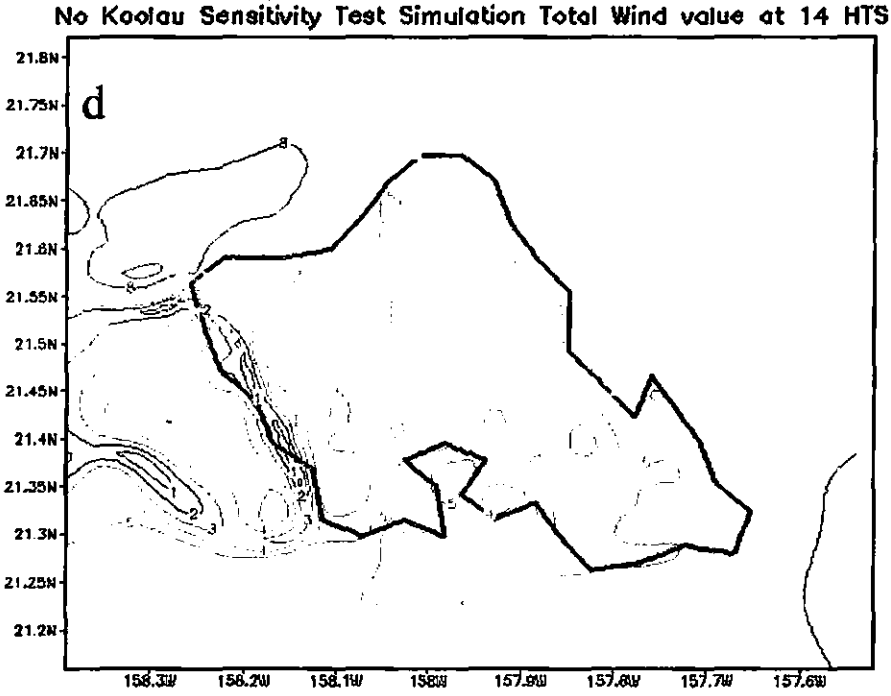

Figure 39 Same as Figs. 36c and 36d but for the no Ko'olau case at (a) 05 HST and (b) 14 HST.

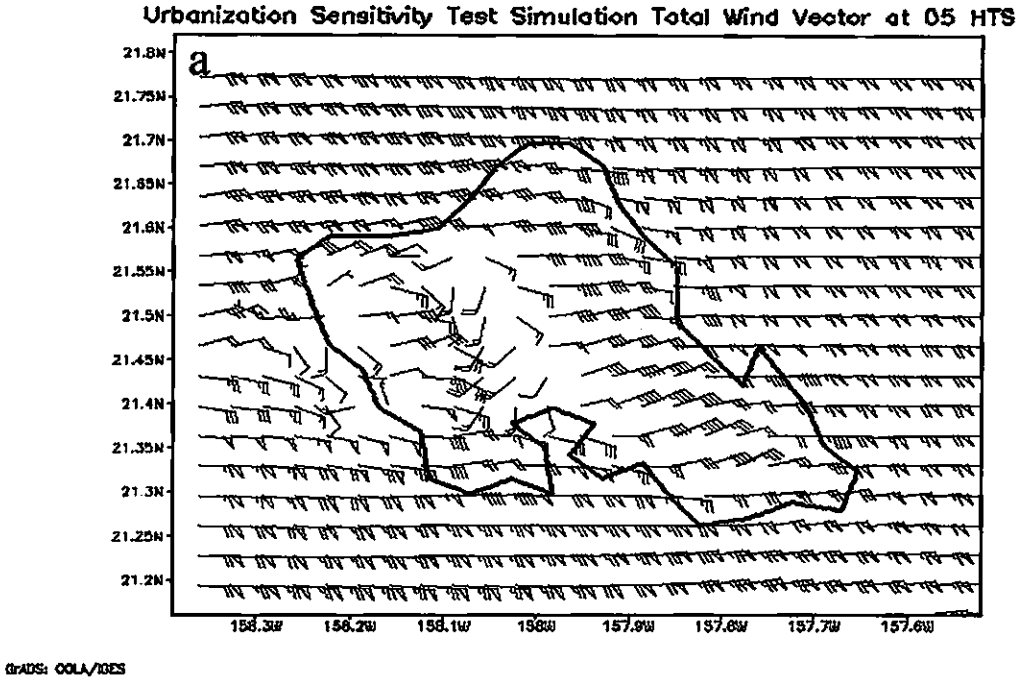

GrADS: COLA/IGES

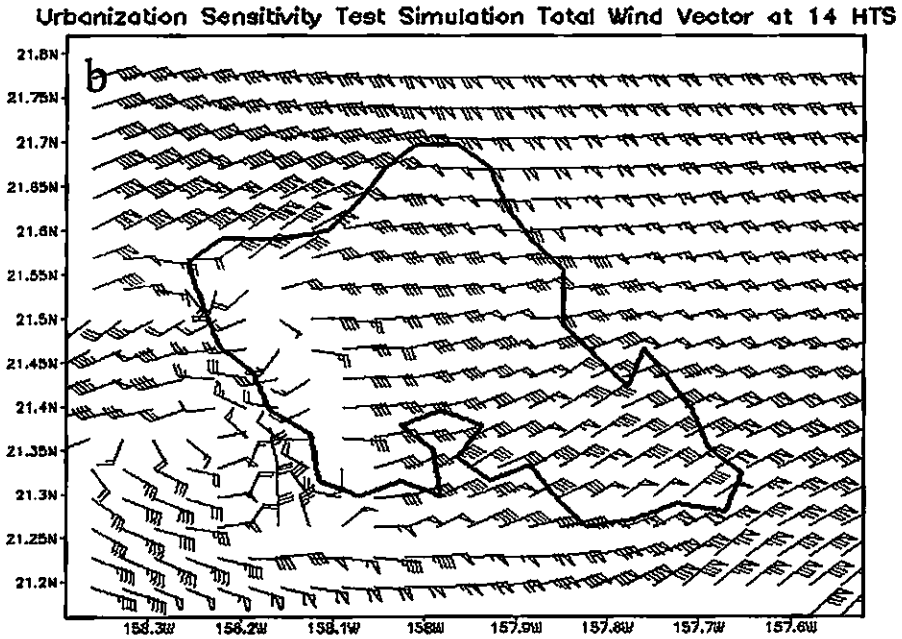

Figure 40 Same as Figs. 36a and 36b but for the urbanization case at (a) 05 HST and (b) 14 HST.

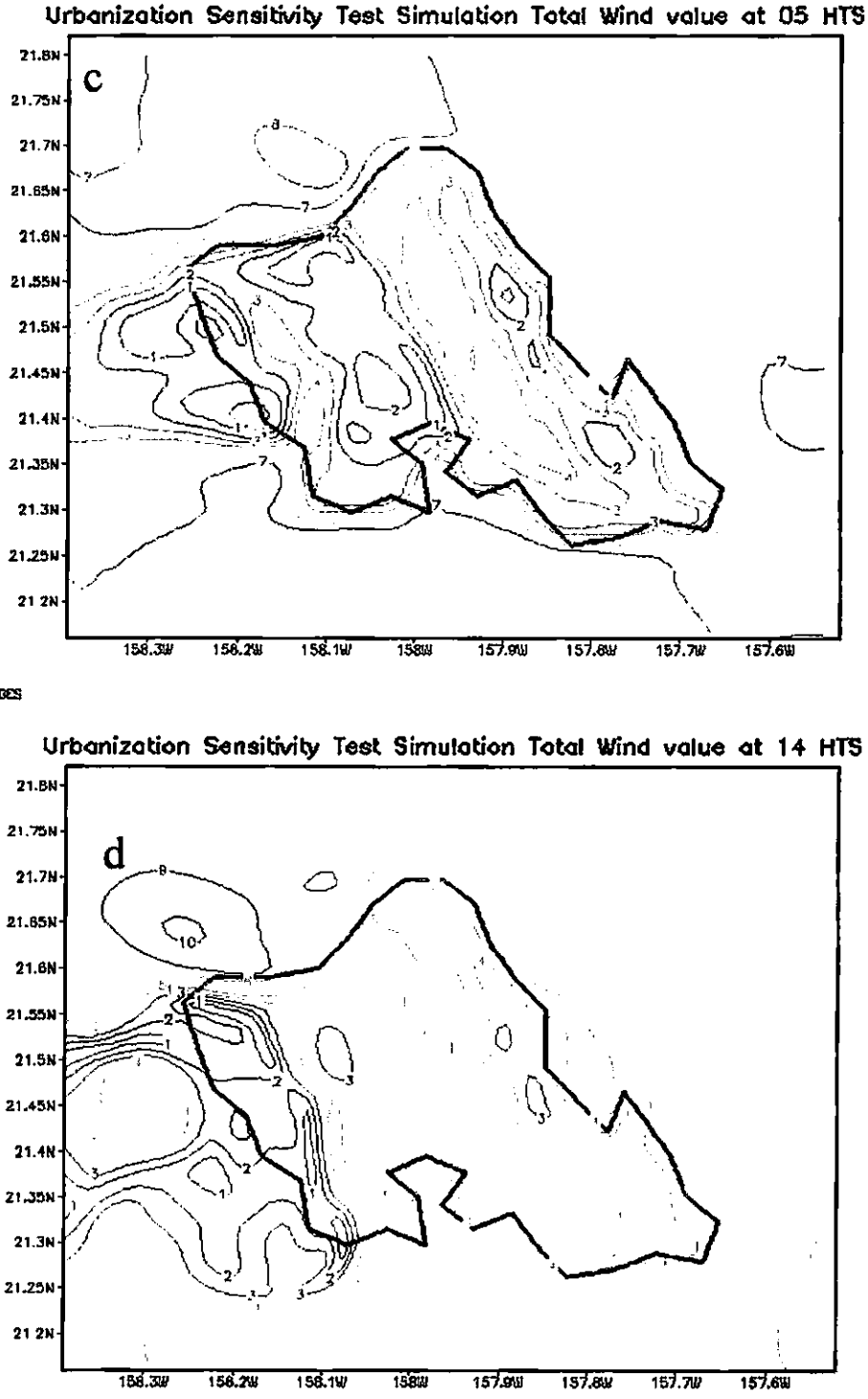

Figure 40 Same as Figs. 36c and 36d but for the urbanization case at (a) 05 HST and (b) 14 HST.

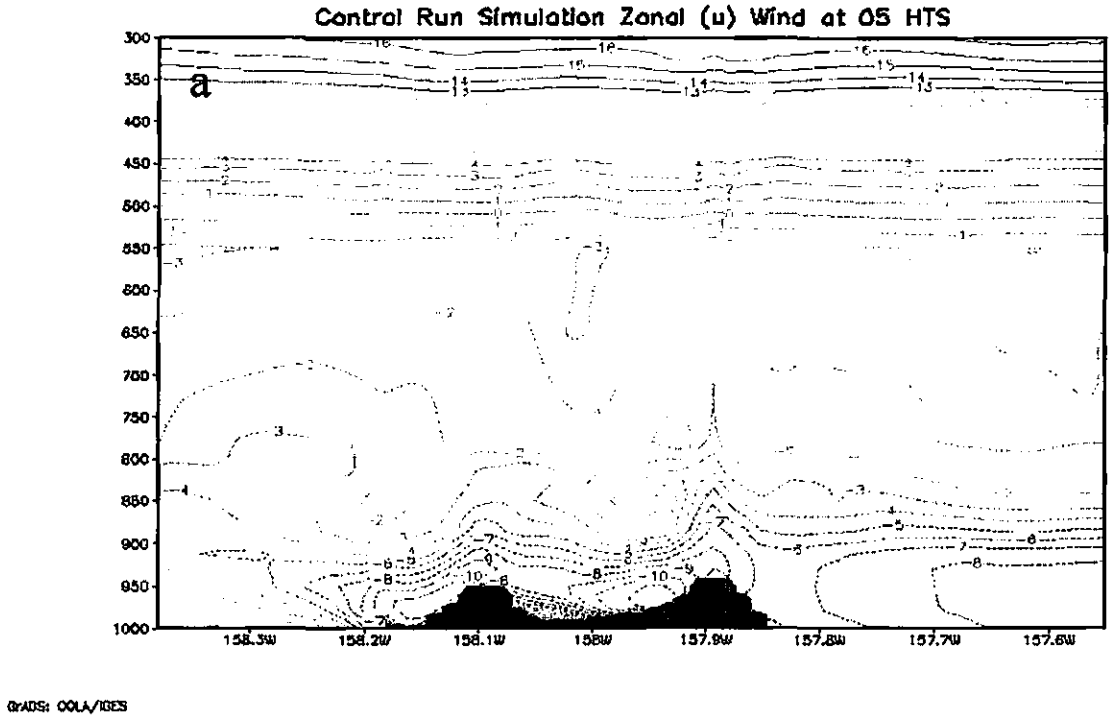

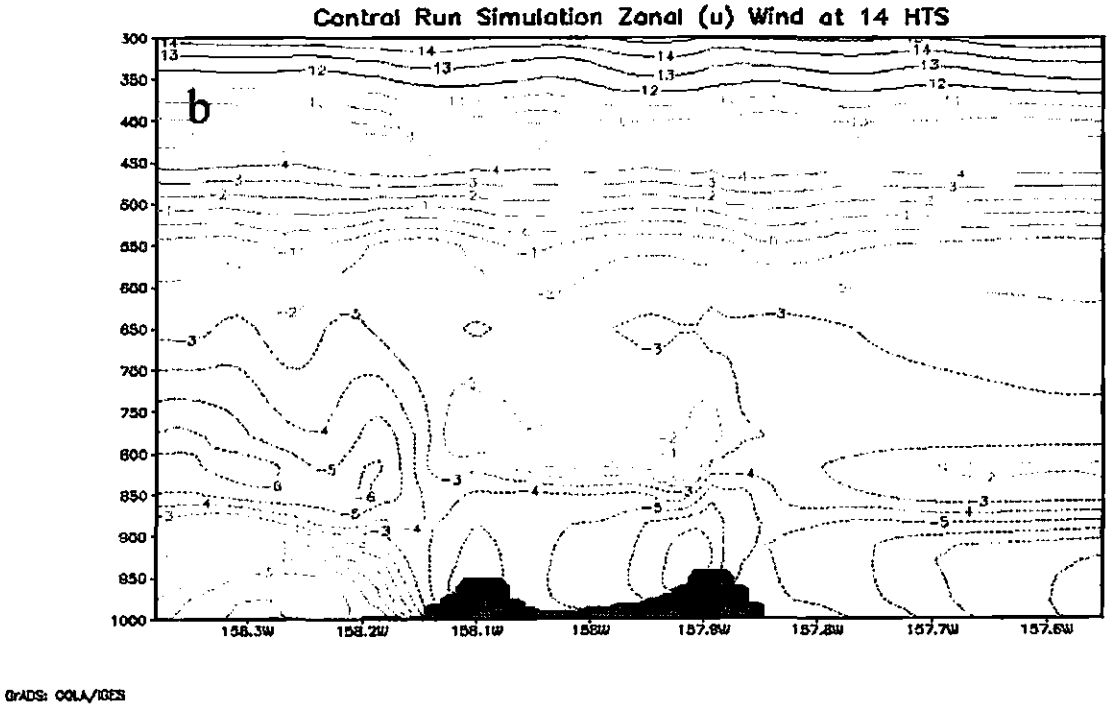

Figure 41 Vertical cross sections of the simulated zonal wind component in the CTRL case at (a) 05 HST and (b) 14 HST for August 09, 2005.

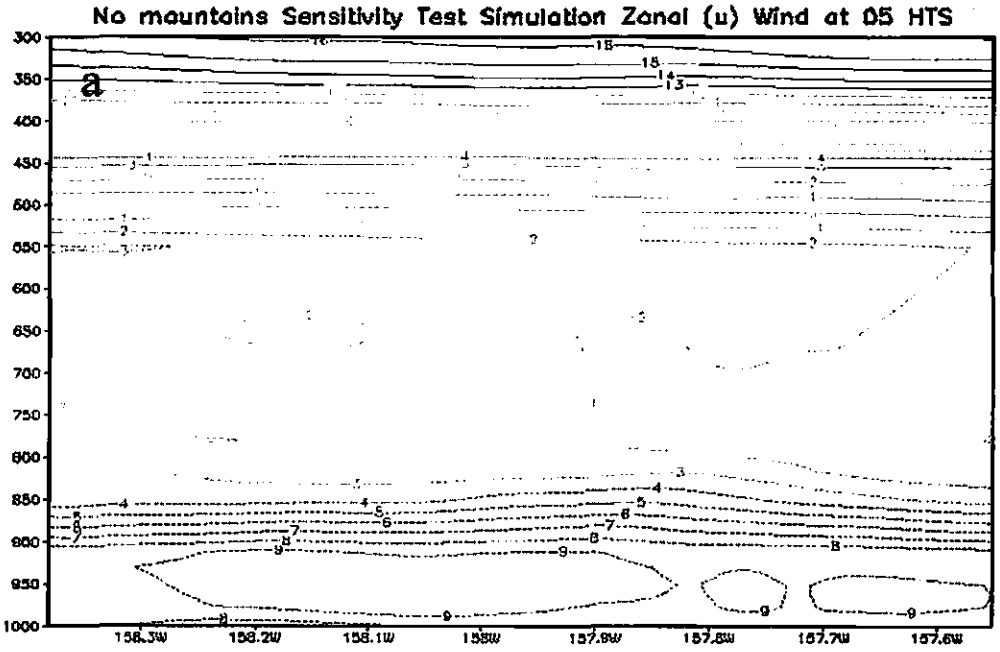

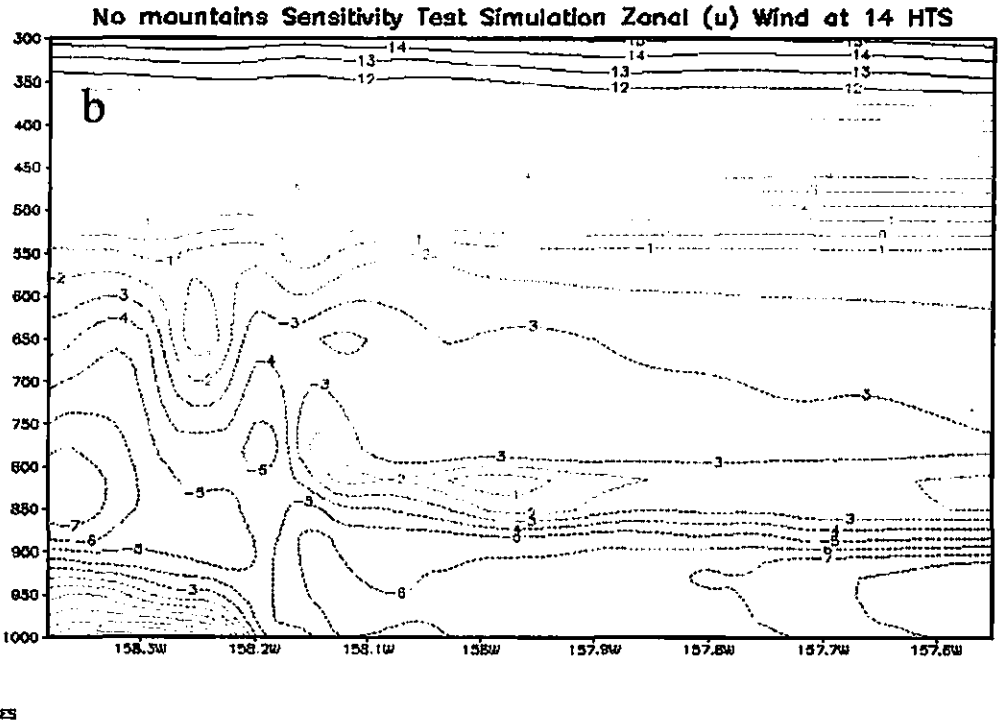

Figure 42 Same as Figs. 41a and 41b but for no mountain case at (a) 05 HST and (b) 14 HST.

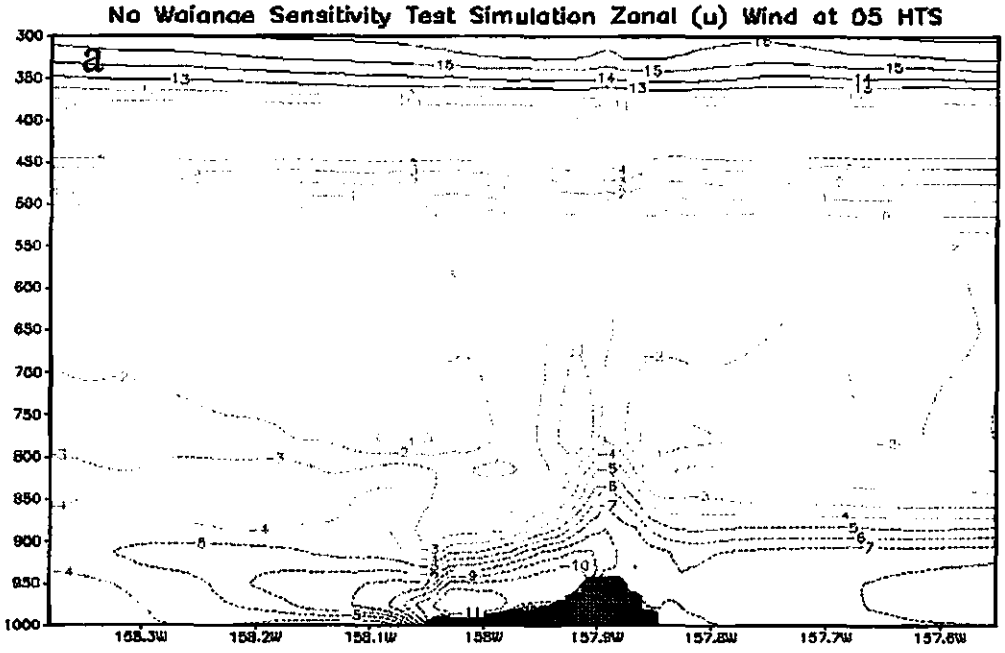

Figure 43 Same as Figs. 41a and 41b but for no Waianae case at (a) 05 HST and (b) 14 HST.

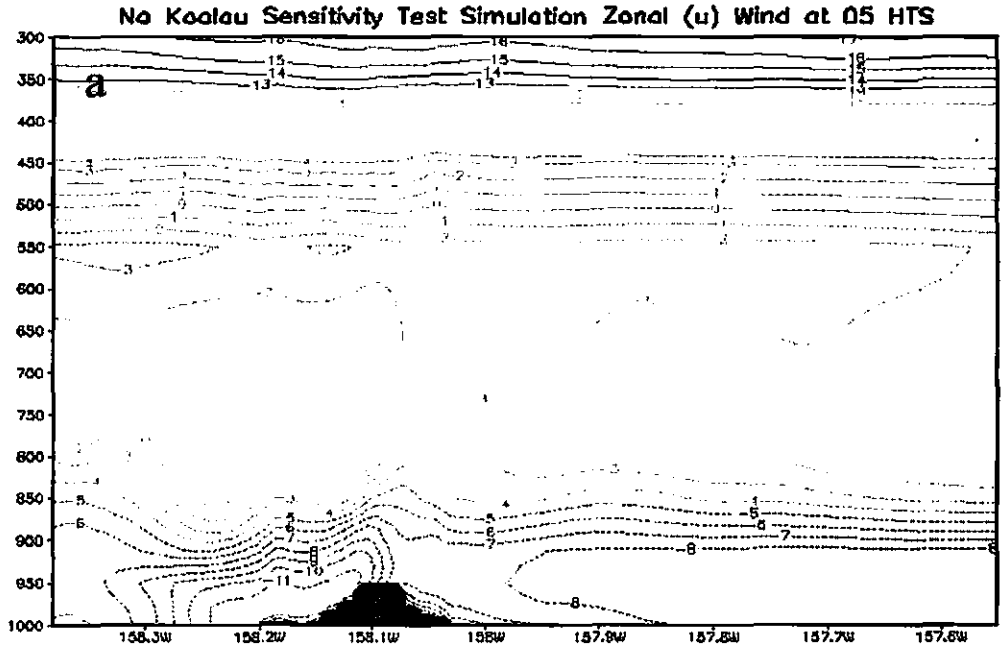

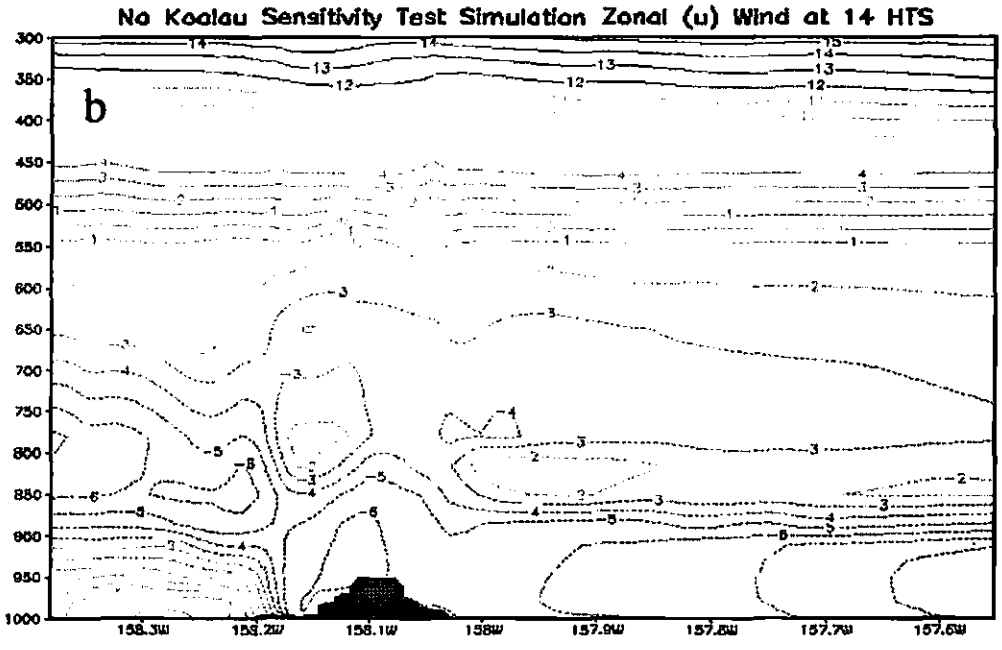

Figure 44 Same as Figs. 41a and 41b but for no Ko'olau case at (a) 05 HST and (b) 14 HST.

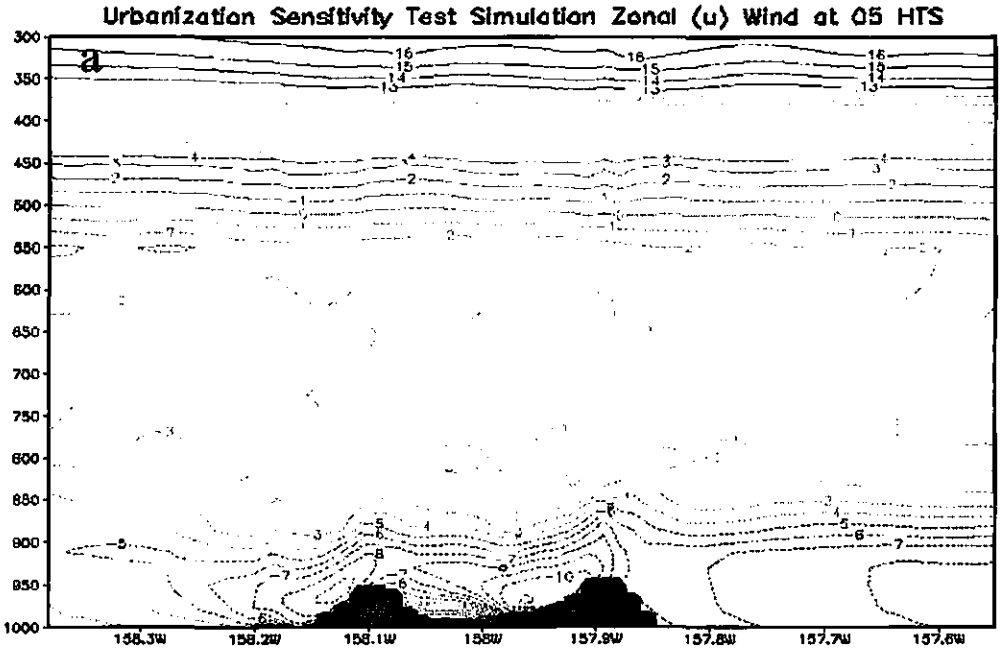

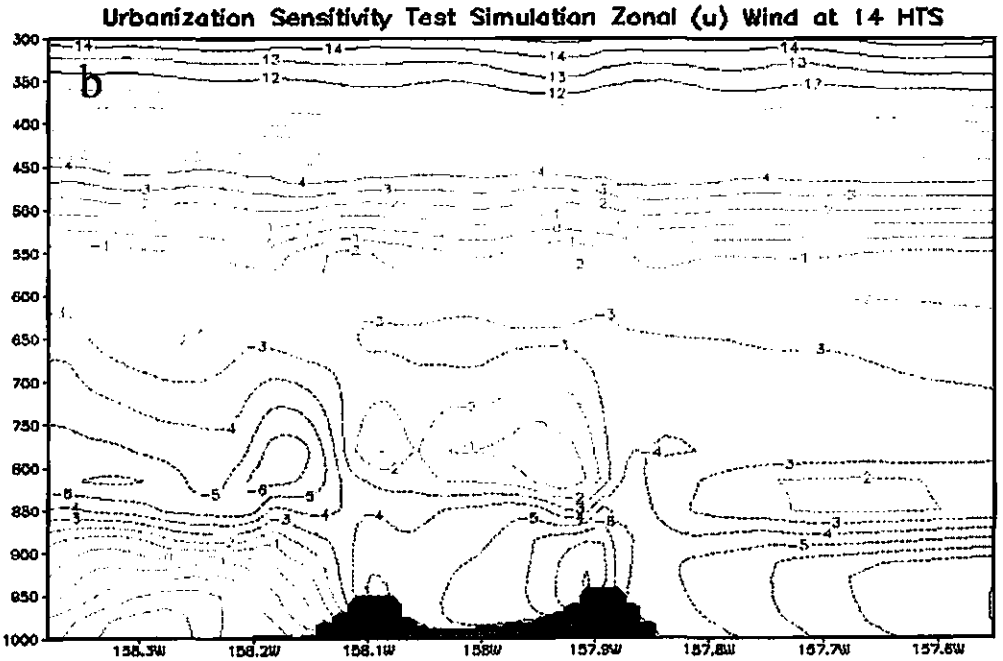

Figure 45 Same as Figs. 41a and 41b but for urbanization case at (a) 05 HST and (b) 14 HST.

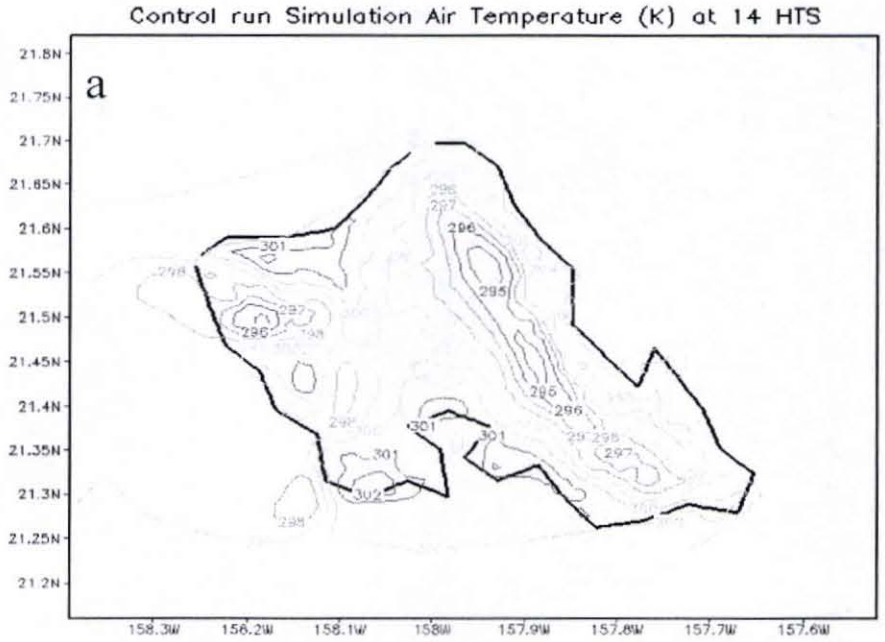

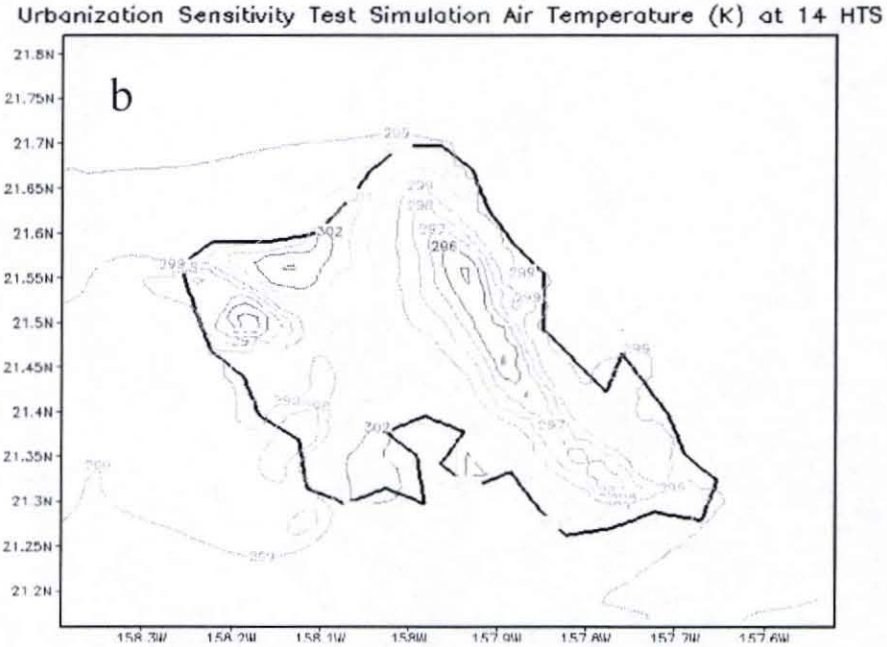

Figure 46 Simulated 2-m air temperatures (K) at 14 HST on 09 August 2005 (a) control run (b) urbanization case.

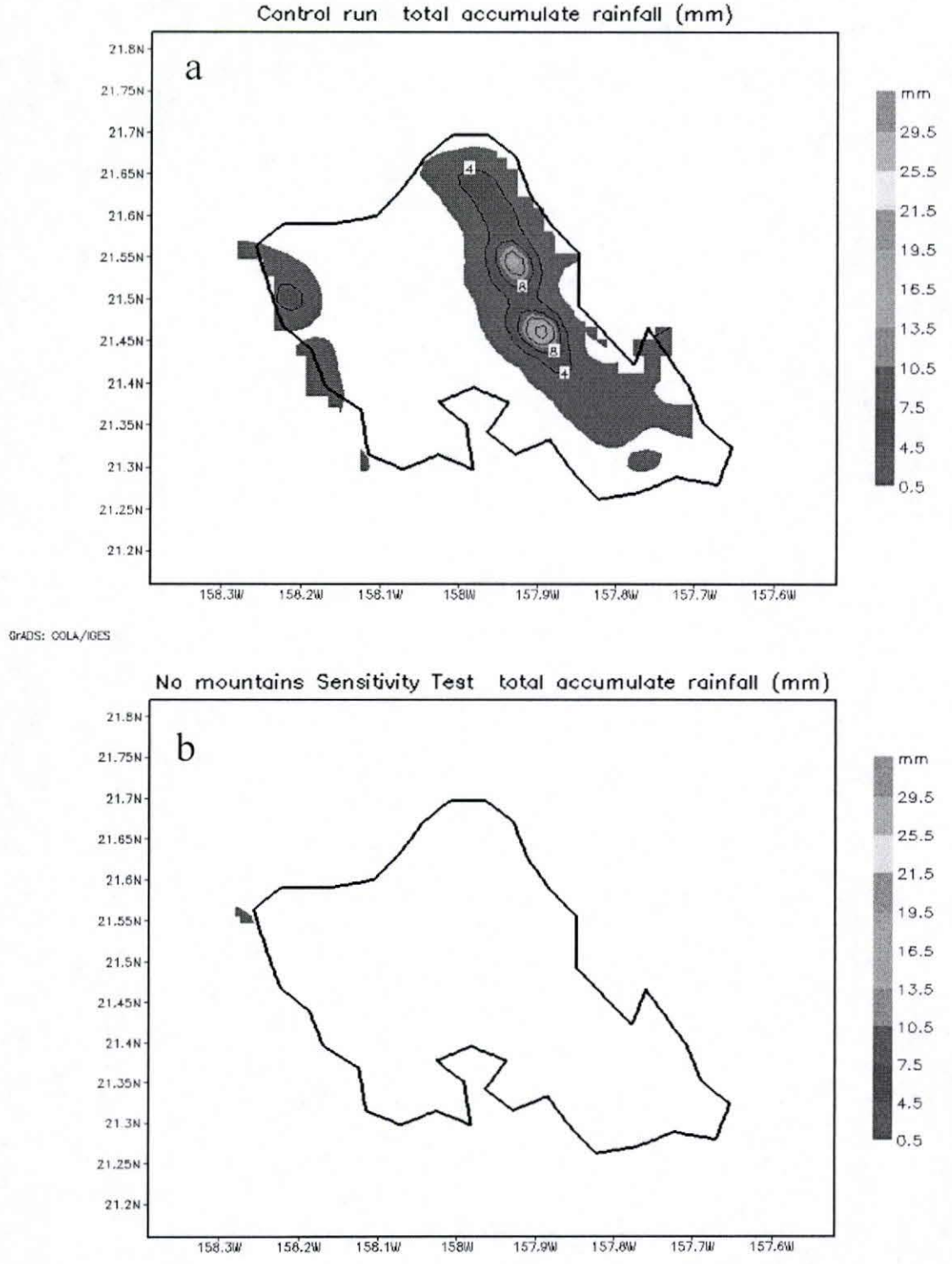

Figure 47 Simulated total rainfall accumulations on 09 August 2005 for (a) the CTRL case and (b) no mountain case.

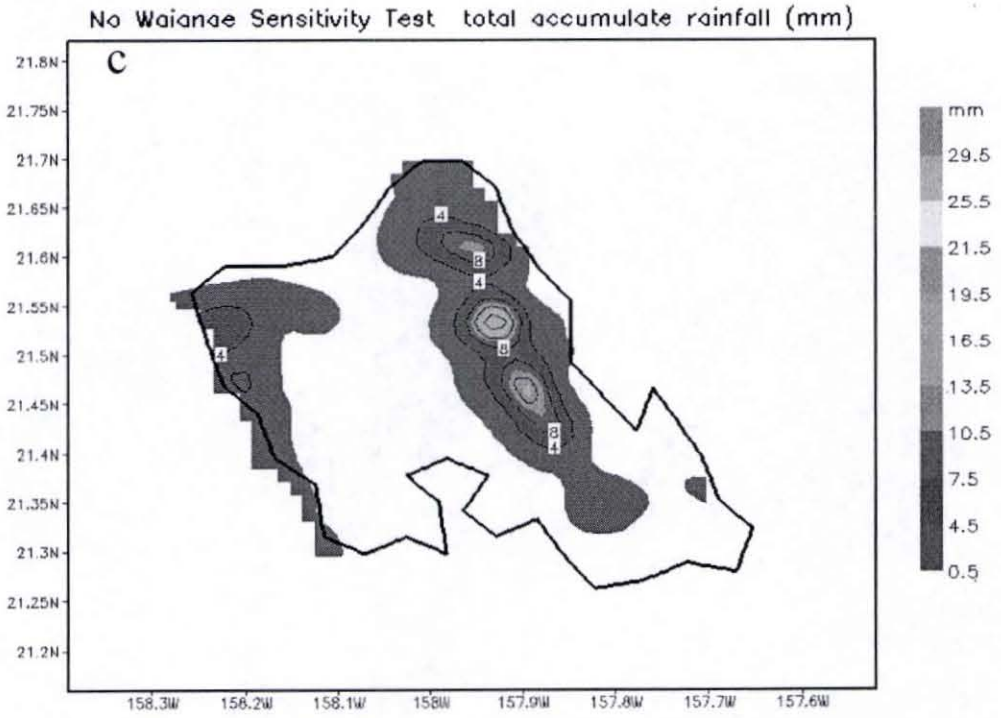

Figure 47c Same as Fig. 39a but for no Waianae case.

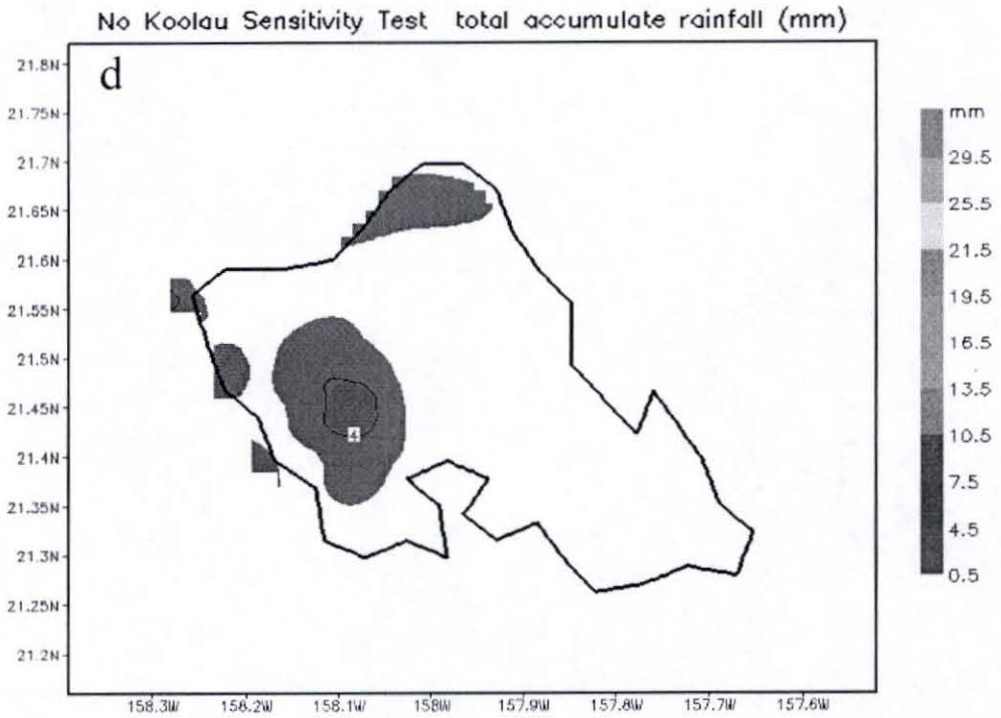

Figure 47d Same as Fig. 39a but for no Ko'olau case.

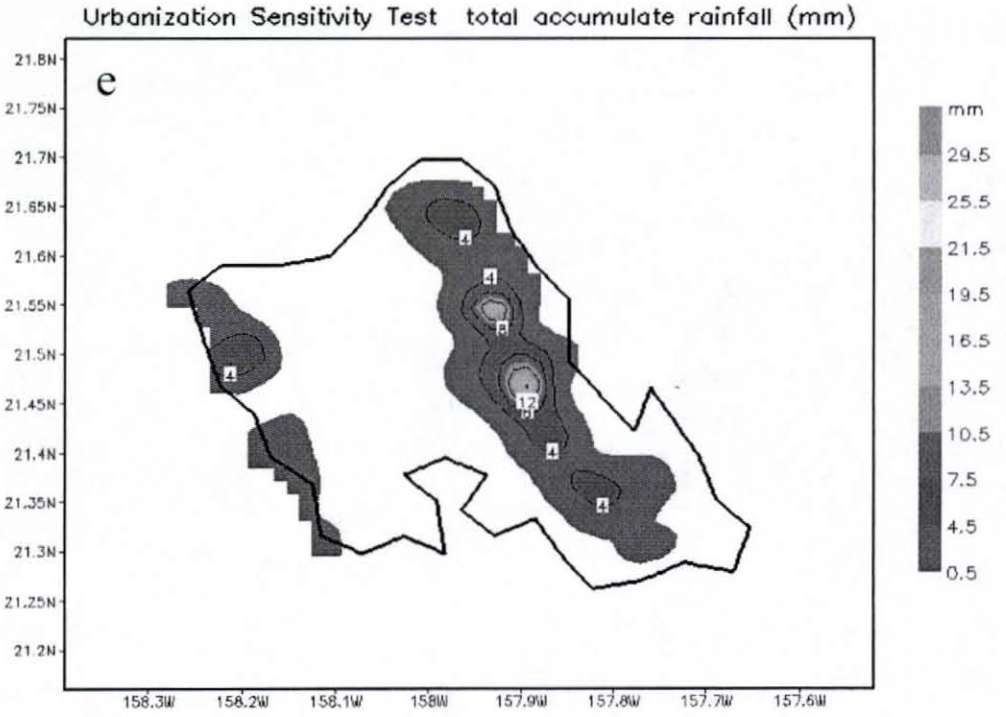

Figure 47e Same as Fig. 39a but for urbanization case.

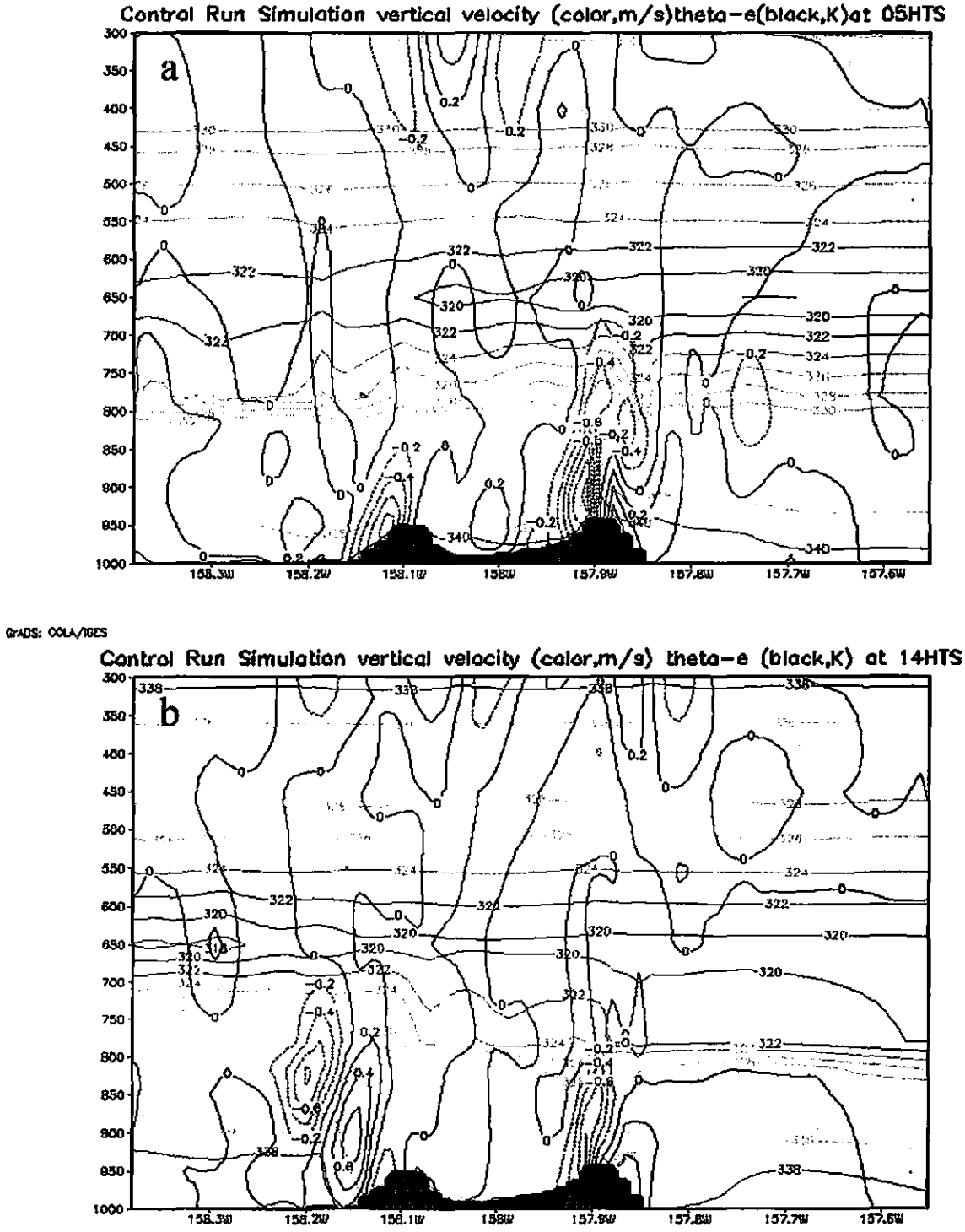

Figure 48 Vertical cross sections of the simulated velocity and equivalent potential temperature on 09 August 2005 at (a) 05 HST and (b)14 HST for the CTRL case.

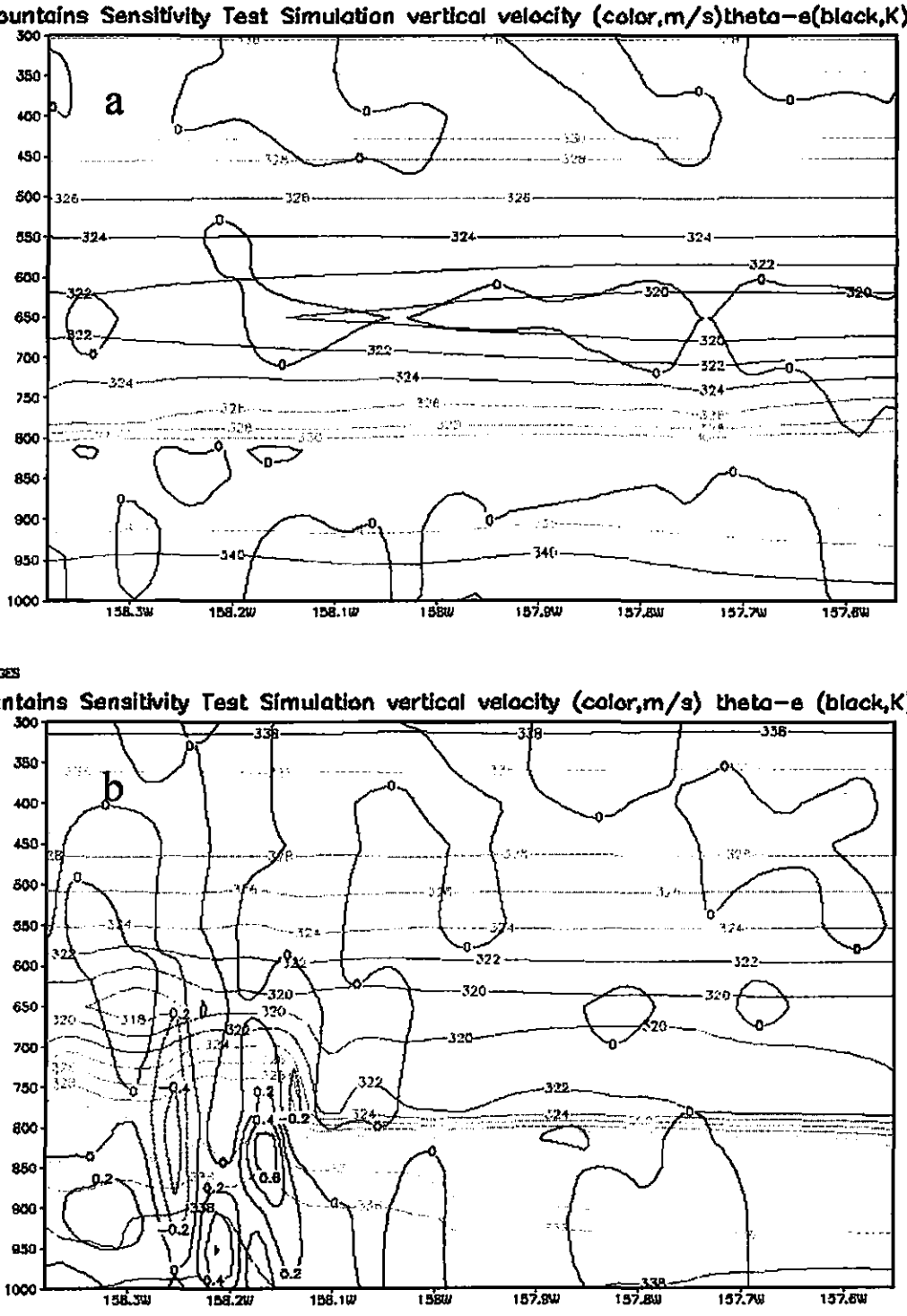

Figure 49 Vertical cross sections of the simulated velocity and equivalent potential temperature on 09 August 2005 at (a) 05 HST and (b) 14 HST for the NM case.

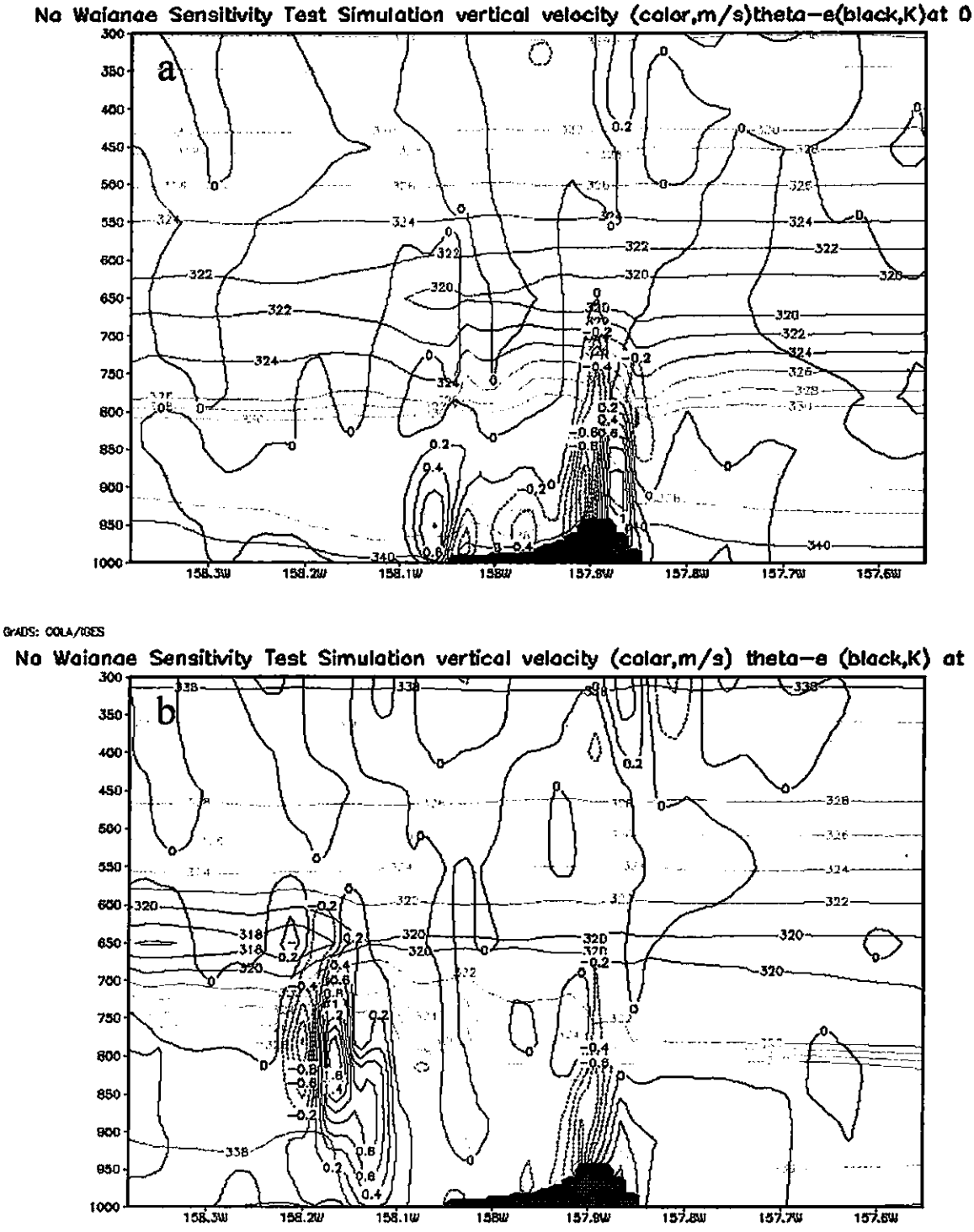

Figure 50 Vertical cross sections of the simulated velocity and equivalent potential temperature on 09 August 2005 at (a) 05 HST and (b) 14 HST for the NW case.

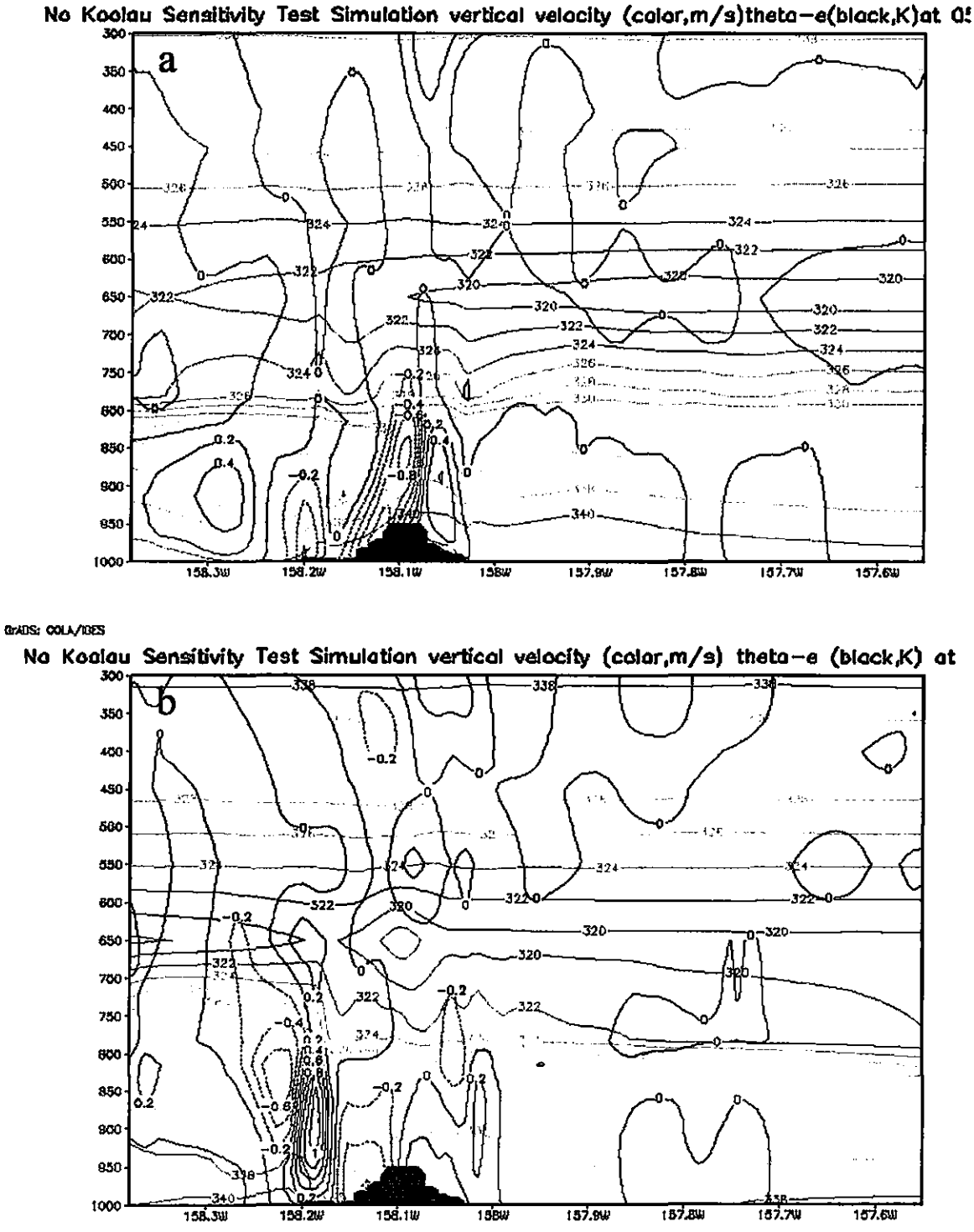

Figure 51 Vertical cross sections of the simulated velocity and equivalent potential temperature on 09 August 2005 at (a) 05 HST and (b) 14 HST for the NK case.

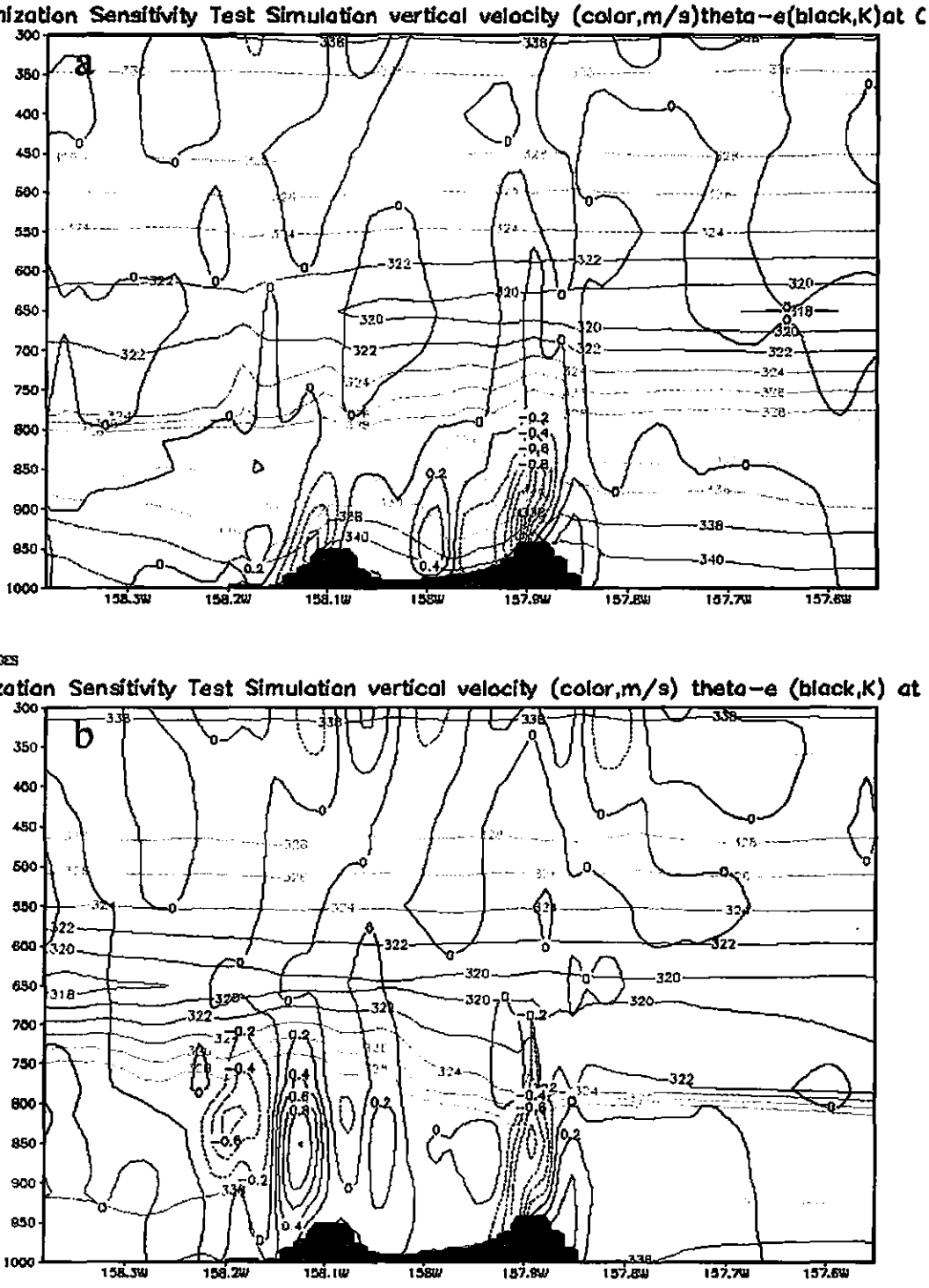

Figure 52 Vertical cross sections of the simulated velocity and equivalent potential temperature on 09 August 2005 at (a) 05 HST and (b) 14 HST for the UB case.

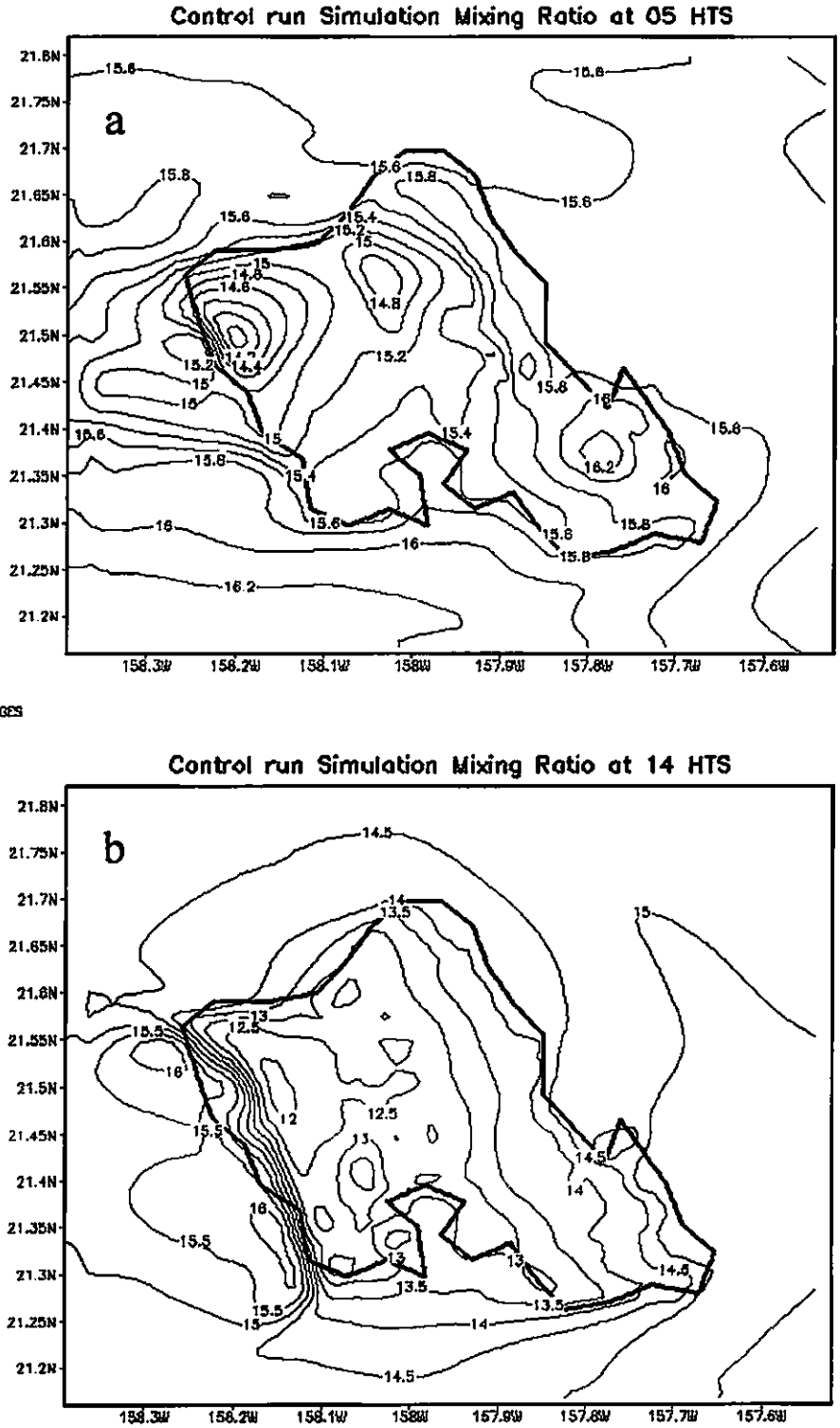

GrADS: COLA/IGES

Figure 53 Simulated mixing ratio (g kg^{-1}) on 09 August 2005 at (a) 05 HST and (b) 14 HST for the CTRL case.

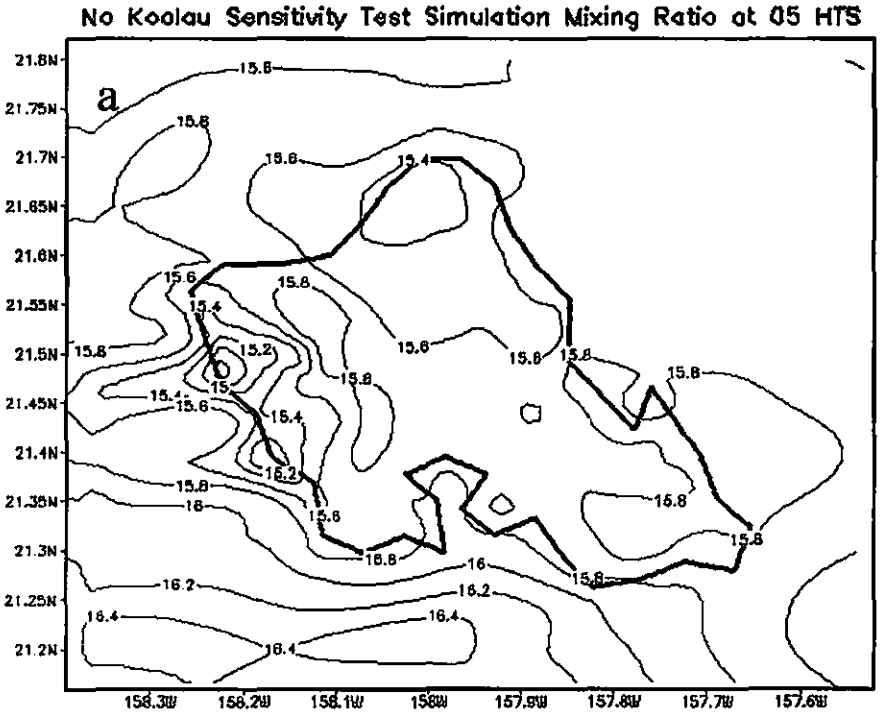

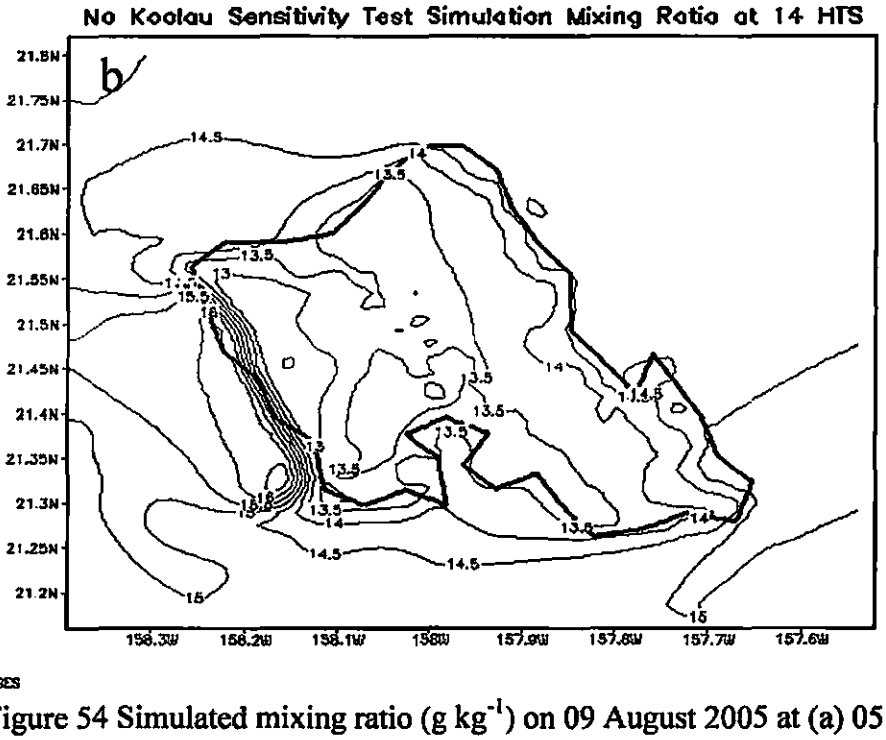

Figure 54 Simulated mixing ratio (g kg^{-1}) on 09 August 2005 at (a) 05 HST and (b) 14 HST for the NK case.

Chapter IV: Summary

The MM5/LSM is used to simulate airflow and weather over Oahu for July and August, 2005. The forecasts from GFS provided by NCEP are used to initialize the model. The effects of trade-wind conditions, terrain height, and landuse on island-scale air flow and weather are investigated.

Even with a relatively small size, the island of Oahu has profound influences on the island airflow and weather. With a 1.5-km resolution, the island effects on airflow and weather are reasonably well simulated by the MM5/LSM model including windward and mauka showers as well as showers over the Ko'olau Mountains at night and early morning, strong easterly downslope winds aloft on the lee-side slopes of both Ko'olau and Waianae mountains at night, weak wind over central Oahu, westerly onshore flow in the afternoon offshore off the Waianae coast and etc.

The simulated spatial variations of mean surface winds are in good agreement with observations. Weaker winds were simulated over the island interior than over the open ocean. The wind direction errors are smaller at stations on the windward side of the Ko'olau Mountains than at stations at other locations. The mean wind speeds are significantly reduced over the island of Oahu due to island blocking and surface roughness. The most significant spatial variations in mean wind directions were simulated and observed over the Waianae Mountains.

Two regions with the strongest wind speeds are simulated over the ocean at the northwestern and southeastern corners of Oahu consistent with previous observational studies (Leopold, 1948; Ramage and Oshiro 1977).

During the diurnal heating cycle, simulated winds agree well with observations. At night winds are weaker than during the day with mountain winds over the Waianae Mountains and weak winds over central Oahu over the Ko'olau Mountains. During the day, winds are stronger and almost uniform wind directions over the entire island. Weak

onshore westerly winds offshore of the Waianae coast were simulated at 14 HST. Wind speed errors during the diurnal cycle are less than or equal to 2 m s^{-1}. Both speed and direction errors (RMSE or MAE) are smaller when winds are stronger during the day.

Surface wind speeds over the island are stronger under strong trades than under weak trades. While the mean wind directions are almost uniform ENE under strong trades, under weak trades they vary over the central Oahu. The trade-wind conditions also have significant effects on the diurnal cycle of island-scale airflow. Under weak trades, wind direction at night is completely opposite to the coming trade-wind directions on the eastern slopes near the top the Ko'olau Mountains. In the afternoon, the westerly onshore flow along the Waianae coast and adjacent waters due to land surface heating is more pronounced under weak trades. A complete reversal of wind directions along the Waianae coast is simulated and observed under weak trades. In contrast, under strong trades, no reversal of wind directions id observed or simulated along the Waianae coast. The onshore/upslope winds on the leeside of the Waianae Mountains in the afternoon hours are also absent.

Simulated winds aloft are also significantly affected by the diurnal heating cycle.

At night, there are strong easterly down-slope winds (>11 m s^{-1}) on the lee-side slopes of both the Ko'olau and the Waianae Mountains. During the day, the surface winds are stronger than at night. The winds aloft on the lee-side slopes are weaker during the day than at night because of the increase in instability during the day.

Simulated rainfalls during the two summer months agree reasonably well with observations. A maximum rainfall over the Ko'olau Mountains, a secondary rainfall maximum occurs at lee-side slopes of the Waianae Mountains and a minimum over central Oahu. During the diurnal cycle, there are two maxima of rainfall at the foothills of the Ko'olau Mountains on the windward side, in agreement with Loos (2004), one at night caused by radiation cooling, stronger wind aloft as well as lower LCL, and the other in the morning. One of the important factors relates to the morning maximum rainfall is

the increase in vertical motion at this time. However, the reason for larger vertical motion in the early morning is still under investigation. Both the simulated and observed rainfalls are about four times larger during strong trades than during weak trades.

The simulated surface air temperatures at 13 stations agree reasonably well with observations. The RSME and MAE values vary from 1.0°C to 2.2°C and from 0.7°C to 1.8°C, respectively. Overall, the simulated temperatures are better at windward stations. Furthermore, the simulated temperatures are better at night than during the day.

The simulation of dew point temperature shows larger MAE during the day (1.8°C) than at night (1.4°C) and the air is moister at night than during the day when the low level air is mixed with dry air aloft. Over the island, the highest moisture area is simulated on the windward side of the Ko'olau Mountains. The island interior and over the Waianae Mountains are much drier.

Sensitivity tests show that in the NM case, at night, the wind directions over the island are rather uniform with about 50% weaker wind speeds than over the open ocean as a result of friction and a stable condition. In the afternoon, decrease in island blocking effects in the NM case results in higher wind speeds over central Oahu and windward coast of the Ko'olau Mountains than in the CTRL. The existence of the onshore flow off the Waianae coast in the absence of island blocking suggests that the onshore flow in the afternoon is a result of both the surface friction and island heating effects.

In the NW case, without the blocking effects of the Waianae Mountains results in increase in wind speeds over the windward coast of the Ko'olau Mountains in the afternoon, and stronger downslope winds at the leeward side of the Ko'olau Mountains at night as well at during the day than in CTRL.

In the NK case, at night, without the blocking effects of the Ko'olau Mountains, no mountain winds were simulated on the eastern slopes of the Waianae Mountains. In addition, the surface wind speeds on the western slopes of the Waianae Mountains are 5-8 m s^{-1} stronger than in CTRL. During the day, surface wind speeds are stronger than

in CTRL on the lee side of the Waianae Mountains, central Oahu, and along the windward coast.

In the UB case, at night, the increase in stability as a result of more significant cooling and the increase in roughness length in urban areas are two main factors that result in weaker wind speed over land than in CTRL. During the day, the simulated onshore flow along the Waianae lee-side coast in the UB case is more significant than in CTRL because of the increase in island heating during the day due to urbanization.

With respect to the effects of landuse on temperature, the UB case shows that urbanization results in an increase in surface temperature about 1 degree or more at 02 HST over the island mainly due to increase in urban heating.

In terms of rainfall, no simulated rainfall over Oahu in the NM case suggests that orographic lifting is crucial factors for the development of showers over Oahu. In the NW case, the increases in vertical motions at windward side of the Ko'olau Mountains at night and at the lee side of the Waianae Mountains in the afternoon is probable a favorable condition for a slight increase in simulated rainfall over the Ko'olau Mountains and the leeward side of the Waianae Mountains than in the CTRL. In the NK case, more rainfall was simulated on the windward side of the Waianae Mountains as compared with the CTRL case. Without the removal of moisture by the Ko'olau Mountains in the NK case, the in-coming trade-wind flow impinges on the windward side of the Waianae Mountains is relative moist as compared with the CTRL case . The Ko'olau Mountains play an important role in rainfall production over the Ko'olau Mountains and dry areas over central Oahu. A slight increase in rainfall was simulated on the lee side of the Waianae Mountains in the UB case maybe due to the increase in onshore flow in the afternoon and on the lee-side slopes of the Waianae Mountains.

Appendix A: The diurnal perturbations of wind from the summer mean state at 3-hour interval

A.1 The diurnal perturbations of wind vector from the summer mean state.

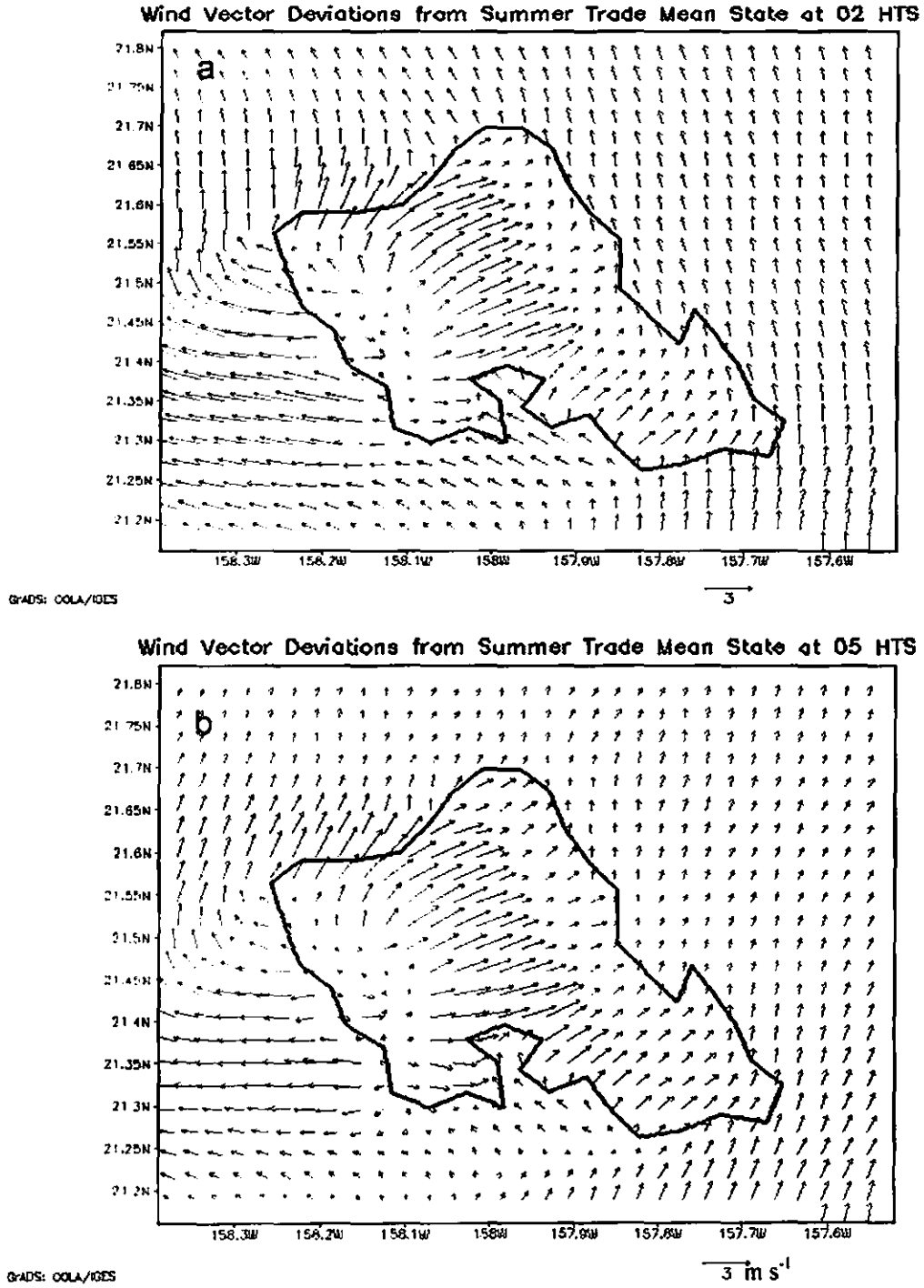

Figure A.1 The diurnal perturbations of wind vector from the summer mean state for (a) at 02 HST. and (b) at 05 HST

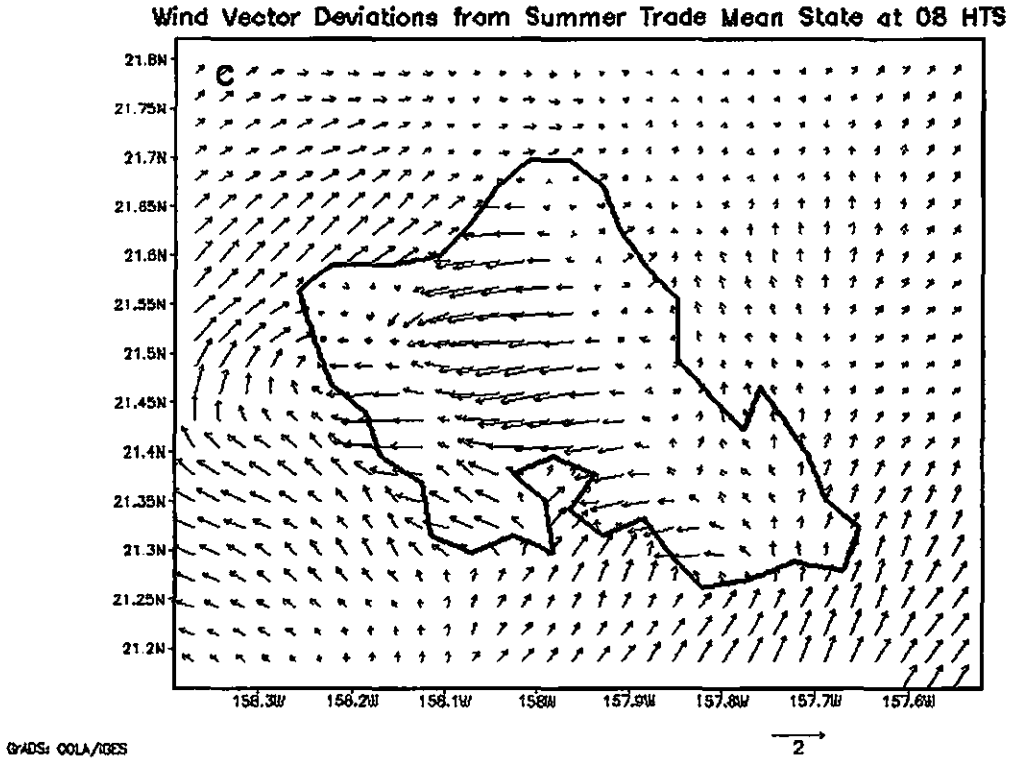

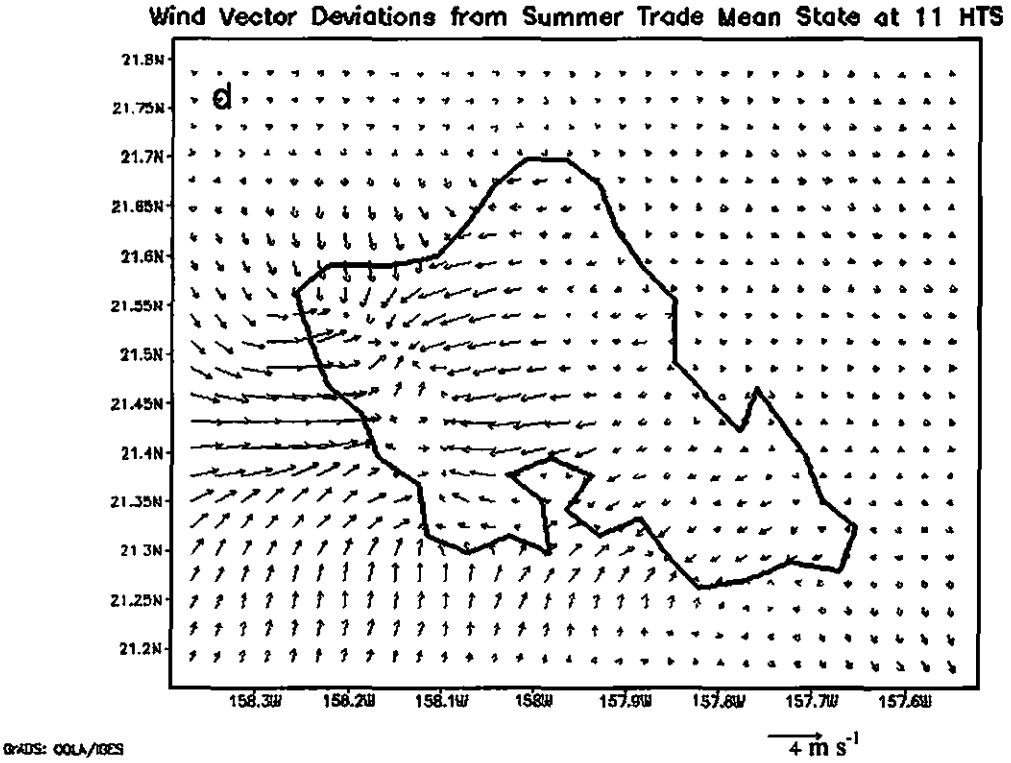

Figure A.1 The diurnal perturbations of wind vector from the summer mean state for (c) at 08 HST, and (d) at 11 HST

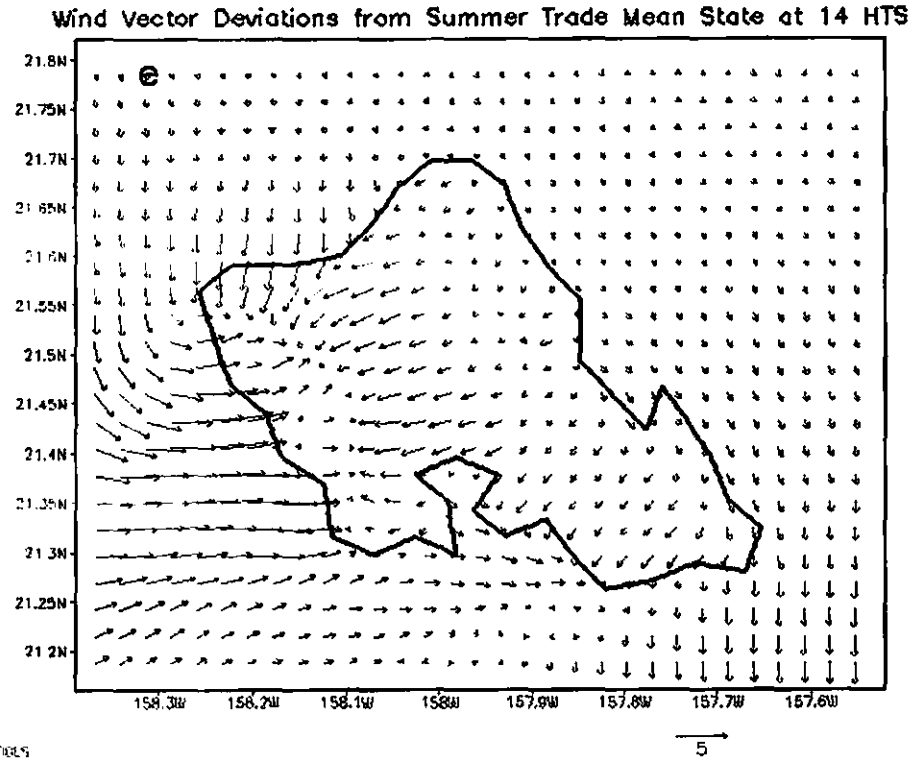

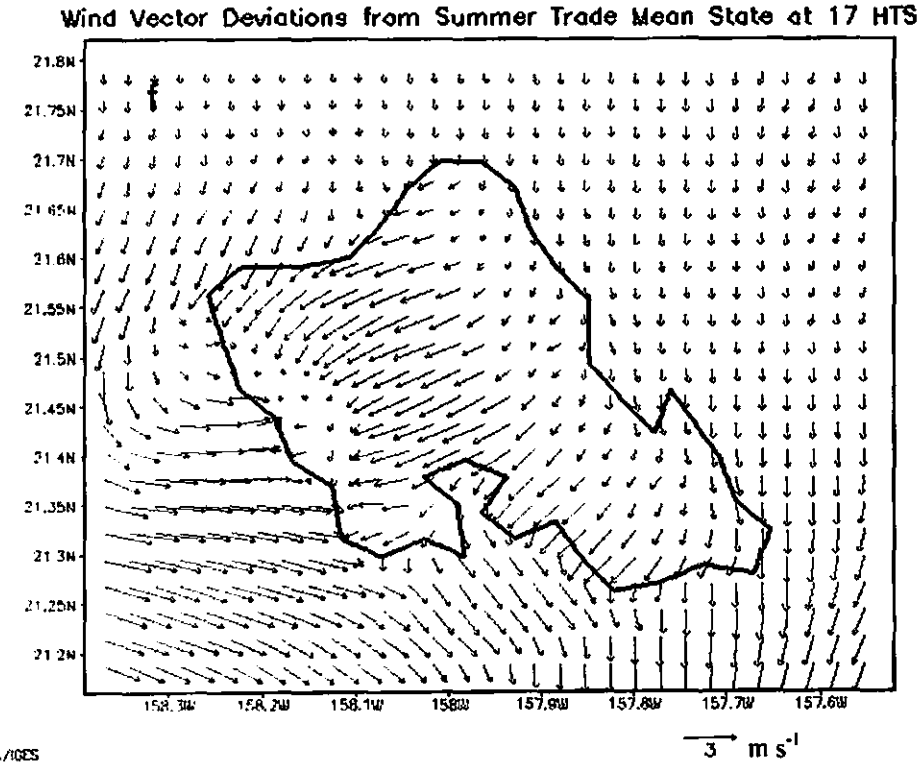

Figure A.1 The diurnal perturbations of wind vector from the summer mean state for (e) at 14 HST. and (f) at 17 HST

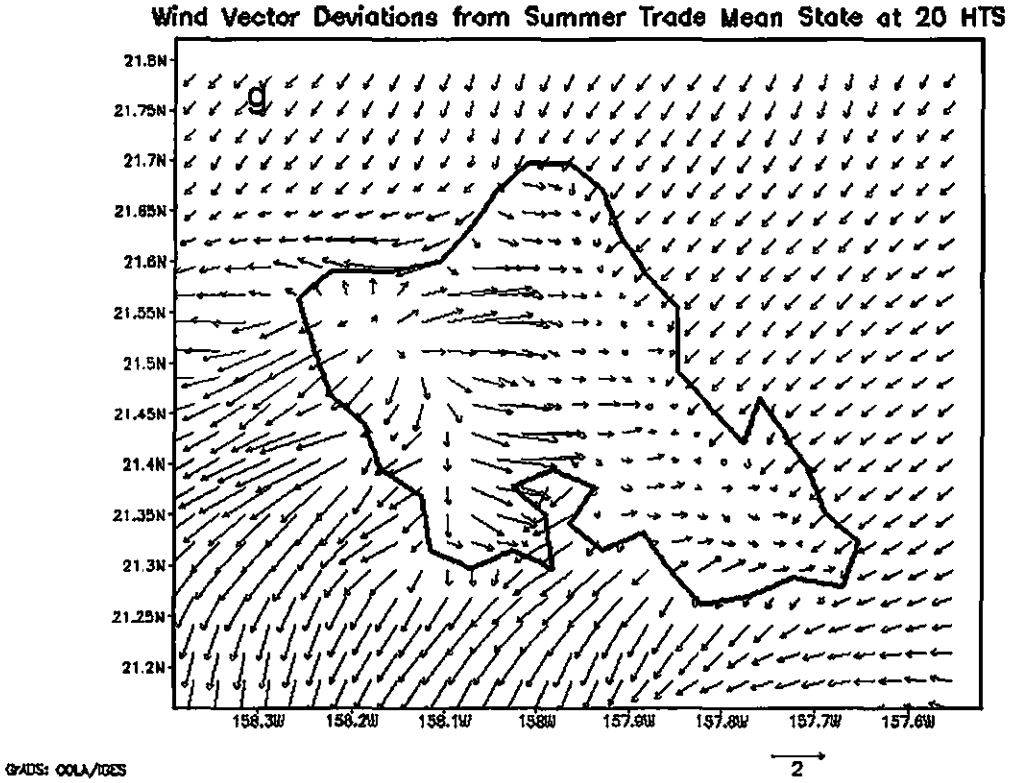

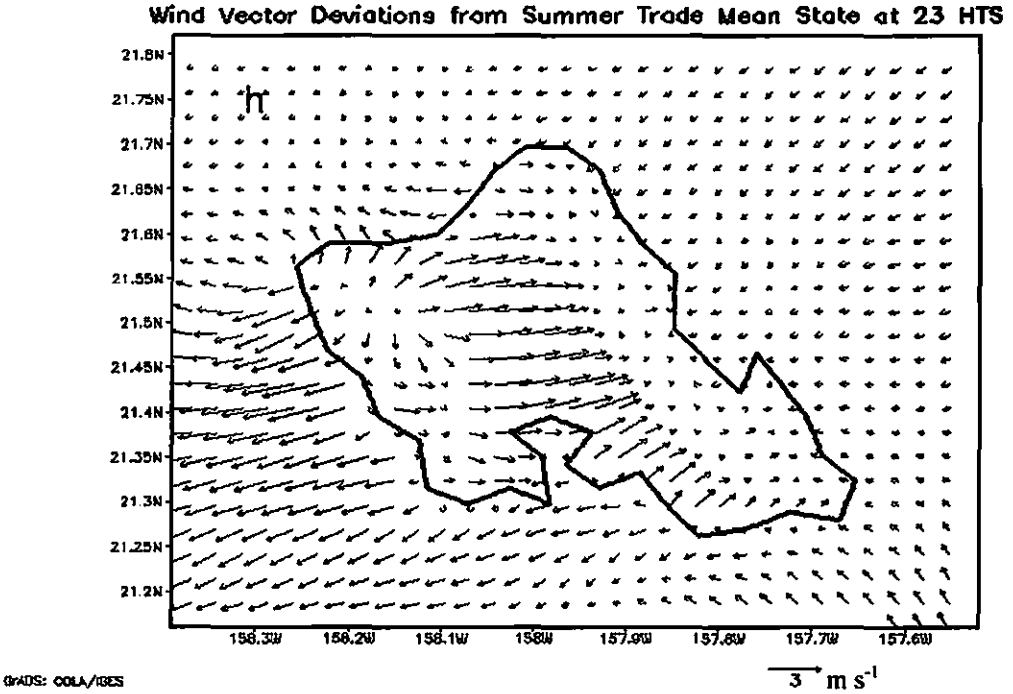

Figure A.1 The diurnal perturbations of wind vector from the summer mean state for (g) at 08 HST, and (h) at 11 HST

A.2 The diurnal perturbations of zonal wind component from the summer mean state.

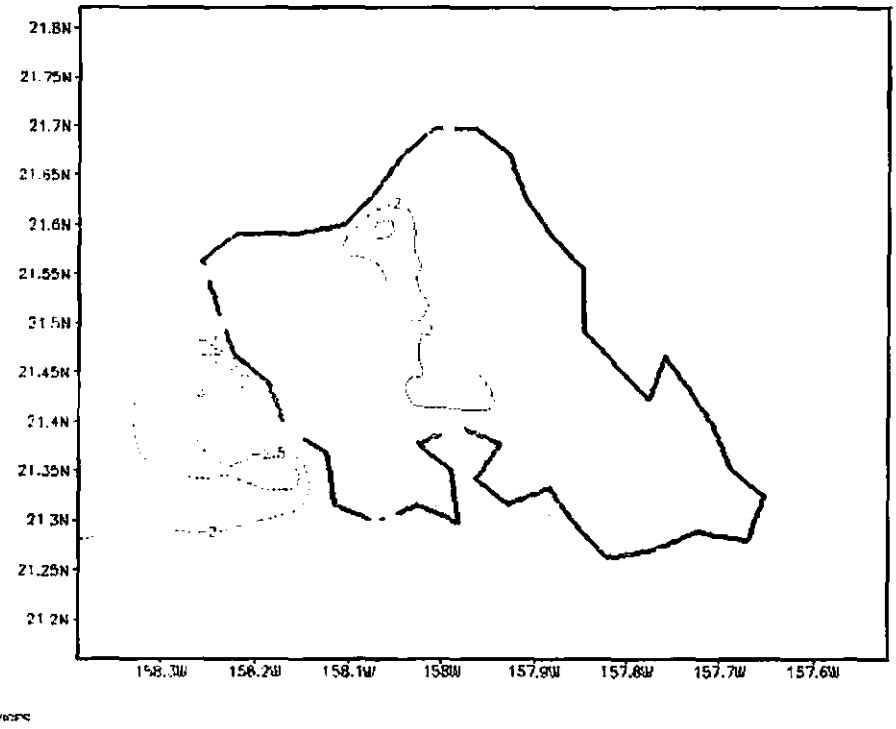

Perturbations of zonal wind component (m s^{-1}) from the summer mean state at 02 HST

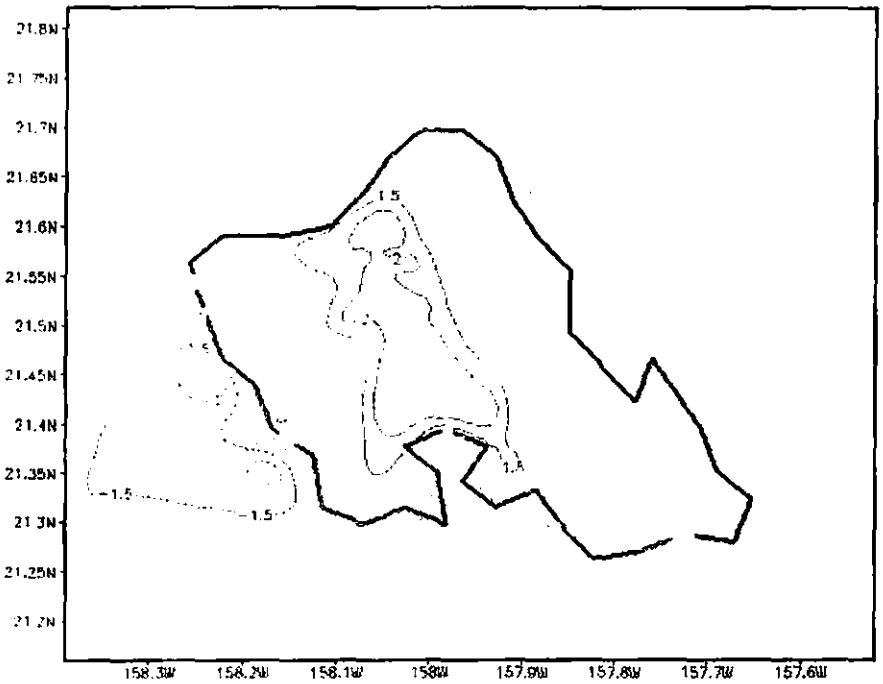

Perturbations of zonal wind component (m s^{-1}) from the summer mean state at 05 HST

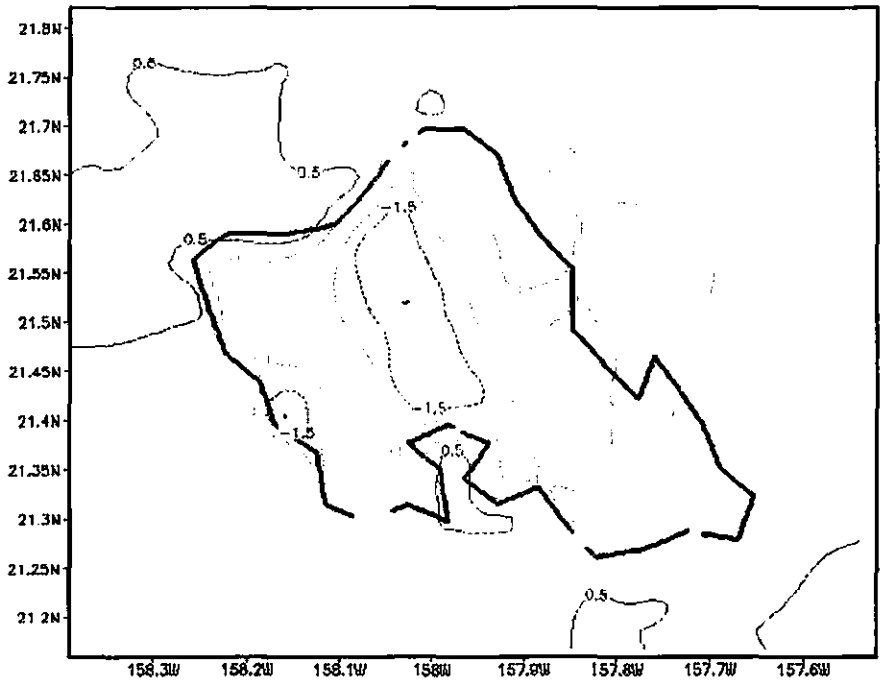

Perturbations of zonal wind component (m s^{-1}) from the summer mean state at 08 HST

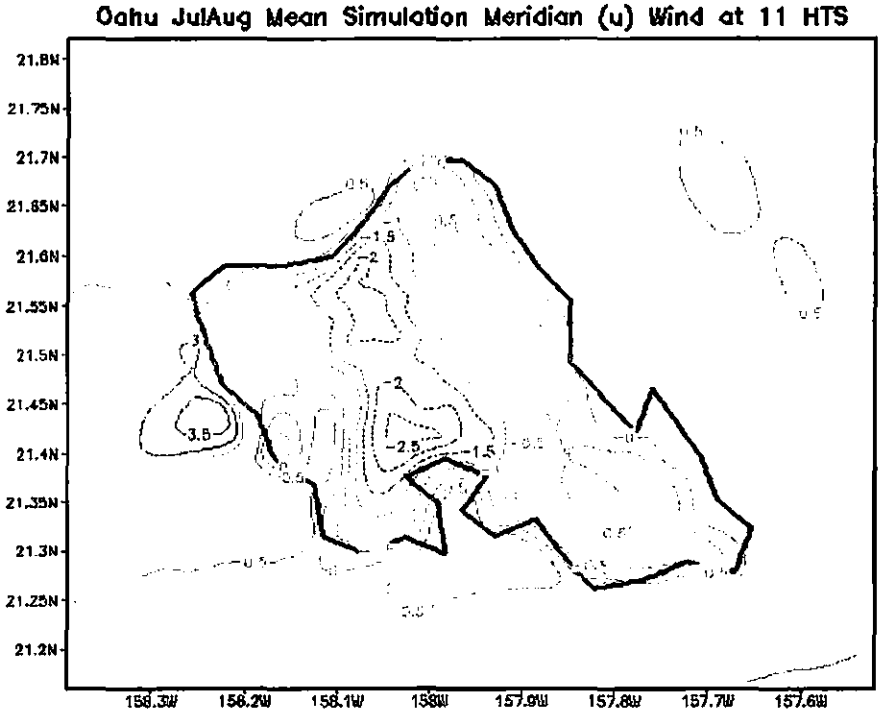

Perturbations of zonal wind component (m s^{-1}) from the summer mean state at 11 HST

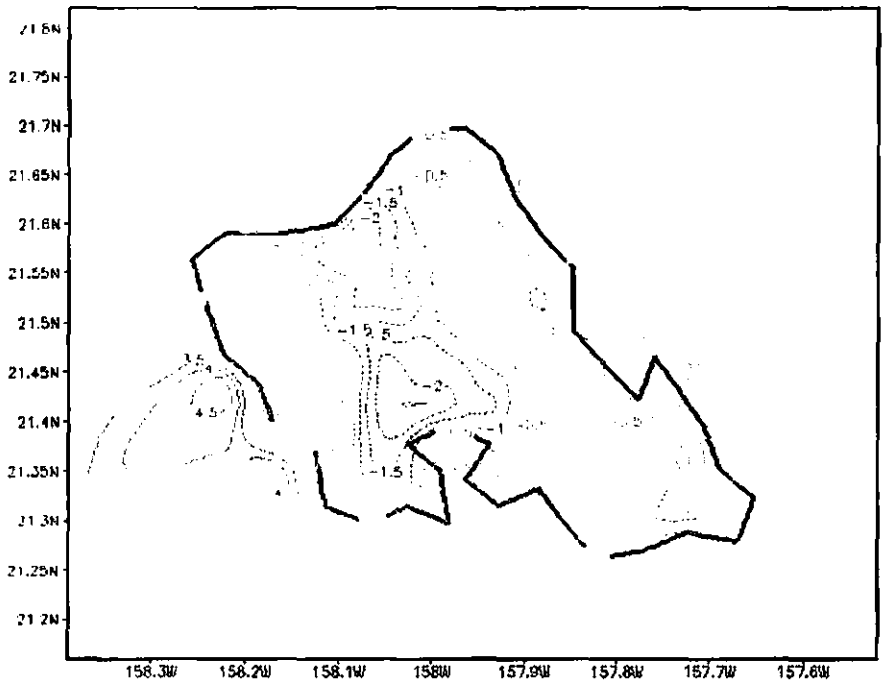

Perturbations of zonal wind component (m s^{-1}) from the summer mean state at 14 HST

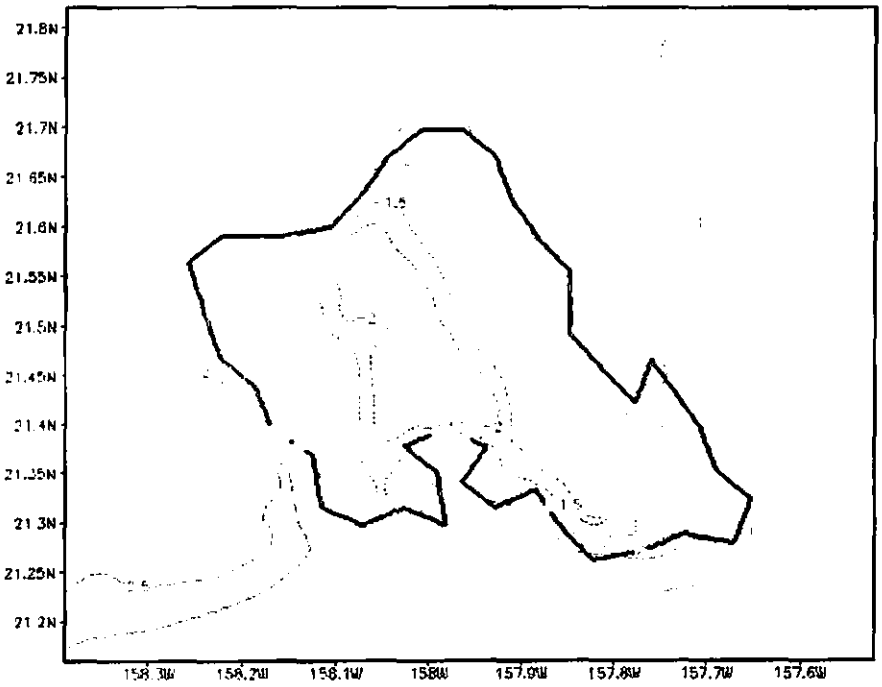

Perturbations of zonal wind component (m s^{-1}) from the summer mean state at 17 HST

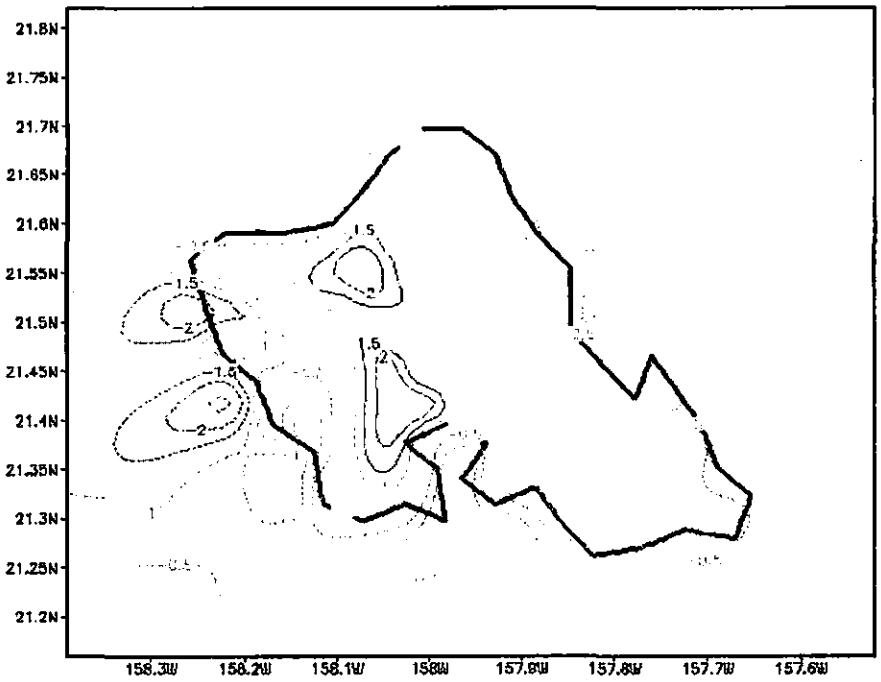

Perturbations of zonal wind component (m s $^{-1}$) from the summer mean state at 20 HST

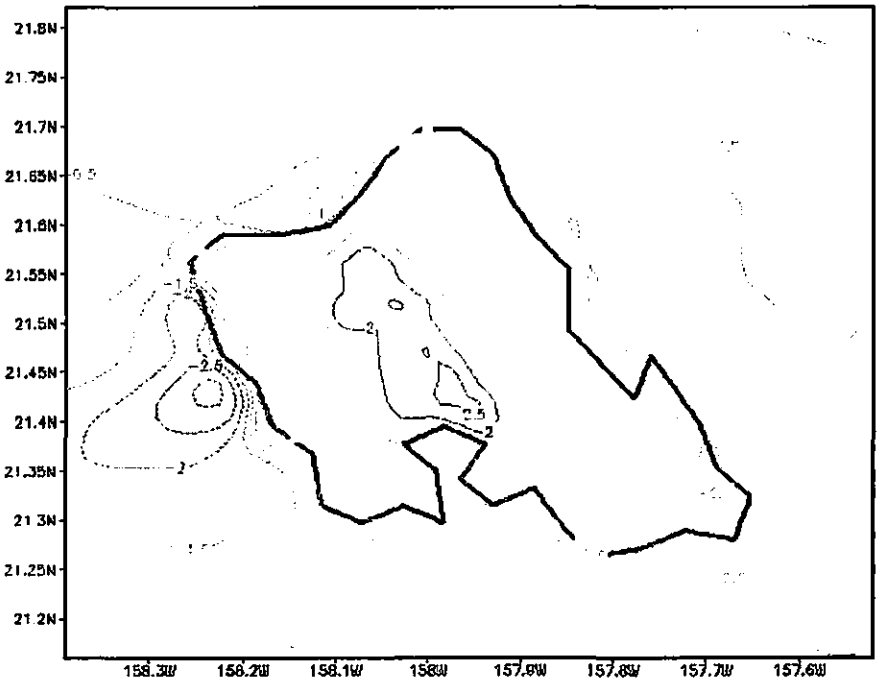

Perturbations of zonal wind component (m s $^{-1}$) from the summer mean state at 23 HST

A.3 Vertical cross sections at (21.45 N) of the diurnal perturbations of zonal wind (m s^{-1}) component from the summer mean state.

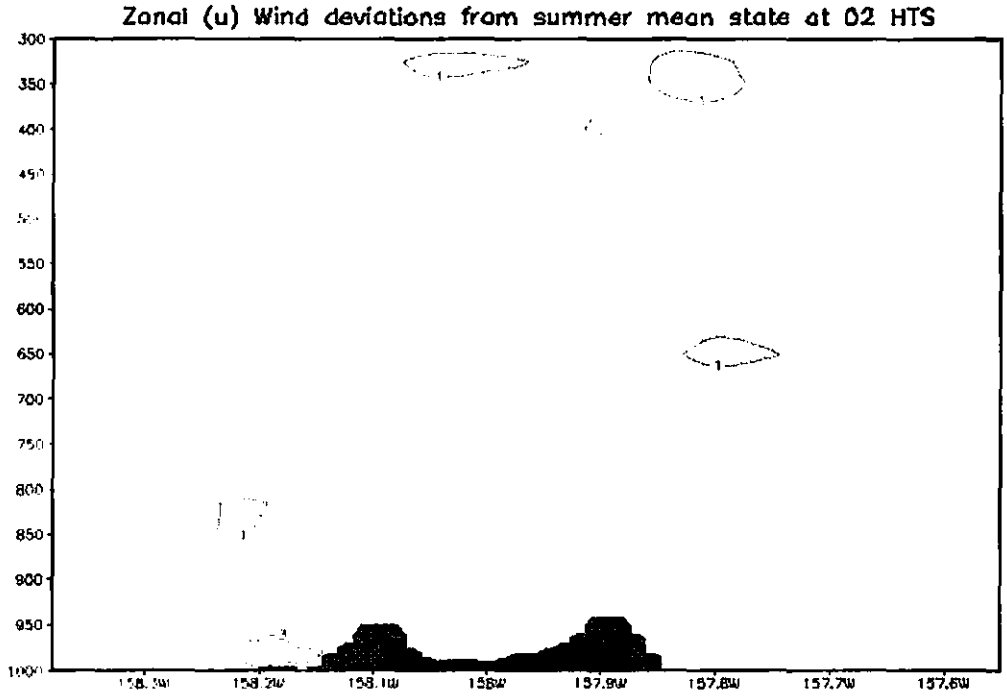

GrADS: COLA/IGES

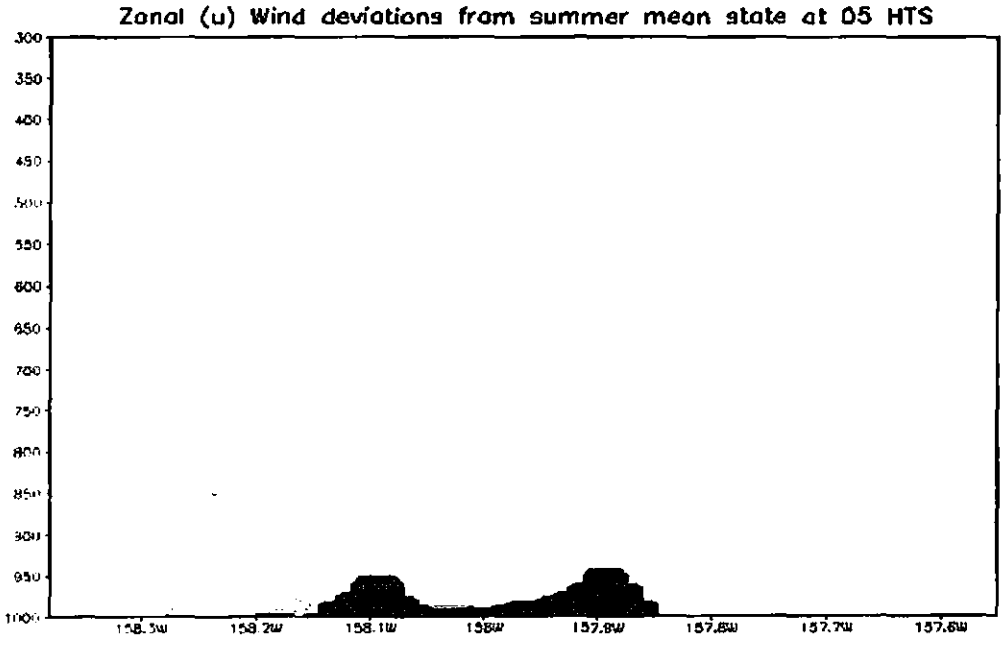

GrADS: COLA/IGES

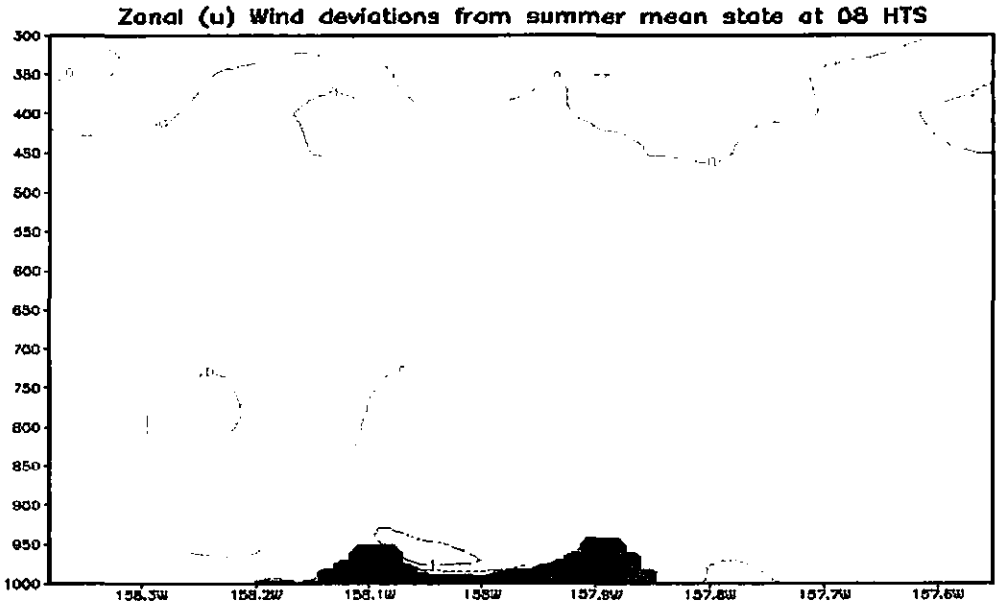
Zonal (u) Wind deviations from summer mean state at 08 HTS
300
350
400
450
500
550
600
650
700
750
800
850
900
950
1000
158.3W
158.2W
158.1W
158W
157.9W
157.8W
157.7W
157.6W
GrADS: COLA/IGES

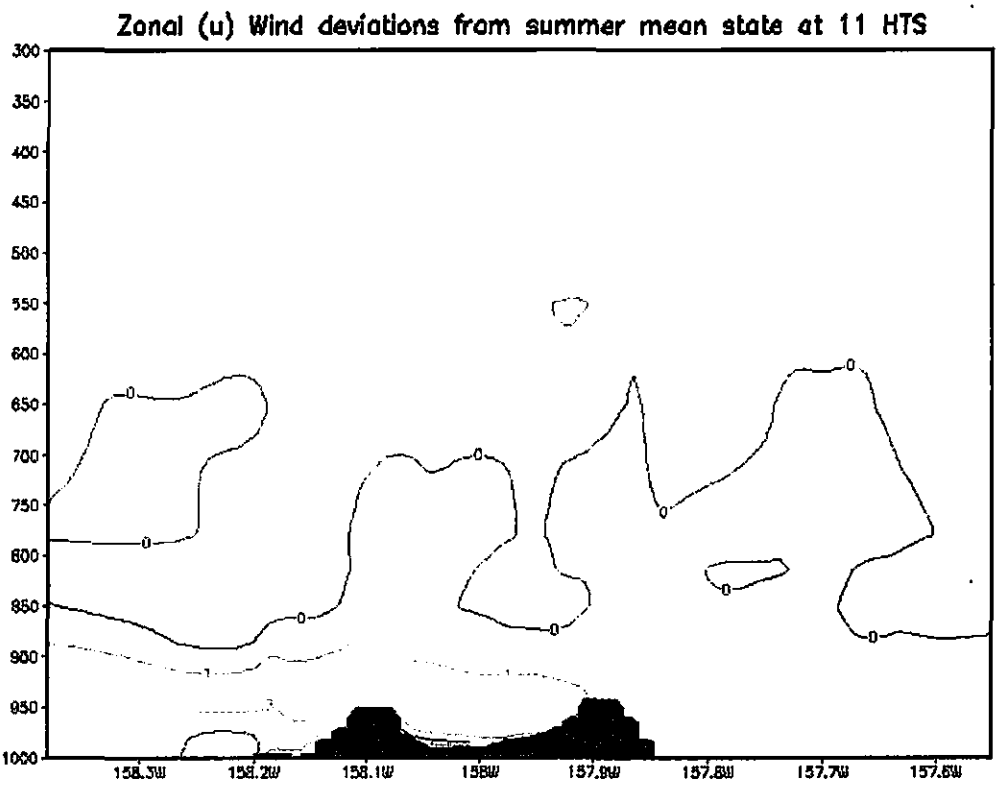
Zonal (u) Wind deviations from summer mean state at 11 HTS
300
350
400
450
500
550
600
650
700
750
800
850
900
950
1000
158.3W
158.2W
158.1W
158W
157.9W
157.8W
157.7W
157.6W
GrADS: COLA/IGES

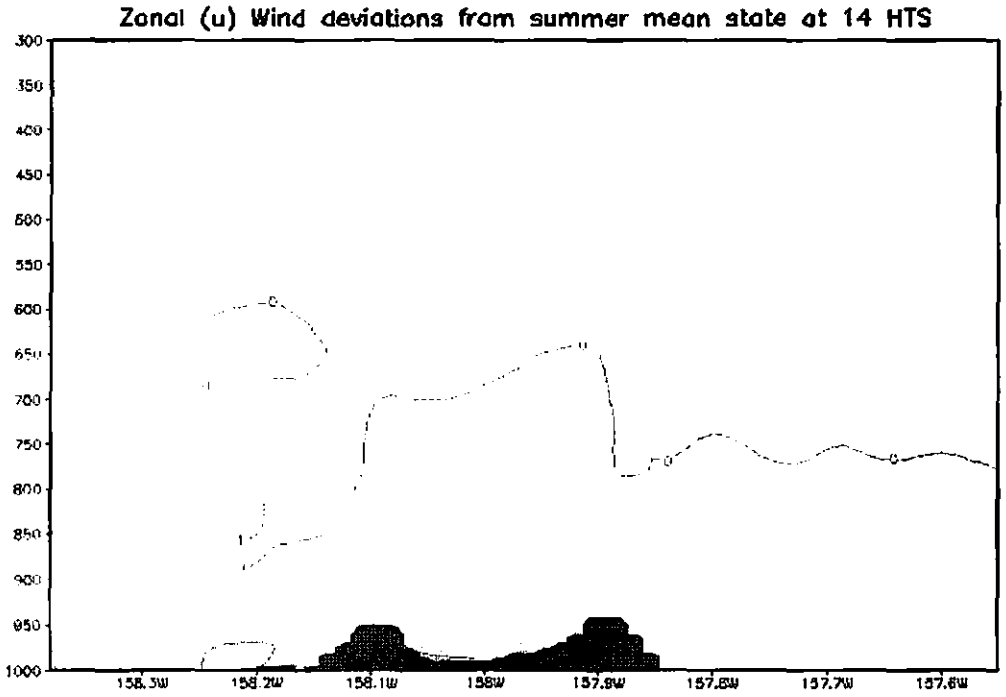
Zonal (u) Wind deviations from summer mean state at 14 HTS
300
350
400
450
500
550
600
650
700
750
800
850
900
950
1000
158.3W
158.2W
158.1W
158W
157.9W
157.8W
157.7W
157.6W
GrADS: COLA/IGES

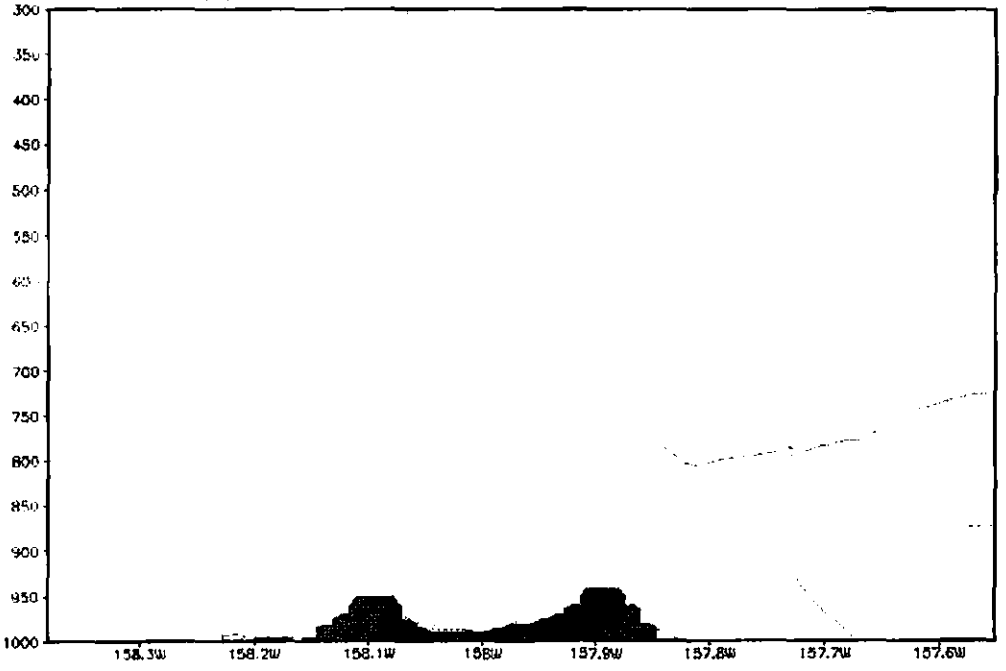
Zonal (u) Wind deviations from summer mean state at 17 HTS
300
350
400
450
500
550
600
650
700
750
800
850
900
950
1000
158.3W
158.2W
158.1W
158W
157.9W
157.8W
157.7W
157.6W
GrADS: COLA/IGES

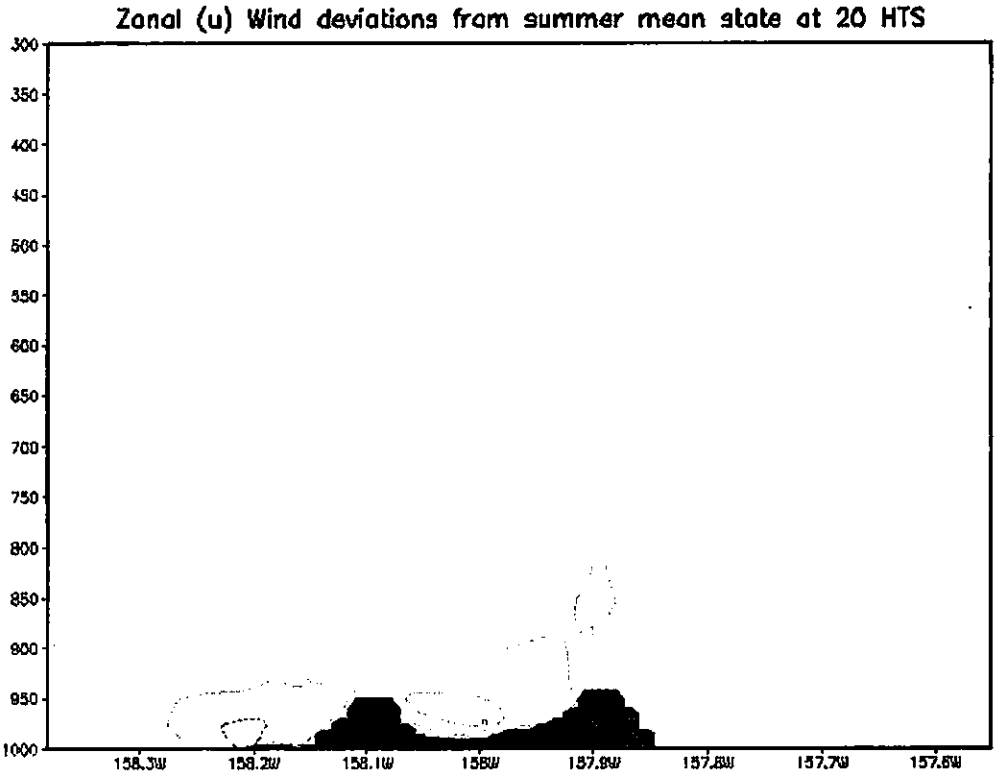

GrADS: COLA/IGES

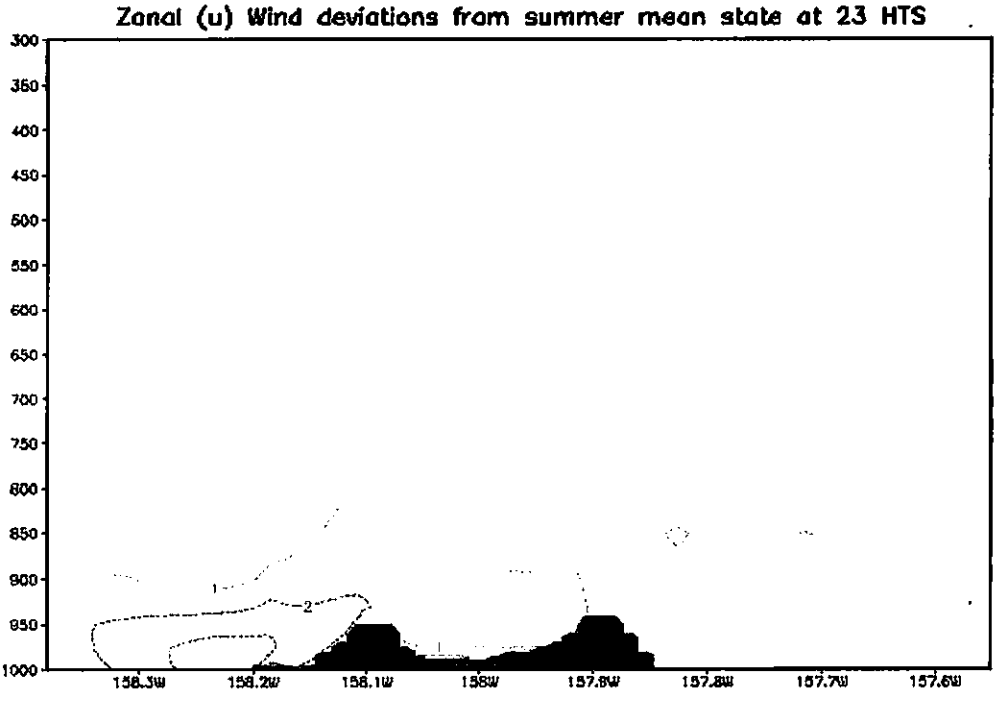

GrADS: COLA/IGES

Appendix B The diurnal perturbations of wind from the mean state at 3-hour interval under strong trades

B.1 The diurnal perturbations of wind vector from the strong-trade mean state

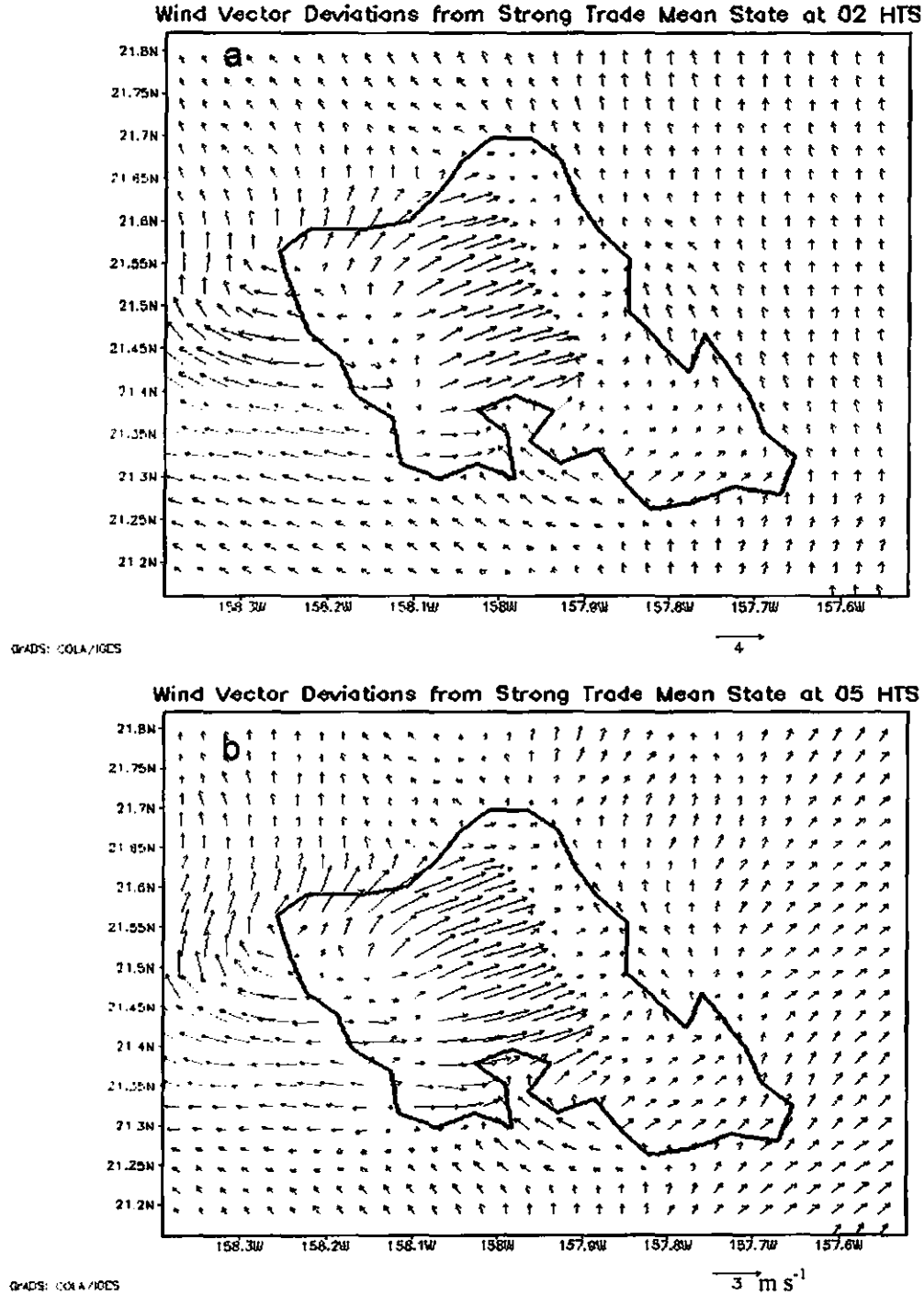

Figure B.1 The diurnal perturbations of wind vector from the strong-trade mean state (a) at 02 HST, and (b) at 05 HST

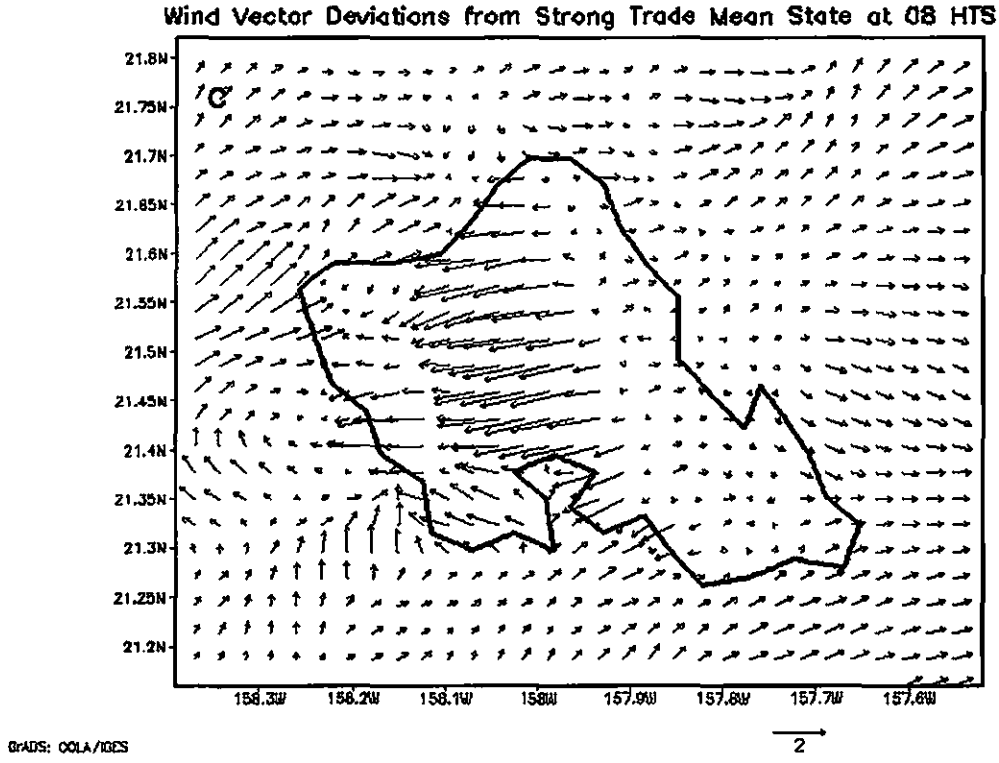

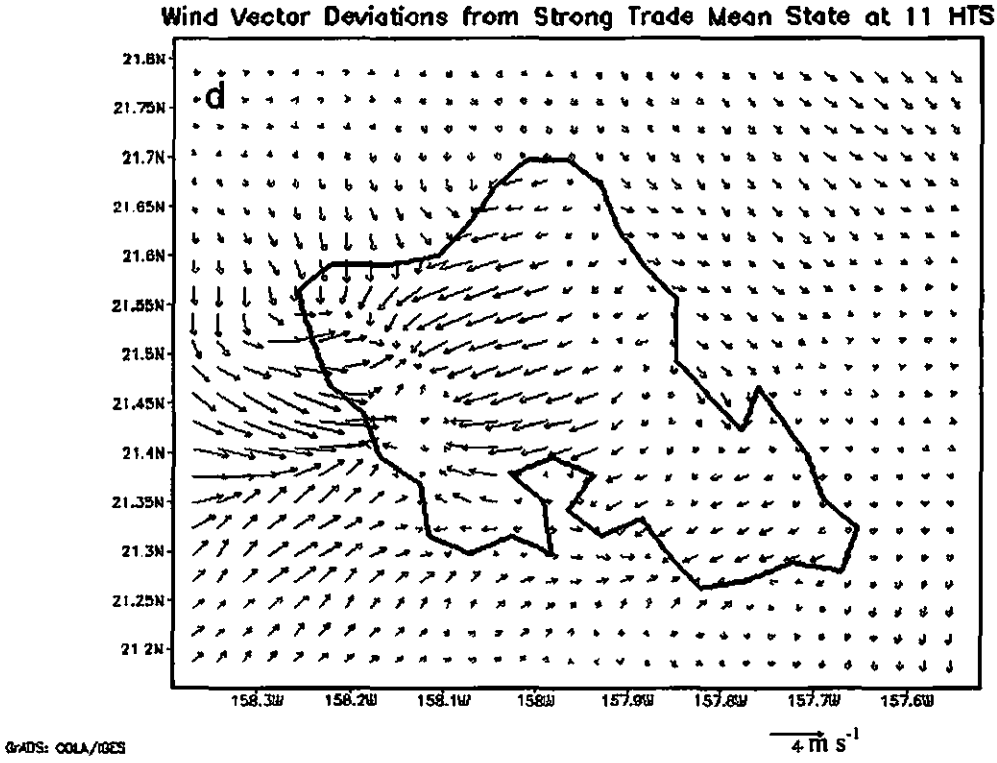

Figure B.1 The diurnal perturbations of wind vector from the strong-trade mean state (c) at 08 HST, and (d) at 11 HST

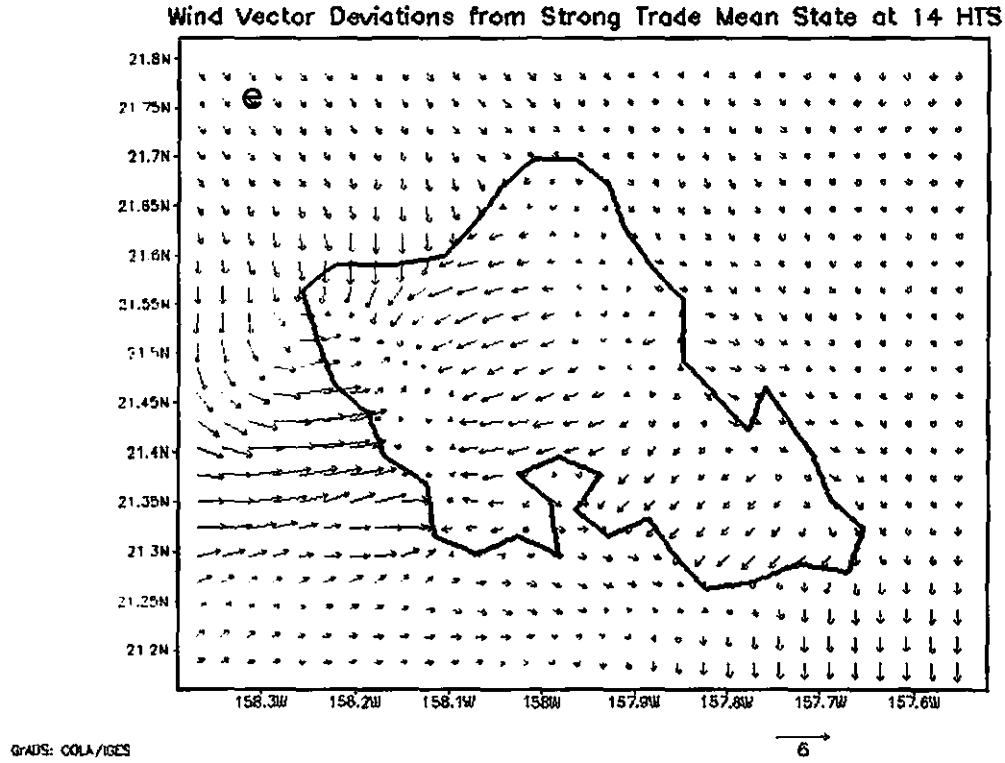

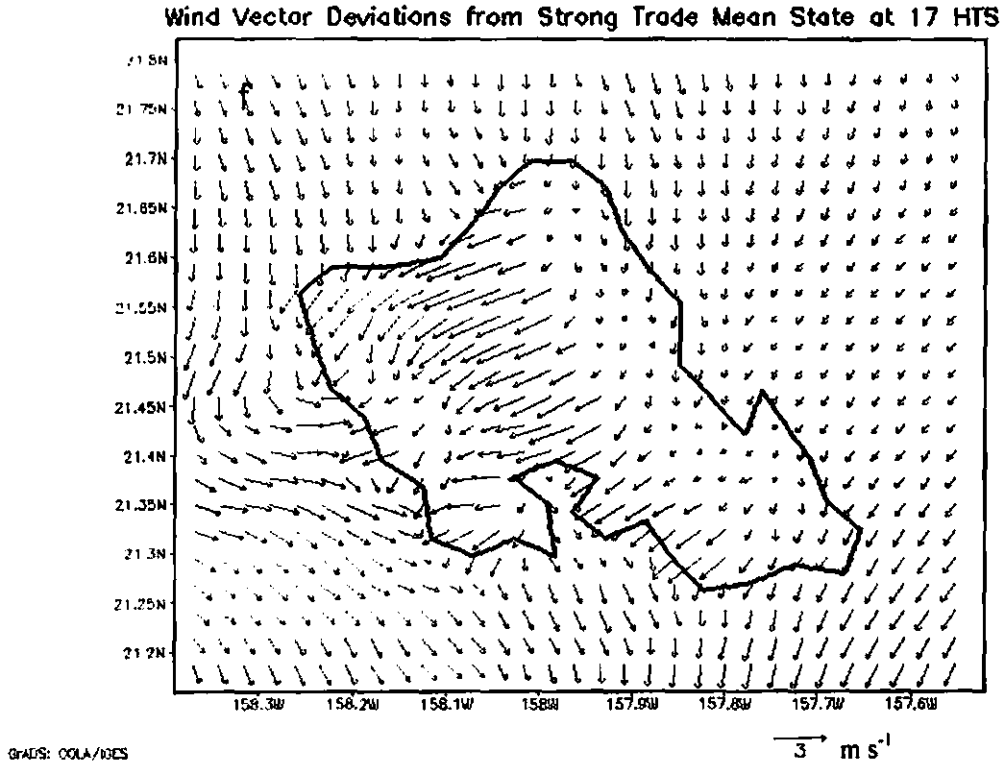

Figure B.1 The diurnal perturbations of wind vector from the strong-trade mean state (e) at 14 HST, and (f) at 17 HST

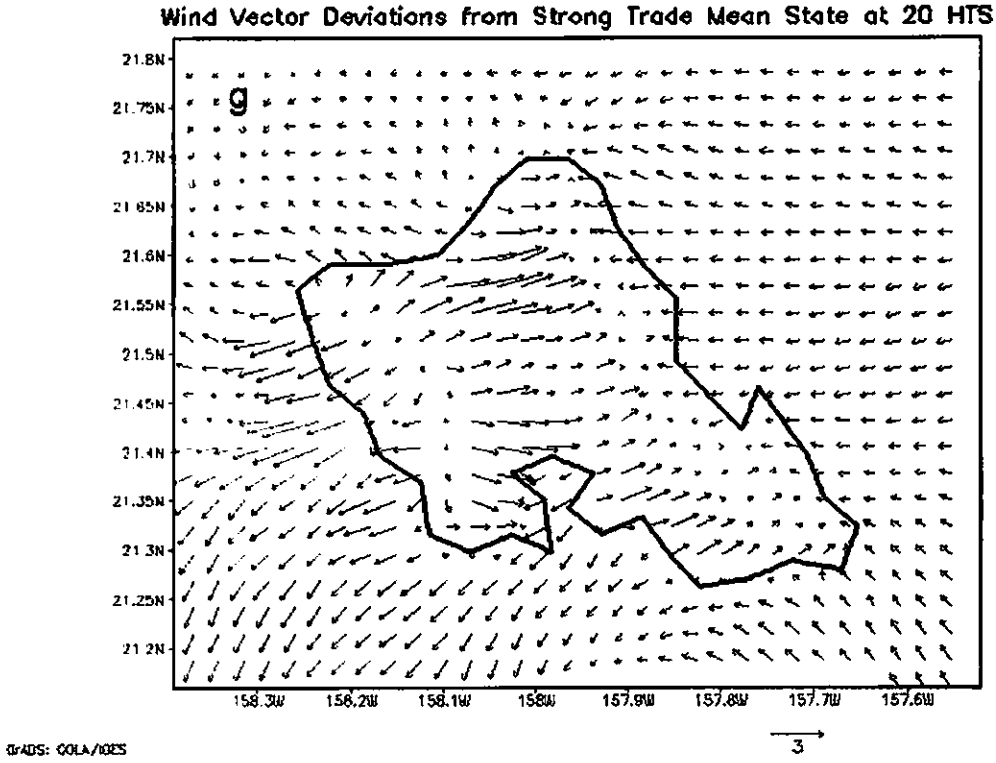

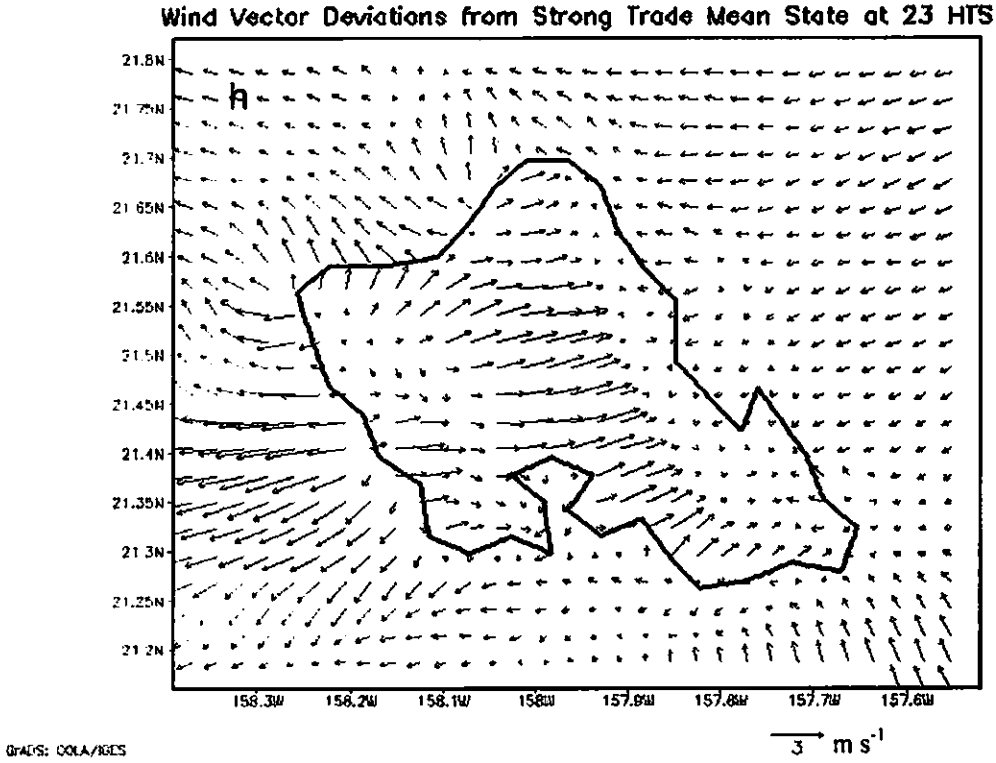

Figure B.1 The diurnal perturbations of wind vector from the strong-trade mean state (g) at 20 HST, and (h) at 23 HST

B.2 The diurnal perturbations of zonal wind component (m s^{-1}) from the strong-trade mean state

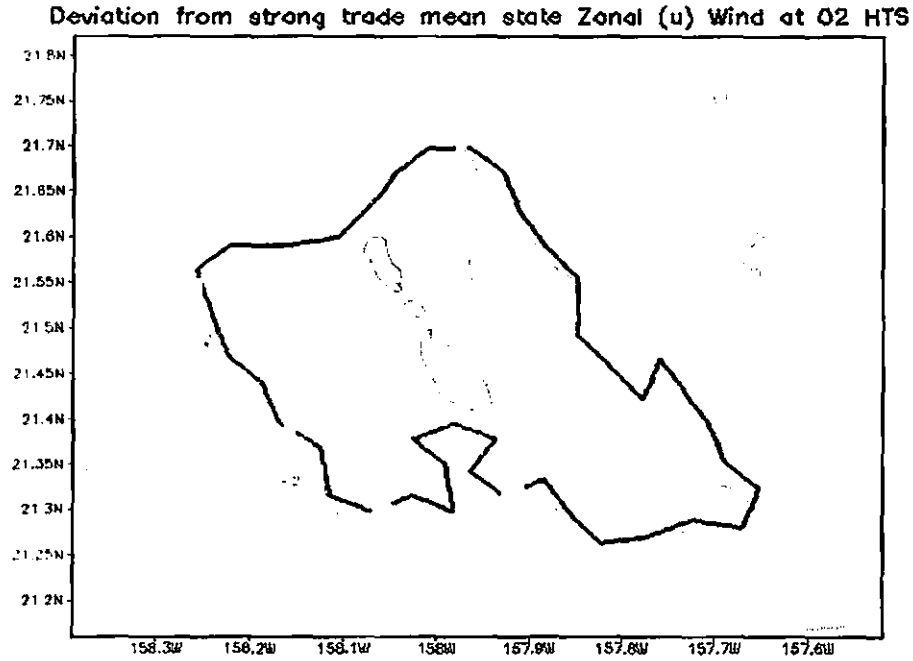

GrADS: COLA/IGES

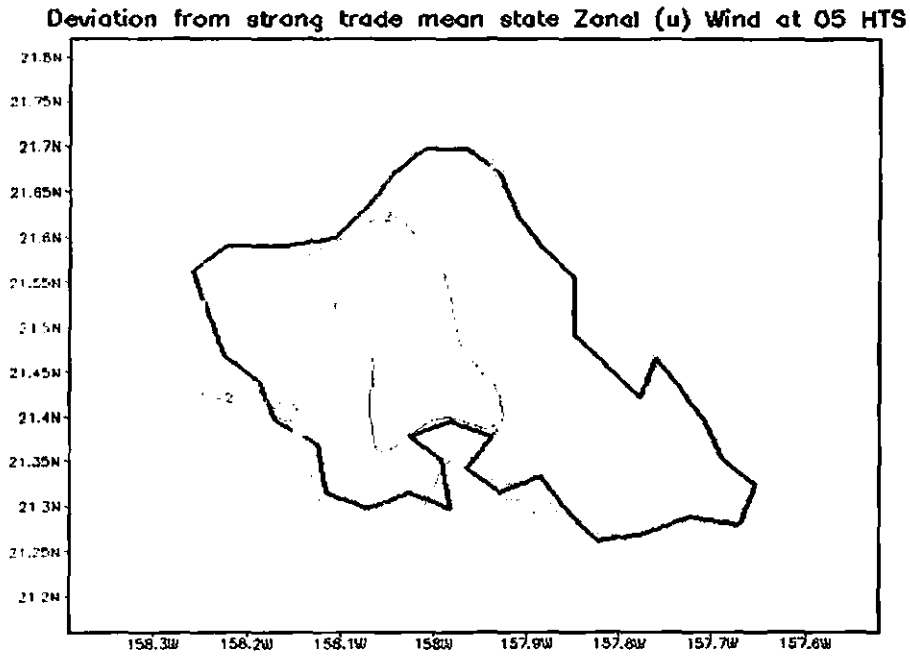

GrADS: COLA/IGES

Deviation from strong trade mean state Zonal (u) Wind at 08 HTS

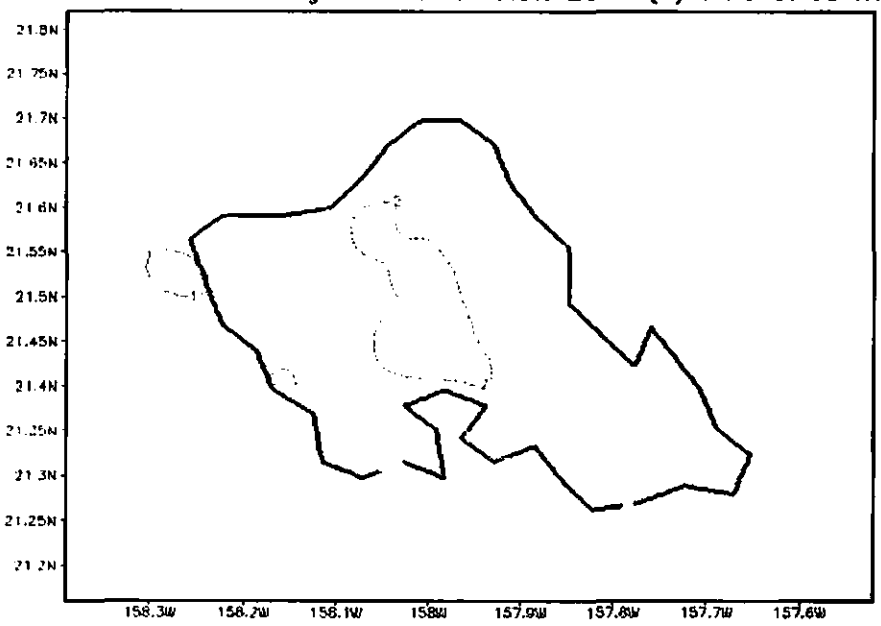

GrADS: COLA/IGES

Deviation from strong trade mean state Zonal (u) Wind at 11 HTS

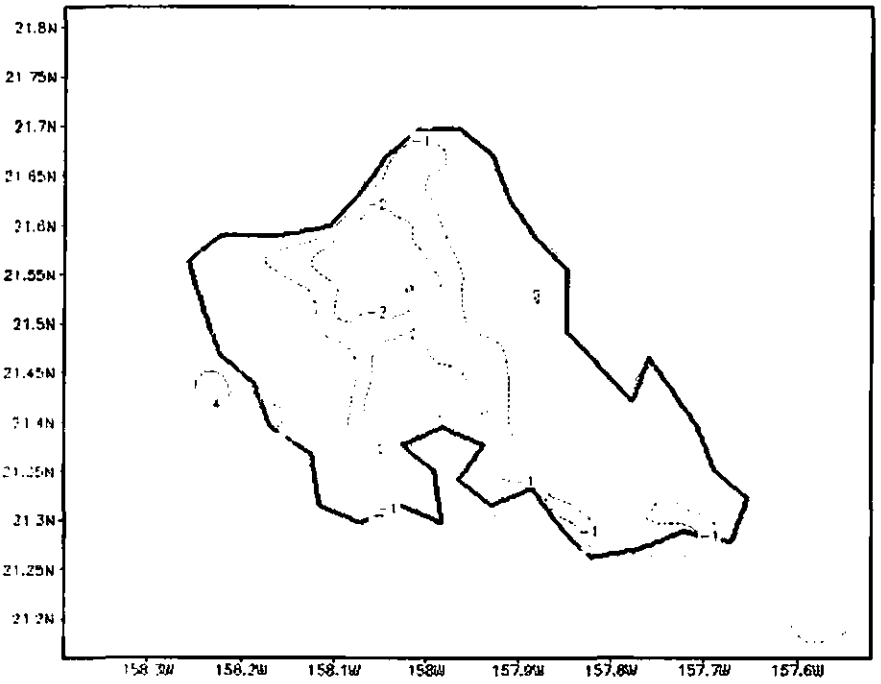

GrADS: COLA/IGES

Deviation from strong trade mean state Zonal (u) Wind at 14 HTS

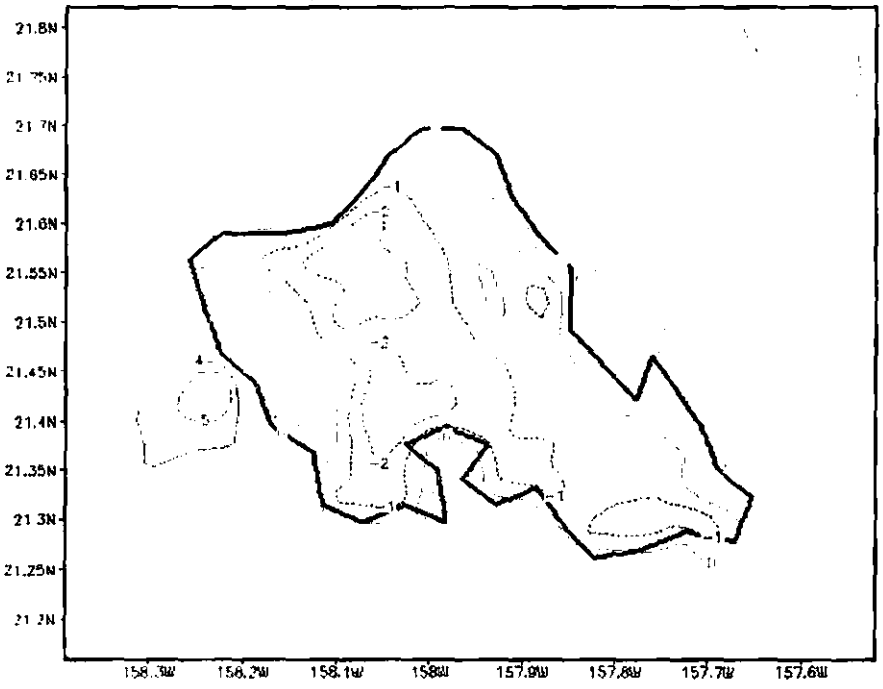

GrADS: COLA/IGES

Deviation from strong trade mean state Zonal (u) Wind at 17 HTS

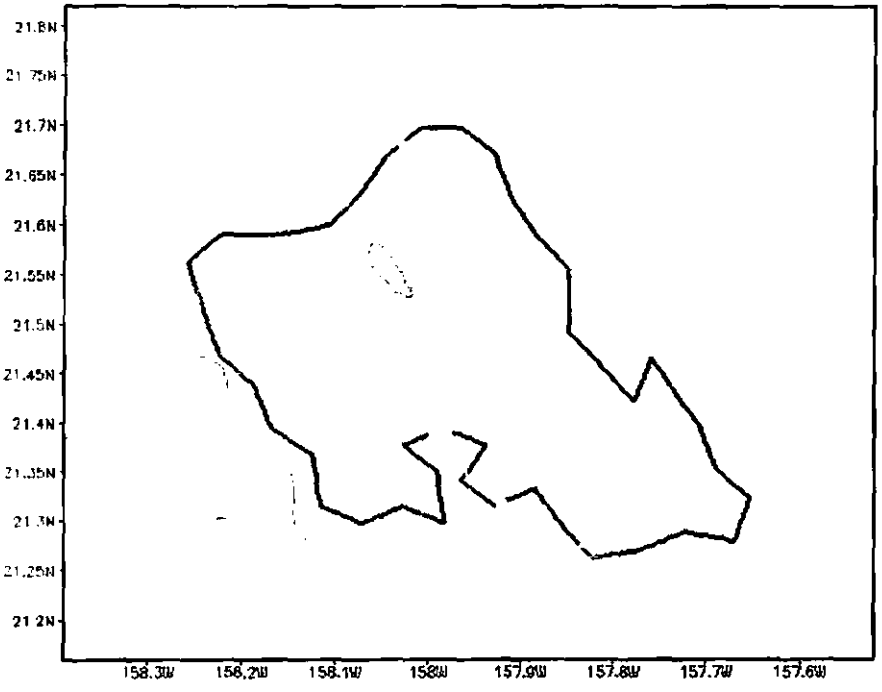

GrADS: COLA/IGES

Deviation from strong trade mean state Zonal (u) Wind at 20 HTS

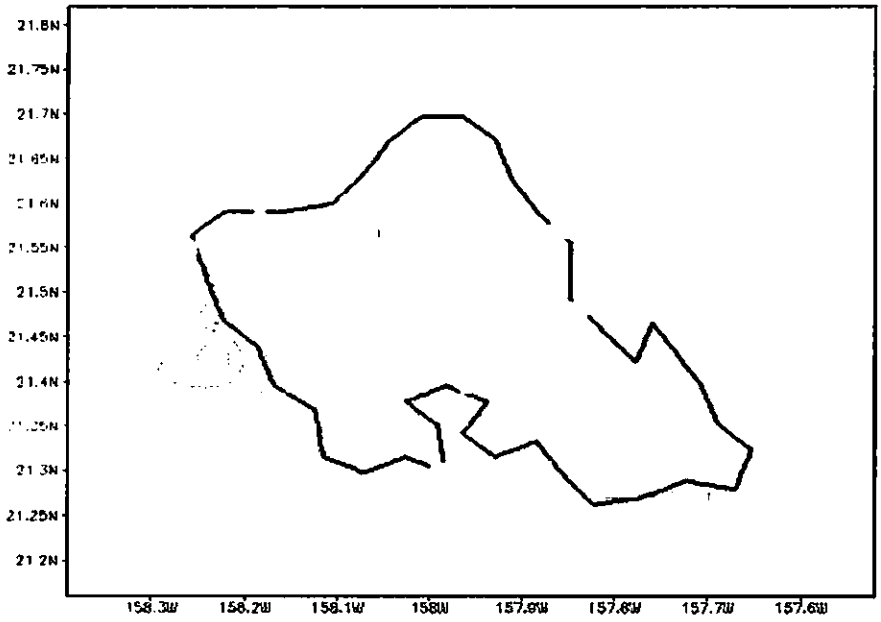

GrADS: COLA/IGES

Deviation from strong trade mean state Zonal (u) Wind at 23 HTS

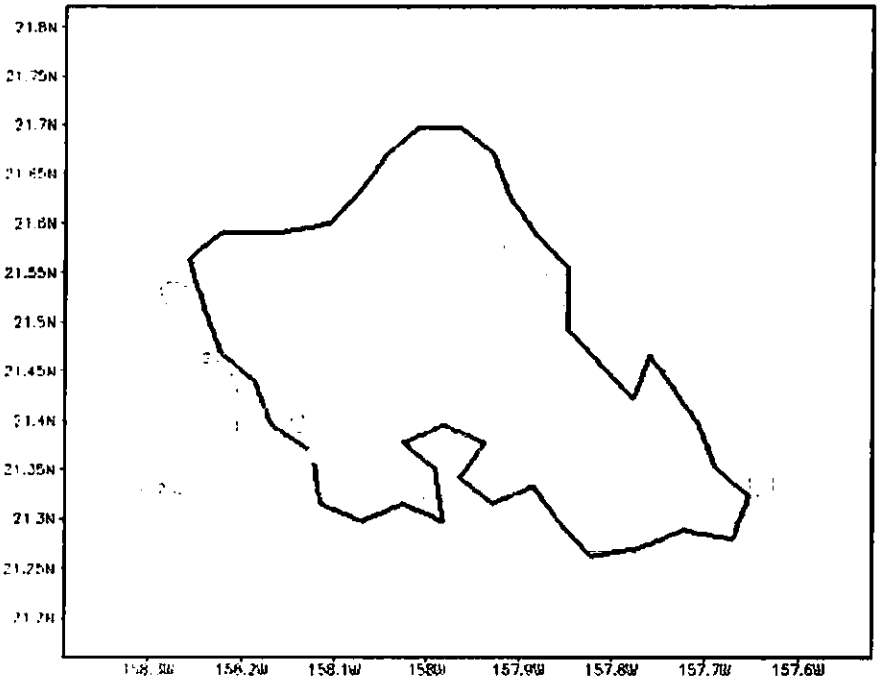

GrADS: COLA/IGES

B.3 Vertical cross sections at (21.45 N) of the diurnal perturbations of zonal wind component (m s^{-1}) from the strong-trade mean state.

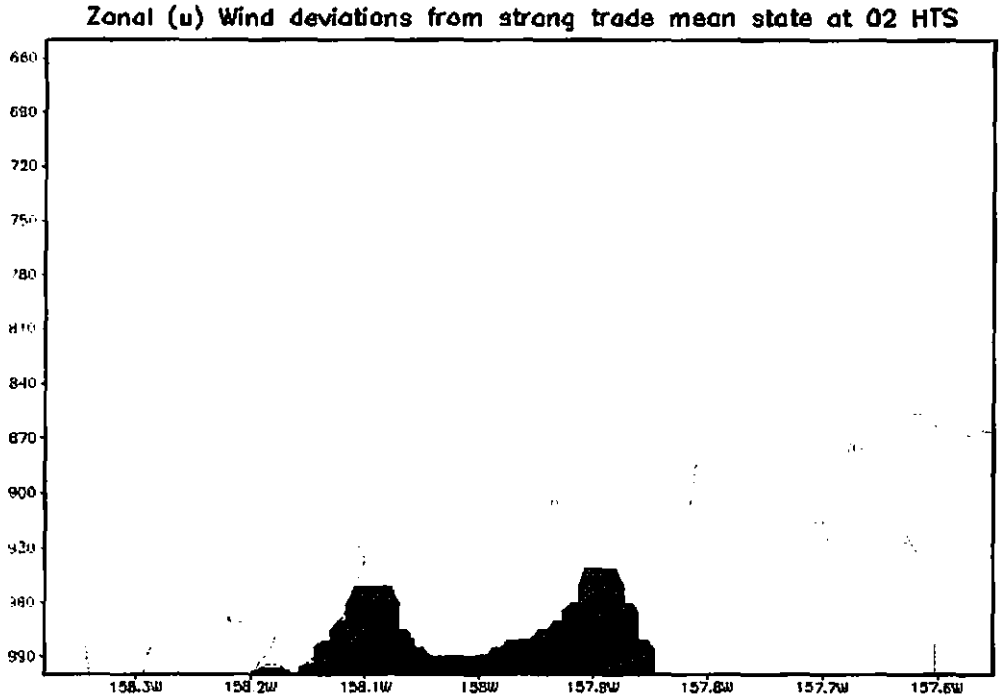

GrADS: COLA/IGES

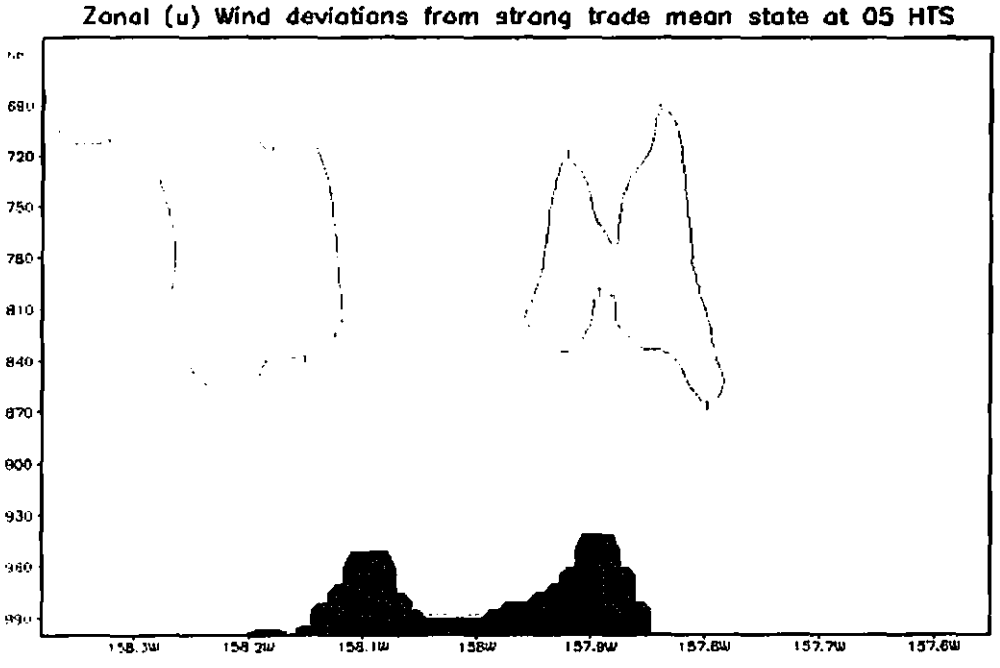

GrADS: COLA/IGES

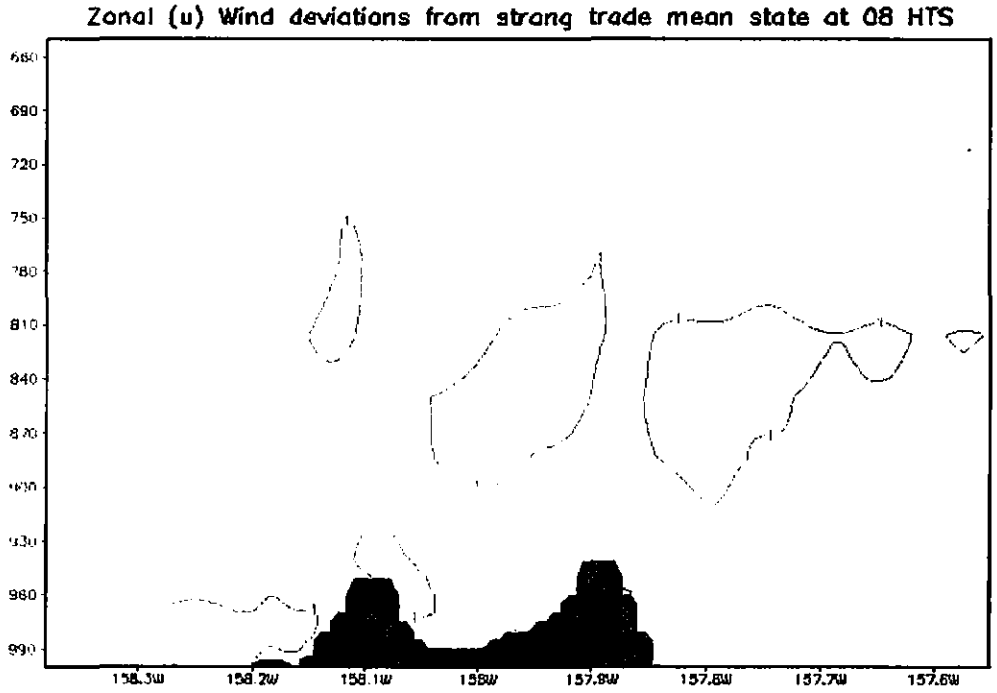

GRADS: COLA/IGES

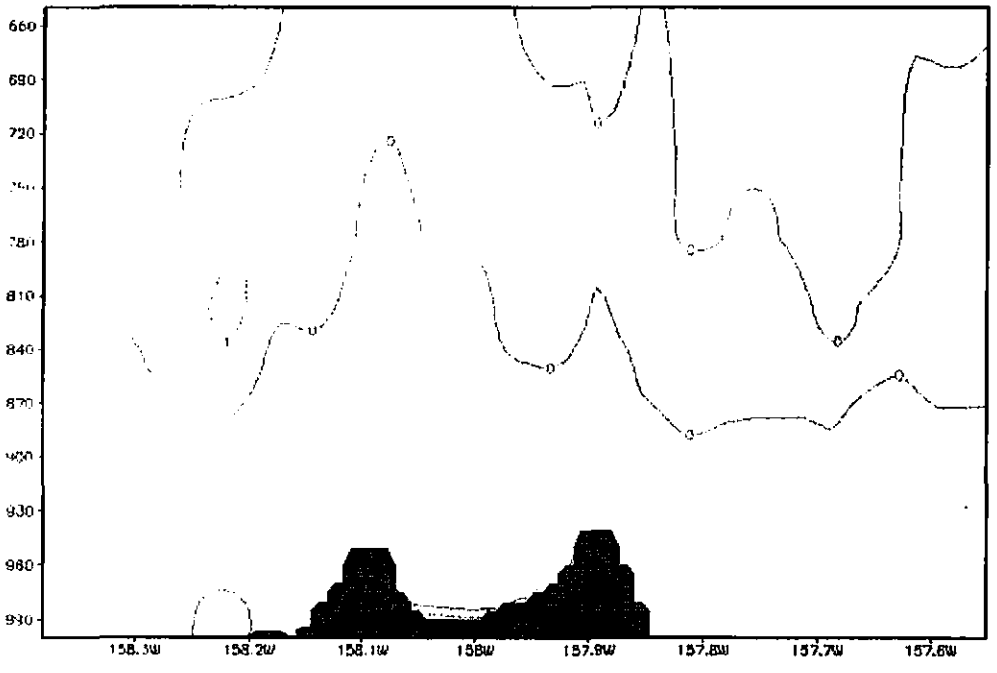

GRADS: COLA/IGES

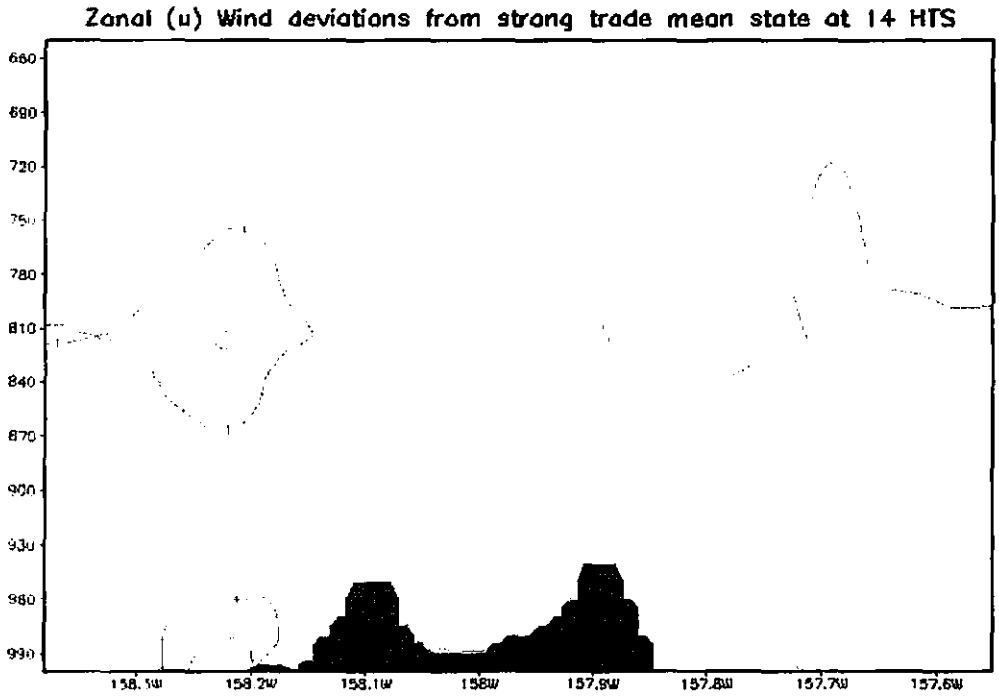

GrADS: COLA/IGES

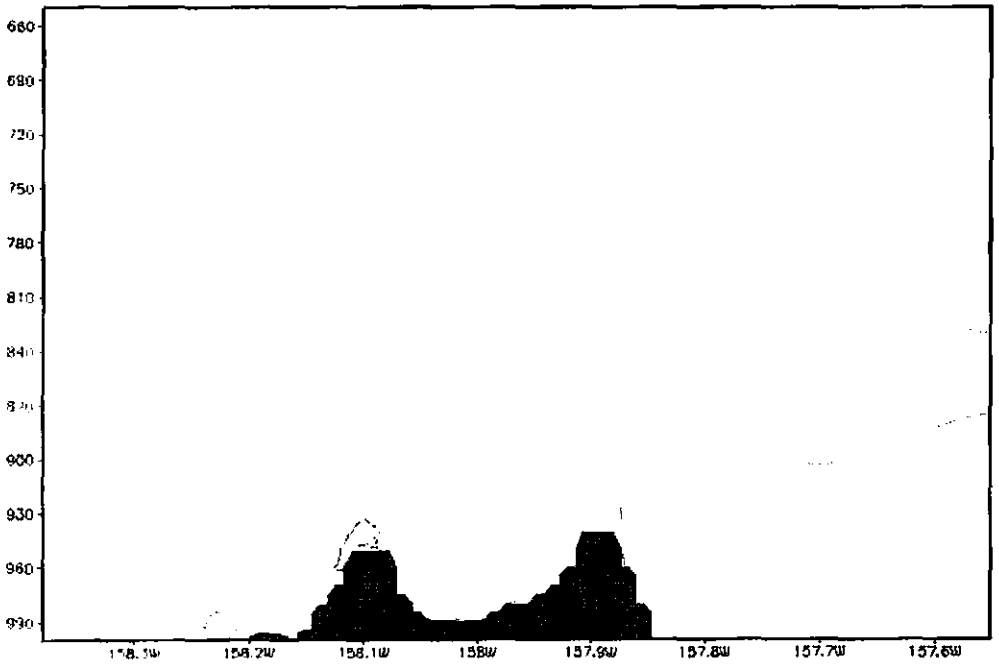

GrADS: COLA/IGES

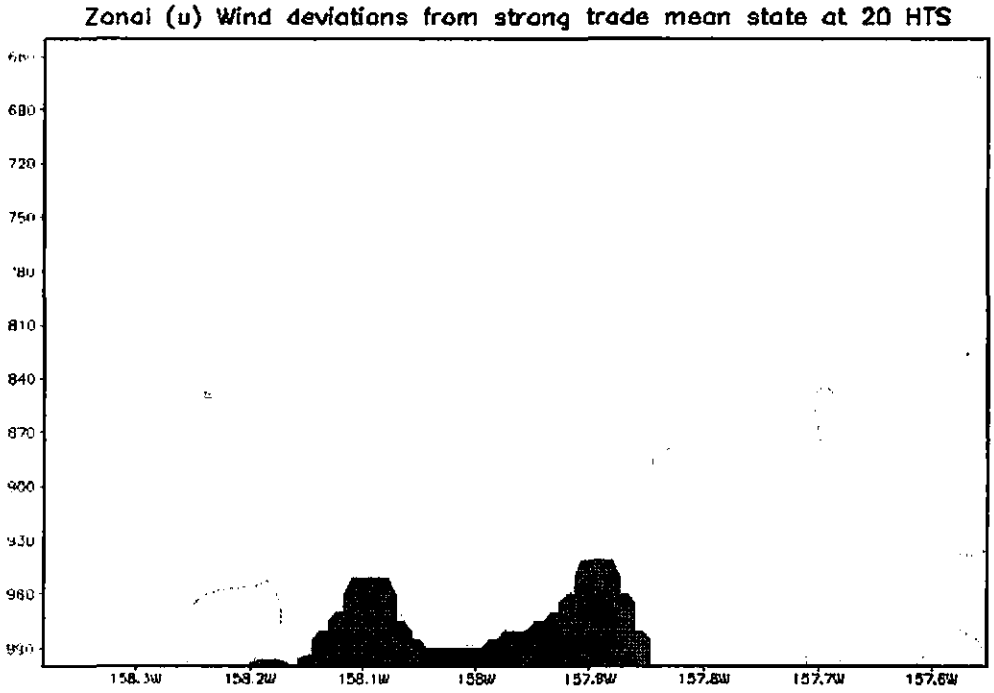
Zonal (u) Wind deviations from strong trade mean state at 20 HTS
680
720
750
780
810
840
870
900
930
960
990
158.3W
158.2W
158.1W
158W
157.9W
157.8W
157.7W
157.6W

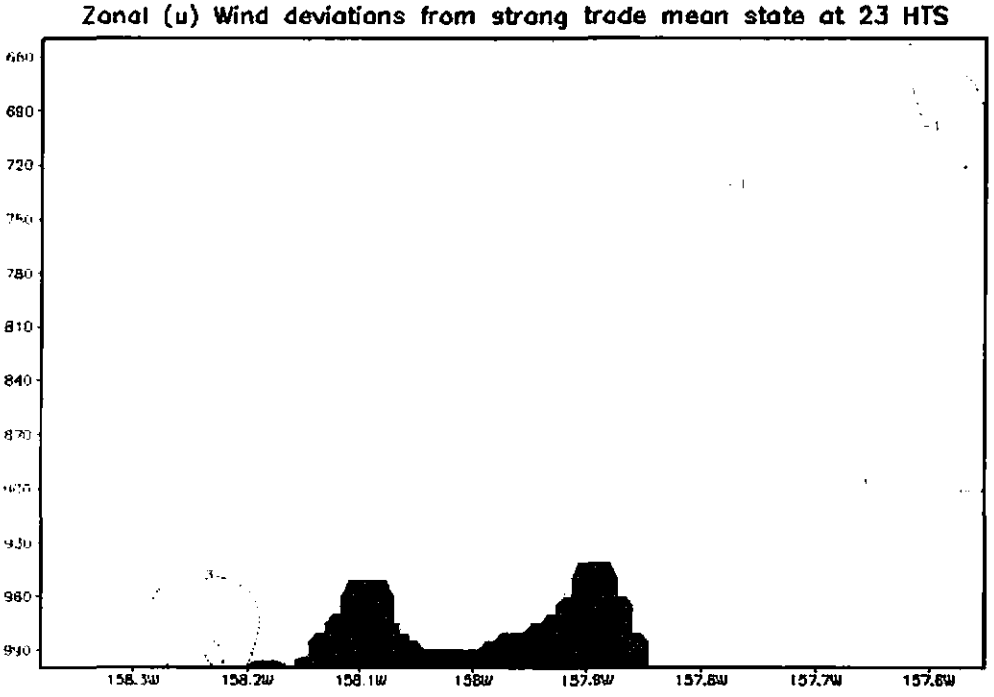
Zonal (u) Wind deviations from strong trade mean state at 23 HTS
680
720
780
810
840
930
960
990
158.3W
158.2W
158.1W
158W
157.9W
157.8W
157.7W
157.6W

Appendix C The diurnal perturbations of wind from the mean state at 3-hour interval under weak trades

C.1 The diurnal perturbations of wind vector from the weak-trade mean state.

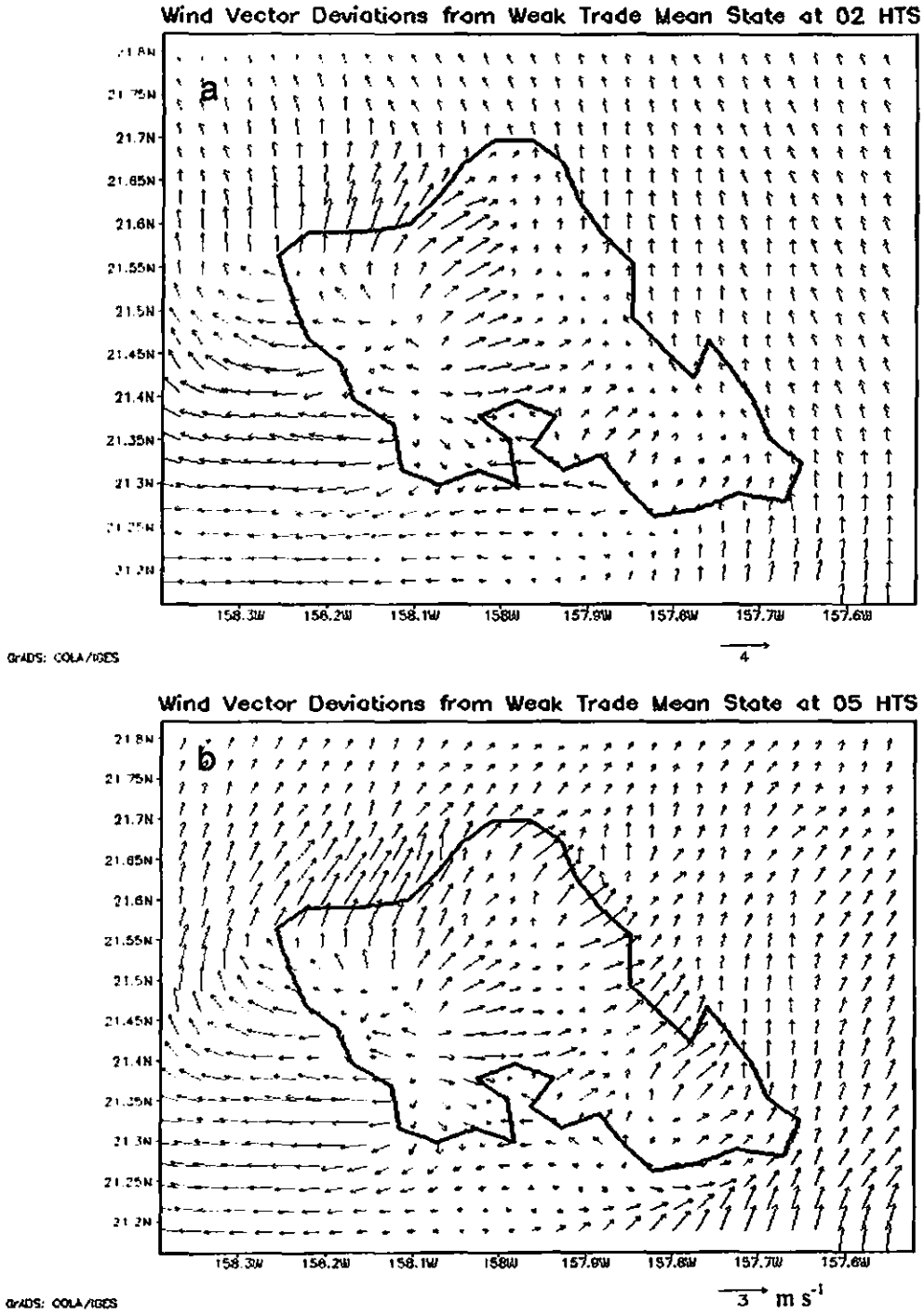

Figure C.1 The diurnal perturbations of wind vector from the weak-trade mean state (a) at 02 HST. and (b) at 05 HST

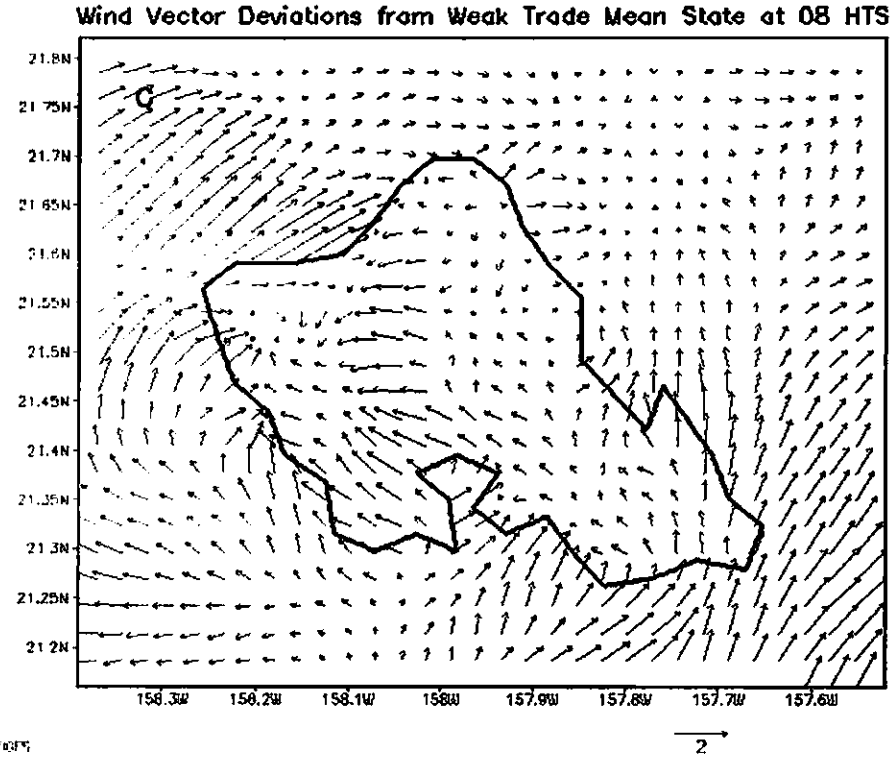

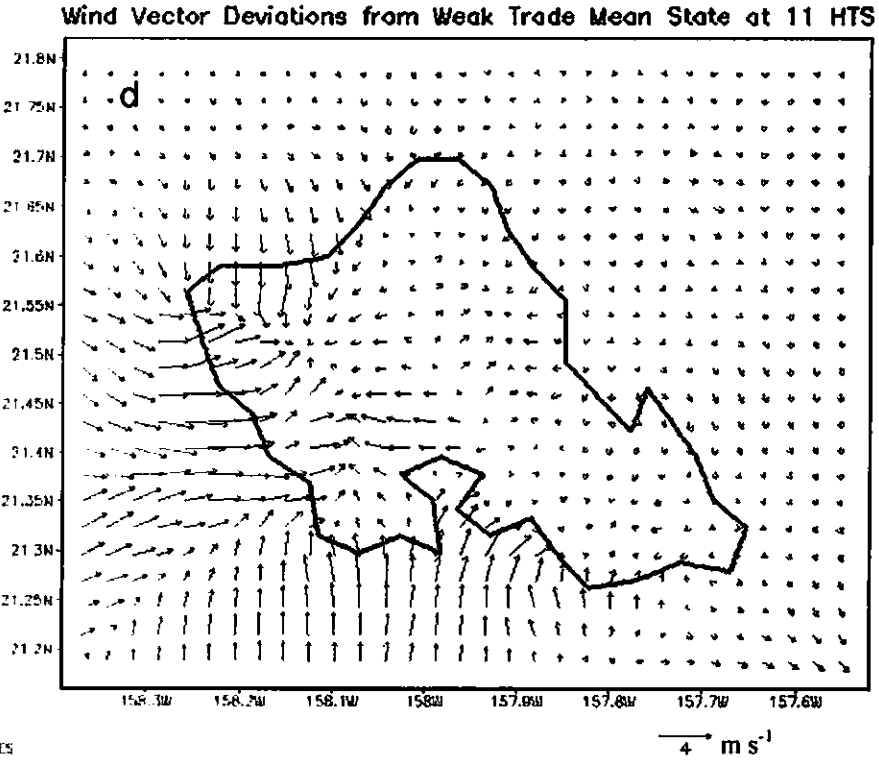

Figure C.1 The diurnal perturbations of wind vector from the weak-trade mean state (c) at 08 HST, and (d) at 11 HST

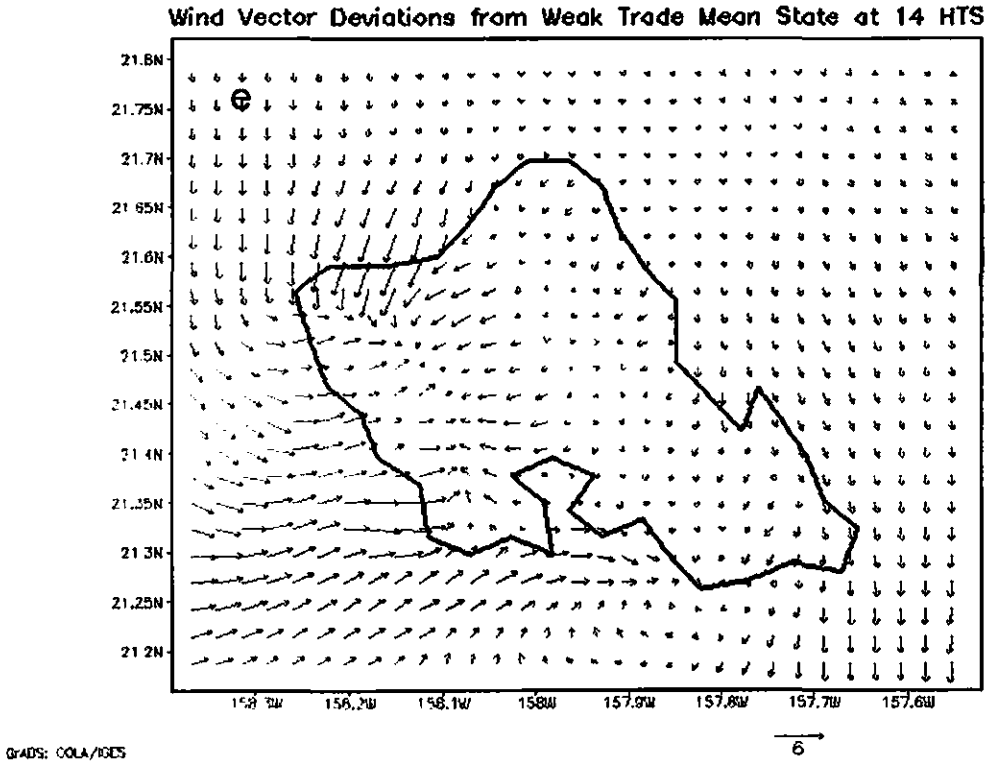

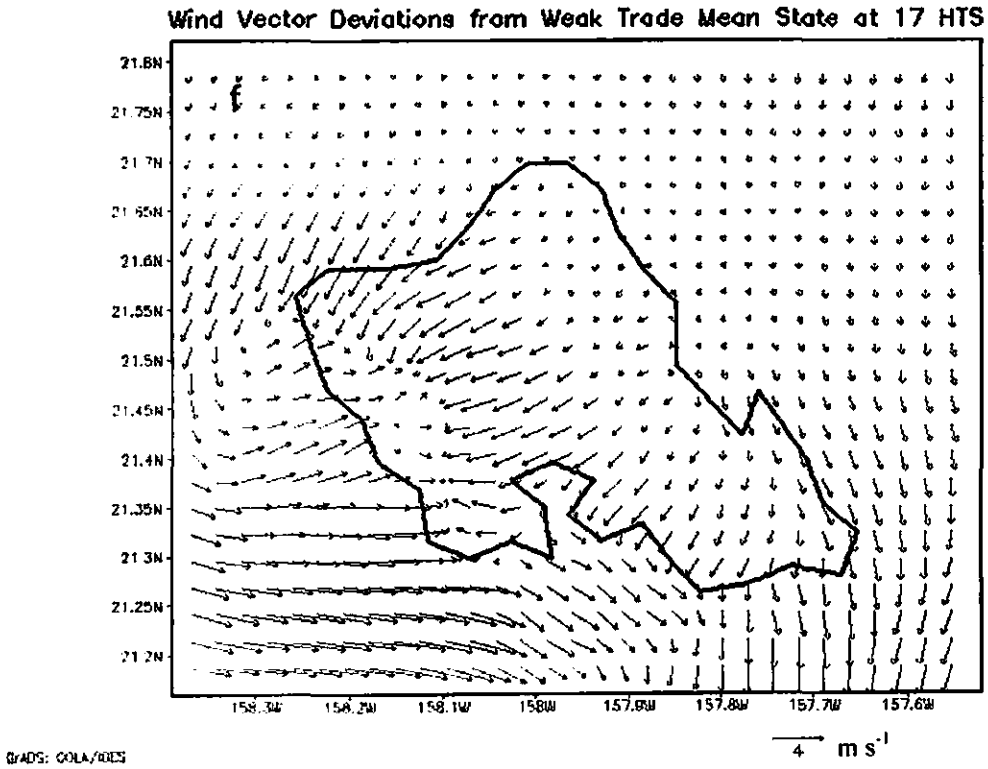

Figure C.1 The diurnal perturbations of wind vector from the weak-trade mean state (e) at 14 HST, and (f) at 17 HST

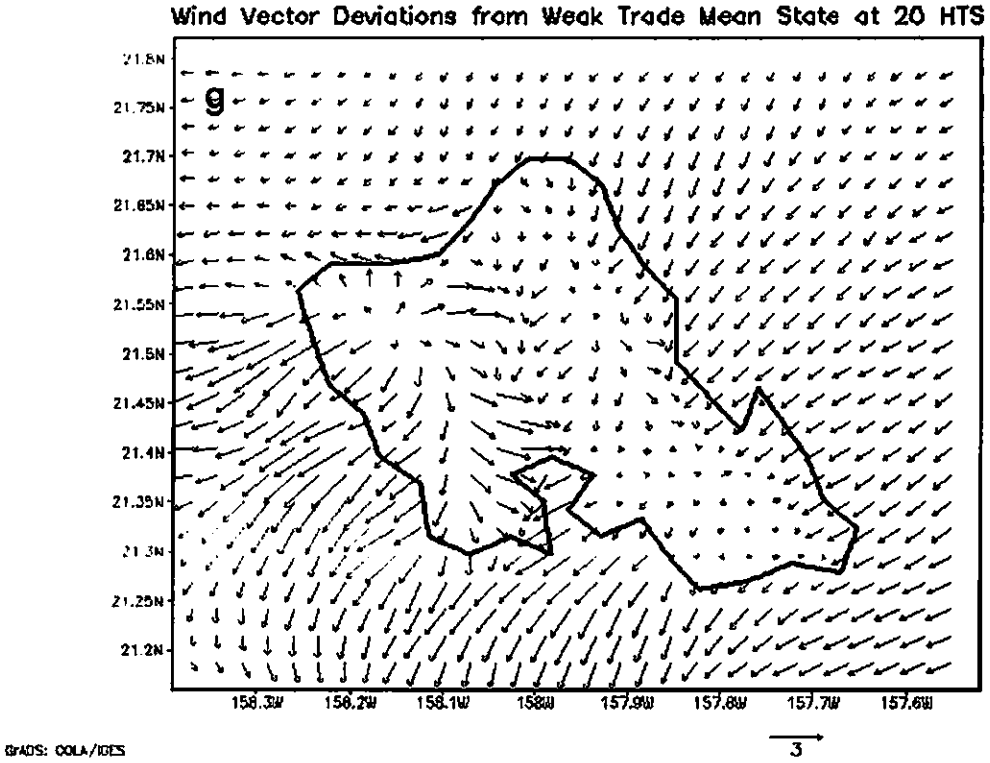

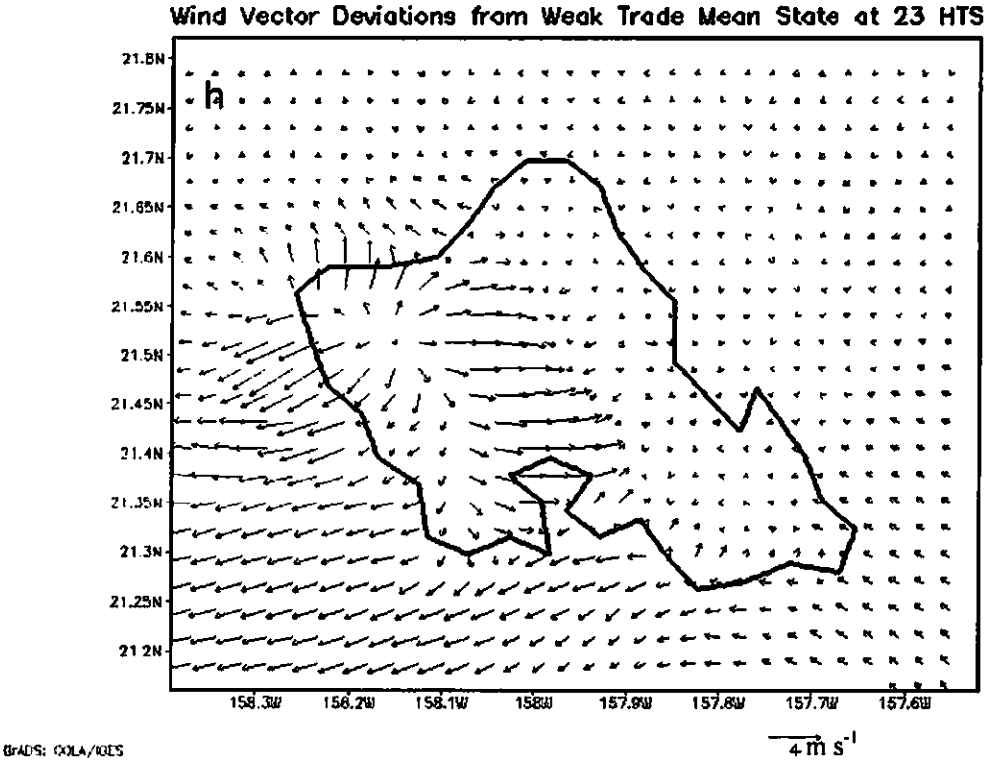

Figure C.1 The diurnal perturbations of wind vector from the weak-trade mean state (g) at 20 HST, and (h) at 23 HST

C.2 The diurnal perturbations of zonal wind component (m s^{-1}) from the weak-trade mean state.

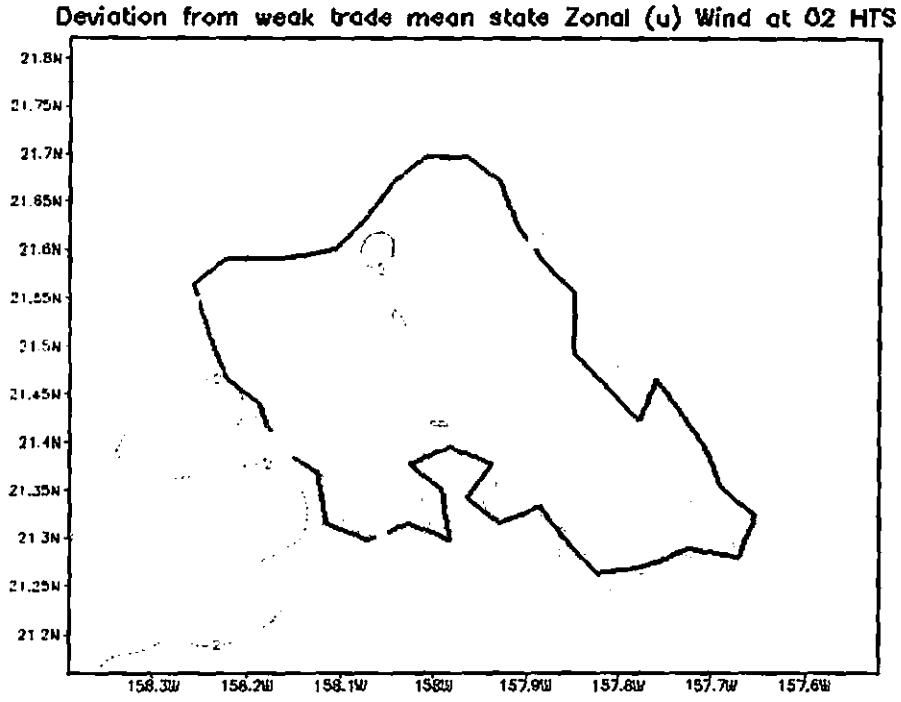

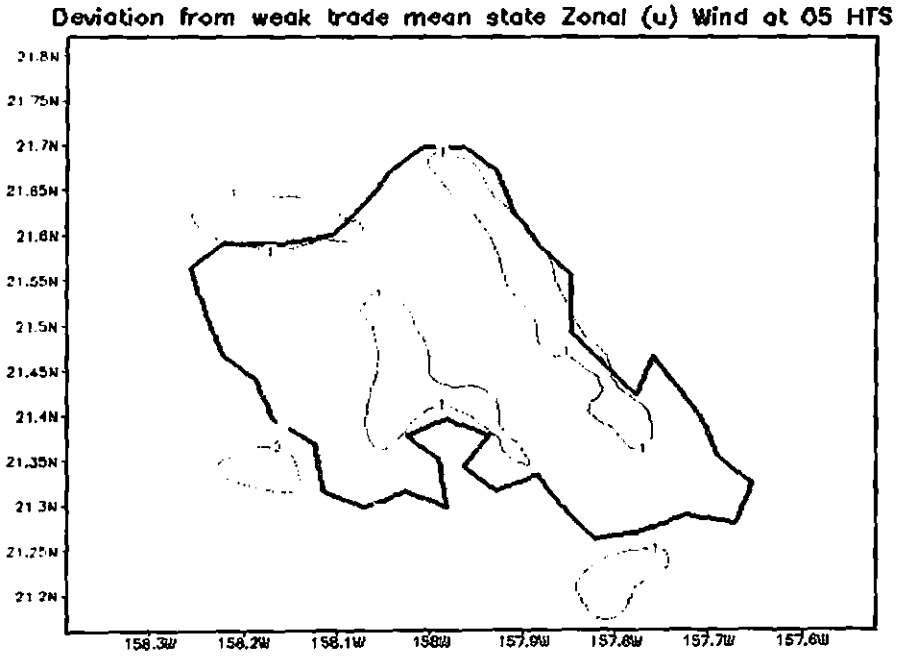

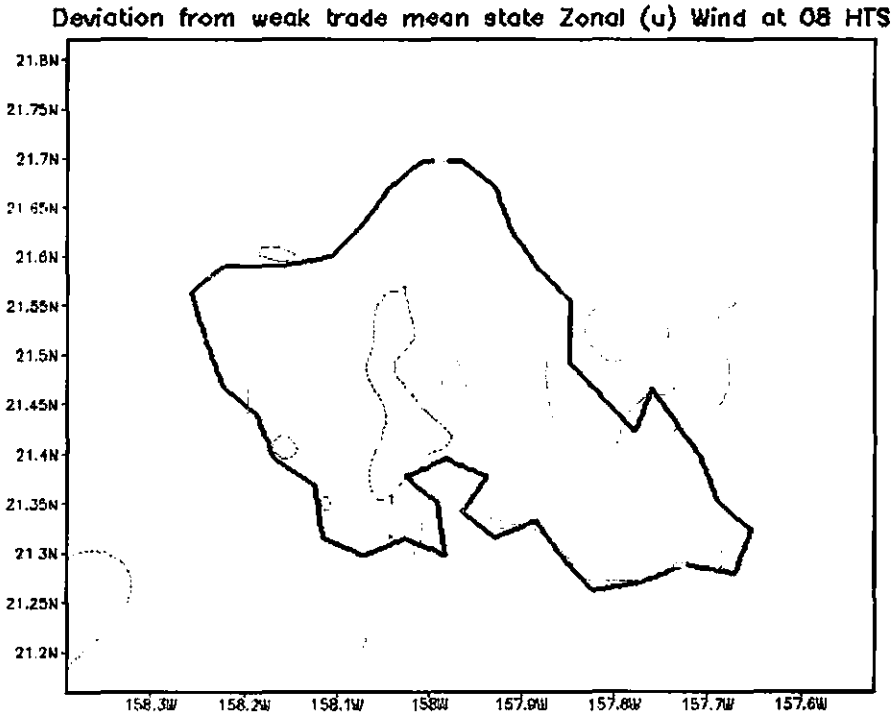
Deviation from weak trade mean state Zonal (u) Wind at 08 HTS
21.8N
21.75N
21.7N
21.65N
21.6N
21.55N
21.5N
21.45N
21.4N
21.35N
21.3N
21.25N
21.2N
158.3W
158.2W
158.1W
158W
157.9W
157.8W
157.7W
157.6W
GrADS: COLA/IGES

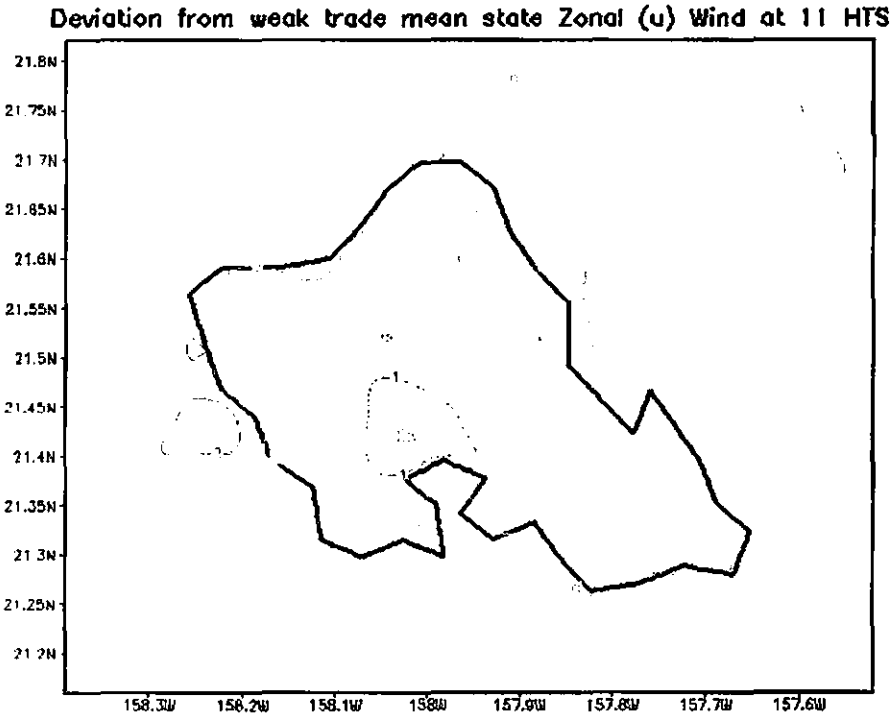
Deviation from weak trade mean state Zonal (u) Wind at 11 HTS
21.8N
21.75N
21.7N
21.65N
21.6N
21.55N
21.5N
21.45N
21.4N
21.35N
21.3N
21.25N
21.2N
158.3W
158.2W
158.1W
158W
157.9W
157.8W
157.7W
157.6W
GrADS: COLA/IGES

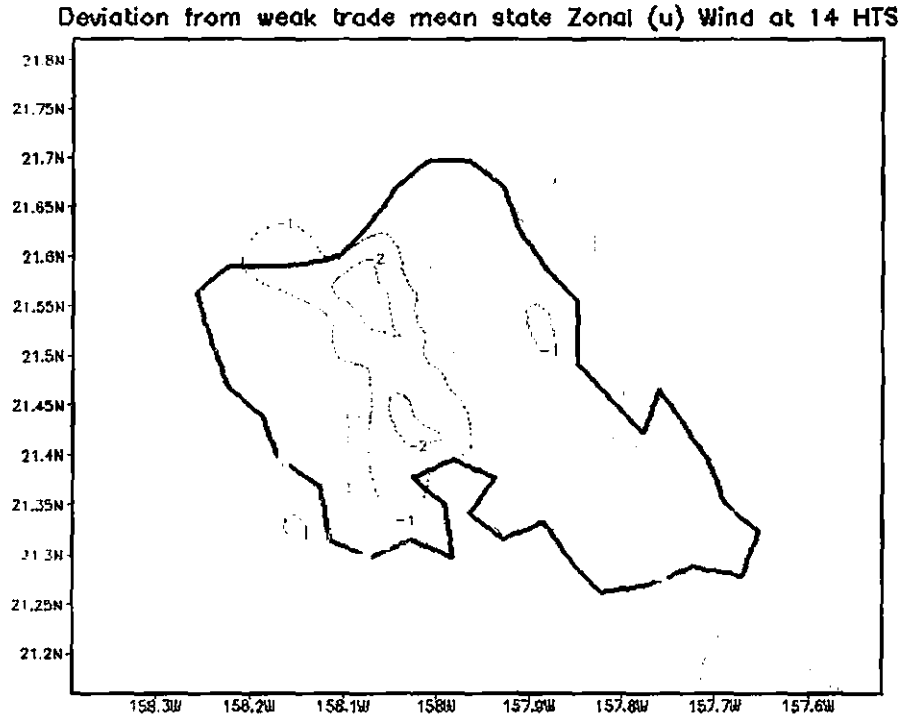
Deviation from weak trade mean state Zonal (u) Wind at 14 HTS
21.8N
21.75N
21.7N
21.65N
21.6N
21.55N
21.5N
21.45N
21.4N
21.35N
21.3N
21.25N
21.2N
158.3W
158.2W
158.1W
158W
157.9W
157.8W
157.7W
157.6W
GrADS: COLA/IGES

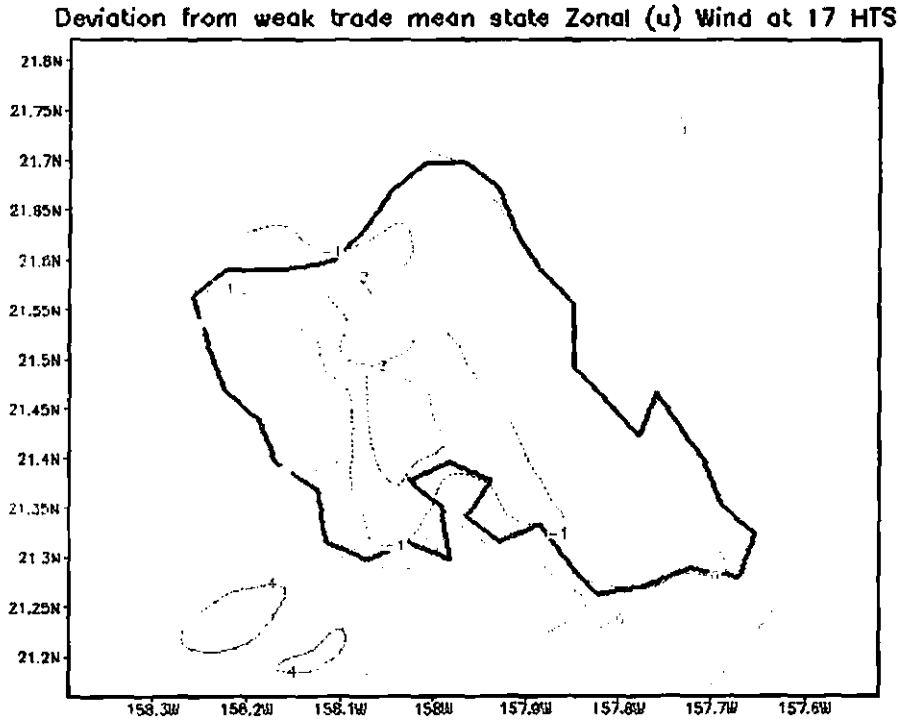
Deviation from weak trade mean state Zonal (u) Wind at 17 HTS
21.8N
21.75N
21.7N
21.65N
21.6N
21.55N
21.5N
21.45N
21.4N
21.35N
21.3N
21.25N
21.2N
158.3W
158.2W
158.1W
158W
157.9W
157.8W
157.7W
157.6W
GrADS: COLA/IGES

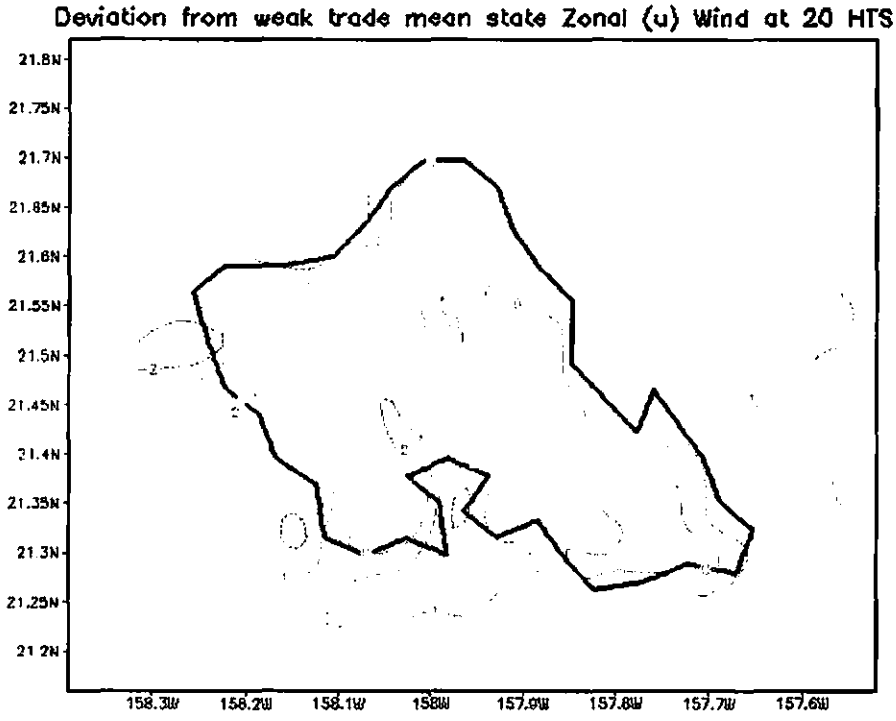
Deviation from weak trade mean state Zonal (u) Wind at 20 HTS
21.8N
21.75N
21.7N
21.65N
21.6N
21.55N
21.5N
21.45N
21.4N
21.35N
21.3N
21.25N
21.2N
158.3W
158.2W
158.1W
158W
157.9W
157.8W
157.7W
157.6W
GrADS: COLA/IGES

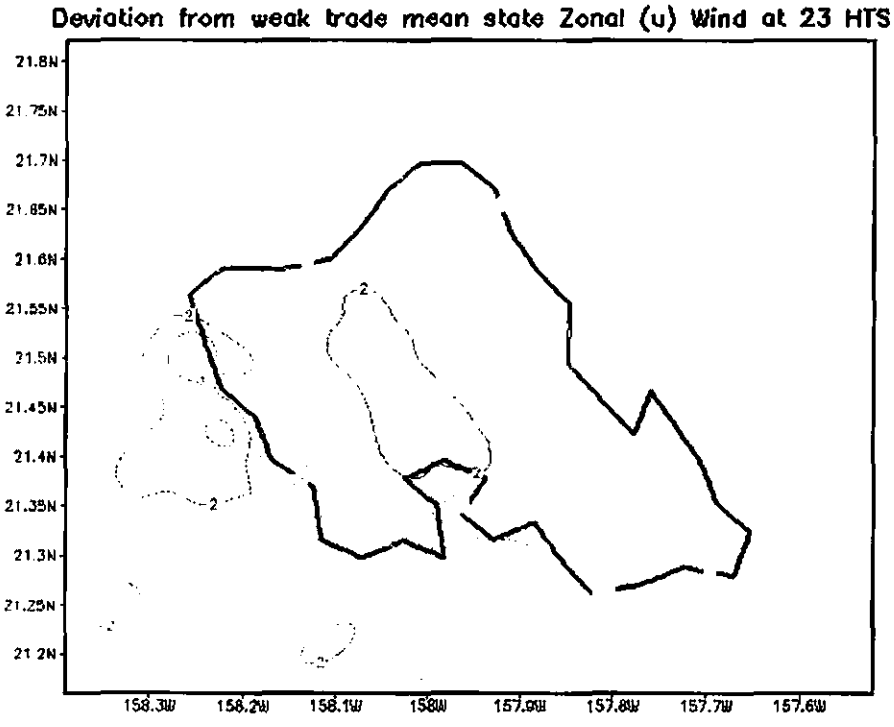
Deviation from weak trade mean state Zonal (u) Wind at 23 HTS
21.8N
21.75N
21.7N
21.65N
21.6N
21.55N
21.5N
21.45N
21.4N
21.35N
21.3N
21.25N
21.2N
158.3W
158.2W
158.1W
158W
157.9W
157.8W
157.7W
157.6W
GrADS: COLA/IGES

C.3 Vertical cross sections at (21.45 N) of the diurnal perturbations of zonal wind component (m s^{-1}) from the weak-trade mean state.

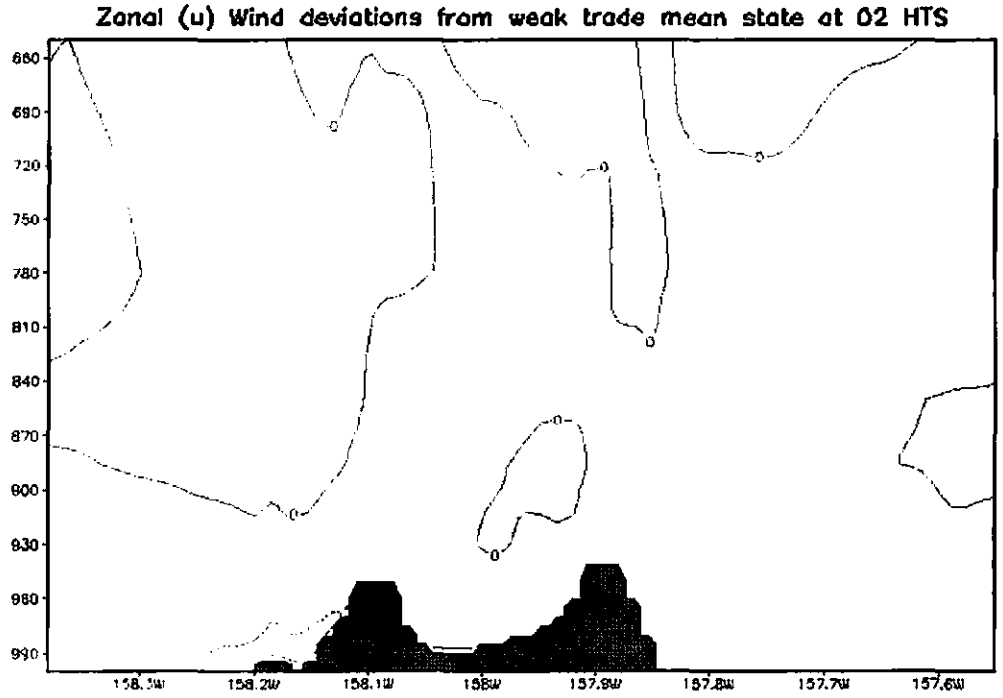

GrADS: COLA/IDES

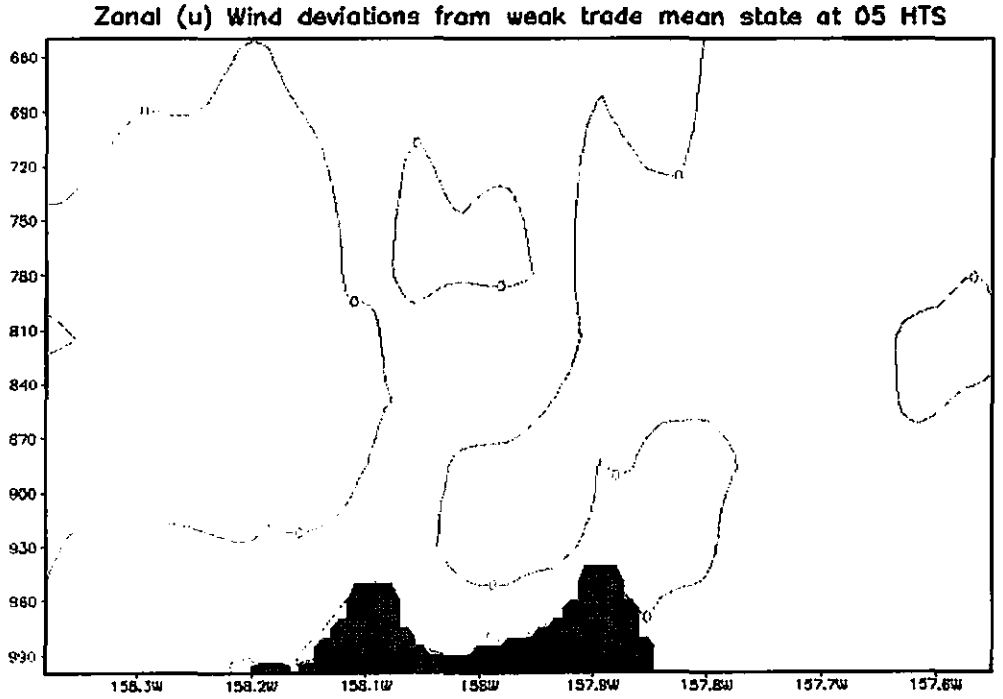

GrADS: COLA/IDES

Zonal (u) Wind deviations from weak trade mean state at 08 HTS

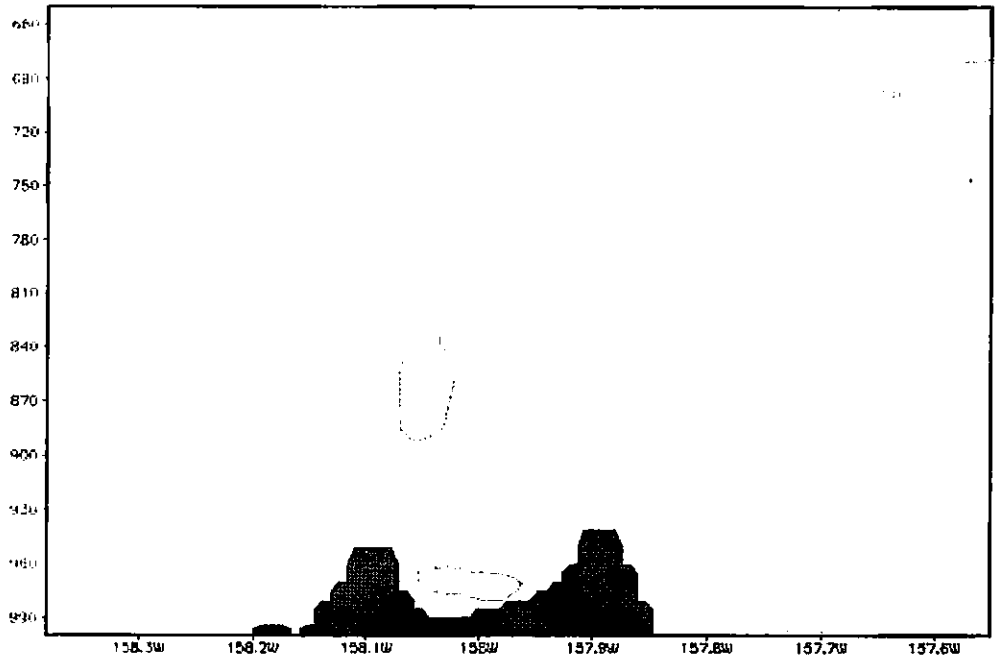

GrADS: COLA/IGES

Zonal (u) Wind deviations from weak trade mean state at 11 HTS .

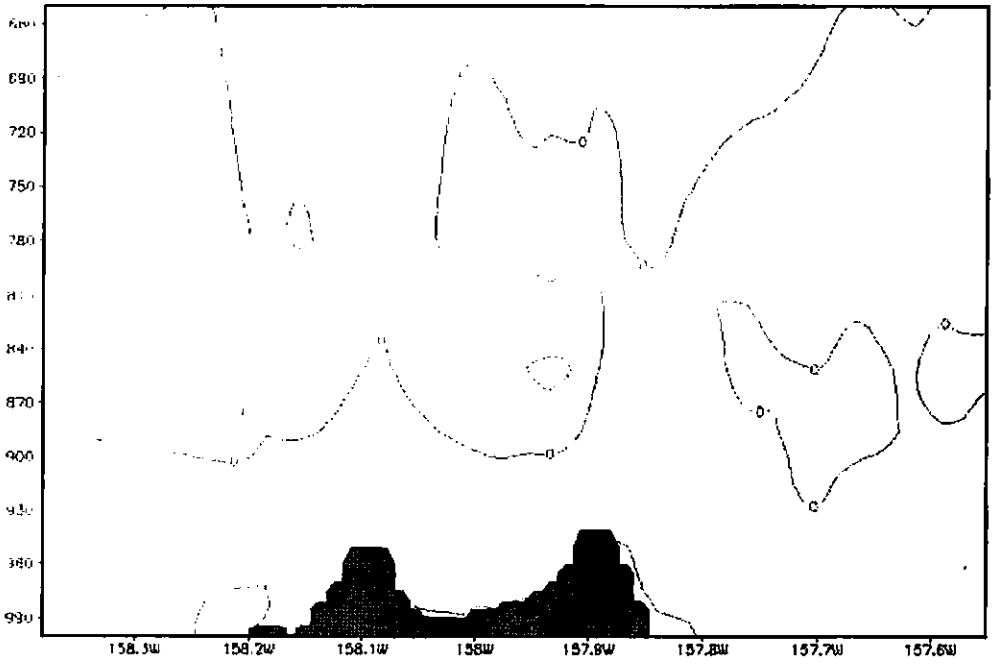

GrADS: COLA/IGES

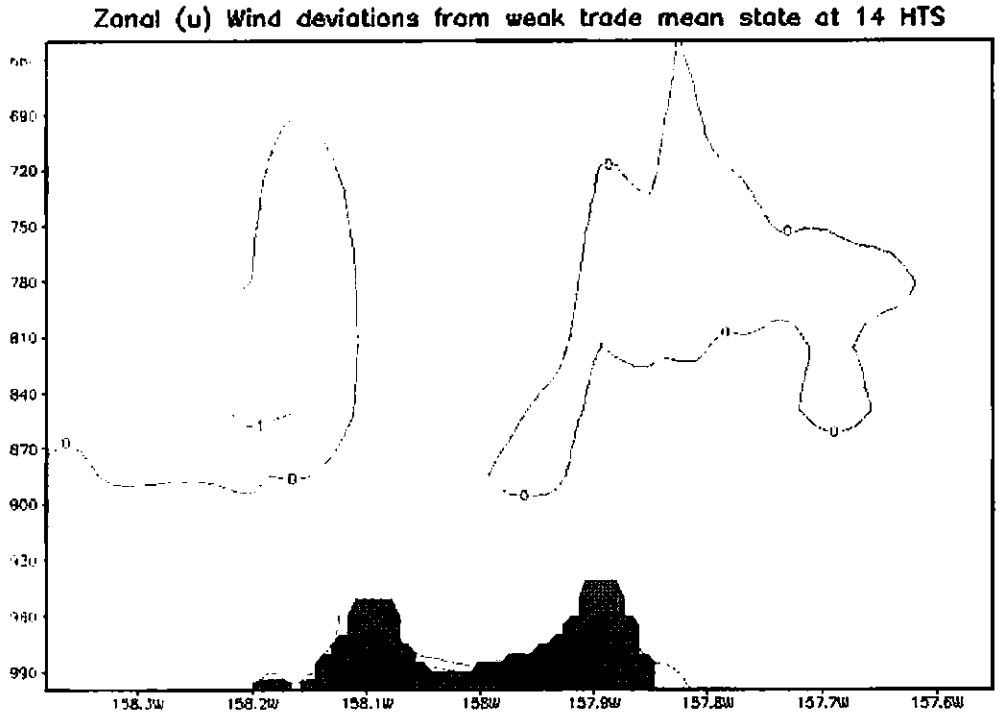

GrADS: COLA/IDES

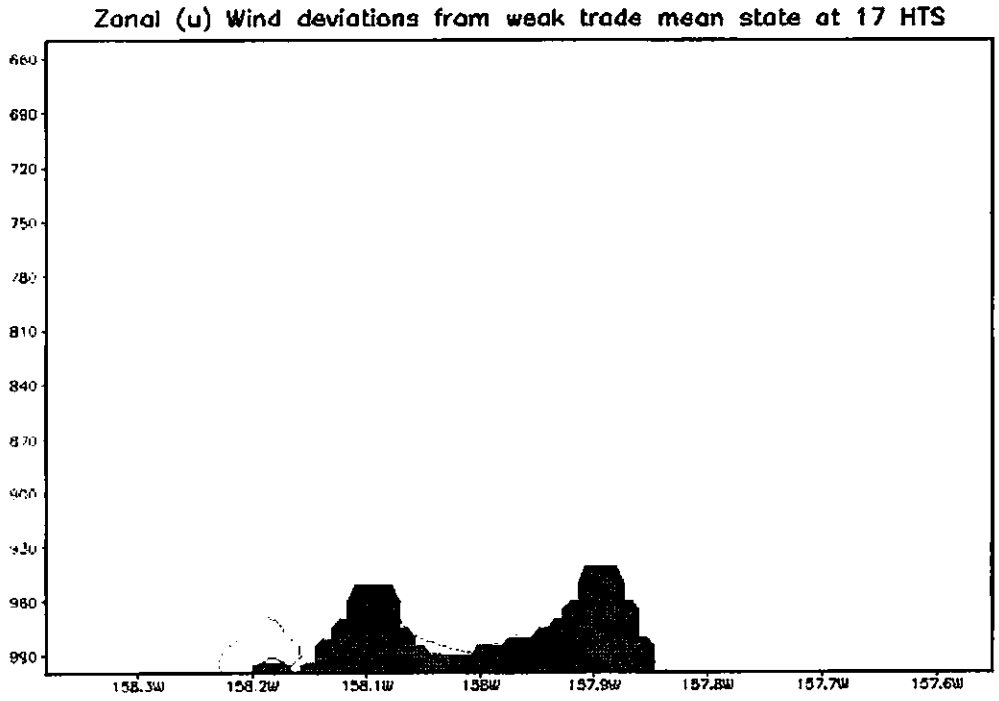

GrADS: COLA/IDES

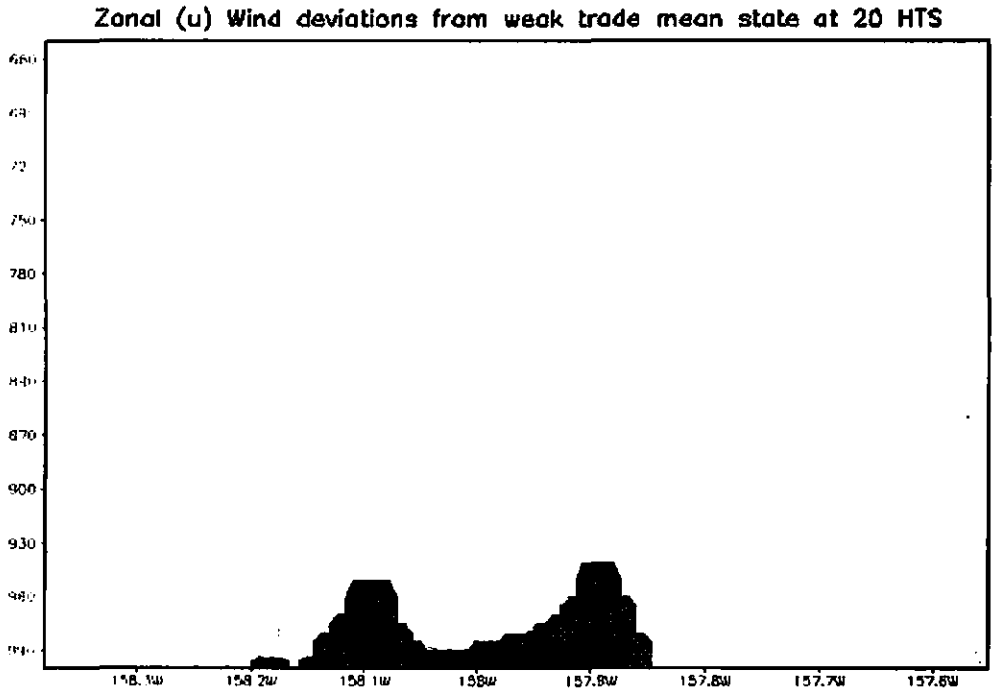

GrADS: COLA/IGES

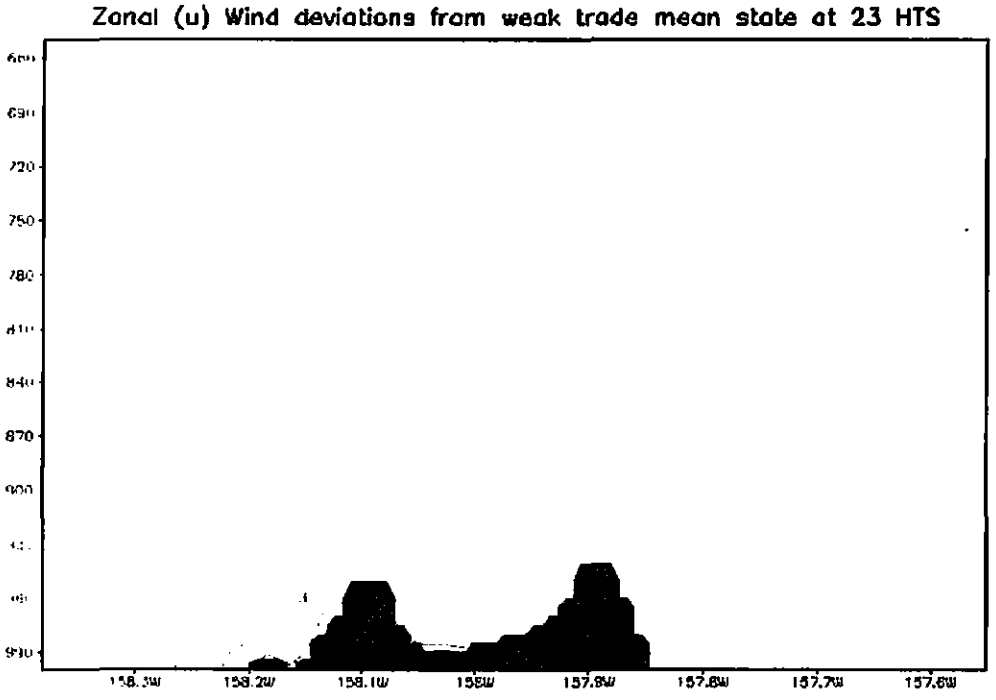

GrADS: COLA/IGES

References

Carbone, R. E., W. A. Cooper, V. Grubisic, and W. C. Lee, 1998: Trade wind rainfall near the windward coast of Hawaii. *Mon. Wea. Rev.*, **126**, 47-63.

Chen, F. and J. Dudhia 2001: Coupling an advanced land surface/hydrological model with the Penn State/NCAR MM5 modeling system. Part I: model implementation and sensitivity. *Mon. Wea. Rev.*, **129**, 569-585.

Chen, Y.-L., and A. J. Nash, 1994: Diurnal variation of surface airflow and rainfall frequencies on the island of Hawaii. *Mon. Wea. Rev.*, **122**, 34-56.

_____, and J. J. Wang, 1994: Diurnal variation of surface thermodynamic fields on the island of Hawaii. *Mon. Wea. Rev.*, **122**, 25-38.

Feng, J. and Y. –L. Chen, 2000: Numerical simulation of airflow and cloud distribution over the windward side of the island of Hawaii. Part I: Nocturnal flow regime. *Mon. Wea. Rev.*, **129**, 35-47.

Frye, J. L., and Y. –L. Chen, 2000: Evolution of downslope flow under strong opposing trade winds and frequent trade-wind rainshowers over the island of Hawaii. *Mon. Wea. Rev.*, **129**, 956-977.

Giambelluca, T. W., M. A. Nullet, and T. A. Schroeder, 1986: Rainfall atlas of Hawaii. Report R76, Department of Land and Natural Resources, State of Hawaii, Honolulu, HI, 267 pp.

Lavoie, R. L., 1974: A numerical model of trade wind weather on Oahu. *Mon. Wea. Rev.*, **102**, 630-637.

Leopold L. B., 1948: Diurnal weather patterns on Oahu and Lanai, Hawaii, *Pacif. Sci.* **2**, 81-95.

_____, 1949: The interaction of trade wind and sea breezes, Hawaii. *J Meteor.*, **6,** 312 – 320.

Li, J., and Y.-L., Chen, 1998: A case study of nocturnal rain showers over the windward coastal region of the island of Hawaii. *Mon. Wea. Rev.*, **127**, 74-92.

Loveridge, E. H., 1924: Diurnal variations of precipitation at Honolulu, Hawaii, *Mon. Wea. Rev.*, **52**, 584-585.

Loos, T., 2004: Diurnal variations of island scale weather over Oahu and Kauai during summer months. M.S. thesis, University of Hawaii, *254* pp. [Available at Department of Meteorology, University of Hawaii, 2525 Correa Rd. Honolulu, Hi. 96822.]

Loos, T. and Y.-L. Chen, 2004: Diurnal variations of island-scale weather over Oahu. AGU Western Pacific Geophysics Meeting, H33B-5, 16-20 August, Honolulu, HI.

Ramage, C.S., and N.E. Oshiro, 1977: Kauai Wind Power Survey -- Part 1: Mobile Sampling Program 19 August to September 1977. Department of Meteorology, University of Hawaii (Report UHMET 77-05).

Schroeder, T. A., B. Kilonsky, and B. Meisner, 1977: Diurnal Variation in Rainfall and Cloudiness. Water Resources Research Center Technical Report No. 112.

Yang, Y., and Y.-L. Chen, 2003: Circulation and rainfall on the lee side of the island of Hawaii during HaRP, . *Mon. Wea. Rev.*, **131**, 25-42.

_____, and Y.-L. Chen, F. M. Fujioka 2005: Numerical simulations of the island-induced circulations over the island of Hawaii during HaRP. *Mon. Wea. Rev.*, ***133***, 93-13.

Zhang, Y., Y.-L. Chen, S.-Y. Hong, K. Kodama, and H.-M. H. Juang, 2005b: Validation of the coupled NCEP Mesoscale Spectral Model and an advanced Land Surface Model over the Hawaiian Islands. Part I: Summer trade wind conditions over Oahu and Heavy rainfall events. *Wea. Forecasting.*, **20**, 847-872.